Exploring Natural Variation in Foliar and Non-Foliar Tissues to Improve Yield Potential in *Pisum sativum*

Alexandra L Milliken

A thesis submitted for the degree of Doctor of Philosophy in Biological Sciences

School of Life Sciences

University of Essex

November 2024

Abstract

As global populations rise exponentially and the impacts of climate change intensify, it is becoming increasingly imperative to increase crop production capable of withstanding future climatic conditions to meet food demands. As genetic approaches have legal restrictions, breeders are focusing on alternative strategies, with natural variation in photosynthetic capacity and stomatal responses remaining an underutilised resource for crop improvements. Studies that have explored natural variation have mainly focused on leaves, however it is becoming increasingly apparent that non-foliar tissues are capable of photosynthesising and are possible compensatory mechanisms for foliar tissues during stress. Although demand for peas are increasing (as an alternative source of protein), their yields are stagnating due to poor conditions. As many different varieties of pea exist, including conventional leafed, semi-leafless and leafless varieties, they provide an ideal model to explore for the identification of beneficial traits in both foliar (leaves and stipules) and non-foliar (pods) tissues. This study utilised IRGA's, chlorophyll fluorescence and surface impressions to determine that photosynthetic capacity/rates, stomatal characteristics and *i*WUE naturally varied amongst the pea accessions utilised and between the different types of foliar tissues. The findings demonstrated that variation in foliar tissues existed in the traits mentioned above when pea accessions were subjected to mild drought. Whilst a bespoke Lawson Lab gas exchange chamber was used to highlight that pea pods were photosynthetically active, naturally varied in measured traits across the pea accessions, had functional stomata and that pod photosynthesis potentially acted as a compensatory mechanism under drought stress. Such findings emphasised that natural variation exists even amongst a small population of peas, with potential for future breeding programmes to explore the accessions and traits presented here, for enhanced pea production under future climatic conditions in order to meet demand.

Acknowledgments

Firstly, I would like to thank my supervisors Professor Tracy Lawson and Professor Phillip Mullineaux for giving me the opportunity to do this PhD. I thank Tracy for her guidance, help and support with everything going on both at work and in my personal life. I thank Phil for his encouragement and support. I would also like to thank the University of Essex and the Perry Foundation for funding this project, with special thanks to Dr Ken Pallett who made me feel welcomed into the Perry family.

I also appreciate all the help the Essex Plant Group (both past and present members) have provided me along the course of my PhD. I want to thank Beata for being there for me and for tending to my plants whilst I was away. I also want to thank Dr Phil Davey whose humour, wit and caring nature has made him like a Lab Uncle, whilst his help with gas exchange (especially the non-foliar chamber) was a lifesaver. I also appreciate the kindness shown by Lorraine and her colleagues, who made the longest days feel less lonely.

Whilst my journeys to the lab were made enjoyable and memorable by my train buddies Shaun and Tim, who I thank for taking a panicked soul under their wings.

I want to thank my friends and both the Milliken and Brightwell Clans for their moral support. I additionally owe the Barker family, specifically Joy and Ken a debt of gratitude for not only allowing me to stay at their home, but for all the love given throughout my life.

To Mum, Dad and Sam, I thank you all for your endless support, love and journeys/lifts to Uni, as well as continually putting up with all my anxiety. Your patience has been truly appreciated. I love you all.

I would also like to give thanks to family members that are no longer with us, time with each of you helped guide me to where I am today. Thus with all my love and thanks, God Bless.

Finally, to the reader I hope that if you ever find yourself struggling, remember to believe in yourself….

Table of Contents

Abbreviation List

A	Assimilation
A100	Steady state *A* at 100 µmol m^{-2} s^{-1} PPFD
A1000	Steady state *A* at 1000 µmol m^{-2} s^{-1} PPFD
AB	Abaxial
ABA	Abscisic Acid
AD	Adaxial
af/AF	Afila gene
A_{max}	CO_2 and light saturating photosynthetic rate
a_{max}	Mean maximum stomatal pore area
A_{sat}	Light saturated rate of *A*
A_{sat400}	CO_2-saturated rate of *A* at 400 µmol mol^{-1} C_a
ATP	Adenosine Triphosphate
C_a	Atmospheric [CO_2]
CA	Carbonic anhydrase
Cam	Cameor pea accession
CAM	Crassulacean Acid Metabolism
CamB	Cameor B pea accession
Cen	Cennia pea accession
C_i	Intracellular [CO_2]
D	Droughted
d	Diffusivity of water in air at 22°C
DW	Dry Weight
Ela	Elatius pea accession
Eth	Ethiopia pea accession
ETR	Electron Transport Rate
F'	Steady state fluorescence in the light
F_m	Maximum fluorescence in the dark
F_m'	Maximum fluorescence in the light
F_o	Minimum fluorescence in the dark
F_o'	Minimum fluorescence in the light
F_q'/F_m'	PSII light operating efficiency
F_q'/F_v'	PSII photochemical quenching factor
F_v'/F_m'	Maximum efficiency of PSII in the light
F_v/F_m	Maximum efficiency of PSII in the dark
GC	Guard Cells
GCL	Guard Cell Length
g_{ias}	Mesophyll conductance through intercellular airspaces
g_{liq}	Mesophyll conductance through liquid phase within cells
g_m	Mesophyll Conductance
GM	Genetic Modification
g_s	Stomatal Conductance
gs100	Steady state g_s at 100 µmol m^{-2} s^{-1} PPFD
gs1000	Steady state g_s at 1000 µmol m^{-2} s^{-1} PPFD
gs_{1500}	Stomatal conductance at 1500 µmol m^{-2} s^{-1} PPFD
gs_{400}	g_s at 400 µmol mol^{-1} C_a
gs_{max}	Maximum anatomical stomatal conductance

g_w	Mesophyll conductance through cell wall
IRGA	Infra-red gas exchange analysers
*i*WUE	intrinsic Water Use Efficiency (calculated as A/g_s)
$iWUE_{max}$	Maximum intrinsic Water Use Efficiency
J_{max}	Maximum rate of electron transport
KW	Kelvedon Wonder pea accession
l	Pore depth
LMA	Leaf mass per unit area
MAS	Marker Assisted Selection
Met	Meteor pea accession
MIMS	Membrane inlet mass spectrometry
NAD-MDH	NAD-dependent malate dehydrogenase
NAD-ME	NAD-dependent malic enzyme
NADPH	Nicotinamide adenine dinucleotide phosphate
Ni11	Near isogenic line 11
Ni16	Near isogenic line 16
Non-GM	Non-genetically Modified
NPQ	Non-photochemical Quenching
OA	Oxaloacetate
PAR	Photosynthetically active radiation
PEPC	Phosphoenolpyruvate carboxylase
PL	Pore Length
PPFD	Photosynthetic photon flux density
PSII	Photosystem Two
PW	Pore width
ROS	Reactive Oxygen Species
RSWC	Relative Soil Water Content
RUBP	Ribulose Bisphosphate
SA	Surface Area
SD	Stomatal Density
SE	Standard Error
SMA	Stipule mass per unit area
SS	Stomatal Size
S_t	Solar Radiation
st/ST	Stipules Reduced gene
tl/TL	Tendriless gene
Tor	Torsdag pea accession
TP	Triose Phosphate
TPU	Triose Phosphate utilisation
v	Molar volume of air at 22^{o}C
Vc_{max}	Maximum rate of Rubisco activity
VPD	Vapour Pressure Deficit
W	Watered
WUE	Water Use Efficiency
WUE_{plant}	Water Use Efficiency at the plant level
Y	Genetic Yield Potential
ε_c	Conversion Efficiency
ε_i	Interception Efficiency
ε_p	Partitioning Efficiency

List of Figures

List of Tables

List of Equations

Chapter 1: Introduction

1.1. Background

With global populations projected to reach 9.7 billion by 2050, croplands (with yields at the current rate) will have to expand by around 69 million ha to meet the predicted 60-110% increase in food demands (Ray et al., 2013; Stagnari et al., 2017; Berners-Lee et al., 2018; Bahar et al., 2020; Furbank et al., 2020; Billen et al., 2024; Galanakis, 2024). However, cropland expansion is being impeded by abiotic and biotic factors, with growing populations heightening urbanisation for housing and manufacturing (de la Peña and Pueyo, 2012; Coyne et al., 2020). Whilst, increased global temperatures (by 0.2-0.3 ^{o}C per decade) from climate change is enhancing desertification, impeding irrigation and reducing the amount of arable land (Elliott et al., 2014; Kennedy et al., 2019; Asseng et al., 2020; Coyne et al., 2020). Rising temperatures and declines in arable land means sustainable improvements to crop productivity is becoming increasingly reliant upon enhancing photosynthetic potential and abiotic/biotic stress tolerance (*e.g.* to drought and disease) in order to meet food demands by 2050 (Ray et al., 2019; Asseng et al., 2020; Furbank et al., 2020).

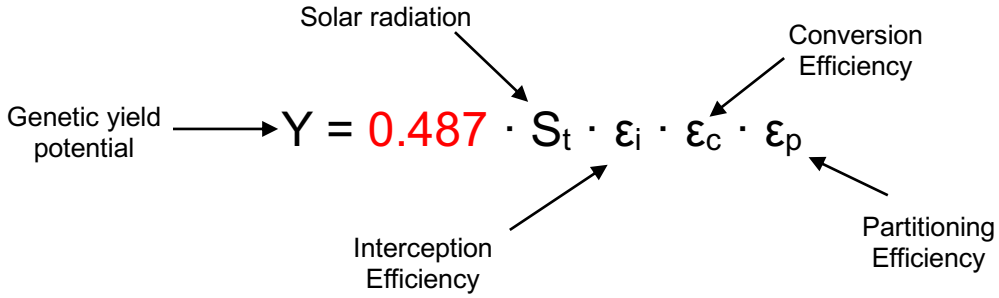

Equation 1.1. Genetic yield potential (Y) equation. Where S_t is the total solar radiation, however less than half (0.487) is absorbed by the leaf, the rest is retransmitted. ε_i is the light interception efficiency defined as the amount of PAR (photosynthetically active radiation; 400-700 nm) intercepted by a crop, with ε_i values reaching 0.8-0.9 which is close to the theoretical maximum in modern varieties through improvements to canopy features (*e.g.* architecture, longevity, development and size) and foliar morphologies (*e.g.* leaf size and number). ε_p is the partitioning efficiency (also known as the harvest index), defined as the amount of energy partitioned into the grain/harvestable product, with values reaching 0.6 mainly due to the selection of varieties (such as those that are semi-dwarfed), which put more biomass into the grain than the stem. ε_c is the conversion efficiency, defined as the amount of intercepted light energy that is converted into biomass, however limited improvements to ε_c have been made with values standing at 0.02 which is much lower than the theoretical maximum of 0.1 for C_3 crops (Zhu et al., 2010; Long et al., 2015; López-Calcagno et al., 2020).

Crop yields are determined by the cumulative rate of photosynthesis (process of light energy capture and conversion to biochemical energy) over the growing period, with maximum yields obtained when crops are grown within optimal conditions (Evans and Fischer, 1999; Timmerman-Vaughan et al., 2005; Evans, 2013; Simkin et al., 2019; Faralli et al., 2019). As a result of the green revolution, global food production tripled with advancements in machinery, industrial fertilisers and semi-dwarfed varieties providing greater harvestable yield (**Y**; yield obtained when biotic/abiotic stresses are absent and efficient management practices are in place) through maximisation of both interception efficiencies (ε_i: amount of solar radiation that is intercepted by a crop) and partitioning efficiencies (ε_p: amount of energy partitioned into the grain/harvestable product) (***Equation.1.1***) (Zhu et al., 2010; Pingali, 2012; Long et al., 2015). As ε_i and ε_p are already near the theoretical maximum, research is now focused on maximising crop conversion efficiencies (ε_c: amount of intercepted light energy converted into biomass) by improving photosynthetic rates (***Equation.1.1***) (Long et al., 2006; Slattery and Ort, 2015; Simkin et al., 2020). Genetic modification (GM) has been utilised to transform crops with Rubisco (ribulose-1,5-bisphosphate carboxylase) containing higher carboxylation capacities (Parry et al., 2011; Whitney et al., 2011; Sharwood, 2017), transferring C_4 concentrating mechanisms into C_3 plants (Raines, 2011; Evans, 2013; Voss-Fels et al., 2019) and creating photorespiration bypass systems (Peterhansel et al., 2013; Hagemann and Bauwe, 2016; Maurino, 2019). However, due to ethical concerns over GM procedures (*e.g.* consumer beliefs), GM crop production is banned in several countries, including the UK (Ricroch et al., 2018; Paarlberg et al., 2024). Subsequently, non-GM pathways are preferred with natural variation in photosynthetic capacity (ability of Rubisco to fix CO_2 and Ribulose Bisphosphate (RUBP) to be regenerated) remaining an untapped resource for

potential crop improvements (Farquhar et al., 1980; Faralli and Lawson, 2020; Yin et al., 2022).

Natural variation in photosynthetic capacity has already been identified in a number of species including wheat (Driever et al., 2014) and soybean (Sakoda et al., 2016), however the potential remains unexamined in many crops such as peas. Variation in photosynthetic capacity can be caused by anatomical, environmental and biochemical differences within and between species (Driever et al., 2014). Identification of high performing cultivars with desirable traits; especially under water limiting environments, can provide an additional potential genetic resource for MAS (Marker Assisted Selection) and conventional breeding programmes for higher yielding crops (van Bezouw et al., 2019). Research into photosynthesis (including natural variation) and carbohydrate acquisition mainly focuses on leaves (Simkin et al., 2020; Lawson and Milliken, 2023). However non-foliar tissues are gaining interest, with evidence of photosynthetic activity previously reported in alfalfa pods (Wang et al., 2016) and barley ears (Maydup et al., 2014). Non-Foliar materials are believed to have the potential to contribute carbohydrates to grain yield and are thought to be a compensatory mechanism for foliar photosynthesis under stress conditions in order to maintain productivity (Araus et al., 2021; Henry et al., 2020; Lawson and Milliken, 2023). Natural variation in non-foliar photosynthesis and yield contributions require further exploration, particularly in peas, with many leafless/semi-leafless varieties grown for ease of harvest and thus must rely upon non-foliar photosynthesis (Nemeskéri et al., 2015; Simkin et al., 2020; Tran et al., 2022; Lawson and Milliken, 2023).

Natural variation in stomatal anatomy and behaviour can also influence photosynthetic rates, especially in response to changing light intensities (Tinoco-Ojanguren and Pearcy, 1993; Matthews et al., 2017; Faralli et al., 2019; Bertolino et al., 2019). Stomata are small pores often found on the surface of photosynthetic tissues, which control the amount of carbon gained for photosynthesis and water lost via transpiration (for evaporative cooling) and thus regulates photosynthetic rates and a plant's water status (Hetherington and Woodward, 2003; Lawson and Blatt, 2014; Faralli et al., 2019; Driesen et al., 2020). These structures (which respond to both internal and external signals, such as light and water availability), are a key determinant of natural variation in water use efficiency (WUE; the measure of water lost compared to carbon gained), with variation in WUE already identified in Arabidopsis (Ferguson et al., 2018) and *B. napus* (Pater et al., 2017), but is yet to be fully quantified within peas (McAusland et al., 2016; Lawson and Vialet-Chabrand, 2019). However, as stomatal responses can be slower than photosynthetic responses to external conditions, a disconnection between stomatal conductance (g_s) and photosynthesis is often generated, leading to detrimental impacts on intrinsic WUE (A/g_s; *i*WUE). Subsequently, identifying accessions with fast/connected stomatal responses in both foliar and non-foliar tissues may highlight those with prominent *i*WUE which can cope under water-limited environments (Lawson and Blatt, 2014; McAusland et al., 2016; Lawson and Vialet-Chabrand, 2019; Stevens et al., 2021; Battle et al., 2024).

Pea yields are currently stagnating, as a result of poor soil regions and water limitations, yet current demands are rising as *Pisum sativum's* potential as an alternative source of protein is gaining popularity. Subsequently, pea production needs to increase to warrant future food security/demands (Tulbek et al., 2017; Rasskazova

and Kirse-Ozolina, 2020; Coyne et al., 2020). This project's exploration into the natural variation in photosynthetic capacity and yield as well as the responses of photosynthesis and stomata (in addition to *i*WUE) to light intensity changes in both foliar and non-foliar pea material, provides the potential to identify desirable accessions with high yields and drought tolerance for increased production under future climatic conditions.

1.2. Importance of Peas

1.2.1. History of Pea Domestication

Pisum sativum is part of the *Leguminosae* (also known as the *Fabaceae*) family (subfamily: *Faboideae*); the second highest producing family globally (after cereals) and third largest flowering family, all of which are eudicots. *Leguminosae* is made up of 650 genera and 18,000 species, consisting of both temperate (*e.g.* lentils, pea, chickpea and faba bean) and tropical legumes (*e.g.* cowpea and mungbean) (Smýkal et al., 2012; Kreplak et al., 2019; Coyne et al., 2020; Lara and Tsiami, 2024; Windsor et al., 2024). There are two *Pisum* species within the *Leguminosae* family; *P. fulvum* (Tawny (wild) pea) and *P. sativum* L. (common/field/garden pea), with *P. sativum* L. also comprising of two subspecies; subsp. *elatius* (wild pea) and subsp. *sativum* (garden pea) (Kosterin, 2017; Smýkal et al., 2017; Weeden, 2018; Gebreegziabher and Tsegay, 2020). The phylogenetic classification of *Pisum* has changed overtime, from five to two distinct species, whilst Jing et al. (2007) proposed *P. abyssinicum* (Ethiopian domesticated pea), made up a third species from its own domestication event, however *P. abyssinicum's* lineage is still being debated (Jing et al., 2007;

Smýkal et al., 2011; Kosterin, 2017; Weeden, 2018; Hanci and Cebeci, 2019; Rispail et al., 2023).

Peas were first domesticated around 10,000 years ago (during the Neolithic period), alongside other leading crop varieties; including cereals (*e.g.* wheat and barley) and other legumes (chickpeas and lentils), within the fertile crescent (a highly fertile area surrounding the Tigris, Euphrates and Nile rivers in the Middle East) (Trněný et al., 2018; Weeden, 2018; Kreplak et al., 2019). The fertile crescent is believed to be where *Pisum* first originated with broad genetic diversity spreading from the Middle East (Syria, Turkey, Israel and Iraq) and into Asia (Pakistan, India and China) (Ljuština et al., 2010; Smýkal et al., 2011). Pea cultivation is thought to have then extended into Russia; via the Danube valley and into Greece, enabling expansion into Northern Europe (Kosterin, 2017; Smýkal et al., 2017). It is believed that peas have been cultivated in Europe since the stone age; providing the early hunter-gathers' diet; with evidence from linguistic and fossil records dating back 12,000 BP (Ljuština et al., 2010). *P. fulvum's* growth is centralised to the fertile crescent, whilst *P. sativum* subspecies *elatius* and *sativum* are naturally found in Europe and Asia, with some expansion into African temporal regions (including Ethiopia). There is deliberation whether Ethiopia is a secondary domestication centre, with *P. abyssinicum* mainly cultivated within Ethiopia and Yemen, although it has never been identified in the wild (Trněný et al., 2018; Weeden, 2018).

This process of continuous domestication/cultivation enabled changes in genotypes and phenotypes within pea species. Although the global pea germplasm consists of 98,000 pea accessions (facilitated by continuous selection), less than 1% of these are

wild pea relatives (subspecies *elatius*). This natural variation currently remains an untapped resource, with the identification of high photosynthetic capacity and WUE within peas being crucial for food production under future climatic conditions (Smýkal et al., 2017; Hradilová et al., 2019; Kreplak et al., 2019). It is worthy noting that *Pisum sativum* has been recently renamed as *Lathyrus oleraceus,* however as this change is only recent and has not been widely adopted due to ongoing debates, for the remainder of this thesis *Pisum sativum* will be used for the scientific/taxonomic name of pea (Lara and Tsiami, 2024).

1.2.2. Pea Productivity and Economic Gains

Peas are spilt into two main categories determined by the FAO; green pea (peas harvested and consumed fresh) and dry/yellow pea (dry pea product used for human consumption and animal feed) and are the second highest grown legume in temperate regions (Smýkal et al., 2011; Olle et al., 2020; Coyne et al., 2020). In 2020, global average green pea production was 20.3 Mt grown across 2.6 Mha, whilst dry pea global average production was 14.7 Mt over 7.2 Mha, this was an increase of 331% and 60.98% respectfully over the past 50 years (***Fig.1.1***) (FAOSTAT, 2024). During the 1960-1990's Eastern and Northern Europe were the main global pea producers; however, this has since shifted to Canada (4.6 Mt), Russia (2.7 Mt) and China (1.4 Mt) for dry peas and China (11.6 Mt), India (5.8 Mt) and France (0.25 Mt) for green peas in 2020 (Warkentin et al., 2015; Olle et al., 2020; FAOSTAT, 2024).

Within the UK, arable crop areas were around 6.1 Mha in 2020, however only 51,600 ha was used to produce 159,805 tonnes of dry peas, whilst 171,213 tonnes of green

peas were produced across 42,904 ha (DEFRA, 2020; FAOSTAT, 2024). As of September 2024, the UK net worth is around £320/t for dry peas and £355/t for green peas, however these values are predicted to increase with a rise in the vegetarian consumer market (Tulbek et al., 2017; Aschemann-Witzel et al., 2020; Windsor et al., 2024; PGRO, 2024). Although, dry and green pea production increased over the last 50 years (***Fig.1.1***), yields are stagnating with cereals being grown on higher quality land (*i.e.*, more fertile), whilst legumes (including peas) have been grown in water limiting and poor nutritional soils, thus identification of greater yielding pea varieties that are able to withstand stressful conditions are required (de la Peña and Pueyo, 2012; Coyne et al., 2020).

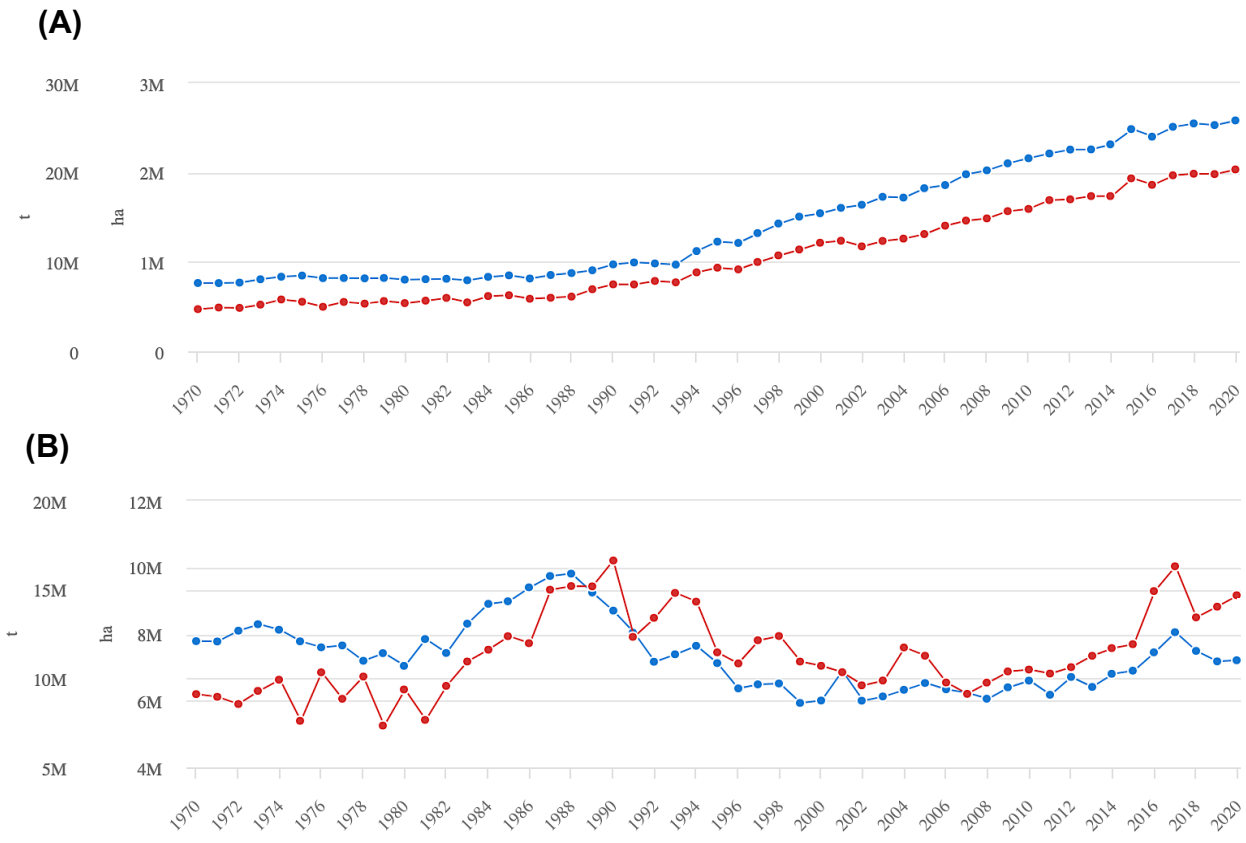

Figure 1.1. Global production and harvest area of (A) green and (B) dry peas from 1970 to 2020. Graphs are supplied by FAOSTAT 2024 Crop and Livestock products for green and dry pea. World area harvested (blue) is measured per hectare (ha), whilst world production (red) is measured in tonnes (t) (FAOSTAT, 2024).

1.2.3. Pea Health Benefits

Peas are historically notable as the first genetic plant model, as used by Gregor Mendel in 1856 to discover the laws of inheritance; including the law of segregation (alleles of the same trait separate during gamete formations) and the law of independent assortment (alleles are sorted independently of each other) (Smýkal et al., 2011; Tayeh et al., 2015). Pea's rapid life cycle, self-fertilization and easy-crossing capabilities made them simple models for Mendel's work (Tayeh et al., 2015). Recent research within peas have highlighted their potential as a source of: alternative plastic (Cano et al., 2015), anti-cancerous isoflavonoids/proteins (TI-1B) (Rungruangmaitree and Jiraungkoorskul, 2017) and a type-II diabetes manager (Becerra-Tomás et al., 2018). Pea consumption has been shown to contribute to increased satiety (via appetite stimulating hormones), which reduces food consumption, obesity risks and thus the likelihood of diabetes (Dahl et al., 2012; Tulbek et al., 2017; Becerra-Tomás et al., 2018).

Peas have gained popularity as an alternative meat source due to their high protein levels (23-25%); rich in tryptophan and lysine amino acids, which alongside chickpea and lentils are the primary protein source for 30% of the global population (Smýkal et al., 2011; Tulbek et al., 2017; Kreplak et al., 2019). High end global companies including ©*BirdsEye*; which launched its ©*Green Cuisine* range in 2019 (with sales already up by 2%), are starting to use pea protein within their meat free ranges (Rasskazova and Kirse-Ozolina, 2020). Proteins are produced within the seed cotyledon, with quantities varying depending on variety and environmental conditions. Field pea proteins also contain 20% less trypsin inhibitors than soybean, which increases the nutritional value. The majority of pea proteins are globular and are often

used within beverages and sauces (Dahl et al., 2012; Tulbek et al., 2017). Whilst peas also contain 50% slow digesting starch and 17-27% dietary fibre, which alongside pea protein and micronutrients (calcium, zinc and iron) makes up pea flour. Pea flour (*e.g.* ©*Novofarina*) can be used within gluten-free snacks, bread and pasta, which supplements the diet of those with celiac disease (Smýkal et al., 2011; Tulbek et al., 2017; Olle et al., 2020).

1.2.4. Pea Agricultural Benefits

As part of the legume family, peas have the capacity for nitrogen fixation, enabling the replenishment of soil fertility, without the requirement for industrial fertilizers (Kreplak et al., 2019). Nitrogen is fixed via symbiotic Rhizobium bacteria, which converts atmospheric dinitrogen gas into ammonium (a more usable form of nitrogen), that enables the production of amino acids and heightens pea protein content (Gresshoff et al., 2015). Nitrogen rhizodeposition; whereby nitrogen-based compounds are released from the roots, enables amino acids to be deposited to the surrounding soil and builds up soil organic matter (de la Peña and Pueyo, 2012). Due to their nitrogen-fixation abilities, peas are often utilised alongside cereals within crop rotations, which have been reported to generate a 13% reduction in total energy usage and a 25% drop in non-renewable energy usage, as fewer synthetic fertilisers are required (Zentner et al., 2004; MacWilliam et al., 2014; Tulbek et al., 2017; Sainju et al., 2019).

Agriculture utilises 70-80% of global water supplies, subsequently crops with sustainable water usage are often preferred by farmers (Blankenagel et al., 2018; Sainju et al., 2019; Mbava et al., 2020). Peas have been identified as being a more

sustainable protein source than meat/dairy products, with legume's water footprint being 1.5 times lower than dairy/poultry and six times lower than beef (Hoekstra, 2015; Tulbek et al., 2017; Ding et al., 2018). Although soybeans have a 10-20% greater protein content than peas, soybean production has led to rainforest deforestation; with nearly 5 Mha of land in South America being cleared since 1980 for pasture and soybean farms, further supporting peas as being a more sustainable protein source (Tulbek et al., 2017; Carlson and Garrett, 2018; Picoli et al., 2020). Yet, despite their sustainable growth and agricultural/health benefits, peas are still underutilised and under-profiled, whilst their natural variation remains untapped (Tulbek et al., 2017).

1.3. Natural Variation in Photosynthetic Capacity

1.3.1. Foliar Tissues

Natural variation is often defined as the within (and between) species phenotypic variation triggered by mutations and environmental conditions, which are maintained within a population through natural (and artificial) selection (Alonso-Blanco et al., 2009). Such variation has been exploited within crops since domestication began, with continuous selection of beneficial traits (*e.g.* selecting crops with more/larger fruit) allowing greater yields (McAusland and Murchie, 2020; Araus et al., 2021). However, domestication and continuous selection for high-yielding cultivars have meant many resourceful genes/phenotypes, such as those coding for drought tolerance or high photosynthetic capacity, have not been captured within current elite varieties (Driever et al., 2014; McAusland et al., 2020; Knorr and Augustin, 2024). Natural variation is currently an underutilised resource (especially within peas) for enhancements in

photosynthesis, productivity and yields. Subsequently, the identification and exploration of natural variation in photosynthesis within pea populations, could enable potential improvements to current varieties through future breeding programmes (van Bezouw et al., 2019; Faralli and Lawson, 2020).

Photosynthetic capacity; the maximum rate of carbon fixation per m^2 per second (μmol m^{-2} s^{-1}), is made up of two major determinates: the maximum rate of carboxylation capacity/Rubisco activity (Vc_{max}) and the maximum rate of electron transport (J_{max}) (Farquhar et al., 1980; Sharkey, 1985; Driever et al., 2014; Sharkey, 2019). Photosynthetic capacity has been reported to vary across 1% of vascular plant species (per unit leaf area) by 40-fold (Hikosaka and Shigeno, 2009), whilst variations in photosynthetic capacity have already been quantified within populations of key crops including wheat (Driever et al., 2014; Silva-Pérez et al., 2020), barely (Stevens et al., 2021), soybean (Gilbert et al., 2011; Sakoda et al., 2016), rice (Gu et al., 2014), cassava (De Souza et al., 2020) and sorghum (Ortiz et al., 2017). Although there is an ongoing debate as to whether photosynthetic capacity directly correlates to yield, with previous studies reporting a lack of relationship (Driever et al., 2014; Silva-Pérez et al., 2020; Stevens et al., 2021), Yoon et al. (2020) reported that a manipulated increase in photosynthetic capacity (through Rubisco overexpression), generated greater grain yield within rice as carbon fixation and nitrogen use efficiencies increased (Yoon et al., 2020; Acevedo-Siaca et al., 2021). Rice yields have been revealed to potentially rise by 22-29% if the natural variation identified within Vc_{max} and J_{max} are fully exploited (Gu et al., 2014), supporting the requirement for identification/quantification of natural variation in photosynthetic capacities within the current pea germplasm as a potential way to improve their productivity (Coyne et al., 2020).

Photosynthetic capacity and photosynthetic rates can be monitored via gas exchange (via infra-red gas exchange analysers (IRGAs)) and chlorophyll fluorescence (Quebbeman and Ramirez, 2016; Barnes et al., 2017; Jiang et al., 2020). IRGAs provide a direct non-invasive measurement of plant photosynthetic capacity, with the differences between reference (air entering the chamber) and sample (air exiting the chamber) CO_2 and water vapour concentrations determining the rates of assimilation (A) and transpiration (Du et al., 2020; Busch, 2024). Stomatal conductance (g_s) and intracellular [CO_2] (C_i) can also be calculated by monitoring environmental parameters such as light, humidity and leaf area (Sharkey, 2016; Du et al., 2020). Plotting A/C_i curves enables the identification of Vc_{max} and J_{max}, as demonstrated by Driever et al. (2014), who identified Vc_{max} and J_{max} naturally varied between 124–161 and 233–280 μmol m^{-2} s^{-1}, respectively, among 64 field-grown wheat cultivars through A/C_i analysis (Driever et al., 2014; Busch, 2024). Chlorophyll fluorescence analysis is often used in conjunction with gas exchange to determine electron transport rates and plant health in response to light (Hossain et al., 2015). Light energy absorbed by a plant can either drive photosynthesis, be released as heat, or re-emitted as fluorescence (McAusland et al., 2019; Lawson and Vialet-Chabrand, 2024). Chlorophyll fluorescence non-invasively measures the amount of re-emitted light (in high resolution) from photosystem two (PSII) and provides an insight into heat dissipation and PSII quantum efficiency (***Fig.1.2***) (Daley et al., 1989; Lawson and Weyers, 1999; Murchie and Lawson, 2013). F_q'/F_m' (also known as φPSII) indicates the PSII light operating efficiency and enables PSII electron transport estimations (predictions of J_{max}), with F_q'/F_m' generated via two products: F_q'/F_v' (PSII photochemical quenching factor) and F_v'/F_m' (maximum efficiency of PSII in the light) (Oxborough and Baker, 1997;

McAusland et al., 2019; McClain and Sharkey, 2020; Li et al., 2020; Lawson and Vialet-Chabrand, 2024). Whilst F_v/F_m determines the maximum efficiency of PSII in the dark (around ~0.83 in healthy leaves) (***Fig.1.2***) (Hossain et al., 2015). Variation within photosynthetic capacity can be the result of physiological, environmental, biochemical and morphological factors influencing Vc_{max} and J_{max}, as they are not fixed parameters (Barnes et al., 2017). Subsequently investigation of the underlining causes of variation in photosynthetic capacity within peas may aid with identification of high yielding and abiotic resistant accessions (Faralli and Lawson, 2020).

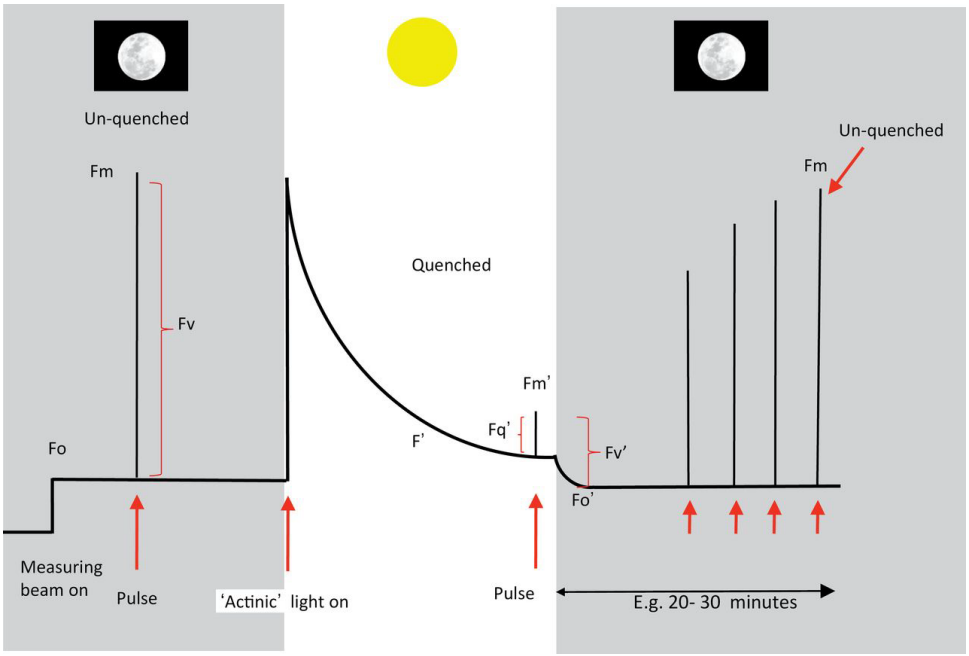

Figure 1.2. Diagram highlighting a fluorescence trace commonly used to determine photochemical and non-photochemical chlorophyll fluorescence parameters. Whereby a fluorescence trace (illustrated by the black line) in the first grey shaded box represents a leaf measured in a dark-adapted state (when non-photochemical quenching (NPQ) is absent and photosystem II (PSII) centres are open). A measuring beam (that is too low to induce photosynthesis) is used to generate a minimum fluorescence (F_o) value, which is followed by a saturating pulse to illicit a maximum fluorescence (F_m) value by closing reaction centres. The difference between the minimum and maximum fluorescence values allows a variable fluorescence (F_v) value to be calculated. When actinic light (represented by the white box) is turned on, steady state fluorescence (F ') can be obtained, whilst application of a saturating pulse is used to determine maximum fluorescence in the light (F_m') by closing the reaction centres (this value is lower than the dark-adapted value as NPQ is also occurring). When the actinic light is turned off (represented by the second grey box) the minimum fluorescence in the light (F_o') can also be obtained. The measurements of F_o, F_m, F_m' and F_o' can then be utilised to determine chlorophyll fluorescent parameters: F_v/F_m (maximum efficiency of PSII in the dark), F_q'/F_m' (PSII operating efficiency in the light), F_v'/F_m' (maximum efficiency of PSII in the light), F_q'/F_v' (PSII photochemical quenching factor) and NPQ (*see* ***Table 2.3*** for chlorophyll fluorescence parameter calculations). Figure has been utilised with permission from Murchie and Lawson (2013).

1.3.2. Factors Influencing Photosynthetic Variation

1.3.2.1. Biochemical Factors

The Farquhar et al. (1980) photosynthetic model; later updated into the Sharkey (1985) model, highlights three potential biochemical limitations of photosynthesis; Vc_{max} (highlighting limitations caused by Rubisco activity), J_{max} (limitations of RUBP regeneration from restricted electron transport) and triose phosphate utilisation (TPU) (Farquhar et al., 1980; Sharkey, 1985; Wullschleger, 1993; Yin et al., 2009; Domingues et al., 2010). Vc_{max} and J_{max} equally limit photosynthetic capacity, but at different levels of C_i, with Vc_{max} limiting photosynthesis at low C_i (typically below 30 Pa), whilst J_{max} becomes limiting at higher C_i concentrations (above 40 Pa) (Kromdijk and Long, 2016; Smith et al., 2019).

Variation within Vc_{max} is often the result of interspecific differences within Rubisco activation, which is influenced by Rubisco-activase activity and discrepancies in nitrogen (N) concentrations (necessary for Rubisco construction) (Faralli and Lawson, 2020; Iñiguez et al., 2021). Rubisco is activated within a reversible reaction involving Rubisco-activase, whereby Rubisco is carbamylated, allowing Rubisco to become active after Mg^{2+} stabilisation (Galmés et al., 2013; Amaral et al., 2024). Vc_{max} declines when Rubisco and/or Rubisco-activase have reduced activity or become de-carbamylated/de-natured, especially under low-light or high temperatures (Sage et al., 2008; Wijewardene et al., 2021). Nunes-Nesi et al. (2016) reported a positive correlation between photosynthetic capacities, Rubisco activity and Rubisco-activase concentrations, with links to greater yielding soybeans, whilst highlighting that

variations in Rubisco activity could be a potential target for future breeding programmes (Nunes-Nesi et al., 2016).

Correlations between nitrogen concentrations and photosynthetic capacities have also been identified, with nitrogen being vital for the structure and function of chlorophyll, enzymes (including Rubisco) and ATP (Wullschleger, 1993; Hikosaka and Shigeno, 2009). Within C_3 plants 20-30% of total leaf nitrogen is utilised by Rubisco (which makes up 50% of soluble leaf protein), therefore changes in leaf nitrogen concentrations often effect Rubisco carboxylation capacities (Faralli and Lawson, 2020; Zhao et al., 2020a). Within many C_3 species, the ratio of Rubisco to total leaf nitrogen (R:N) varies, with spinach and pea reported to have a higher R:N with increased nitrogen content (Makino and Osmond, 1991), whilst nitrogen content showed no influence on wheat R:N (Cheng and Fuchigami, 2000). Variations in nitrogen utilisation by Rubisco (and therefore variations in photosynthetic capacity at a given leaf nitrogen) can be caused by differences in nitrogen availability/partitioning and Rubisco activity (Evans, 1989). For instance, low nitrogen availability causes decreased Rubisco levels; however, Rubisco activation often increases to compensate for low Rubisco content (Li et al., 2020). Within legumes (including peas), Vc_{max} variations can be caused by differences in N-fixation abilities (*e.g.* associations to rhizobium bacterium and cell division rates), with many studies now being undertaken to assess the variation in N-fixation affiliations/abilities and the impact on yield, as seen by Dhillon et al. (2022) who found that N-fixation capacities across 20 pea lines ranged between 50-80% (Boussadia et al., 2010; Abi-Ghanem et al., 2013; Wang et al., 2018; Dhillon et al., 2022). Highlighting that variations in N-fixation within

peas, may additionally assist in identifying pea varieties with higher photosynthetic capacities and yield (Makino, 2003; Abi-Ghanem et al., 2011; Wang et al., 2018).

Variations in J_{max} can be attributed to the content/activity of the remaining Calvin cycle enzymes (*e.g.* SBPase), TPU limitations and the ability of the light-dependent reaction to produce ATP and NADPH for RuBP regeneration (Quebbeman and Ramirez, 2016; Sharkey, 2019). A decrease in quantity/activity of regenerative Calvin cycle enzymes have been reported to reduce J_{max}, as end product conversions decrease (Driever et al., 2017). As reported by Harrison et al. (2001) who found a 38-57% reduction in SBPase activity decreased J_{max}, with greater SBPase reductions causing further J_{max} declines whilst also lowering Vc_{max} (Harrison et al., 2001). J_{max} and Vc_{max} often influence each other, as RuBP regeneration is required for Rubisco activation and vice versa. Therefore, variations in one photosynthetic capacity component often causes variations in the other (Harrison et al., 2001; Driever et al., 2017). TPU limitation is caused by the restriction of phosphate regeneration from the production of photosynthetic end products (starch and sucrose), which limits carbon assimilation, especially when carboxylation and electron transport rates are high (Sharkey, 1985; Wullschleger, 1993; Sharkey, 2019). TPU varies between species due to differences in enzymatic activity and Triose phosphate (TP) concentrations. When TP concentrations are too high within the chloroplast, sucrose and starch production becomes inhibited, causing a decreased photosynthetic rate (McClain and Sharkey, 2020). If TP sources deplete, then Calvin cycle intermediates cannot be reproduced, creating reduced RUBP regeneration and therefore J_{max} declines (Sharkey, 2019). However TPU limitations are rarely found in natural/ambient conditions and thus are

often considered negligible when considering the impacts on photosynthetic capacity (Lombardozzi et al., 2018; McClain et al., 2023).

1.3.2.2. Stomatal Factors

Photosynthesis is dependent upon the uptake of atmospheric CO_2 to the site of carboxylation, via stomata (small pores often found on the surface of photosynthetic tissues which enable gaseous flow between internal and external environments) (Hetherington and Woodward, 2003; Lawson and Blatt, 2014; Nunes-Nesi et al., 2016; Lawson and Matthews, 2020). Stomatal aperture is regulated via two guard cells (GC) which surround the pore and respond to environmental cues that change their turgidity (Daszkowska-Golec and Szarejko, 2013). Movement of inorganic ions (K^+ and Cl^-) into and organic solute (malate and sucrose) metabolism within the GC generate a water influx that increases GC turgidity; as water potential (ψ) declines, causing the GC to bow out and the pore to open (Araújo et al., 2011; Lawson and Matthews, 2020; Blatt et al., 2022). Whereas a loss of turgidity from inorganic ion and organic solute export causes stomatal closure (Daszkowska-Golec and Szarejko, 2013; Roux and Leonhardt, 2018). Variations in stomatal morphology, distribution, density and responses all generate variation within CO_2 availability, which influences Vc_{max} and J_{max} (as well as *i*WUE; *see* ***Section 1.5***) (Tanaka et al., 2013; Yin et al., 2020; Lawson and Matthews, 2020). Therefore, stomatal limitation variations provide a potential route for screening pea germplasms for varieties with higher photosynthetic rates/capacity (Geber and Dawson, 1997; Faralli and Lawson, 2020).

The CO_2 diffusion pathway is also influenced by mesophyll conductance (g_m) which often generates variation in photosynthetic capacity (Han et al., 2019). g_m is the movement of CO_2 to the stroma from the intercellular airspaces, which consists of three different diffusion phases; conductance through the leaf intercellular airspaces (g_{ias}), the cell wall (g_w) and a liquid phase within the cells (g_{liq}), with g_{liq} being the most significant contributor towards variation (Evans and von Caemmerer, 1996; Evans, 2020; Kromdijk et al., 2020). g_{liq} is dictated by cell wall thickness and the exposed surface area of chloroplasts and mesophyll to intercellular airspaces (Han et al., 2019). However, calculations and measurements of g_m are often considered to have high amounts of uncertainty and are restricted by low through-put phenotyping (as reviewed by Leverett and Kromdijk, 2024), subsequently analysis of variation in stomatal conductance (g_s; inverse of stomatal resistance), are preferred, with fluctuations in g_m often impacted by differences in g_s (Faralli and Lawson, 2020). Increases in g_s have been reported to enhance *A* and therefore yield, however, g_s declines have been shown to restrict CO_2 entering the leaf, which can reduce photosynthetic rates by 20% in C_3 plants (Faralli et al., 2019; Faralli and Lawson, 2020; Matthews et al., 2020). Variation within g_s arises from interspecific and intraspecific differences in stomatal morphologies and their kinetic responses to the environment, both of which can be targeted to heighten carboxylation and *A* (Lawson and Blatt, 2014; Takahashi et al., 2015; McAusland et al., 2016; Faralli and Lawson, 2020; Battle et al., 2024). Differences in stomatal morphologies can derive from diversity in stomatal densities (SD), apertures/sizes of the guard cells and pore and the presence of subsidiary cells (Bertolino et al., 2019; Evans, 2020).

One of the most renowned sources of stomatal variation is the evolutionary differences in adaptions between monocots and eudicots to their environment (Vatén and Bergmann, 2012; Chater et al., 2017). In monocots (including wheat and barley), stomata can be found in regular patterns of parallel rows surrounded predominantly by dumbbell-shaped guard cells and adjoining subsidiary cells, on both the upper (adaxial) and lower (abaxial) epidermis. In contrast, eudicots (such as peas and beans), consist of irregularly distributed stomata which are surrounded by kidney-shaped guard cells upon both epidermis (Brownlee, 2018; Hepworth et al., 2018; Conklin et al., 2019; McKown and Bergmann, 2020; Harrison et al., 2020). Stomatal morphological differences can impact kinetic responses to environmental conditions, with dumbbell-shaped guard cells providing greater control over pore aperture and enabling faster responses (Brownlee, 2018; Harrison et al., 2020). The presence of subsidiary cells within monocots have been shown to act alongside dumbbell-shaped guard cells as a single unit, enabling ion exchange for rapid responses to internal and external stimuli (Nunes et al., 2020; McKown and Bergmann, 2020). Although subsidiary cells are also present alongside some kidney-shaped eudicot guard cells, they have a lower incorporation into the stomatal complex (consisting of the stomatal pore, guard cells and subsidiary cells) and thus factors other than subsidiary cell mechanisms (such as stomatal density and size) are of a greater importance in pea stomatal regulation (Bertolino et al., 2019; Gray et al., 2020; Harrison et al., 2020).

Stomatal densities (SD; amount of stomata per unit area) and stomatal sizes (SS) are frequently reported to impact g_s and in turn photosynthetic rates and/or capacity, whilst they are also the key determinants of theoretical maximum anatomical stomatal conductance (gs_{max}) (***Fig.1.3***) (*see* ***Section 1.5.3***) (Lawson and Blatt, 2014; Dow et

al., 2014a; Dow et al., 2014b). However the impact of SD and SS on photosynthetic rates and g_s have been reported to differ within/between species, with Yin et al. (2020) reporting a negative correlation between SD and the CO_2 and light saturating photosynthetic rate (A_{max}) between 45 woody plants on the Loess Plateau. Whereas Tanaka et al. (2013) identified a positive relationship between SD and g_s, with enhanced SD through overexpression of STOMAGEN increasing photosynthetic rates by 30% and showing a positive effect on Vc_{max} (Tanaka et al., 2013). Whilst Xiong et al. (2018), found that there were no significant associations between stomatal size (SS) and A_{max} across ten species (Xiong et al., 2018), in contrast to Battle et al. (2024) who found a positive correlation in SD and SS to g_s and A after a photosynthetic induction across 43 Sorghum accessions. Several other studies have also highlighted that a greater density of smaller stomata leads to increased g_s and photosynthetic rates, due to their enhanced surface area to volume ratio (SA:V), which enables rapid responses to biochemical and environmental stimuli (Drake et al., 2013; Tran et al., 2013; Lawson and Blatt, 2014; Hong et al., 2018; Bertolino et al., 2019). As shown by Kardiman and Ræbild (2018), who found SS negatively correlated to rapidity of stomatal opening, with smaller stomata reaching 50% g_s at a much faster rate (Kardiman and Ræbild, 2018). Yet, Zhang et al., (2019a), indicated that smaller stomata in *Ozyra* do not always benefit photosynthesis and yields, as smaller stomata (in comparison to larger stomata) showed a lower initial g_s and a faster decrease in C_i, which reduced Rubisco activation and Vc_{max}, emphasising that larger stomata can provide potential advantages especially under stress (Zhang et al., 2019a). Further indicating that natural variation in photosynthetic capacity can be influenced by stomata (Faralli and Lawson, 2020).

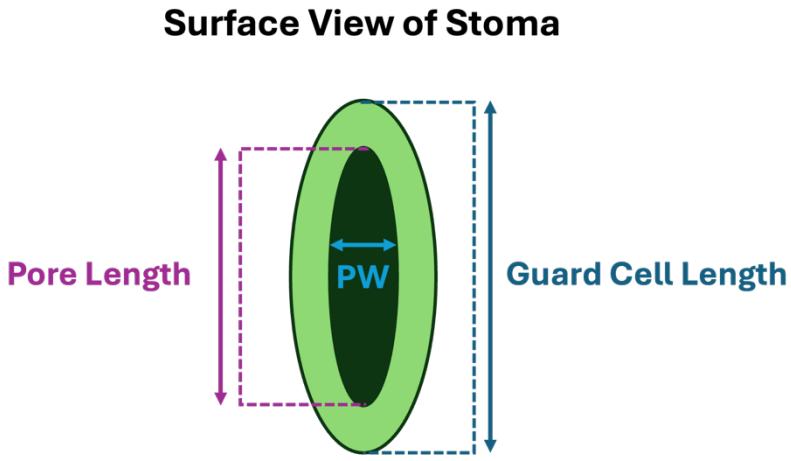

Figure 1.3. Stomatal anatomy components often used to generate the theoretical maximum anatomical stomatal conductance (gs_{max}). gs_{max} is based on stomatal anatomy components including stomatal density, pore length, guard cell length, pore width (PW) and pore depth. Stomatal density, pore length and guard cell length are often measured traits, whereas pore depth is assumed to be half the guard cell length and the mean maximum stomatal pore area (a_{max}) for elliptical stomata is calculated from assumptions that the major axis is equal to the pore length and minor axis is equal to half the pore length (*see* ***Equation 2.1*** for the calculation of gs_{max}) (Lawson et al., 1998; Dow et al., 2014a). Image has been adapted from Lawson et al. 1998.

1.3.2.3. Environmental Factors

Biochemical and physiological sources of natural variation are often impacted by environmental factors, including temperature, light and water-availability, leading to greater variations in photosynthetic capacity (Cen and Sage, 2005; Elsheery and Cao, 2008; Huang et al., 2014; Faralli and Lawson, 2020; Baslam et al., 2020). Many studies exploring variations in photosynthetic capacity have only utilised controlled steady-state environments or only considered one/two environmental factors (Ali et al., 2015). In reality, environmental conditions continuously fluctuate, with acclimation abilities to dynamic environments also being a source of photosynthetic variation (Kaiser et al., 2015). In the majority of cases, stomatal closure occurs under low-light, droughted environments (high vapour pressure deficit; VPD) and abundant CO_2 (Lawson and Blatt, 2014; Pantin and Blatt, 2018).

Increases in global temperatures are generating significant impacts on photosynthetic rates and capacities (Zlatev and Lidon, 2012; Zargar et al., 2017; Cassia et al., 2018; Crous et al., 2022). High temperatures directly impact photosynthetic biochemical reactions via changes in enzymatic activity and stomatal closure from increased VPD (Pantin and Blatt, 2018). Rubisco activation decreases under heat stress (> 40°C in C_3 plants); causing Vc_{max} to decline, as Rubisco-activase denatures (Cen and Sage, 2005; Galmés et al., 2013; Crous et al., 2022). Heat stress can also cause the decline of ATP, whereby high temperatures cause ATP synthesis to become uncoupled from electron transport, reducing ATP production, RuBP regeneration and Rubisco-activase activity leading to a decrease in Vc_{max} and J_{max} (Yamori and von Caemmerer, 2009; Chovancek et al., 2021). Vc_{max} can also decline from increased photorespiration (Rubisco fixes O_2 instead of CO_2), whereby Rubisco's affiliation with CO_2 declines as CO_2 solubility decreases (Chovancek et al., 2021). Photorespiration rates varies across species, with the spatial and temporal separations of CO_2 uptake and carboxylation mechanisms utilised by C_4 and crassulacean acid metabolic (CAM) species (respectively), enabling high CO_2 concentrations to be supplied to Rubisco, leading to higher Vc_{max} under heat and/or drought stress in these species (*e.g.* sorghum and pineapples) (Peterhansel et al., 2013; Edwards, 2019). In contrast, C_3 species (including peas) have to rely upon stomatal and biochemical responses to ensure survival, yet these responses to environmental conditions often vary between/within species (Yamori et al., 2014; Kumar et al., 2019).

Stomata open under high temperatures to enable evaporative cooling (via transpiration), which prevents heat damage and limits photorespiration (Yamori et al., 2014). Whilst under droughted environments, stomata close to prevent water

loss/desiccation, yet this limits carbon fixation (as CO_2 diffusion becomes restricted) and therefore photosynthetic rates and yields (variation in the responses to drought stress is examined in ***Section 1.5***) (Elsheery and Cao, 2008; Pantin and Blatt, 2018). Stomatal responses can be slower than photosynthetic responses to external conditions, causing a disconnection between g_s and photosynthesis and negatively impacting *i*WUE (*see* ***Section 1.5***) (Lawson and Blatt, 2014; Faralli et al., 2019). A recent study by Stevens et al. (2021) illustrated that variation in g_s time constants (defined therein as the time take for g_s to rise by 63%) existed across Barley varieties, ranging between 3.3 and 6.3 minutes. However, variation in stomatal lags are yet to be fully explored in peas, subsequently, identifying accessions with fast/connected stomatal responses in pea germplasms, may highlight those with higher photosynthetic capacity and *i*WUE for greater pea production (Lawson and Blatt, 2014; Stevens et al., 2021; Battle et al., 2024).

Variations in photosynthetic capacity can also be influenced by light intensity and wavelength fluctuations, which dictate performance/fitness via morphological and photosynthetic changes (Vialet-Chabrand et al., 2017; Faralli et al., 2019). The amount of sun or shade a plant is acclimated to can drive intraspecific variations in photosynthetic capacity, with sun-grown plants reported to have higher Rubisco activity and RuBP regeneration (Lombardini et al., 2009; Huang et al., 2014). Sun-grown plants develop thicker leaves (than shaded individuals), which increases photosynthetic capacity, as chlorophyll development and Rubisco content increases allowing enhanced light use for photosynthesis, as highlighted by Huang et al. (2014) who found sun-grown tobacco leaves had higher Rubisco content than shaded leaves (Huang et al., 2014; Yamori et al., 2014; Li et al., 2020). Different light intensities

heavily impact J_{max}, which is often referred to as the photosynthetic light limitation (Quebbeman and Ramirez, 2016). Greater light intensities are reported to increase J_{max}, as more electron transport occurs, providing increased energy (ATP and NADPH) for RuBP regeneration (Ye et al., 2020). When high-light becomes damaging, intraspecific variations in J_{max} can be attributed to differences in photodamage recovery, through variations in antioxidant activity/concentrations and non-photochemical quenching (NPQ) activity (removal of excess light energy as heat via the xanthophyll cycle) (Foyer, 2018). Under natural settings, the amount of light a plant receives can even be influenced by small cloud cover or overlapping leaves, with both photosynthetic and stomatal responses varying under dynamic light conditions (Tinoco-Ojanguren and Pearcy, 1993; Matthews et al., 2017; Long et al., 2022). Subsequently, natural variation in photosynthetic capacity requires measurements taken under dynamic environments (including those under differing light intensities and water availability) to ensure realistic/sustainable pea cultivar selection for potentially high-yielding peas under future climatic conditions (Lawson et al., 2012; Faralli et al., 2019; McAusland et al., 2020).

1.3.2.4. Morphological Factors

Photosynthetic capacity (as well as some of the influencing factors mentioned above; ***Section 1.3.2.1-1.3.2.3***) can additionally be impacted by morphological differences in foliar tissues. Leaf mass per unit area (LMA) is a well-renowned source of morphological variation that can influence photosynthetic capacity, with both positive (He et al., 2019; Song et al., 2020) and negative (Wright et al., 2004; Hikosaka and Shigeno, 2009) associations previously identified (Poorter et al., 2009; Ren et al.,

2019; Silva-Pérez et al., 2020; Jiao et al., 2022). It is believed that positive relationships involve increased leaf thickness which can enable greater exposure of chloroplast to intracellular airspaces through heightened mesophyll cell spacing and reduced cell-cell contact (Ren et al., 2019). However, negative relationships are related to greater enhancements to cell walls and reductions in g_m, which come at a cost of photosynthetic capacity investments, but can confer greater drought tolerance, with thicker cuticles and reduced leaf area limiting water loss (Poorter et al., 2009; de la Riva et al., 2016; Münchinger et al., 2023).

Interestingly, peas have two main types of lamina foliar tissues; leaflets (henceforth called leaves) and stipules, which differ in their morphological structure, with stipules reported to have reduced tissue organisation due to rounder palisade cells and greater compaction of mesophyll cells in comparison to leaves, potentially leading to differences in photosynthesis and WUE (Côté and Grodzinski, 1990; Côté et al., 1992; Giovanardi et al., 2018; Chen et al., 2024). These different foliar tissues have enabled the development of an assortment of semi-leafless and leafless pea varieties since the 1970's, utilising Afila (AF) and Stipules Reduced (ST) genes to convert leaves into tendrils and stipules into reduced structures for greater lodging resistance, ease of harvest and higher yields (Côté and Grodzinski, 1990; Tran et al., 2022). Both Syrovy et al. (2015) and Ćupina et al. (2010), reported a 5-12% increase in yield due to the combined growth mixtures of semi-leafless and leafed pea varieties in comparison to monoculture growth, with changes in canopy morphology believed to increase lodging resistance and weed suppression (Ćupina et al., 2010; Syrovy et al., 2015). Whilst a previous study by Sharma et al. (2012) identified stomatal traits (SD and SS) were similar, yet photosynthetic rates varied between the leaves and stipules depending on

the pea variety (*i.e.,* conventional vs semi-leafless) (Sharma et al., 2012; Tran et al., 2022). However, (to date) differences between leaves and stipules are yet to be fully evaluated for variation in photosynthetic capacity and responses of photosynthesis and stomata to changes in light intensity (under both watered and droughted conditions using modern physiological techniques) for the identification of beneficial traits under future climatic conditions (Nemeskéri et al., 2015).

1.4. Non-Foliar Photosynthesis

1.4.1. Non-Foliar Photosynthesis Mechanisms

Research on photosynthesis (including natural variation in photosynthetic capacity) and carbohydrate acquisition mainly focuses on leaves (Han et al., 2018; Simkin et al., 2020; Lawson and Milliken, 2023). However, non-foliar tissues are gaining interest, with evidence of photosynthetic activity in: fruits (Tanaka et al., 1974; Aschan and Pfanz, 2003; Sui et al., 2017), stems (Hu et al., 2019; AuBuchon-Elder et al., 2020), pods (Atkins et al., 1977; Puthur et al., 2013; Wang et al., 2016; Lawson and Milliken, 2023; Milliken et al., 2024), grass ears/panicles (Tambussi et al., 2007; Maydup et al., 2014; Sanchez-Bragado et al., 2016; Chang et al., 2020) and cotton bracts (Hu et al., 2012; Zhan et al., 2014) (*see* ***Table.1.1***). As explored in ***Section 1.3.2.4*** many different varieties of semi-leafless and leafless peas have been produced, with leafless varieties lacking any form of foliar tissue and thus must rely upon some form of non-foliar photosynthesis for carbohydrate acquisition and survival (Simkin et al., 2020; Tran et al., 2022; Lawson and Milliken, 2023). Whilst recent studies by Stepanova et al. (2024a) and (2024b) have explored non-foliar photosynthetic activity of peas via

chlorophyll a fluorescence, they primarily focus on the seeds. Subsequently, to date variation in photosynthetic activity and stomatal responses using modern physiological techniques are yet to be examined in the pods of peas for enhanced pea cultivar selection (Lawson and Milliken, 2023; Milliken et al., 2024).

Unlike foliar tissues, non-foliar tissues have two CO_2 sources: atmospheric and recycled/refixed CO_2. Whereby, atmospheric CO_2 enters through the stomata and is assimilated via Rubisco into sugars (similar to the C_3 pathway), whilst refixed CO_2 is supplied by mitochondrial respiration (Simkin et al., 2020; Henry et al., 2020). Under stress (such as low-light and drought) stomatal closure prevents atmospheric CO_2 fixation, therefore refixed CO_2 compensates to enable non-foliar photosynthesis, whilst reducing photorespiration and increasing WUE as transpiration rates decline (Han et al., 2018; Hu et al., 2019; Simkin et al., 2020; Lawson and Milliken, 2023). This compensatory mechanism has been reported in wheat, whereby under water stress wheat ear photosynthesis provided a secondary source of photo-assimilates when leaf photosynthesis was prevented, in order to maintain productivity/yields (Tambussi et al., 2005; Faralli and Lawson, 2020; Simkin et al., 2020). As wheat ears have greater osmotic adjustment abilities, CO_2 refixation and delayed chloroplastic degradation, they are able to withstand water limiting environments (Maydup et al., 2010; Henry et al., 2020). Likewise, in *L. sativus* (grass pea) stems were reported to become the main carbohydrate source under NaCl stress, due to the stem's ability to activate an alternate electron transport pathway after the reconstruction of stem PSII (Tokarz et al., 2021). C_4 and CAM metabolisms within non-foliar tissues have also been reported to enable photosynthesis under water-restricted regions (Henry et al., 2020). Non-Foliar C_4 metabolites/enzymes (*e.g.* Phosphoenolpyruvate carboxylase;

PEPC and malate) have been identified within C_3 plants including cucumber fruits, barley seeds and tobacco stems (Hibberd and Quick, 2002; Sui et al., 2017). Whilst, C_4 expression in late filling barley seeds and wheat bracts have been found to increase under drought conditions, supporting productivity when leaf photosynthesis is compromised (Zhang et al., 2019b). Yet, the ability of pea pods to act as a compensatory component under droughted environments is yet to be investigated.

Table 1.1. Examples of previously reported non-foliar photosynthetic activity. Whereby ETR is electron transport rate, PAR is photosynthetic active radiation and PPFD is photosynthetic photon flux density.

Species	Non-Foliar Tissue	Evidence of Photosynthetic Activity	Reference
Barley	Awns	Contribute 90% of total ear photosynthesis and ear photosynthesis contributes 50% towards yields.	Maydup et al., 2014
Cotton	Capsule walls and Bracts	Photosynthetic rates of 20.4-26.3% and 60.3-72.8% within bracts and capsule walls, respectively.	Zhan et al., 2014
Cotton	Stems	Stem shading decreased seed weight by 16%.	Hu et al., 2012
Cucumber	Fruit	Cucumber fruit exocarp photosynthesis contributed 9.4% towards Carbon assimilation.	Sui et al., 2017
Green Olive	Fruit	Refixation rate of 40-80%.	Aschan and Pfanz, 2003
Pea	Seed Coat	ETR of 21.3 ± 0.8 μmol electrons m^{-2} s^{-1} when 8% of PAR triggers photosynthesis.	Tschiersch et al., 2011
Pea	Tendrils	30-50% contribution to photosynthetic rates.	Côté and Grodzinski, 1990
Rice	Panicles	17–54 nmol s^{-1} at 2000 μmol m^{-2} s^{-1} PPFD.	Chang et al., 2020
Sorghum	Stems and Spikes	Stem and spike photosynthesis contributes 40% to grain weight.	AuBuchon-Elder et al., 2020
Soybean	Pod and Seed	Pod and seed photosynthesis contributed 13-14% to seed weight.	Cho et al., 2023
Tomato	Fruit	Tomato fruit contribute 10-15% of total Carbon fixed.	Tanaka et al., 1974
Wheat	Ears	Ear shading caused a 16.35% decrease in grain filling.	Elazab et al., 2021
Wheat	Awns	Contribute 50% of total ear CO_2 fixation, evidence of light harvesting gene expression.	Maydup et al., 2010
Wheat	Stems	Stem and sheath photosynthesis contributed 10% to yield.	Rivera-Amado et al., 2020

1.4.2. Measuring Non-Foliar Photosynthesis

In order to determine/quantify non-foliar photosynthetic activity many different methodologies/technologies can be utilised including carbon isotope discriminations, chlorophyll fluorescence and infra-red gas exchange (Henry et al., 2020; Tambussi et al., 2021; Milliken et al., 2024).

Carbon isotope discrimination; between ^{12}C and ^{13}C, can be utilised to detect non-foliar photosynthesis in a non-invasive manner (Henry et al., 2020). When tissues photosynthesise fixation of the lighter ^{12}C isotope is preferred, causing an abundance of ^{13}C (Gresset et al., 2014). Variations in ^{13}C can be generated through differences in carbon assimilation and diffusion, caused by tissue permeability/thickness (*e.g.* wheat ears have a lower permeability compared to flag leaves) (Sanchez-Bragado et al., 2014). Refixation from respiratory processes is known to deplete ^{13}C sources, potentially due to the lack of ^{13}C discrimination in PEPC, enabling non-foliar photosynthetic traits to be distinguished (between atmospheric fixation and refixation strategies) (Hu et al., 2019; Garrido et al., 2023). Carbon isotope discrimination was used by Sanchez-Bragado et al. (2014) to estimate 47-100% yield contributions were from wheat ear photosynthesis (Sanchez-Bragado et al., 2016; Henry et al., 2020). Radioactive ^{14}C labelling has also been utilised to determine carbon fixation rates within pea pods, with Atkins et al. (1977) identifying 42% of carbon fixation occurred in pea pod endocarp (innermost pod layer) compared to 58% in the mesocarp (middle pod layer) and exocarp (outermost pod layer), where chlorophyll concentrations were greater. Although Atkins et al. (1977) explored pea pod carboxylation capacities, an increasing number of modern physiological techniques (*e.g.* non-foliar gas exchange

chambers) have become available to provide more accurate/reliable quantifications (Ismail et al., 2014; Milliken et al., 2024).

Similar to leaf photosynthetic measurements (*see* ***Section 1.3.1***), chlorophyll fluorescence and gas exchange can be used to determine the photosynthetic rates of non-foliar tissues (Faralli and Lawson, 2020; Simkin et al., 2020; Milliken et al., 2024). Chlorophyll fluorescence was previously utilised by Tschiersch et al. (2011), who reported pea embryos were photosynthetically active, whilst the quantum yield of PSII varied across pea embryo surfaces (Tschiersch et al., 2011). Simkin et al. (2020) also identified tomato and strawberry fruits were capable of photosynthetic electron transport (via chlorophyll fluorescence), with F_q'/F_m' reaching 0.7 within tomato fruits. Highlighting the potential utilisation of chlorophyll fluorescence to differentiate between high and low ETR (electron transport rate) regions in non-foliar pea tissues (Simkin et al., 2020; Lawson and Milliken, 2023). To measure non-foliar gas exchange, a bespoke chamber is required to enable correct air mixing and to prevent stagnant air, for accurate results (Chang et al., 2020; Milliken et al., 2024). Maydup et al. (2010) utilised an airtight periglass chamber attached to a CIRAS IRGA, to determine that wheat ear photosynthesis varied between varieties and environmental conditions. Whilst utilisation of a rice panicle (P) chamber (aluminium periglass chamber attached to LICOR 6400) by Chang et al. (2020) highlighted rice panicles were able to photosynthesise at 20-38% to that of the flag leaf. More recently, Lawson and Milliken (2023) and Milliken et al. (2024) illustrated the potential for pea pod photosynthetic rates to be measured within a bespoke Lawson Lab non-foliar gas exchange chamber, whilst also providing information on pod stomatal kinetics and *i*WUE. However, non-foliar chambers often struggle with over-heating; yet, the above examples utilise a

mixture of cooling fans and water-cooling systems to overcome this (Maydup et al., 2010; Chang et al., 2020; Lawson and Milliken, 2023; Milliken et al., 2024). Furthermore, due to the complex 3D structures and difficulties calculating C_i (due to the different CO_2 sources) photosynthetic capacity measurements, equations and calculations are still being determined (Milliken et al., 2024; Song and Zhu, 2024).

Membrane inlet mass spectrometry (MIMS) can also be used in conjunction to gas exchange and chlorophyll fluorescence to provide insight into variations in photosynthesis, through correlations between photoreductions of CO_2 and O_2 and energy dissipation (Burlacot et al., 2020). MIMS utilises a semi-permeable membrane to enable dissolved CO_2 and O_2 to be measured (within a vacuum), without water and PSII entering the system. CO_2 and O_2 are detected (after ionisation), via their mass:charge (Shevela et al., 2018). Providing a quick and high-resolution measurement of photosynthetic activity, with potential to be used on non-foliar material (Shevela et al., 2018; Burlacot et al., 2020). This study will utilise some of the above techniques to determine natural variations in photosynthetic rates in pea pod tissues and their ability to act as a compensatory mechanism under drought stress.

1.4.3. Natural Variation in Non-Foliar Photosynthesis

Similar to leaves (*see* ***Section 1.3.2***), non-foliar photosynthesis is believed to naturally vary with differences in morphology, biochemistry and the environment (Simkin et al., 2020; Lawson and Milliken, 2023). Non-Foliar morphologies can generate variations in photosynthesis, including pod/seed thickness, shape, colour and stomatal presence (Bean et al.,1963; Atkins et al., 1977; Wang et al., 2016; Sui et al., 2017; Garrido et

al., 2023). Variations in photosynthesis in cucumbers can arise from whether epicuticular waxes are present, which has been reported to cover cucumber guard cells and hinder gas exchange (Simkin et al., 2020). Sui et al. (2017) found epicuticular wax presence meant only 8% of carbon assimilation was from exocarp photosynthesis in comparison to 88% from refixation (Sui et al., 2017; Henry et al., 2020). Whilst the different layers of pea pods and seeds have also been shown to vary in photosynthetic ability, with the endocarp receiving less atmospheric CO_2 and light than the exocarp (Garrido et al., 2023). As highlighted by Atkins et al. (1977) who found 96% ^{14}C was present in the mesocarp and exocarp, compared to 4% in the endocarp, due to the large diffusion pathway required to reach the internal pod compartments. Similar results were identified within pea seeds by Tschiersch et al. (2011), who found lower light absorption within inner pea seed regions compared to external regions, leading to significant variations in ETR (21.3 ± 0.8 μmol m^{-2} s^{-1} outer regions to 6.2 ± 1.0 μmol m^{-2} s^{-1} in inner regions) and therefore photosynthesis (Tschiersch et al., 2011). Pod and ear/panicle shapes and distributions can also naturally vary, leading to changes in assimilation (Henry et al., 2020). For instance, the number of Alfalfa pod coils have been shown to influence yields with seed weight per pod varying by 16% in one spiralled pods and 35% within two coiled pods (Wang et al., 2016). Chang et al. (2020) highlighted reduced spikelet density in rice panicles correlated to increased spikelet photosynthesis, with a 402% higher net panicle photosynthetic rate found between Indicia (less dense panicles) and Japonica (densely packed panicles) rice varieties.

Photosynthesis in non-foliar tissues have often been seen to reduce with maturity, with Bean et al. (1963) identifying a decrease in fruit chlorophyll content with maturation in oranges and lemons correlated with reduced photosynthetic rates. Non-Foliar SD and

functionality have also been demonstrated to vary with age, with *Brassica* pod g_s peaking at 30-days post-anthesis, whilst older chickpea pods have been reported to contain more leaky stomata which increased transpiration and lowered WUE (Ma et al., 2001; Garrido et al., 2023). Stomatal densities on fruit/pod surfaces have been found to vary significantly depending on the species, with strawberries reported to have very low SD (6 mm^{-2}) compared to the satsuma mandarin with evidence of 300 mm^{-2} SD (Blanke, 2002; Hiratsuka et al., 2015). SD can also vary amongst non-foliar tissues, with wheat ear SD differing between the glumes (32 mm^{-2}), awns (70 mm^{-2}) and lemmas (10-20 mm^{-2}) (Simkin et al., 2020). Tissues with reduced non-foliar SD are believed to have greater contributions from refixed CO_2 and are often shown to contain greater amounts of PEPC (Henry et al., 2020). As mentioned in ***Section 1.4.1***, environmental conditions such as drought can also influence photosynthetic activity of non-foliar materials with PEPC and Rubisco being upregulated as water stress increases (Zhang et al., 2019b). Variation in non-foliar photosynthesis, WUE and their ability to act as compensatory mechanisms under stress require further exploration, with the identification/exploitation of pea varieties with efficient capacity for non-foliar photosynthesis, stomatal conductance and WUE, providing further targets/resources for genetic modifications and future breeding programmes (Simkin et al., 2020; Henry et al., 2020; Araus et al., 2021; Lawson and Milliken, 2023).

1.5. Natural Variation in WUE

1.5.1. What is WUE

Agriculture utilises over 70% of freshwater supplies, however a prominent cause of yield loss in many crop species is due to drought, with drought reducing yield by around 30-90% depending on the species (Blankenagel et al., 2018; Dietz et al., 2021). As global food demands increase, the necessity to increase water use efficiency (WUE) in key crops has heightened (Hatfield and Dold, 2019). Many legumes (including peas) are often grown within marginal lands with water-limiting soils, therefore identification of pea varieties with fast and connected stomatal responses and greater WUE could highlight beneficial traits for increased productivity under future climatic conditions (Coyne et al., 2020; Battle et al., 2024). WUE definitions vary with data collection, scales and stakeholders (*e.g.* farmer and scientists) (Leakey et al., 2019). At the plot level, WUE defines the ratio of grain/biomass yield to evapotranspiration. At the plant-level (WUE_{plant}), it is determined as biomass accumulation compared to transpiration, which establishes plant productivity (Blankenagel et al., 2018). Whilst at the leaf level, intrinsic WUE (*i*WUE) is measured as carbon assimilation (A) relative to stomatal conductance (g_s) (A/g_s) (Kantar et al., 2010; Guerrieri et al., 2019). High *i*WUE is beneficial under droughted-conditions, which is often achieved via low g_s generated through stomatal closure to minimise transpiration (Easlon et al., 2014). Yet reduced g_s can negatively implicate yields as carbon uptake decreases, meaning plants need to mitigate the trade-off between carbon assimilation and water loss (Elsheery and Cao, 2008; Blankenagel et al., 2018; Battle et al., 2024).

1.5.2. Determining *i*WUE

*i*WUE can be measured non-invasively using chlorophyll fluorescence, gas exchange (which determines A and g_s; as explored in ***Section 1.3.1***) and carbon isotope discriminations (Hatfield and Dold, 2019). *i*WUE is monitored using carbon isotope ratios of intercellular to atmospheric CO_2 (C_i:C_a), with discriminations of ^{13}C identified, as Rubisco prefers ^{12}C (Farquhar et al., 1982; Condon et al., 2002; Seibt et al., 2008). Higher *i*WUE lines are distinguished as having lower ^{13}C discrimination values, as stomatal closure reduces the availability of atmospheric ^{12}C (Flexas et al., 2010; Easlon et al., 2014; Guerrieri et al., 2019). As highlighted by Tomás et al. (2012), who described ^{13}C discrimination decreased within grapevine species between well-watered (from -31‰ to -27‰) and droughted (between -26‰ to -24.7‰) conditions. Recent development of an *i*WUE machine, provides high-throughput screening and precise *i*WUE calculations under changing conditions, via combined chlorophyll fluorescence and thermal imaging systems. The combined approach determines A and g_s via temporal responses and spatial images, which highlighted imaged *i*WUE varied in Arabidopsis between 0.0025 μmol CO_2/mmol H_2O m^{-2} s^{-1} to 0.05 μmol CO_2/mmol H_2O m^{-2} s^{-1} (McAusland et al., 2013). *i*WUE can be used to evaluate WUE_{plant}, as WUE_{plant} gravimetric measurements are long and destructive. However, these extrapolations are often error-prone due to photorespiration and dark respiration effects on WUE_{plant} not being incorporated within *i*WUE measurements (Blankenagel et al., 2018). Nonetheless, *i*WUE provides a non-invasive and simple physiological assessment of carbon assimilation to water loss (Blankenagel et al., 2018; Hatfield and Dold, 2019). *i*WUE can be improved within crop species (including peas) via better management practices and selecting varieties with high *i*WUE via some of the above techniques (Blankenagel et al., 2018; Battle et al., 2024).

1.5.3. Drivers of Natural Variation in *i*WUE

Significant natural variation in *i*WUE also exists, with variation recorded within crop (avocado, rice and soybean) and non-crop species (Arabidopsis and perennial grasses) (Bota et al., 2001; Easlon et al., 2014; Pater et al., 2017; Acosta-Rangel et al., 2018). For instance, Bota et al. (2001) found *i*WUE across 20 irrigated Mediterranean grapevine cultivars ranged from 38-64 μmol mol^{-1}. Whilst Acosta-Rangel et al. (2018) reported *i*WUE ranged from 82 ± 30 to 141 ± 33 μmol mol^{-1} amongst 24 well-watered avocado cultivars. *i*WUE has also been identified as being higher in non-foliar tissues than foliar tissues, whereby the ears of durum wheat and barley have been reported to have lower C^{13} discriminations compared to the flag leaf, indicating the greater *i*WUE of the ears (Tambussi et al., 2007). Variations within *i*WUE can be due to morphological, physiological, environmental and genetic influences (Easlon et al., 2014; Pignon et al., 2021a).

Stomata play a key role in optimising *i*WUE, especially within droughted environments (Lawson et al., 2012). Therefore, differences in stomatal characteristics (such as densities, sizes and patterning) and responses to the environment are major contributors to *i*WUE variations (Pignon et al., 2021a). gs_{max} (determined by SD and SS, represents the theoretical maximum anatomical stomatal conductance (***Fig.1.3***)) is frequently associated with WUE, whereby a greater gs_{max} is often related to a lower WUE as stomata are assumed to be fully open, enabling greater water loss, as highlighted by Dow et al. (2014a) who found a negative correlation between anatomical gs_{max} and *i*WUE in Arabidopsis (Dow et al., 2014a; Bertolino et al., 2019). Many studies investigating stomatal variations have reported that higher g_s (and gs_{max}) is attributed to a high frequency of smaller stomata (Dittberner et al., 2018). Smaller

stomata can also lead to reduced g_s and higher *i*WUE, as they respond rapidly to environmental stimuli (as greater surface area to volume ratios permit rapid guard cell changes), as seen within droughted rice and Arabidopsis (Ouyang et al., 2017; Dittberner et al., 2018; Lawson and Vialet-Chabrand, 2019). Larger stomata are often associated with a lag in stomatal responses, leading to increased transpiration and reduced WUE as stomata can take longer to close (Bertolino et al., 2019). This lag causes a disconnection between g_s and photosynthesis and therefore *i*WUE (Lawson and Blatt, 2014). Such disconnections were reported to cause a 13% and 5% loss in carbon assimilation and *i*WUE, respectfully, within cassava cultivars (De Souza et al., 2020). However, the speed of g_s responses are not always correlated with differences in SD and SS, with variations in biochemical and structural features of stomata also playing key roles. For instance stomatal responses can vary with presence/density of guard cell actin microfibrils, with more actin providing quicker stomatal regulation due to greater aperture control (Kim et al., 1995; Lawson and Vialet-Chabrand, 2019; Battle et al., 2024). The identification of pea varieties with fast stomatal responses may highlight those with greater *i*WUE for enhanced pea production under future climatic conditions (Lawson and Blatt, 2014; Battle et al., 2024).

Environmental conditions can provide additional sources of variation in *i*WUE (Pignon et al., 2021a). Changes in light dynamics can influence stomatal mechanisms (*see* ***Section 1.3.2.3***) and generate *i*WUE variations. *i*WUE under dynamic light have been shown to vary between/within species (De Souza et al., 2020; Acevedo-Siaca et al., 2021). Acevedo-Siaca et al. (2021) identified a 77% difference in average *i*WUE with a light induction between the highest and lowest performing flag leaf within *Oryza* accessions. Whilst De Souza et al. (2020) found a two-fold difference in *i*WUE

between the highest and lowest performing cassava cultivars under dynamic light. Blue light can also negatively implicate *i*WUE, as it triggers stomatal opening even when carbon-assimilation is high, with g_s increases driving greater water loss (Matthews et al., 2020).

The ability of plants to tolerate drought conditions also vary, with differences in root and foliar/non-foliar morphologies dictating *i*WUE variations (Ruggiero et al., 2017). Within field peas and chickpeas, drought tolerance has been attributed to greater root biomass and root length densities within deeper soils (> 100 cm) (Blessing et al., 2018). Increased root biomass is facilitated by long taproots that reach ground-water supplies whilst secondary lateral roots maximise surface water uptake (Purushothaman et al., 2017). Although deeper taproots are beneficial under drought, they do not always result in greater yields, as deeper roots require higher energy investments leading to stunted growth (as seen across chickpea accessions) (Serraj et al., 2004; Blessing et al., 2018). Subsequently, care must be taken to prevent selection of high *i*WUE traits at the cost of yield (Blankenagel et al., 2018). *i*WUE can also be influenced by nitrogen-fixation abilities, with rhizobium and mycorrhizae symbiosis increasing surface area for water uptake (Ruggiero et al., 2017). However, under drought nitrogen-fixation declines as nodule senescence increases. Loss of nitrogen fixation requires greater g_s to facilitate photosynthetic requirements, therefore *i*WUE declines as water loss increases (Kantar et al., 2010; Blessing et al., 2018).

At non-foliar and foliar levels, water and CO_2 diffusion pathways can be affected by surface area, trichome abundance and impermeable wax presence (Palliotti et al., 2001; Müller et al., 2017). Müller et al. (2017) found greater wax epicuticular thickness

in date palm, inhibited water loss and increased WUE. Whilst Palliotti et al. (2001) reported high epicuticular wax (in conjunction with other foliar traits) caused a 31% increase in WUE in grapevine. Greater trichome (hair-like structures) abundance increases the trapped air-layer over stomata (called boundary layer resistance), which can heighten *i*WUE as g_s and water loss decline (Galdon-Armero et al., 2018; Bertolino et al., 2019). For instance, Galdon-Armero et al. (2018) reported an increased trichome to stomata ratio caused greater *i*WUE within *Solanum lycopersicum* leaves. Within peas, WUE variations can be attributed to differences in semi-leafless, leafless and leafed morphologies, with semi-leafless and leafless varieties often described as having improved drought tolerance due to reduced foliar area for water loss (Nemeskéri et al., 2015; Checa et al., 2020). As previously mentioned, non-foliar tissues have been reported as having greater *i*WUE, as CO_2 refixation enables photosynthesis without detrimental impacts of water loss, due to restricted g_s (Wang et al., 2016; Simkin et al., 2020). Natural variation in *i*WUE remains unquantified in many species, with variation in *i*WUE in foliar (leaves and stipules) and non-foliar tissues (pods) yet to be fully explored within peas using modern physiological techniques, with potential to distinguish cultivars with beneficial traits under future climates (Li et al., 2017; Hatfield and Dold, 2019; Driscoll et al., 2020; Lawson and Milliken, 2023).

1.6. Aims and Objectives

Natural variation in photosynthesis and WUE have been identified amongst a variety of plant/crop species, although, these studies mainly focus upon conventional leaf tissues (Faralli and Lawson, 2020; Lawson and Milliken, 2023; Milliken et al., 2024). However an assortment of conventional leafed, semi-leafless and leafless varieties of peas exist, with natural variation in photosynthetic capacity and stomatal responses to light intensity changes (and *i*WUE) yet to be fully explored in both types of foliar tissue (leaves and stipules) (Tran et al., 2022). Although non-foliar photosynthetic activity has been previously established within the pod walls of *P. sativum*, physiological methodologies have since advanced, with examination utilising new methodologies (such as gas exchange and chlorophyll fluorescence) yet to be fully investigated within *P. sativum* (Atkins et al., 1977; Simkin et al., 2020).

The aims of this project were to determine the extent of natural variation in photosynthetic capacity/rates and yield, alongside the responses of photosynthesis and stomata to light intensity changes in foliar (leaves and stipules) and non-foliar (pods) pea tissues when subjected to watered and droughted conditions. Infra-red gas exchange analysis was used to determine the extent of natural variation in pea foliar photosynthetic capacity, whilst step increases in light intensity and surface impressions were also utilised to determine variation in *i*WUE, stomatal kinetics and anatomy (*see* ***Chapter 2***). Findings from ***Chapter 2*** (such as photosynthetic capacity, stomatal and *i*WUE performances) as well as pea accession characteristics (*e.g.* foliar morphologies and heritage), were used to select accessions that were examined for the impact of drought on functional traits and the extent of natural variation in the traits mentioned above (*see* ***Chapter 3***). Whilst a bespoke Lawson Lab non-foliar gas

exchange chamber was utilised to explore the extent of natural variation in non-foliar photosynthesis and stomatal conductance under watered and droughted conditions (*see* ***Chapter 4***).

By exploring the natural variation within foliar and non-foliar pea tissues, productivity gains could be made if high photosynthetic capacity, fast stomatal responses and prominent *i*WUE accessions are identified. Identified accessions could be used to provide phenotypes for marker establishment for MAS and conventional breeding programmes, supplying potentially high-yielding peas able to withstand future climatic conditions (Faralli and Lawson, 2020; Simkin et al., 2020; Lawson and Milliken, 2023).

Chapter 2: Improving Yield Potential by Exploiting Natural Variation in Pea (*Pisum sativum*)

2.1. Introduction

As temperatures rise and arable land declines, crop productivity is becoming increasingly reliant upon enhanced photosynthetic potential and abiotic/biotic stress tolerance in order to meet food demands by 2050 (Ray et al., 2019; Asseng et al., 2020; Furbank et al., 2020; Billen et al., 2024). Genetic modification (GM) of photosynthetic processes have already been used to improve crop productivity (Raines, 2011; Evans, 2013; Voss-Fels et al., 2019). However, GM crop production is still not accepted in all countries; including the UK, due to ethical concerns (Ricroch et al., 2018). Subsequently, non-genetically modified (non-GM) pathways are preferred with natural variation in photosynthetic capacity (ability of Rubisco to fix CO_2 (Vc_{max}) and Ribulose Bisphosphate (RUBP) to be regenerated (J_{max})), remaining an untapped and unexamined resource for potential crop improvements especially within peas (*P. sativum*) (Lawson et al., 2012; Driever et al., 2014; Faralli and Lawson, 2020; Burgess et al., 2023).

Natural variation is defined as the within (and between) species phenotypic variation generated through spontaneous mutations, which is evolutionarily conserved through natural and artificial selection (Alonso-Blanco et al., 2009). Natural variation in photosynthetic capacity can be the result of anatomical, environmental and biochemical differences and has been identified in a number of species including wheat (Driever et al., 2014; Silva-Pèrez et al., 2020; McAusland et al., 2020), rice (Giuliani et al., 2013; Acevedo-Siaca et al., 2021), barley (Stevens et al., 2021) and soybean (Sakoda et al., 2016). A study by Gu et al. (2014), revealed that rice yields have the potential to increase by 22-29% if the natural variation identified in Vc_{max} and J_{max} are fully exploited (Gu et al., 2014), reinforcing the need to exploit the natural

variation within current crop germplasms (such as peas) to improve productivity by identification of high yielding and abiotic stress resistant/tolerant lines (Faralli and Lawson, 2020; Coyne et al., 2020; Burgess et al., 2023). Biochemical sources of variation in Vc_{max} can be attributed to differences in Rubisco content and activation, which is influenced by Rubisco-activase activity and nitrogen concentrations (vital for enzymatic function). Whilst variation in J_{max} often reflect differences in electron transport and regeneration of Calvin cycle enzymes (*e.g.* SBPase concentrations) (Driever et al., 2017; Faralli and Lawson, 2020; Burgess et al., 2023).

Photosynthesis is reliant upon CO_2 uptake via stomata, thus differences in stomatal density, aperture, morphology, distributions and responses all influence photosynthetic rates (Lawson and Blatt, 2014; Nunes-Nesi et al., 2016). Anatomical/stomatal and biochemical factors are influenced by environmental conditions, with changes in temperature (which influences enzyme activity), light (which determines electron transport) and water availability (which impacts stomatal conductance; g_s), causing greater variations in photosynthetic performance and capacity (Faralli and Lawson, 2020; Burgess et al., 2023). Stomatal responses to external/fluctuating conditions (*e.g.* light quantity and quality changes) can also be slower than photosynthetic responses, causing a disconnection between g_s and photosynthesis. Slow stomatal responses negatively effects intrinsic water use efficiency (*i*WUE), as slow stomatal closure results in water loss for limited CO_2 uptake (Lawson and Blatt, 2014; Faralli et al., 2019; Faralli et al., 2022). Variation in stomatal lags are yet to be fully evaluated in peas, subsequently, identifying accessions with rapid responding stomata in pea germplasms, may highlight those with reduced limitation in naturally dynamic

environments, which could be beneficial for enhanced pea production (Lawson and Blatt, 2014).

Peas are gaining popularity as an alternative meat source, due to their high protein levels (23-25%), with pea protein already being used within ©*BirdsEye Green Cuisine* range (vegan-based meals), ©*BeyondMeat* burgers and ©*MightyPea* milk (Smýkal et al., 2011; Tulbek et al., 2017; Rasskazova and Kirse-Ozolina, 2020; Pilorgé et al 2021). Peas also replenish soil fertility due to their nitrogen fixation capacity, reducing the requirement for industrial fertilisers, which lowers carbon emissions, as shown by the 24% decline in non-renewable energy usage (Kreplak et al., 2019; Sainju et al., 2019; Uhlarik et al., 2022; Vouraki et al., 2023). However, as water restrictions and poor soil conditions are limiting pea yields, there is a heightened need to increase pea production to meet growing demands (de la Peña and Pueyo, 2012; Tulbek et al., 2017; Rasskazova and Kirse-Ozolina, 2020; Coyne et al., 2020; Bagheri et al., 2023).

Since the 1970's production of leafless and semi-leafless pea varieties; to improve standing/lodging-resistance and reduce canopy diseases, have provided an added source of variation (Syrovy et al., 2015; Shen et al., 2022). Leafless/semi-leafless varieties are controlled by three main genes: Stipules Reduced (*ST*), Afila (*AF*) and Tendriless (*TL*), with WT peas being dominant for all three genotypes (*AFAF*, *STST*, *TLTL*). Whilst different combinations of these genes convey variations of semi-leafless and leafless phenotypes (***Table.2.1&Fig.2.1***) (Mikic et al., 2011; Moreau et al., 2018; Tran et al., 2022; Tayeh et al., 2023). Semi-leafless varieties have been reported to have a greater whole plant photosynthetic capacity in comparison to leafless varieties, with Mikic et al. (2011), depicting that semi-leafless cultivars in 2011 made up 80% of

dry pea production in the EU (Lafond and Evans, 1981; Mikic et al., 2011; Syrovy et al., 2015; Tran et al., 2022). Subsequently, variation in pea leaf morphology provides an additional layer of variation yet to be fully explored in pea, whilst comparisons to other pea accessions using modern physiological techniques remains untapped (Mikic et al., 2011).

The aim of this study was to determine the extent of natural variation in foliar photosynthetic capacity and yield in pea populations, whilst also establishing and quantifying differences in stomatal and photosynthetic responses to light intensity changes. Pea accessions were subjected to infra-red gas exchange analysis to determine the extent of natural variation in pea foliar photosynthetic capacity, whilst step increases in light intensity and surface impressions explored the variation in *i*WUE, stomatal kinetics and anatomy.

Table 2.1. Genetic variations conferring the different type of leaf morphologies in pea (P. sativum). Derived from Mikic et al. (2011), Moreau et al. (2018), Tran et al. (2022) and Tayeh et al. (2023). Stipules Reduced (*ST*), Afila (*AF*) and Tendriless (*TL*) genes.

Name	Phenotype	Genotype
WT/Conventional Dominant	Has leaves, stipules and tendrils.	***STST*, *AFAF*, *TLTL***
Fully Leafless	No leaves or stipules but has tendrils.	***stst*, *afaf*, *TLTL***
Semi-leafless: Afila	No leaves but has stipules and tendrils.	***STST*, *afaf*, *TLTL***
Semi-leafless: Stipules Reduced	Reduced stipules but has leaves and tendrils.	***stst*, *AFAF*, *TLTL***

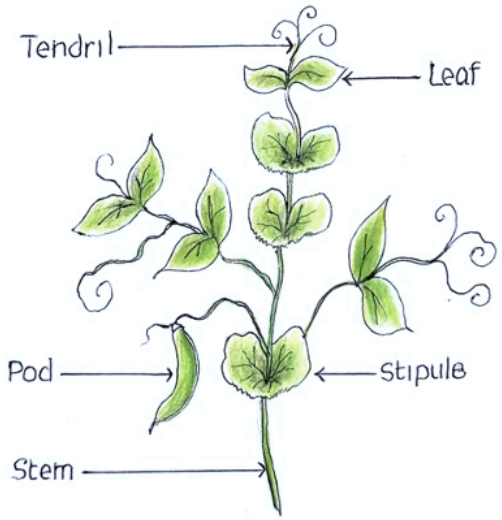

Figure 2.1. Schematic of a pea plant's anatomy. Highlighting the difference between leaflets (leaves) and stipules (leaves attached to the stem).

2.2. Material and Methods

2.2.1. Plant Materials and Growth

P. sativum accessions were selected based on whether they were elite, landrace, semi-leafless, commercial and/or contained potentially beneficial traits (such as heat/drought tolerance) (***Table.2.2***) (Professor Claire Domoney and Dr Noel Ellis, John Innes Centre Germplasm Resource Unit, Norwich; Mr. Fothergill's, Newmarket, Suffolk; Thompson & Morgan, Ipswich, Suffolk; Associate Professor Jim Weller, University of Tasmania, Australia). Accessions were chitted in petri-dishes at room temperature (23 ^{o}C) and moved into 12 cm deep pots containing peat-based compost (Levingtons F2S, Everris, Ipswich, UK), upon germination. Pots were then placed into a controlled growth room at 23 ^{o}C, 400 µmol mol^{-1} CO_2 concentration, 65 % relative humidity and a 16/8 light/dark cycle (with a photosynthetic photon flux density (PPFD) of 300 µmol m^{-2} s^{-1} ± 10 µmol m^{-2} s^{-1} during the artificial day) to try and mimic optimal external conditions (with the exception of light intensity, which was set to the growth rooms maximum). All *P. sativum* accessions were randomly sown across a four-week period, utilising Cameor as an experimental control (Cam grown in week one and CamB in week four) to enable examination of constant conditions (***Table.2.2***). To prevent environmental heterogeneity, plants were regularly rotated within trays and around the growth room. Unless stated otherwise, six plants were measured per accession between 21-30 days old between 7 am and 4 pm. Plants were sprayed with Rose Clear Ultra (Evergreen Garden Care UK Ltd, Surrey, UK) at around 44 days old to combat Powdery Mildew and prevent/minimise damage to plants and final yield.

Table 2.2. Description of the P. sativum accessions utilised. Supplied by Professor Claire Domoney and Dr Noel Ellis, John Innes Centre Germplasm Resource Unit, Norwich; Mr. Fothergill's, Newmarket, Suffolk; Thompson & Morgan, Ipswich, Suffolk; Associate Professor Jim Weller, University of Tasmania, Australia. Accessions supplied by the John Innes Centre Germplasm Resource Unit have a JI coding. Stipules Reduced (*ST*), Afila (*AF*) and Tendriless (*TL*) genes.

Accession Name (Abbreviation)	**Accession Type (Supplier)**	**Accession Name (Abbreviation)**	**Accession Type (Supplier)**
Alaska	Elite (JI2015)	**Kelvedon Wonder (KW)**	Commercial Elite (*Thompson & Morgan* ©)
Cameor (Cam)	Elite (JI3253)	**Meteor (Met)**	Commercial Dwarf (*Mr. Fothergill's* ©)
Cameor B (CamB)	Elite (JI3253)	**Near isogenic line 11 (Ni11)**	Near isogenic line Semi-leafless Stipules Reduced; *stst*, *AFAF*, *TLTL* (JI3310)
Cennia (Cen)	Elite (JI0399)	**Near isogenic line 16 (Ni16)**	Near isogenic line WT Dominant; *STST, AFAF, TLTL* (JI3315)
Ethiopia (Eth)	Landrace (JI0281)	**Pacco**	Commercial Semi-leafless Afila; *STST*, *afaf*, *TLTL* (*Thompson & Morgan* ©)
Elatius (Ela)	Landrace (JI1095)	**Torsdag (Tor)**	Landrace (Professor Jim Weller)
JI2822	Inbred Line: RIL (JI0015 x JI0399)	**Wando**	Elite Heat and Drought Tolerant (JI2483)

2.2.2. Chlorophyll Fluorescence Imaging

Plants were imaged using a chlorophyll fluorescence imager (Fluorimager; Technologica., Colchester, UK), as previously described (Murchie and Lawson, 2013). After a predetermined 30-minute dark-adaption period (where all photosystem II (PSII), centres were fully open and non-photochemical quenching (NPQ), was absent), minimum fluorescence (F_o) was obtained followed by maximum fluorescence (F_m) using a predetermined 800 ms saturating pulse of 6231 µmol m^{-2} s^{-1} PPFD. These were used to determine the maximum efficiency of PSII in the dark (F_v/F_m), via the equation in ***Table.2.3***. After determining F_v/F_m the actinic growth light was increased to 300 µmol m^{-2} s^{-1} PPFD, and the induction of photosynthesis was assessed using the PSII operating efficiency in the light (F_q'/F_m'). Steady state fluorescence in the light (*F'*) was obtained immediately before a saturating pulse (as above) was used to determine the maximum fluorescence in the light (F_m') at 10-minute intervals. Together these measurements were used to calculate F_q'/F_m', the maximum efficiency of PSII in the light (F_v'/F_m') and PSII photochemical quenching factor (F_q'/F_v') using the equations in ***Table.2.3***. The minimum fluorescence in the light (F_o') was calculated according to Oxborough and Baker. (1997). Plant relaxation responses in F_v/F_m were measured every minute for 10-minutes following the cessation of actinic light. A light curve was determined at a range of light intensities with a saturating pulse applied three minutes after light intensity was altered (1500, 1250, 1000, 500, 250,150, 50 and 0 µmol m^{-2} s^{-1} PPFD), with the F_v'/F_m', F_q'/F_m', F_q'/F_v' and NPQ calculated according to ***Table.2.3***. Leaves and stipules were isolated using the Fluorimager software.

Table 2.3. Chlorophyll fluorescent parameter calculations. Calculations used for chlorophyll fluorescence imaging were adapted from Murchie and Lawson. (2013). Whereby F_m is the maximum fluorescence in the dark, F_o is the minimum fluorescence in the dark, F_m' is the maximum fluorescence in the light, F_o' is the minimum fluorescence in the light, F' is the steady state fluorescence in the light and PSII is photosystem II.

Parameter	Definition	Calculation
F_v/F_m	Maximum efficiency of PSII in the dark	$(F_m-F_o)/F_m$
F_q'/F_m'	PSII operating efficiency in the light	$(F_m'-F')/F_m'$
F_v'/F_m'	Maximum efficiency of photosystem II in the light	$(F_m'-F_o')/F_m'$
F_q'/F_v'	PSII photochemical quenching factor	$(F_m'-F')/(F_m'-F_o')$
NPQ	Non-Photochemical Quenching	$(F_m-F_m')/F_m'$

2.2.3. Gas Exchange

A Li-Cor 6800 portable gas exchange system (Li-Cor, Lincoln, Nebraska, USA) was utilised for all gas exchange measurements (assimilation; *A* and stomatal conductance; g_s) and carried out at a constant flow rate of 500 µmol s^{-1}, 23 ^oC, 400 µmol mol^{-1} CO_2 concentration, a vapor pressure deficit of 1.2 (± 0.2) kPa and a light intensity of 1500 µmol m^{-2} s^{-1} PPFD (unless otherwise stated). The youngest fully expanded leaf and stipule were used per accession. Leaf/stipule areas were calculated via ImageJ (version 1.53) using images of the leaf/stipule in the chamber.

2.2.3.1. Light Response (*A*/*Q*) Curves

Leaves/Stipules were acclimated to the conditions in ***Section 2.2.3***, after waiting 15 minutes for stabilisation of *A* and g_s, responses of *A* and g_s were monitored with light intensity changes (1500, 1300, 1100, 900, 700, 550, 400, 250, 150, 100, 50 and 0 µmol m^{-2} s^{-1} PPFD). Measurements were taken after *A* had stabilised to each new light

intensity (predetermined min wait: 60 s and max wait: 120 s). Mean *A*/*Q* curves were generated by plotting *A* as a function light intensity. Mean light-saturated rate of *A* (A_{sat}) and mean g_s at 1500 µmol m^{-2} s^{-1} PPFD (gs_{1500}) were also calculated, by averaging the highest *A* measured for each accession and the g_s measured at 1500 µmol m^{-2} s^{-1} PPFD for each accession.

2.2.3.2. *A*/C_i Response Curves

Leaves/Stipules were stabilised to the conditions in ***Section 2.2.3***, after waiting 15 minutes for stabilisation of *A* and g_s, responses of *A* and g_s were measured following changes in CO_2 concentrations (400, 250, 150, 100, 50, 400, 550, 700, 900, 1100, 1300, 1500 and 400 µmol mol^{-1}). Measurements were taken after *A* had stabilised to each new CO_2 concentration (predetermined min wait: 60 s and max wait: 120 s). Only the first 400 CO_2 concentration value was used in data analysis, as this was representative of the true stabilised value. Mean *A*/C_i curves were generated by plotting *A* as a function of intercellular CO_2 concentration (C_i) and utilised to determined photosynthetic capacity parameters; Vc_{max} (maximum rate of Rubisco activity) and J_{max} (maximum rate of electron transport) via the plantecophys RStudio package (using the "fitacis" function), which models the data derived from the *A*/C_i curves by fitting the Farquhar-Berry-von Caemmerer model (*see* Duursma, 2015).

2.2.3.3. Step Increases in Light Intensity

Leaves/Stipules were acclimated to the conditions described in ***Section 2.2.3***, with the exception that the light intensity was at 100 µmol m^{-2} s^{-1} PPFD. When both *A* and g_s were stable, measurements were recorded every 20 s for 10-minutes before PPFD

was increased to 1000 µmol m^{-2} s^{-1} for 30-minutes. Changes in intrinsic water use efficiency (*i*WUE) were calculated as *i*WUE = A/g_s. Steady state *A* and g_s at 100 µmol m^{-2} s^{-1} PPFD (*A100* and *gs100*) were calculated from the average of the last five data points before PPFD was increased to 1000 µmol m^{-2} s^{-1}, whilst steady state *A* and g_s at 1000 µmol m^{-2} s^{-1} PPFD (*A1000* and *gs1000*) were calculated from the average of the last five data points at 1000 µmol m^{-2} s^{-1}. The maximum *i*WUE ($iWUE_{max}$) was calculated from the average of five data points (observations 45-49) after PPFD was increased to 1000 µmol m^{-2} s^{-1}, where *i*WUE was generally at the highest and most stable rate. Vialet-Chabrand et al. (2013) sigmoidal model was utilised to parametrise *A* and g_s responses. This model determined the lag-time (initial temporal delay in the response of *A* and g_s to a light intensity change) and time constants (time taken for *A* and g_s to reach steady state) in *A* and g_s (*see* McAusland et al., 2016).

2.2.4. Total Protein Content

Three 0.5 cm^2 and three 1 cm^2 leaf and stipule disk samples were taken from three plants per accession. Samples were ground to a fine powder in liquid nitrogen, mixed with 400 µL Bicine extraction buffer (100 mM Bicine NaOH (pH 8), 20 mM MgCl2, 2 mM NaEDTA, 5.1 mM DTT, 10 mg/ml PVPP, 2 % (v/v) Tween-20) and spun for 10-minutes at 15,000 rpm within a centrifuge. 20 µL of the extracted supernatant were added into microplate wells (two technical replicates used per sample), alongside 20 µL of each premade BSA dilution series (*see* MACHEREY-NAGEL Protein Quantification Assay 2023 manual). 40 µL protein solving buffer (PSB) and 40 µL quantification reagent were added to each well and left to incubate for 30-minutes at room temperature. A FLUOstar Omega Microplate Reader (BMG Labtech, Offenburg, Germany) was used to measure light extinction photometrically at 570 nm, with protein

concentration calculated in relation to the BSA dilution series and standardised via leaf/stipule disk fresh weights.

2.2.5. Surface Impressions

Surface impressions were taken from the youngest fully expanded leaf and stipule on the adaxial (AD) and abaxial (AB) surfaces, using activated Xantropen dental impression material (Xantopren, Heraeus, Germany). Once the impression had dried clear nail varnish generated a positive microscope slide impression (*see* Weyers and Johansen (1985)). Stomatal densities (SD) were calculated by counting stomata at 200x magnification in a 1 mm^2 grid (nine grids per impression). Stomatal sizes (SS) were calculated by measuring five stomatal pore lengths (PL) and guard cell lengths (GCL) per impression at 400x magnification. Utilising SD and SS, mean maximum anatomical g_s (gs_{max}) was generated following the Dow et al. (2014a) method (***Equation.2.1***). A Leica ATC 2000 microscope (Leica Microsystems, Milton Keynes, UK), Swiftcam digital eyepiece (© 2021 Swift Optical Instruments, Schertz, Texas) and Swift Imaging software (Mac version 3.0) were used for SD and SS.

$$(d \times \mathrm{SD} \times a_{max}) / \left(v \times \left(l + (\pi / 2) \times \sqrt{(a_{max} / \pi)} \right) \right)$$

Equation 2.1. Theoretical maximum anatomical stomatal conductance (gs_{max}) calculation. Whereby d is the diffusivity of water in air ($m^2\ s^{-1}$ at 22 °C), SD is stomatal density, v is the molar volume of air ($m^3\ mol^{-1}$ at 22 °C), π is the mathematical constant 3.142, l is pore depth (μm) which is equal to guard cell width at the stoma centre and assumed to be half the guard cell length and a_{max} is the mean maximum stomatal pore area (μm^2) generated with the assumptions that stomata were elliptical and that the major axis was equal to the pore length and minor axis was equal to half the pore length (*see* Dow et al., 2014a).

2.2.6. Foliar Anatomical Measurements

Individual leaf and stipule samples were taken to generate leaf and stipule mass per area (LMA and SMA) (n = 6), with dry weights (DW) measured after two weeks in a 60 ^{o}C oven. Whilst ImageJ (version 1.53) calculated leaf/stipule area using a ruler as a known scale.

2.2.7. Yield Calculations

Plants were harvested after being left to fully dry out within their controlled growth room (*see* ***Section 2.2.1***). Grain yield parameters from each accession were represented by the mean number of pods, number of seeds, pod length (calculated using a ruler as a known scale via ImageJ; version 1.53), pod DW, seed DW and total pod DW (summed pod DW for all the pods from one plant). Whilst biomass yield parameters were represented by mean plant height, plant DW, mean number and DW of stems, leaves and stipules and mean tendril DW for plants that survived to harvest (n = 3-6) (*see* ***Section 2.2.1***).

2.2.8. Data Analysis/Statistics

Mean ± standard error (SE) were calculated for each measurement. A Shapiro-Wilk test and Levene's test were utilised (respectively) to check if data was normally distributed and had equal variance and thus met the assumptions of an ANOVA. A one-way ANOVA and TukeyHSD test were utilised between *P. sativum* accessions and yield parameters (***Appendix Table.A1.1***). Two-way and/or multi-way ANOVAs were also calculated for each measured physiological parameter between *P. sativum* accession and foliar tissues, followed by TukeyHSD tests. A multi-way ANOVA was

also performed for each chlorophyll fluorescence parameter between PPFD/time, foliar tissue and *P. sativum* accession, followed by TukeyHSD tests which were calculated on data at the end of the chlorophyll fluorescent protocol (*i.e.,* at 10 or 20 minutes of induction/relaxation or at 1500 μmol m^{-2} s^{-1} PPFD of the chlorophyll fluorescent light curve). TukeyHSD results for each physiological parameter were compared between the leaves and stipules (for accessions that had both types of foliar tissues) to determine differences between leaf and stipule physiology within each individual accession. Whilst multi-way ANOVAs and TukeyHSD tests were also carried out for SD, SS and gs_{max} between the AD and AB surface, foliar tissue and *P. sativum* accession, with TukeyHSD results compared between the leaves and stipules and between the AD and AB surfaces to determine differences within each individual accession. Spearman's correlation coefficients (R) and linear regression equations were run between SD, SS, gs_{max} and against g_s (at 400 μmol mol^{-1} $[CO_2]$ measured from the A/C_i data) to determine if stomatal anatomy impacted g_s and/or gs_{max}. Whilst Spearman's correlation coefficients and linear regression equations were additionally carried out between photosynthetic capacity and LMA/SMA, between photosynthetic capacity and protein content and between photosynthetic capacity and each yield parameter. Graphs and statistics were generated within RStudio (Mac version 2024.04.0+735).

2.3. Results

2.3.1. Variation in Chlorophyll Fluorescence Parameters in Response to Light

2.3.1.1. Variation in Response to an Induction and Relaxation in Light Intensity

Chlorophyll fluorescence parameters (F_q'/F_m', F_q'/F_v' and F_v'/F_m') were monitored during a light induction and relaxation (***Fig.2.2&2.3***). In the induction phase, significant variation was identified in F_q'/F_m' between the different *P. sativum* accessions in both the leaves ($F_{(12)} = 29.6$, $P < 0.001$) and stipules ($F_{(12)} = 16.1$, $P < 0.001$) (***Fig.2.2***), and significant variation in F_q'/F_v' and F_v'/F_m' were also apparent between accessions in both the leaves ($F_{(12)} = 53.3$, $P < 0.001$; $F_{(12)} = 26.3$, $P < 0.001$) and stipules ($F_{(12)} = 28.7$, $P < 0.001$; $F_{(12)} = 14.8$, $P < 0.001$) (***Fig.2.3***).

At the end of the 10 min induction, Ji2822 leaves displayed the highest F_q'/F_m' (0.67 ± 0.01) and was significantly different to Alaska, CamB, Cen and Torsdag (TukeyHSD; $P < 0.05$) (***Fig.2.2A&Table.2.4A***). Whilst CamB had a significantly lower leaf F_q'/F_m' (0.59 ± 0.01) at 10 mins to Eth, Ni11 and Ji2822 (TukeyHSD; $P < 0.05$) (***Fig.2.2A&Table.2.4A***). Elatius had the highest (0.63 ± 0.01), and Alaska (0.6 ± 0.01) the lowest stipule F_q'/F_m' after 10 mins of induction (although these were not significantly different to the other accessions (TukeyHSD; $P > 0.05$)) (***Fig.2.2B&Table.2.4B***). Quenching parameters illustrated that the greater F_q'/F_m' at the end of the induction in Ji2822 leaves were possibly generated by a higher value of F_q'/F_v', which were significantly different to CamB, Cen and Met leaves (TukeyHSD; $P < 0.05$) (***Fig.2.3A&Table.2.5A***). Whilst the greater F_q'/F_m' in Elatius stipules at the end of the induction were potentially generated via F_v'/F_m' and F_q'/F_v' (although no

significant differences were identified to the other accessions in either parameter (TukeyHSD; $P > 0.05$)) (***Fig.2.3D&Table.2.5B***). CamB leaves exhibited significantly lower values of F_v'/F_m' to Met (TukeyHSD; $P < 0.05$) and F_q'/F_v' to Eth, Ji2822, Ni11 and Wando (TukeyHSD; $P < 0.05$) at 10 mins, which possibly drove the low F_q'/F_m' in CamB leaves (***Fig.2.3C&Table.2.5A***). The low F_q'/F_m' in Alaska stipules at the end of the induction, may have been driven by a significantly lower F_q'/F_v' to Eth, Ji2822, Pacco and Wando (TukeyHSD; $P < 0.05$) (***Fig.2.3B&Table.2.5B***). After 10 mins of the induction no significant differences were identified in F_q'/F_m' between the leaves and stipules within each individual accession (TukeyHSD; $P > 0.05$) (***Fig.2.2***).

In the relaxation phase there were significant variation identified in F_v/F_m between the accessions for both the leaves ($F_{(12)} = 29.2$, $P < 0.001$) and stipules ($F_{(12)} = 25.4$, $P < 0.001$) (***Fig.2.2***). Ji2822 exhibited the highest F_v/F_m for the leaves (0.82 ± 0.003) and stipules (0.81 ± 0.003) at the end of the relaxation protocol, with a significant difference in leaf F_v/F_m to Alaska, Cen, KW and Wando (TukeyHSD; $P < 0.05$) and in stipule F_v/F_m to Ni16 (TukeyHSD; $P < 0.05$) (***Fig.2.2&Table.2.4***). In contrast, KW leaves (0.77 ± 0.02) and Ni16 stipules (0.78 ± 0.01) had the lowest F_v/F_m at the end of the relaxation protocol, with a significant difference to Eth and Ji2822 in leaf (TukeyHSD; $P < 0.05$) and stipule (TukeyHSD; $P < 0.05$) F_v/F_m respectively (***Fig.2.2&Table.2.4***). At the end of the relaxation protocol no significant differences were identified in F_v/F_m between the leaves and stipules within each individual accession (TukeyHSD; $P > 0.05$) (***Fig.2.2***).

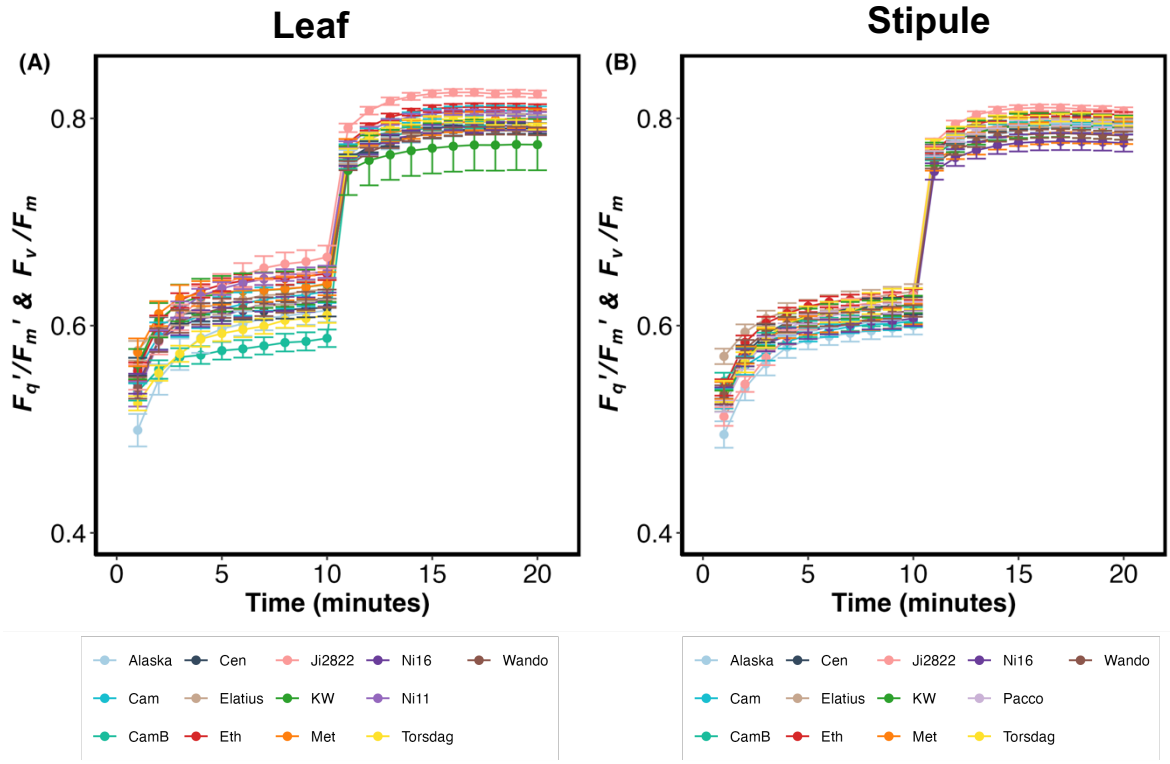

Figure 2.2. Variation in chlorophyll fluorescence induction and relaxation responses across P. sativum accessions. Induction responses were monitored as F_q'/F_m' (operating efficiency of photosystem II in the light) and recovery of F_v/F_m (photosystem II maximum efficiency in the dark) in both **(A)** leaves and **(B)** stipules. Accessions were dark adapted for 30-min before being measured within a Fluorimager. Error bars represent mean ± SE (n = 6). Whilst the presence of * of the same colour indicates a significant difference in either F_q'/F_m' or F_v/F_m within an individual accession between the leaves and stipules, whereby * is $P < 0.05$, ** is $P < 0.01$ and *** is $P < 0.001$ (TukeyHSD). Significant differences in either F_q'/F_m' at 10 minutes or F_v/F_m at 20 minutes between the *P. sativum* accessions can be found in ***Table.2.4***.

Table 2.4. Significant differences in chlorophyll fluorescence induction and relaxation parameters across P. sativum accessions. Induction responses were monitored as F_q'/F_m' (operating efficiency of photosystem II in the light) and recovery of F_v/F_m (photosystem II maximum efficiency in the dark) in ***Fig.2.2***. The different letters within the **(A)** leaf and **(B)** stipule tables indicate a significant difference in either F_q'/F_m' at 10 mins or F_v/F_m at 20 mins between the different *P. sativum* accessions ($P < 0.05$; TukeyHSD).

(A)

Accession	Leaves	
	F_q'/F_m'	F_v/F_m
Alaska	bc	bc
Cam	abc	abc
CamB	c	abc
Cen	bc	bc
Elatius	abc	abc
Eth	ab	ab
Ji2822	a	a
KW	abc	c
Met	abc	abc
Ni16	abc	abc
Ni11	ab	abc
Torsdag	c	abc
Wando	abc	bc

(B)

Accession	Stipules	
	F_q'/F_m'	F_v/F_m
Alaska	a	ab
Cam	a	ab
CamB	a	ab
Cen	a	ab
Elatius	a	ab
Eth	a	a
Ji2822	a	a
KW	a	ab
Met	a	ab
Ni16	a	b
Pacco	a	ab
Torsdag	a	ab
Wando	a	ab

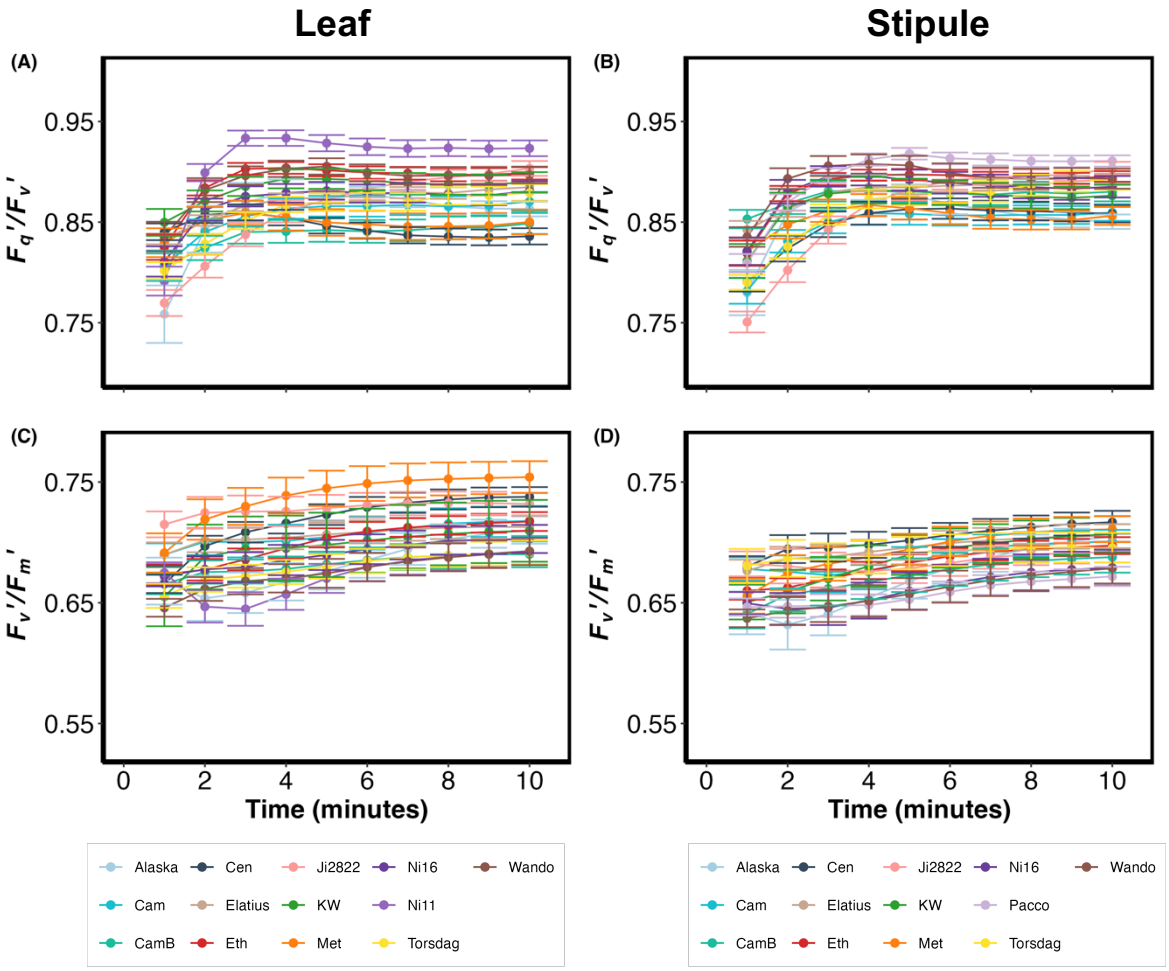

Figure 2.3. Variation in chlorophyll fluorescence induction parameters across P. sativum accessions. Induction responses were monitored as F_q'/F_v' (PSII photochemical quenching factor) in the **(A)** leaves and **(B)** stipules and as F_v'/F_m' (PSII maximum efficiency) in the **(C)** leaves and **(D)** stipules. Accessions were dark adapted for 30-minutes before being measured within a Fluorimager. Error bars represent mean ± SE (n = 6). Significant differences in either F_q'/F_v' or F_v'/F_m' at 10 minutes between the *P. sativum* accessions can be found in ***Table.2.5***.

Table 2.5. Significant differences in chlorophyll fluorescence induction parameters across P. sativum accessions. Induction responses were monitored as F_q'/F_v' (PSII photochemical quenching factor) and as F_v'/F_m' (PSII maximum efficiency) in ***Fig.2.3***. The different letters within the **(A)** leaf and **(B)** stipule tables indicate a significant difference in either F_q'/F_v' at 10 mins or F_v'/F_m' at 10 mins between the different *P. sativum* accessions ($P < 0.05$; TukeyHSD).

(A)

Accession	Leaves	
	F_q'/F_v'	F_v'/F_m'
Alaska	bcd	ab
Cam	bcd	ab
CamB	cd	b
Cen	d	ab
Elatius	bc	ab
Eth	ab	ab
Ji2822	ab	ab
KW	abc	ab
Met	cd	a
Ni16	bc	ab
Ni11	a	b
Torsdag	bc	b
Wando	ab	b

(B)

Accession	Stipules	
	F_q'/F_v'	F_v'/F_m'
Alaska	d	a
Cam	bcd	a
CamB	abcd	a
Cen	bcd	a
Elatius	abcd	a
Eth	ab	a
Ji2822	a	a
KW	abcd	a
Met	cd	a
Ni16	abcd	a
Pacco	a	a
Torsdag	abcd	a
Wando	abc	a

2.3.1.2. Photosynthetic Efficiency Light Response Curves

Chlorophyll fluorescence parameters (F_v'/F_m', F_q'/F_m', F_q'/F_v' and NPQ), were assessed as a function of irradiance, with significant variation observed in F_v'/F_m' ($F_{(11)}$ = 5.32, $P < 0.001$), F_q'/F_v' ($F_{(11)}$ = 7.09, $P < 0.001$), F_q'/F_m' ($F_{(11)}$ = 11.57, $P < 0.001$) and NPQ ($F_{(11)}$ = 6.58, $P < 0.001$) between the different accessions and foliar tissues (***Fig.2.4***). However, there were no significant difference in F_v/F_m (at 0 µmol m^{-2} s^{-1} PPFD) between the different accessions and foliar tissues ($F_{(11)}$ = 1.09, P = 0.363) (***Fig.2.4***).

At the highest light intensity (1500 µmol m^{-2} s^{-1} PPFD) Ji2822 had a significantly greater leaf F_q'/F_m' (0.33 ± 0.01) to all accessions (excluding Cam, Eth, KW and Met) (TukeyHSD; $P < 0.05$) (***Fig.2.4A&Table.2.6A***). Whilst CamB exhibited the lowest leaf F_q'/F_m' (0.24 ± 0.01) at 1500 µmol m^{-2} s^{-1} PPFD and was significantly different to Ji2822, KW and Met (TukeyHSD; $P < 0.05$) (***Fig.2.4A&Table.2.6A***). Observations of quenching parameters highlighted that the high F_q'/F_m' in Ji2822 leaves were potentially driven by significantly higher values of F_v'/F_m' to Alaska, Ni16, Ni11 and Wando (TukeyHSD; $P < 0.05$) and F_q'/F_v' to CamB, Cen, Elatius and Torsdag (TukeyHSD; $P < 0.05$) (***Fig.2.4A,C,E&Table.2.6A***). In contrast, the low F_q'/F_m' experienced by CamB leaves were primarily driven by a significantly lower value of F_q'/F_v' to all accessions (excluding Elatius and Torsdag) (TukeyHSD; $P < 0.05$) (***Fig.2.4A&E&Table.2.6A***).

Ji2822 also exhibited a significantly higher stipule F_q'/F_m' at 1500 µmol m^{-2} s^{-1} PPFD (0.29 ± 0.01) to Alaska, CamB, Ni16, Pacco and Wando (TukeyHSD; $P < 0.05$) (***Fig.2.4B&Table.2.6B***). Whereas Wando was significantly lower in stipule F_q'/F_m' at

1500 µmol m^{-2} s^{-1} PPFD (0.24 ± 0.004) to Ji2822, KW and Torsdag (TukeyHSD; P < 0.05) (***Fig.2.4B&Table.2.6B***). Quenching parameters illustrated that the high F_q'/F_m' observed in Ji2822 stipules were primarily driven by a significantly higher value of F_q'/F_v' to Alaska, CamB, Elatius, Ni16, Pacco and Wando (TukeyHSD; P < 0.05) (***Fig.2.4F&Table.2.6B***). Whilst the lowest stipule F_v'/F_m' seen in Wando possibly drove the low F_q'/F_m' in Wando stipules (with a significant difference in F_v'/F_m' to CamB, Elatius and Torsdag (TukeyHSD; P < 0.05)) (***Fig.2.4D&Table.2.6B***). However no significant differences were observed in F_q'/F_m' at 1500 µmol m^{-2} s^{-1} PPFD between the leaves and stipules within each individual accession (TukeyHSD; P > 0.05) (***Fig.2.4A&B***).

Wando leaves (3.33 ± 0.1) and stipules (3.58 ± 0.1) had the highest NPQ at 1500 µmol m^{-2} s^{-1} PPFD, which were significantly different to CamB, Cen, Elatius, Ji2822, KW, Met and Torsdag in leaf NPQ (TukeyHSD; P < 0.05) and to all accessions (excluding Alaska and Cam) in stipule NPQ (TukeyHSD; P < 0.05) (***Fig.2.4G&H&Table.2.6***). In contrast, Met leaves (2.34 ± 0.13) and Torsdag stipules (2.64 ± 0.08) exhibited the lowest NPQ at 1500 µmol m^{-2} s^{-1} PPFD, with a significant difference to Cam, Eth, Ni16, Ni11 and Wando in leaf NPQ (TukeyHSD; P < 0.05) and to Alaska, Cam, Eth, Ni16 and Wando in stipule NPQ (TukeyHSD; P < 0.05) (***Fig.2.4G&H&Table.2.6***). However at 1500 µmol m^{-2} s^{-1} PPFD there were no significant differences seen in NPQ between the leaves and stipules within each individual accession (TukeyHSD; P > 0.05) (***Fig.2.4G&H***).

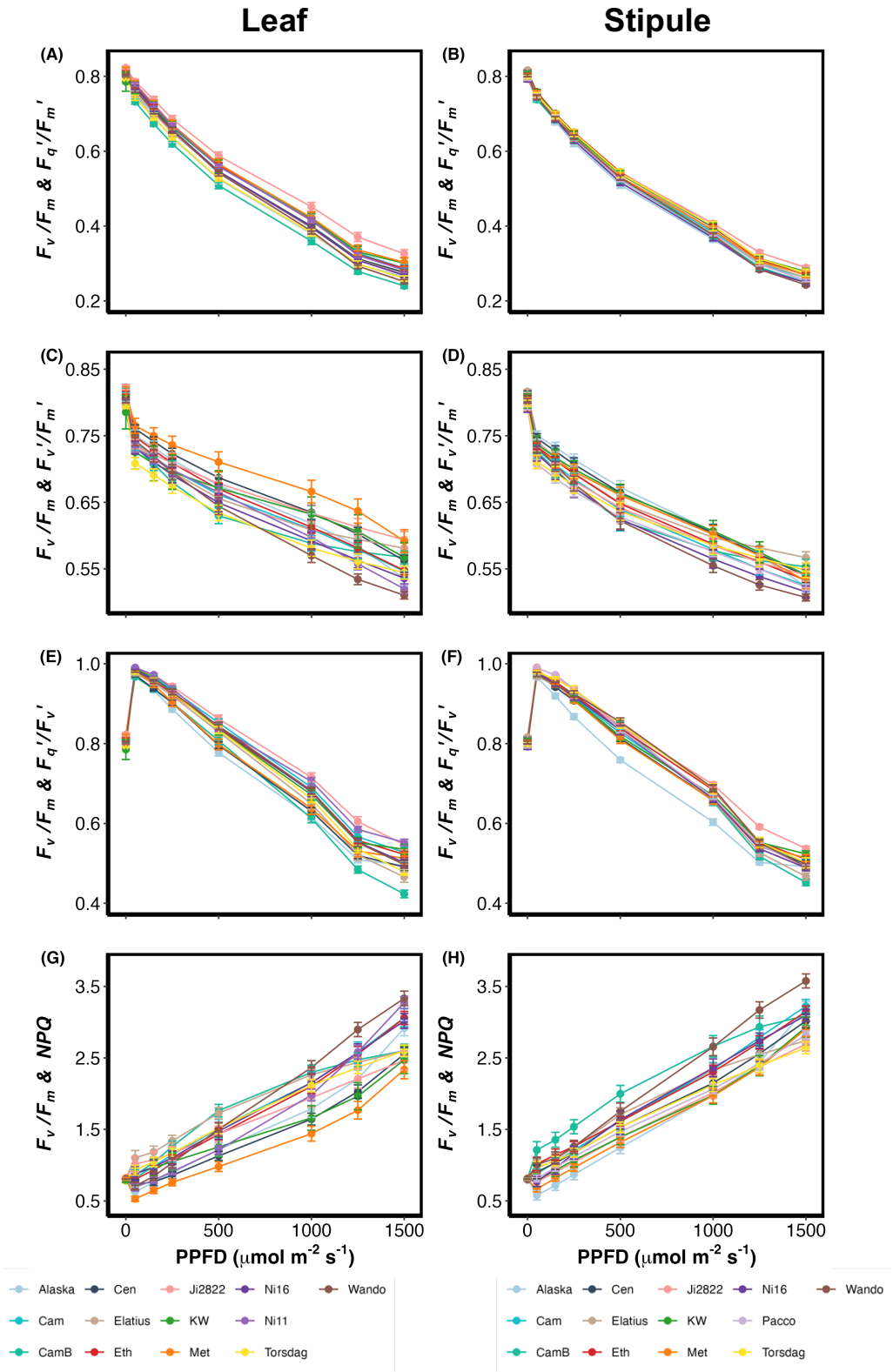

Figure 2.4. Variation in chlorophyll fluorescence light curve parameters across P. sativum accessions. Chlorophyll fluorescent responses to light intensity changes were monitored initially in the dark as F_v/F_m (photosystem II maximum efficiency in the dark) in all graphs, followed by measurements in the light monitored as F_q'/F_m' (operating efficiency of photosystem II; PSII) in the **(A)** leaves and **(B)** stipules, F_v'/F_m' (PSII maximum efficiency) in the **(C)** leaves and **(D)** stipules, F_q'/F_v' (PSII photochemical quenching factor) in the **(E)** leaves and **(F)** stipules and as NPQ (non-photochemical quenching) in the **(G)** leaves and **(H)** stipules. Accessions were dark adapted for 30-minutes before being measured at different photosynthetic photon flux densities (PPFD) within a Fluorimager. Error bars represent mean ± SE (n = 6). Whilst the presence of * of the same colour indicates a significant difference in either F_q'/F_m' or NPQ within an individual accession between the leaves and stipules, whereby * is $P < 0.05$, ** is $P < 0.01$ and *** is $P < 0.001$ (TukeyHSD). Significant differences in either F_q'/F_m', F_v'/F_m', F_q'/F_v' or NPQ at 1500 µmol m^{-2} s^{-1} PPFD between the *P. sativum* accessions can be found in ***Table.2.6***.

Table 2.6. Significant differences in chlorophyll fluorescence light curve parameters across P. sativum accessions. Chlorophyll fluorescent responses to light intensity changes were monitored in ***Fig.2.4*** as F_q'/F_m' (operating efficiency of photosystem II; PSII), F_v'/F_m' (PSII maximum efficiency), F_q'/F_v' (PSII photochemical quenching factor) and as NPQ (non-photochemical quenching). The different letters within the **(A)** leaf and **(B)** stipule tables indicate a significant difference in either F_q'/F_m', F_v'/F_m', F_q'/F_v' or NPQ at 1500 µmol m^{-2} s^{-1} photosynthetic photon flux density between the different *P. sativum* accessions ($P < 0.05$; TukeyHSD).

(A)

Accession	Leaves			
	F_q'/F_m'	F_v'/F_m'	F_q'/F_v'	NPQ
Alaska	bc	bcd	bcde	abc
Cam	abc	abcd	abcd	ab
CamB	c	abc	f	bc
Cen	bc	abc	cde	c
Elatius	bc	ab	ef	bc
Eth	abc	abcd	abcd	ab
Ji2822	a	a	ab	c
KW	ab	abc	abc	c
Met	ab	a	abcde	c
Ni16	bc	bcd	bcde	ab
Ni11	bc	cd	a	a
Torsdag	bc	abcd	def	bc
Wando	c	d	bcde	a

(B)

Accession	Stipules			
	F_q'/F_m'	F_v'/F_m'	F_q'/F_v'	NPQ
Alaska	bc	abc	bcd	abc
Cam	abc	abc	abc	ab
CamB	bc	ab	d	bcd
Cen	abc	abc	abc	bcd
Elatius	abc	a	cd	bcd
Eth	abc	abc	abc	bc
Ji2822	a	abc	a	cd
KW	ab	abc	ab	bcd
Met	abc	abc	abc	bcd
Ni16	bc	bc	bcd	bc
Pacco	bc	bc	bc	bcd
Torsdag	ab	ab	abc	d
Wando	c	c	bc	a

2.3.2. Photosynthetic Rates in Response to Changing Light Intensity

Leaf and stipule *A* and g_s were monitored as a function of light intensity across the *P. sativum* accessions, with variation apparent between the accessions in both tissue types for *A* and g_s (***Fig.2.5***). Leaves and stipules displayed a typical hyperbolic response for *A* with increasing irradiance (***Fig.2.5A&B***), whilst g_s remained relatively constant (***Fig.2.5C&D***). A significant difference in the light-saturated rate of *A*; A_{sat} ($F_{(11)}$ = 2.84, $P < 0.01$) and g_s at 1500 µmol m^{-2} s^{-1} PPFD; gs_{1500} ($F_{(11)}$ = 2.16, $P < 0.05$), between the different accessions and foliar tissues were identified (***Fig.2.6***).

Met exhibited a significantly higher leaf A_{sat} (21.1 ± 0.59 µmol m^{-2} s^{-1}), to half of the accessions (TukeyHSD; $P < 0.05$), including Alaska, Cam, Elatius, Eth, Torsdag and Wando (***Fig.2.6A***). Alaska displayed the lowest leaf A_{sat} (12.35 ± 0.58 µmol m^{-2} s^{-1}), with a significant difference to the remaining accessions (TukeyHSD; $P < 0.05$), excluding Cam, Elatius, Eth, Torsdag and Wando (***Fig.2.6A***). The highest stipule A_{sat} was observed by Ni16 (16.8 ± 2.85 µmol m^{-2} s^{-1}), which was significantly higher than all other accessions (TukeyHSD; $P < 0.05$), with the exception of Cam, Cen, Eth, Ji2822, KW and Met (***Fig.2.6B***). Whilst Elatius exhibited a significantly lower stipule A_{sat} (6.69 ± 0.31 µmol m^{-2} s^{-1}) to all accessions (TukeyHSD; $P < 0.05$), excluding Alaska, CamB, Ji2822, Pacco, Torsdag and Wando (***Fig.2.6B***). Ni16 had the highest leaf (0.51 ± 0.07 mol m^{-2} s^{-1}) and stipule (0.34 ± 0.07 mol m^{-2} s^{-1}) gs_{1500} and was significantly higher than Alaska, Cam and CamB in leaf gs_{1500} (TukeyHSD; $P < 0.05$) and significantly greater than CamB, Elatius and Wando in stipule gs_{1500} (TukeyHSD; $P < 0.05$) (***Fig.2.6C&D***). In contrast Cam leaves (0.24 ± 0.03 mol m^{-2} s^{-1}) and Wando

stipules (0.17 ± 0.01 mol m^{-2} s^{-1}) had the lowest gs_{1500} and was significantly different to Cen, Ji2822, KW, Met and Ni16 for leaf gs_{1500} (TukeyHSD; $P < 0.05$), and to Ni16 for stipule gs_{1500} (TukeyHSD; $P < 0.05$) (***Fig.2.6C&D***).

The leaves generally had a greater A_{sat} and gs_{1500} than the stipules, with a significant difference identified in A_{sat} between the leaves and stipules within each individual accession (TukeyHSD; $P < 0.05$), excluding Alaska, Cam, Cen, Eth, Ni16 and Torsdag (***Fig.2.6***). A significant difference was also seen in gs_{1500} between the leaves and stipules within the individual accessions of Elatius (TukeyHSD; $P < 0.001$), Ji2822 (TukeyHSD; $P < 0.01$), Met (TukeyHSD; $P < 0.01$) and Wando (TukeyHSD; $P < 0.01$) (***Fig.2.6***).

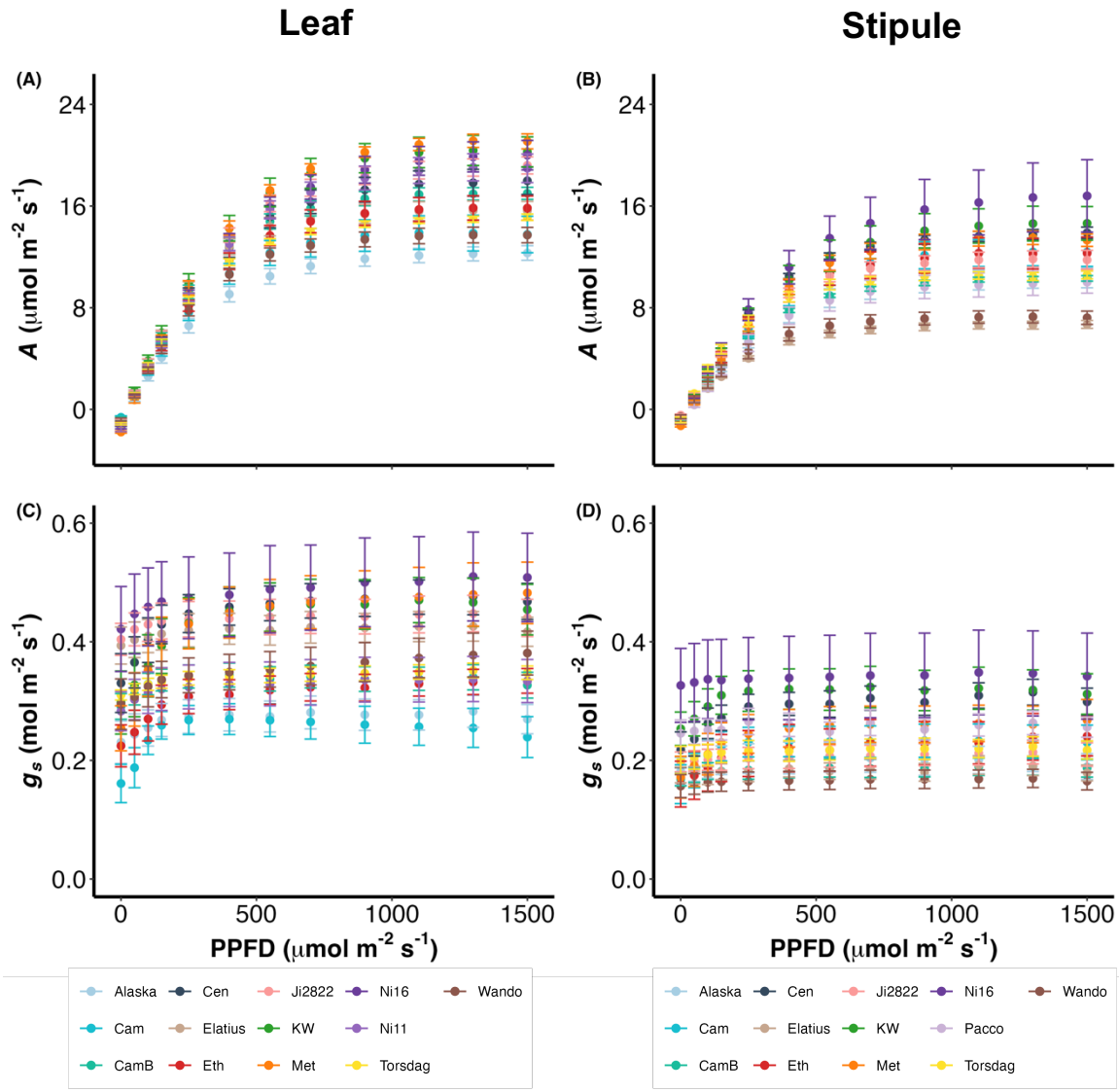

Figure 2.5. Variation in carbon assimilation (A) and stomatal conductance (g_s) in response to light across P. sativum accessions. Changes in **(A)** leaf and **(B)** stipule assimilation and **(C)** leaf and **(D)** stipule stomatal conductance was measured against increasing photosynthetic photon flux densities (PPFD) within a Li-Cor 6800 at 23ºC and 400 µmol mol^{-1} [CO_2]. Error bars represent mean ± SE (n = 6).

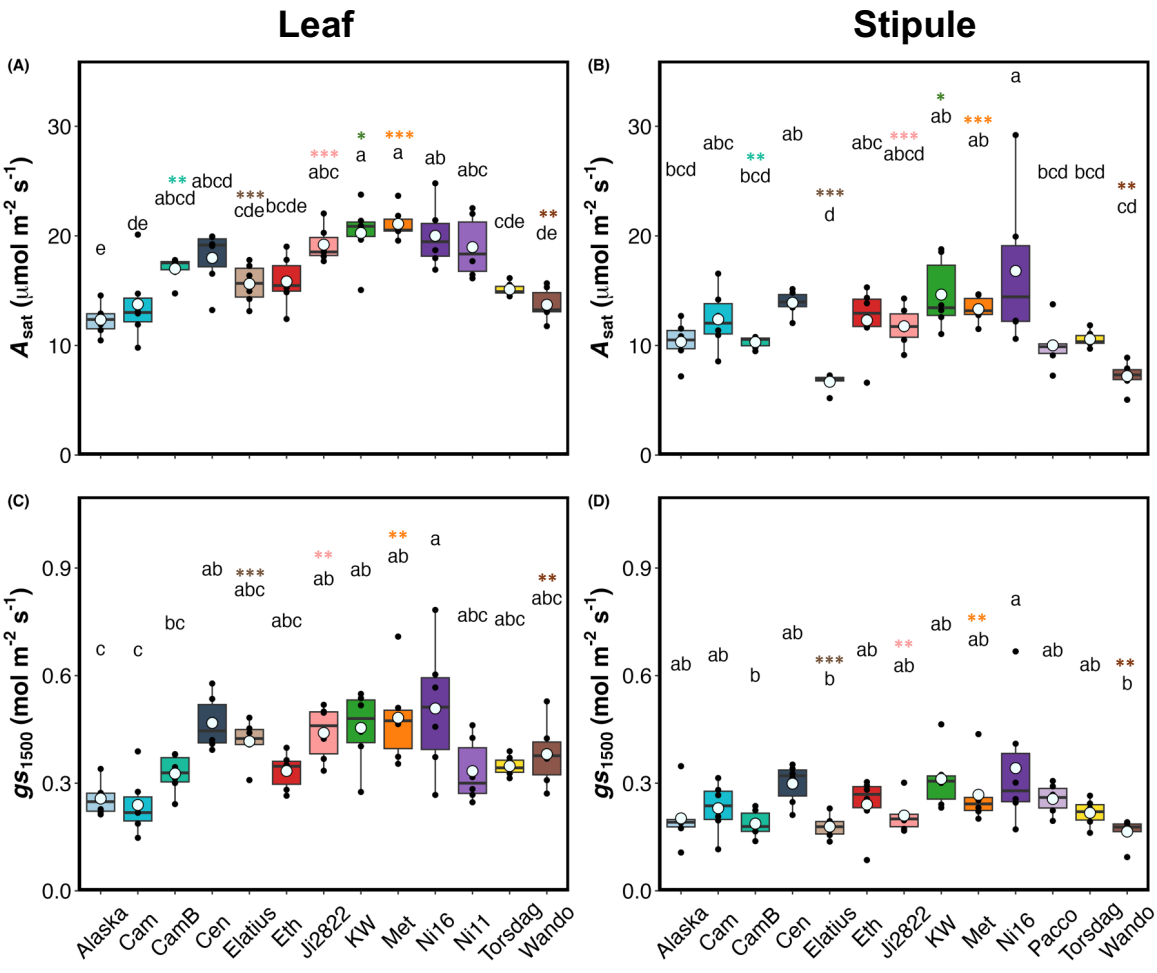

Figure 2.6. Variation in leaf and stipule light-saturated rate of A (A_{sat}) and g_s at 1500 µmol m^{-2} s^{-1} PPFD (gs_{1500}) across P. sativum accessions. Changes in **(A)** leaf and **(B)** stipule light-saturated rate of assimilation (A_{sat}) and **(C)** leaf and **(D)** stipule stomatal conductance at 1500 µmol m^{-2} s^{-1} photosynthetic photon flux density (gs_{1500}). Measured within a Li-Cor 6800 at 23 ºC and 400 µmol mol^{-1} [CO_2]. White dots symbolise the mean, whilst error bars represent mean ± SE (n = 6). Different letters above each error bar indicate a significant difference in either A_{sat} or gs_{1500} between *P. sativum* accessions ($P < 0.05$; TukeyHSD). Whilst the presence of * of the same colour indicates a significant difference in either A_{sat} or gs_{1500} within an individual accession between the leaves and stipules, whereby * is $P < 0.05$, ** is $P < 0.01$ and *** is $P < 0.001$ (TukeyHSD).

2.3.3. Variation in Photosynthetic Capacity

To determine differences in photosynthetic capacity, leaf and stipule *A* were measured as a function of internal [CO_2] (C_i), with variation apparent between the accessions in both tissue types for *A* and g_s (***Fig.2.7&2.8***). Both leaves and stipules exhibited a hyperbolic response in *A* (***Fig.2.7A&B***), whilst little change in g_s was noted (***Fig.2.7C&D***). KW and Met had the greatest overall leaf g_s, whilst Eth, Alaska and Ni11 generally had lowest at all C_i (***Fig.2.7C***). Cam displayed the highest overall stipule g_s, and Elatius, Eth, Wando and Alaska had the lowest at all C_i (***Fig.2.7D***).

Significant variation in the maximum rate of Rubisco activity; Vc_{max} ($F_{(11)} = 2.64$, $P < 0.01$) and maximum rate of electron transport; J_{max} ($F_{(11)} = 2.95$, $P < 0.01$) were observed between the different accessions and foliar tissues (***Fig.2.8***). KW had the highest leaf (97.25 ± 3.51 μmol m^{-2} s^{-1}) and stipule (64.01 ± 3.32 μmol m^{-2} s^{-1}) Vc_{max} and was significantly different in leaf Vc_{max} to Alaska, Cen, Elatius, Eth, Torsdag and Wando (TukeyHSD; $P < 0.05$), and significantly different in stipule Vc_{max} to Alaska, CamB, Elatius, Eth, Pacco, Torsdag and Wando (TukeyHSD; $P < 0.05$) (***Fig.2.8A&B***). KW also had the highest leaf J_{max} (153.6 ± 7.06 μmol m^{-2} s^{-1}) that was significantly greater than Alaska, Cen, Elatius, Eth, Ni11, Torsdag and Wando (TukeyHSD; $P < 0.05$) and stipule J_{max} (103.8 ± 7.34 μmol m^{-2} s^{-1}) which was significantly greater than Alaska, CamB, Elatius, Eth, Pacco, Torsdag and Wando (TukeyHSD; $P < 0.05$) (***Fig.2.8C&D***). In contrast, Eth (50.15 ± 3.75 μmol m^{-2} s^{-1}) and Wando (76.67 ± 5.18 μmol m^{-2} s^{-1}) leaves had the lowest leaf Vc_{max} and J_{max}, respectively, with a significant difference in leaf Vc_{max} identified between Eth to all accessions (TukeyHSD; $P < 0.05$),

excluding Alaska, Elatius, Torsdag and Wando, whilst Wando had a significantly lower leaf J_{max} than all accessions (TukeyHSD; $P < 0.05$), with the exception of Alaska, Elatius, Eth and Torsdag (***Fig.2.8A&C***). Elatius had the lowest stipule Vc_{max} (28.71 ± 1.44 µmol m^{-2} s^{-1}) and J_{max} (47.84 ± 2.29 µmol m^{-2} s^{-1}), with a significantly lower stipule Vc_{max} identified to all accessions (TukeyHSD; $P < 0.05$), excluding Alaska, CamB, Eth, Pacco, Torsdag and Wando, and a significantly lower stipule J_{max} identified to all accessions (TukeyHSD; $P < 0.05$), exempting Alaska, CamB, Eth, Pacco, Torsdag and Wando (***Fig.2.8B&D***).

The leaves generally had a greater Vc_{max} and J_{max} compared to the stipules, with a significant difference seen in Vc_{max} between the leaves and stipules within each individual accession (TukeyHSD; $P < 0.01$), excluding Alaska, Cen, Eth, Torsdag and Wando (***Fig.2.8***). A significant difference was also seen in J_{max} between the leaves and stipules within each individual accession (TukeyHSD; $P < 0.05$), excluding Alaska, Cen, Eth and Wando (***Fig.2.8***).

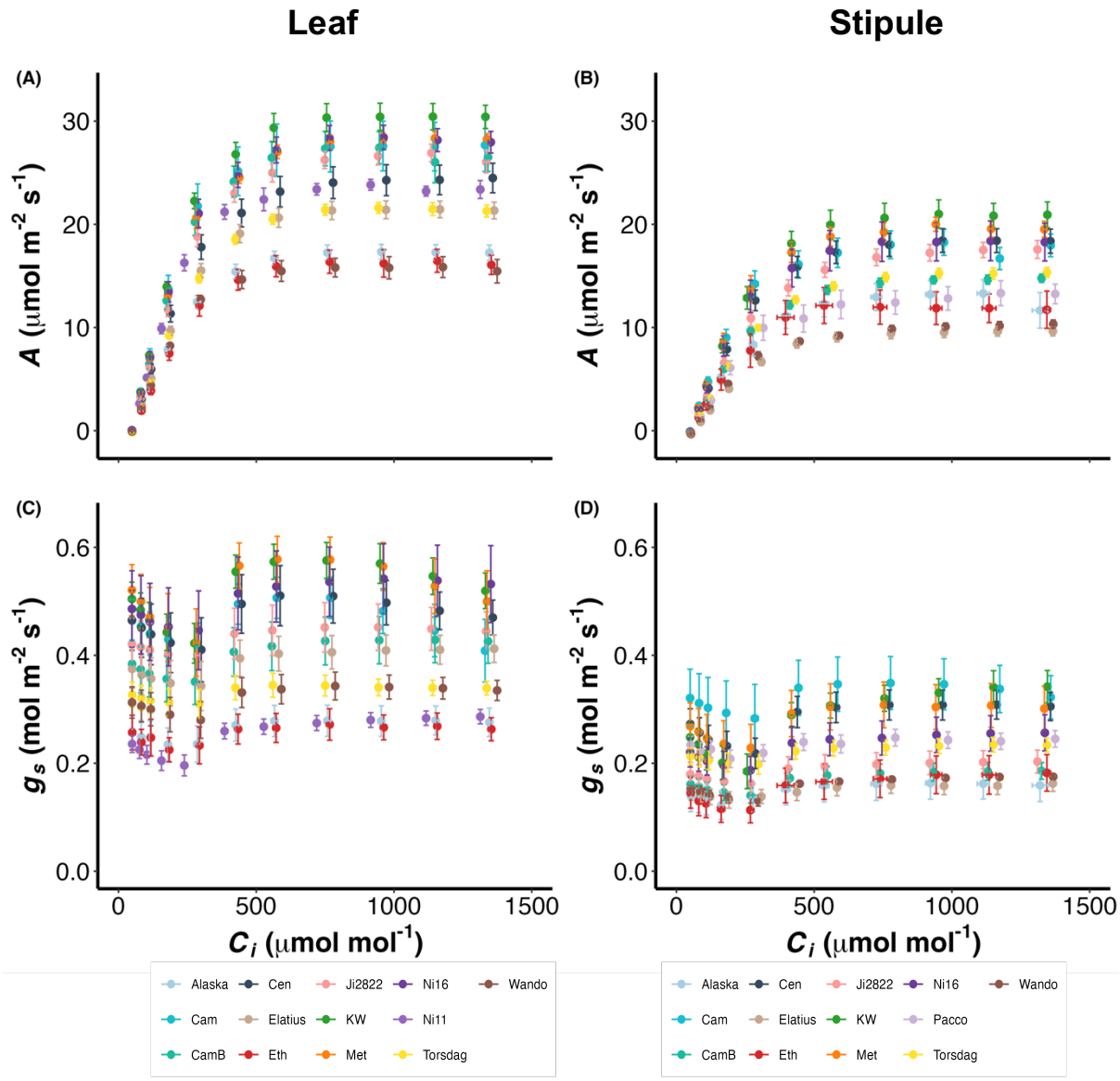

Figure 2.7. Variation in carbon assimilation (A) and stomatal conductance (g_s) in response to changing internal CO_2 concentration (C_i) across P. sativum accessions. Changes in **(A)** leaf and **(B)** stipule assimilation and **(C)** leaf and **(D)** stipule stomatal conductance were measured against increasing C_i within a Li-Cor 6800 at 23 °C and 1500 µmol m^{-2} s^{-1} photosynthetic photon flux density. Error bars represent mean ± SE (n = 6).

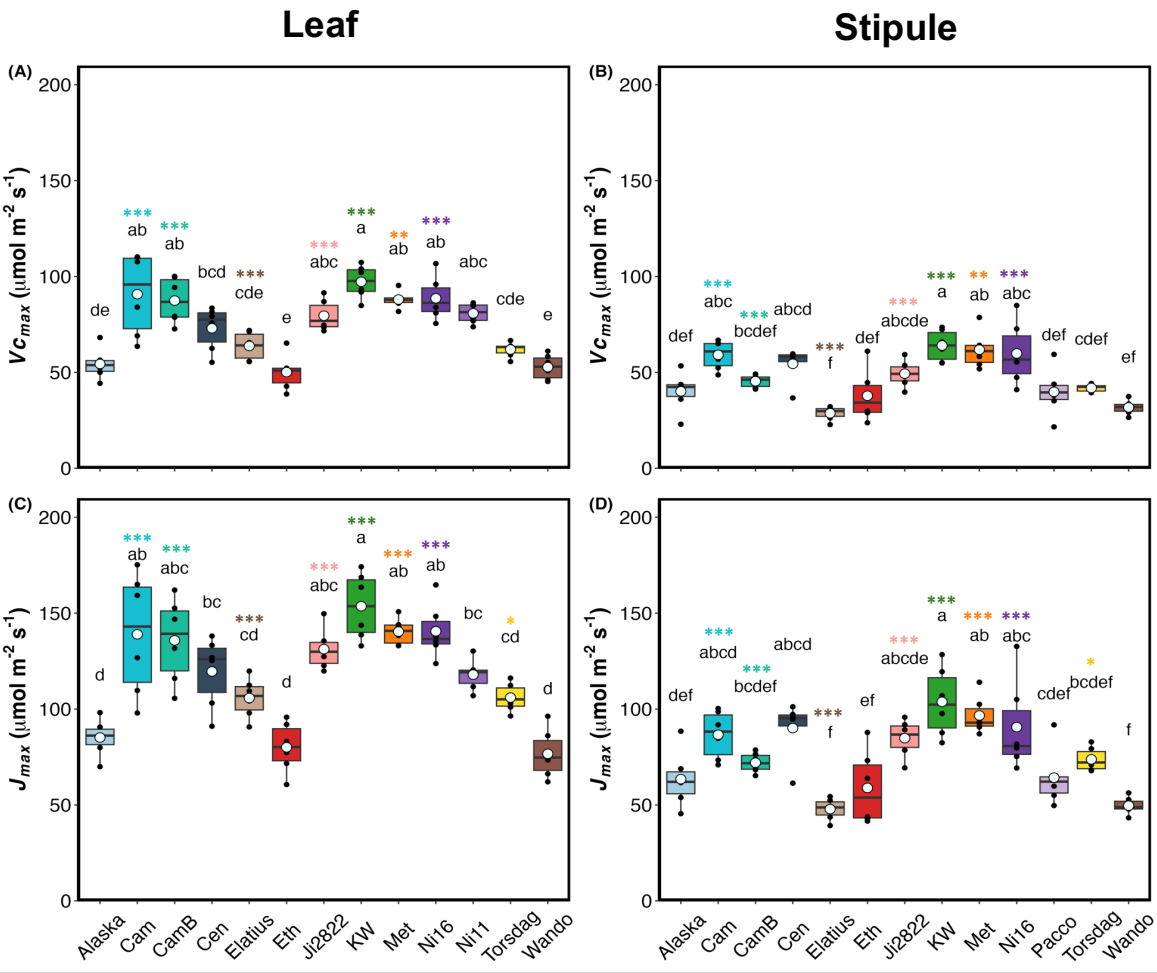

Figure 2.8. Variation in photosynthetic capacity across P. sativum accessions. Photosynthetic capacity were monitored as Vc_{max} (maximum rate of Rubisco activity) in the **(A)** leaves and **(B)** stipules and as J_{max} (maximum rate of electron transport) in the **(C)** leaves and **(D)** stipules. Measured within a Li-Cor 6800 at 1500 µmol m^{-2} s^{-1} photosynthetic photon flux density and 23 ^{o}C (n = 6). White dots symbolise the mean, whilst error bars represent mean ± SE. Different letters above each error bar represent significant differences in either Vc_{max} or J_{max} between *P. sativum* accessions ($P < 0.05$; TukeyHSD). Whilst the presence of * of the same colour indicates a significant difference in either Vc_{max} or J_{max} within an individual accession between the leaves and stipules, whereby * is $P < 0.05$, ** is $P < 0.01$ and *** is $P < 0.001$ (TukeyHSD).

2.3.4. Variation in Total Protein Content

Leaf and stipule total protein content significantly varied between the *P. sativum* accessions and foliar tissues ($F_{(11)} = 2.69$, $P < 0.01$) (***Fig.2.9***). Ji2822 had the highest leaf (327.6 ± 12.41 µg/g) and stipule (460 ± 72.36 µg/g) total protein content, which were significantly different to all accessions (TukeyHSD; $P < 0.05$), except from Cam, Cen and Ni11 in the leaves (***Fig.2.9***). The lowest total protein content were found in Met leaves (51.41 ± 19.95 µg/g) and Elatius stipules (63.85 ± 28.37 µg/g), whereby a significant difference were identified in leaf total protein content in Met to Cam, Cen, Ji2822 and Ni11 (TukeyHSD; $P < 0.05$), whilst Elatius was significantly different to Ji2822 and Pacco in stipule total protein content (TukeyHSD; $P < 0.05$) (***Fig.2.9***). However there were no significant differences identified in total protein content between the leaves and stipules within each individual accession (TukeyHSD; $P > 0.05$) (***Fig.2.9***). There were also no significant correlations identified between leaf or stipule Vc_{max} or J_{max} to total protein content ($P > 0.05$) (***Fig.2.10***).

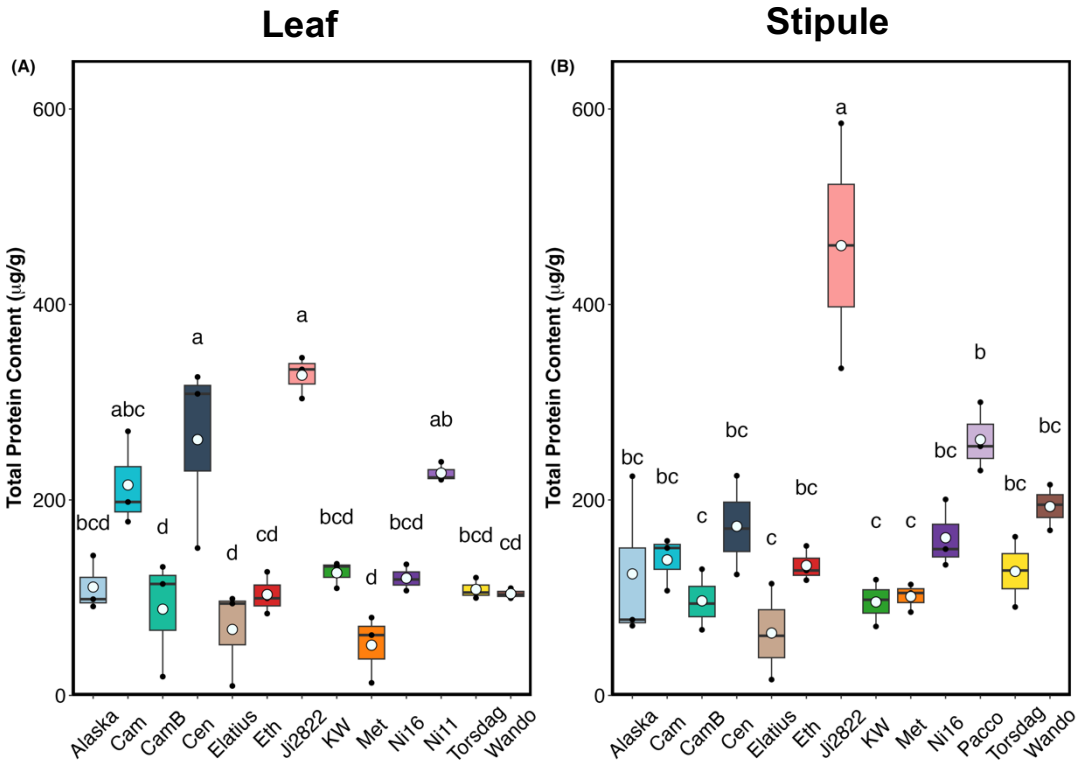

Figure 2.9. Variation in (A) leaf and (B) stipule total protein content across P. sativum accessions. Protein was extracted from three 0.5 cm^2 and three 1 cm^2 leaf disks via the MACHEREY-NAGEL protein extraction kit and standardised via leaf/stipule disk fresh weights. White dots symbolise the mean, whilst error bars represent mean ± SE (n = 3). Different letters above each error bar represent significant differences in total protein content between *P. sativum* accessions ($P < 0.05$; TukeyHSD). Whilst the presence of * of the same colour indicates a significant difference in total protein content within an individual accession between the leaves and stipules, whereby * is $P < 0.05$, ** is $P < 0.01$ and *** is $P < 0.001$ (TukeyHSD).

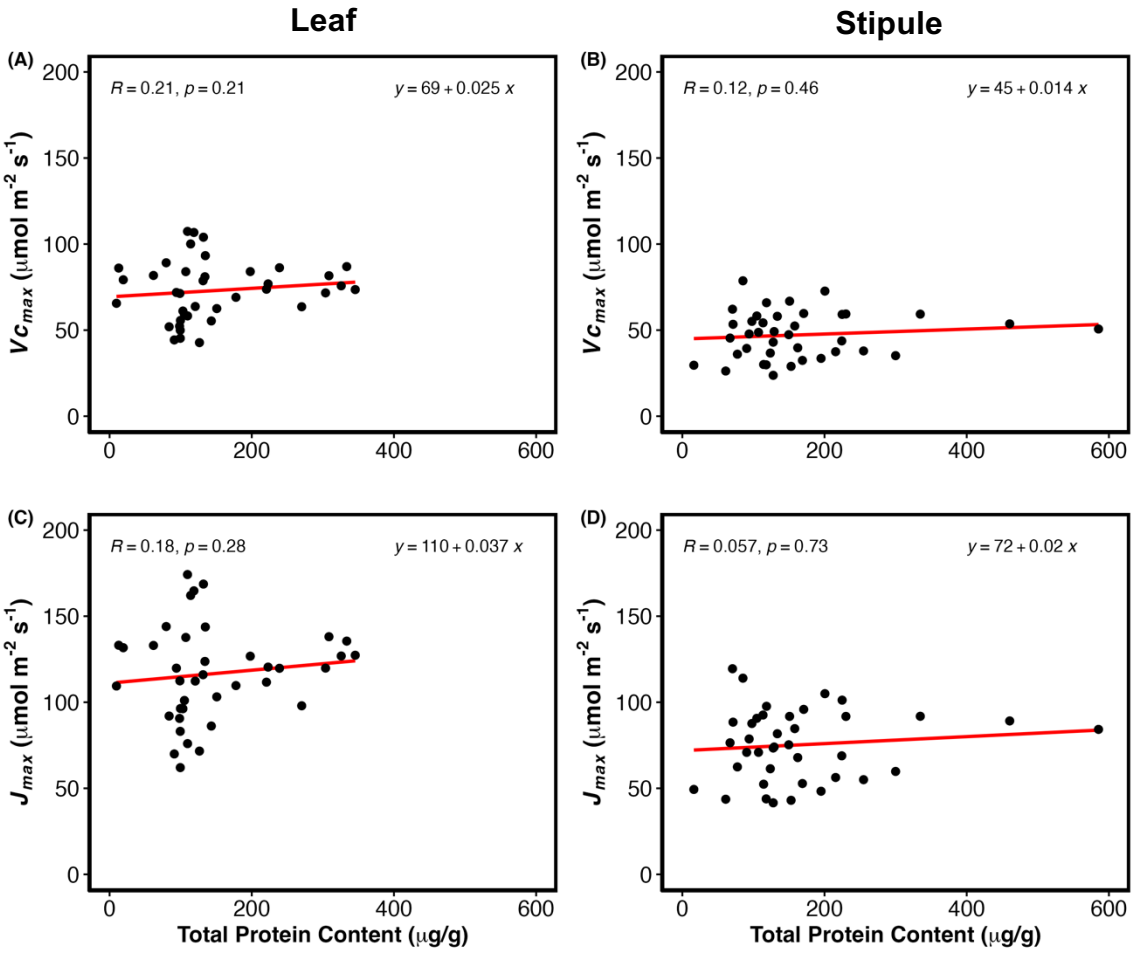

Figure 2.10. Spearmans correlation between photosynthetic capacity and total protein content in the leaves and stipules. Spearman's correlation coefficients (R) and linear regressions (represented as equations and red lines) were calculated between Vc_{max} (maximum rate of Rubisco activity) and total protein content in the **(A)** leaves and **(B)** stipules and between J_{max} (maximum rate of electron transport) and total protein content in the **(C)** leaves and **(D)** stipules. Gas exchange was measured within a Li-Cor 6800 at 1500 µmol m^{-2} s^{-1} photosynthetic photon flux density and 23 °C. Protein was extracted from three 0.5 cm^2 and three 1 cm^2 leaf disks via the MACHEREY-NAGEL protein extraction kit and standardised via leaf/stipule disk fresh weight. $P < 0.05$ indicates a significant relationship (n = 3).

2.3.5. Variation in Stomatal Characteristics

2.3.5.1. Stomatal Densities

Variation in leaf and stipule adaxial (AD) and abaxial (AB) stomatal densities (SD) were monitored across *P. sativum* accessions (***Fig.2.11***). Significant variations were apparent in stomatal densities between the different *P. sativum* accessions for the leaf AD ($F_{(12)}$ = 20.6, P < 0.001) and AB ($F_{(12)}$ = 5.23, P < 0.001) and stipule AD ($F_{(12)}$ = 19.63, P < 0.001) and AB ($F_{(12)}$ = 8.60, P < 0.001) surfaces, whilst an overall significant difference was also identified in SD between the different accessions and foliar tissues ($F_{(11)}$ = 2.59, P < 0.01) (***Fig.2.11***).

Leaf AD SD was greatest in Cam (191.5 ± 4.58 mm^{-2}), and significantly higher than Alaska, Elatius, Eth, Ni11, Torsdag and Wando (TukeyHSD; P < 0.05) (***Fig.2.11A***). Whilst CamB displayed the highest leaf AB density (201.3 ± 12.2 mm^{-2}), which was significantly greater than Elatius, Eth and Torsdag (TukeyHSD; P < 0.05) (***Fig.2.11C***). The lowest leaf SD were seen in Elatius on both the AD (98.38 ± 7.8 mm^{-2}) and AB (130.8 ± 2.55 mm^{-2}) surfaces, whereby a significant difference in leaf AD SD were apparent to all accessions (TukeyHSD; P < 0.05), except Eth, Torsdag and Wando, whilst a significantly lower leaf AB SD was identified to Cam, CamB, KW, Met and Ni16 (TukeyHSD; P < 0.05) (***Fig.2.11A&C***). In stipules, Ni16 had the highest AD SD (172.2 ± 9.19 mm^{-2}) and was significantly different to all accessions (TukeyHSD; P < 0.05), except Cam, CamB, Cen, Ji2822 and KW (***Fig.2.11B***). Meanwhile, Cam exhibited the greatest stipule AB SD (208.3 ± 6.01 mm^{-2}) and was significantly greater than Alaska, Elatius, Eth, Ji2822, Pacco and Torsdag (TukeyHSD; P < 0.05) (***Fig.2.11D***). The lowest stipule densities were observed in Torsdag (86.08 ± 2.24 mm^{-2}) for the AD surface and

in Eth (125.3 $\pm$ 6.89 mm^{-2}) for the AB surface, with a significantly lower stipule AD SD compared to all accessions (TukeyHSD; $P < 0.05$), excluding Elatius and Eth, whilst a significantly lower stipule AB SD was apparent between Eth to Cam, CamB, Cen, KW, Met, Ni16 and Wando (TukeyHSD; $P < 0.05$) (***Fig.2.11B&C***).

In general, the AB surface exhibited a greater SD than the AD surface for both the leaves and stipules, with a significant difference seen between the surfaces for Elatius (TukeyHSD; $P < 0.001$), Met (TukeyHSD; $P < 0.001$) and Torsdag (TukeyHSD; $P < 0.001$) stipules and for Eth leaves (TukeyHSD; $P < 0.01$) (***Table.2.7&Fig.2.11***). However there were no significant differences identified in either AD or AB SD between the leaves and stipules within each individual accession (TukeyHSD; $P > 0.05$) (***Fig.2.11***).

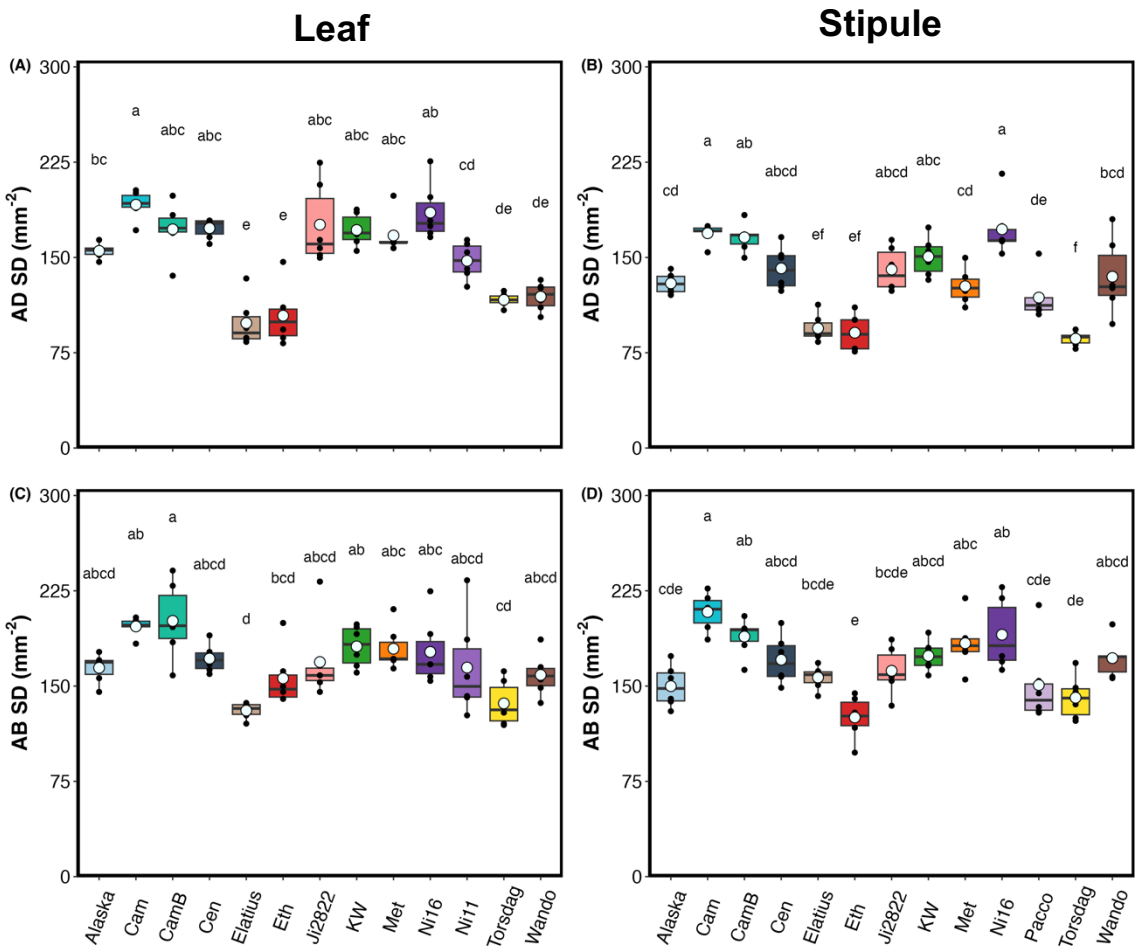

Figure 2.11. Variation in adaxial and abaxial leaf and stipule stomatal densities across P. sativum accessions. Stomatal densities (SD) were calculated for the adaxial (AD) **(A)** leaf and **(B)** stipule surface and for the abaxial (AB) **(C)** leaf and **(D)** stipule surface. Stomata were counted at 200x magnification in a 1 mm^2 grid (n = 6). White dots symbolise the mean, whilst error bars represent mean ± SE. Different letters above each error bar represent significant differences in either AD or AB SD between *P. sativum* accessions ($P < 0.05$; TukeyHSD). Whilst the presence of * of the same colour indicates a significant difference in either AD or AB SD within an individual accession between the leaves and stipules, whereby * is $P < 0.05$, ** is $P < 0.01$ and *** is $P < 0.001$ (TukeyHSD). Significant differences in SD between the AD and AB surfaces can be found in ***Table.2.7***.

Table 2.7. Statistical P values between adaxial (AD) and abaxial (AB) stomatal densities (SD). Statistical differences were generated from ***Fig.2.11*** via TukeyHSD comparisons of AD vs AB SD of the same foliar tissue for each individual accession, whereby * is $P < 0.05$, ** is $P < 0.01$ and *** is $P < 0.001$ (TukeyHSD). Stomata were counted at 200x magnification in a 1 mm^2 grid (n = 6).

Accession	AD vs AB SD *P* values	
	Leaves	Stipules
Alaska	1.00	1.00
Cam	1.00	0.20
CamB	0.88	1.00
Cen	1.00	0.87
Elatius	0.68	**2.62E-05***
Eth	**3.01E-03** **	0.51
Ji2822	1.00	1.00
KW	1.00	1.00
Met	1.00	**4.50E-04***
Ni16	1.00	1.00
Ni11	1.00	NA
Pacco	NA	0.68
Torsdag	1.00	**9.10E-04***
Wando	0.18	0.32

2.3.5.2. Stomatal Sizes

Variation in leaf and stipule AD and AB stomatal sizes (SS: consisting of pore length; PL and guard cell length; GCL) were monitored across *P. sativum* accessions (***Fig.2.12***). Significant variation were apparent in stomatal sizes between the different *P. sativum* accessions for both the leaf AD ($F_{(12)} = 3.83$, $P < 0.001$) and AB ($F_{(12)} = 7.03$, $P < 0.001$) PL and AD ($F_{(12)} = 2.83$, $P < 0.01$) and AB ($F_{(12)} = 4.97$, $P < 0.001$) GCL, as well as the stipule AD ($F_{(12)} = 2.68$, $P < 0.01$) and AB ($F_{(12)} = 2.77$, $P < 0.01$) PL and AD ($F_{(12)} = 2.99$, $P < 0.01$) and AB ($F_{(12)} = 3.16$, $P < 0.01$) GCL. An overall significant variation were also identified in PL ($F_{(11)} = 4.08$, $P < 0.001$) and GCL ($F_{(11)} = 2.74$, $P < 0.01$) between the different accessions and foliar tissues (***Fig.2.12***).

Pore length was lowest in Cam on both leaf surfaces (AD; 14.05 $\pm$ 0.44 µm, AB; 14.74 $\pm$ 0.49 µm) with significant differences compared to Ni11 and Torsdag (TukeyHSD; $P < 0.05$) for the AD surface and to CamB, Eth, Met, Ni11 and Torsdag (TukeyHSD; $P < 0.05$) for AB surface (***Fig.2.12A&C***). In contrast, Torsdag and Met exhibited the largest leaf AD (17.43 $\pm$ 0.48 µm) and AB (19.4 $\pm$ 0.61 µm) PL respectively, with Torsdag leaf AD PL being significantly greater than Cam, Cen, Elatius and KW (TukeyHSD; $P < 0.05$), whilst Met leaf AB PL was significantly different to all accessions (TukeyHSD; $P < 0.05$), excluding CamB, Eth, Ni11 and Torsdag (***Fig.2.12A&C***). KW exhibited the largest (18.39 $\pm$ 0.59 µm), whereas Alaska had the smallest (15.43 $\pm$ 0.54 µm) stipule AD PL, with a significant difference identified between them (TukeyHSD; $P < 0.05$) (***Fig.2.12B***). The greatest stipule AB PL was found in Ji2822 (18.36 $\pm$ 0.54 µm), which was significantly different to Cam and Alaska (smallest stipule AB PL; 15.52 $\pm$ 0.73 µm and only significantly smaller than Ji2822) (TukeyHSD; $P < 0.05$) (***Fig.2.12D***). AB GCL

was greatest in Torsdag leaves (26.92 ± 0.56 µm) and Elatius stipules (26.21 ± 0.34 µm), with a significant difference in the leaf AB GCL to Cam and KW (TukeyHSD; $P < 0.05$) and a significant difference in stipule AB GCL to Cam (smallest stipule AB GCL; 22.38 ± 0.63 µm) (TukeyHSD; $P < 0.05$) (***Fig.2.12G&H***). Whilst Cam was significantly smaller than Elatius, Eth and Ji2822 in stipule AB GCL (TukeyHSD; $P < 0.05$) (***Fig.2.12H***). Cam also exhibited the smallest leaf AB GCL (22.4 ± 0.68 µm) with a significant difference to CamB, Met, Ni11 and Torsdag (TukeyHSD; $P < 0.05$) (***Fig.2.12G***). However, no significant differences were identified in leaf or stipule AD GCL between any of the accessions (TukeyHSD; $P > 0.05$) (***Fig.2.12E&F***).

In general, both the leaves and stipules exhibited larger PL and GCL on the AB surfaces than the AD, however, the only significant difference detected was in CamB leaves between AD and AB GCL (TukeyHSD; $P < 0.05$) (***Table.2.8&Fig.2.12***). AD PL were generally larger in the stipules than the leaves, with a significant difference identified in AD PL between KW leaves and stipules (TukeyHSD; $P < 0.001$) (***Fig.2.12***). However there were no significant differences identified in AD GCL or in AB PL or GCL between the leaves and stipules within each individual accession (TukeyHSD; $P > 0.05$) (***Fig.2.12***).

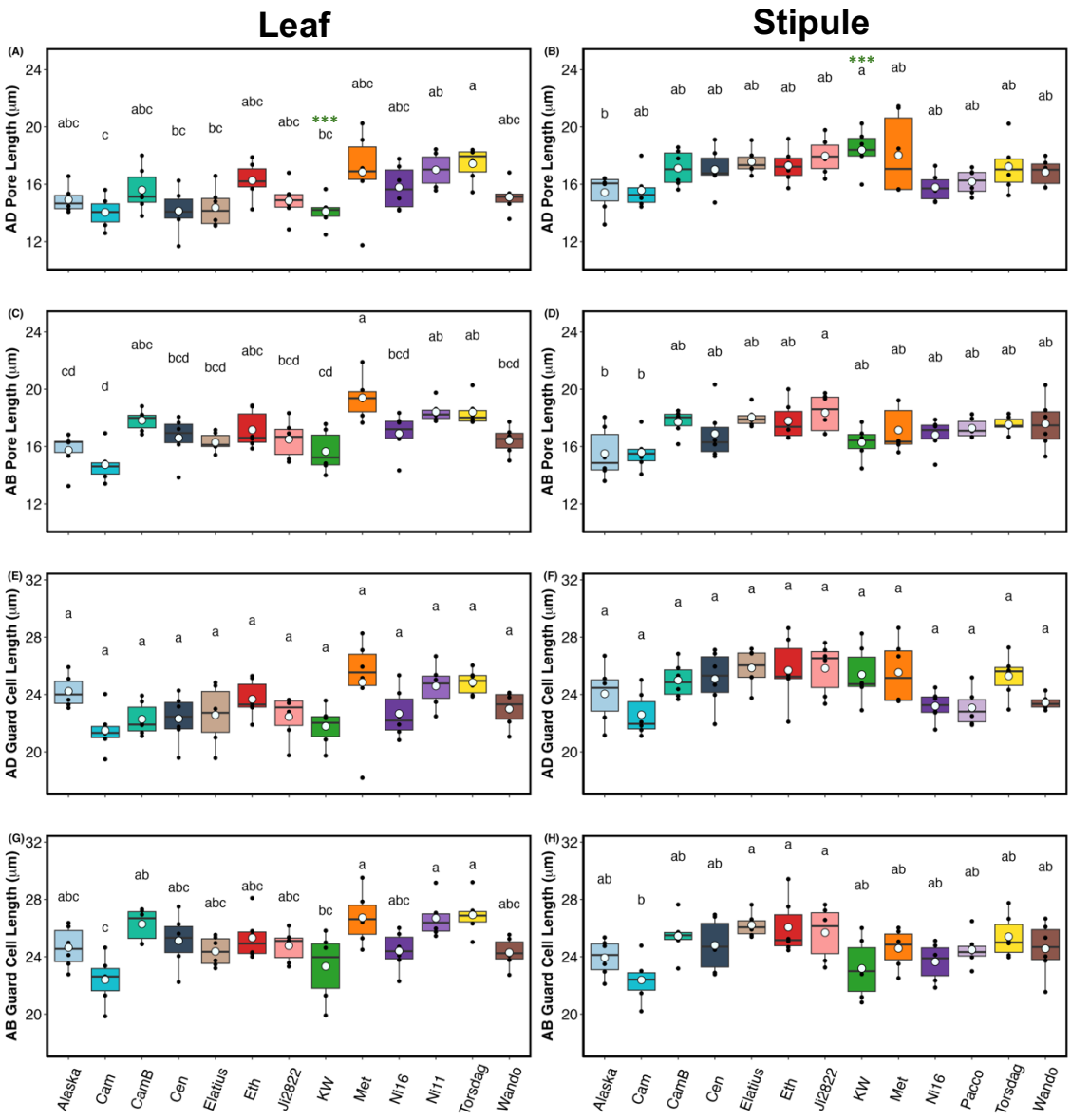

Figure 2.12. Variation in leaf and stipule adaxial and abaxial stomatal sizes across P. sativum accessions. Stomatal sizes were calculated as pore length (PL) for the adaxial (AD) **(A)** leaves and **(B)** stipules, and for the abaxial (AB) **(C)** leaves and **(D)** stipules, and as guard cell length (GCL) for the AD **(E)** leaves and **(F)** stipules and for the AB **(G)** leaves and **(H)** stipules. Stomatal sizes were measured at 400x magnification (n = 6). White dots symbolise the mean, whilst error bars represent mean ± SE. Different letters above each error bar represent significant differences in either AD or AB PL or GCL between *P. sativum* accessions ($P < 0.05$; TukeyHSD). Whilst the presence of * of the same colour indicates a significant difference in either AD or AB PL or GCL within an individual accession between the leaves and stipules, whereby * is $P < 0.05$, ** is $P < 0.01$ and *** is $P < 0.001$ (TukeyHSD). Significant differences in stomatal size between the AD and AB surfaces can be found in ***Table.2.8***.

Table 2.8. Statistical P values between adaxial (AD) and abaxial (AB) stomatal sizes. Statistical differences were generated from ***Fig.2.12*** via TukeyHSD comparisons of AD vs AB pore length (PL) or guard cell length (GCL) of the same foliar tissue for each individual accession, whereby * is $P < 0.05$, ** is $P < 0.01$ and *** is $P < 0.001$ (TukeyHSD). Stomatal sizes were measured at 400x magnification (n = 6).

Accession	AD vs AB PL *P* values		AD vs AB GCL *P* values	
	Leaves	Stipules	Leaves	Stipules
Alaska	1.00	1.00	1.00	1.00
Cam	1.00	1.00	1.00	1.00
CamB	0.80	1.00	**0.02***	1.00
Cen	0.56	1.00	0.67	1.00
Elatius	0.97	1.00	1.00	1.00
Eth	1.00	1.00	1.00	1.00
Ji2822	1.00	1.00	0.96	1.00
KW	1.00	0.89	1.00	0.98
Met	0.47	1.00	1.00	1.00
Ni16	1.00	1.00	1.00	1.00
Ni11	1.00	NA	0.99	NA
Pacco	NA	1.00	NA	1.00
Torsdag	1.00	1.00	0.99	1.00
Wando	1.00	1.00	1.00	1.00

2.3.5.3. Maximum Anatomical g_s

SD and SS were used to calculate the maximum anatomical g_s (gs_{max}), whereby significant differences in gs_{max} were identified between the different *P. sativum* accessions for the leaf AD ($F_{(12)} = 11.75$, $P < 0.001$) and AB ($F_{(12)} = 3.28$, $P < 0.001$) and stipule AD ($F_{(12)} = 10.91$, $P < 0.001$) and AB ($F_{(12)} = 8.25$, $P < 0.001$) surfaces, whilst a significant difference were also identified in gs_{max} between the different accessions and foliar tissues ($F_{(11)} = 1.84$, $P < 0.05$) (***Fig.2.13***).

KW had the highest leaf AD gs_{max} (1.20 ± 0.04 mol m^{-2} s^{-1}) and was significantly different to Elatius, Eth, Torsdag and Wando (TukeyHSD; $P < 0.05$), whilst Eth displayed the lowest leaf AD gs_{max} (0.61 ± 0.03 mol m^{-2} s^{-1}), and was significantly different to all other accessions (TukeyHSD; $P < 0.05$), excluding Elatius, Torsdag and Wando (***Fig.2.13A***). CamB had the highest leaf AB gs_{max} (1.42 ± 0.10 mol m^{-2} s^{-1}), whereas Torsdag had the lowest (1.00 ± 0.07 mol m^{-2} s^{-1}), with a significant difference identified between CamB AB leaves to Elatius and Torsdag (TukeyHSD; $P < 0.05$), whilst Torsdag AB leaves were significantly different to CamB and Ni11 (TukeyHSD; $P < 0.05$) (***Fig.2.13C***). CamB displayed the greatest AD (1.22 ± 0.03 mol m^{-2} s^{-1}) and AB (1.45 ± 0.04 mol m^{-2} s^{-1}) stipule gs_{max}, with a significantly higher stipule AD gs_{max} to Alaska, Elatius, Eth, Pacco and Torsdag (TukeyHSD; $P < 0.05$), whilst a significant difference in stipule AB gs_{max} was identified to Alaska, Eth, Pacco and Torsdag (TukeyHSD; $P < 0.05$) (***Fig.2.13B&D***). Torsdag AD (0.64 ± 0.04 mol m^{-2} s^{-1}) and Eth AB (0.96 ± 0.06 mol m^{-2} s^{-1}) exhibited the lowest stipule gs_{max}, with a significant difference identified to all accessions excluding Alaska, Elatius, Eth and Pacco in stipule AD gs_{max} (TukeyHSD; $P < 0.05$), and to all accessions with the exception of

Alaska, Elatius, Pacco and Torsdag in stipule AB gs_{max} (TukeyHSD; $P < 0.05$) (***Fig.2.13B&D***).

The AB surface of the leaves and stipules generally had a greater gs_{max} than the AD surface, with a significant difference seen between the surfaces for Eth (TukeyHSD; $P < 0.001$) and Wando (TukeyHSD; $P < 0.05$) leaves and for Elatius (TukeyHSD; $P < 0.001$) and Torsdag (TukeyHSD; $P < 0.01$) stipules (***Table.2.9&Fig.2.13***). However there were no significant differences identified in either AD or AB gs_{max} between the leaves and stipules within each individual accession (TukeyHSD; $P > 0.05$) (***Fig.2.13***).

2.3.5.4. Relationship Between Stomatal Densities, Sizes and Conductance

A significant negative correlation was identified between stipule PL and SD (R = -0.21, $P < 0.01$) and between stipule GCL and SD (R = -0.29, $P < 0.001$) (***Fig.2.14***). Whilst a significant positive correlation were found between gs_{max} and SD in the leaves (R = 0.74, $P < 0.001$) and stipules (R = 0.8, $P < 0.001$) (***Fig.2.15***) and between stipule PL and gs_{max} (R = 0.24, $P < 0.01$) (***Fig.2.16***). Significant positive correlations were also identified between g_s and AD SD (R = 0.35, $P < 0.01$), as well as g_s and AB SD in the leaves (R = 0.24, $P < 0.05$) (***Fig.2.17***). Leaf AD PL and g_s were negatively correlated (R = -0.35, $P < 0.01$), as was leaf AD GCL and g_s (R = -0.37, $P < 0.001$) and stipule AB GCL and g_s (R = -0.23, $P < 0.05$) (***Fig.2.18***).

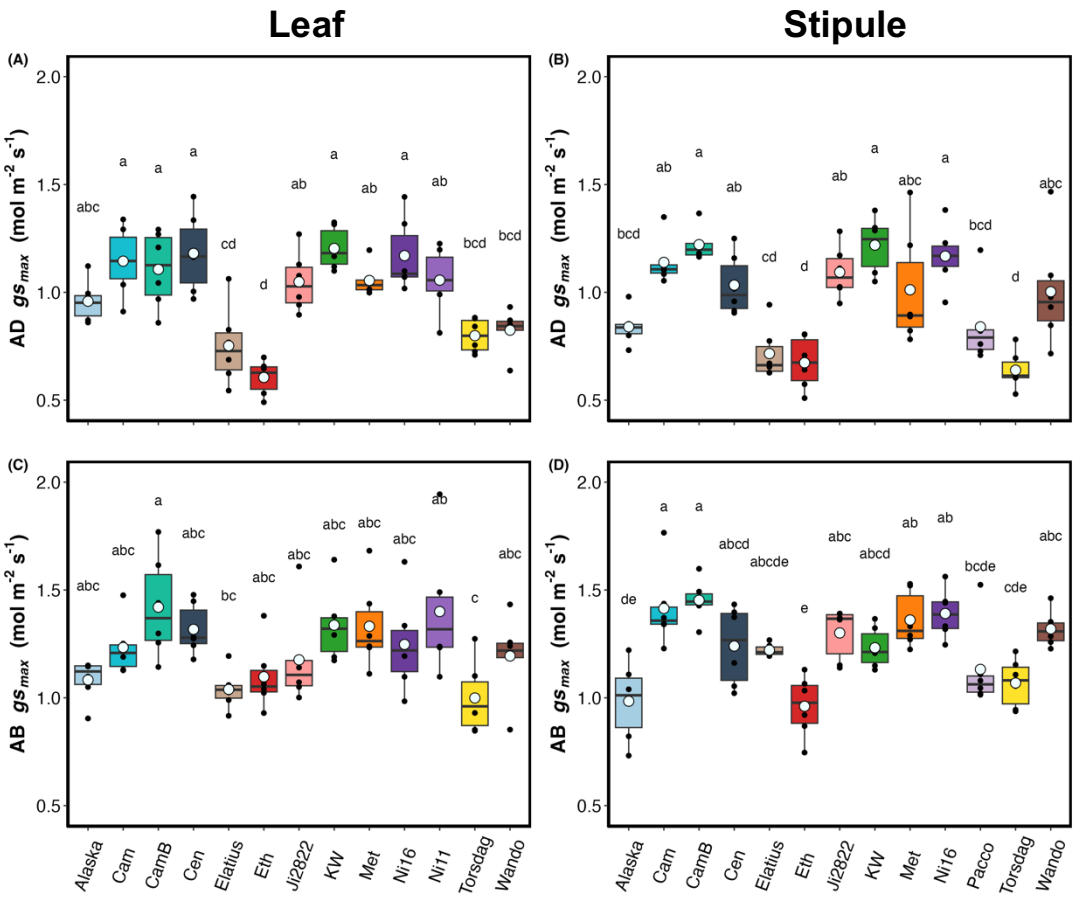

Figure 2.13. Variation in adaxial and abaxial leaf and stipule gs_{max} across P. sativum accessions. Mean maximum anatomical g_s (gs_{max}) were generated for the adaxial (AD) **(A)** leaves and **(B)** stipules, and for the abaxial (AB) **(C)** leaves and **(D)** stipules, via the Dow et al. (2014a) method using stomatal densities and sizes from the AD and AB surfaces. Stomata were counted at a 200x magnification in a 1 mm^2 grid, whilst stomatal sizes (pore and guard cell length) were measured at 400x magnification (n = 6). White dots symbolise the mean, whilst error bars represent mean ± SE. Different letters above each error bar represent significant differences in either AD or AB gs_{max} between *P. sativum* accessions ($P < 0.05$; TukeyHSD). Whilst the presence of * of the same colour indicates a significant difference in either AD or AB gs_{max} within an individual accession between the leaves and stipules, whereby * is $P < 0.05$, ** is $P < 0.01$ and *** is $P < 0.001$ (TukeyHSD). Significant differences in gs_{max} between the AD and AB surfaces can be found in ***Table.2.9***.

Table 2.9. Statistical P values between adaxial (AD) and abaxial (AB) maximum anatomical stomatal conductance (gs_{max}). Statistical differences were generated from ***Fig.2.13*** via TukeyHSD comparisons of AD vs AB gs_{max} of the same foliar tissue for each individual accession, whereby * is $P < 0.05$, ** is $P < 0.01$ and *** is $P < 0.001$ (TukeyHSD). gs_{max} was calculated via the Dow et al. (2014a) method using stomatal densities and sizes from the AD and AB surfaces. Stomata were counted at a 200x magnification in a 1 mm^2 grid, whilst stomatal sizes (pore and guard cell length) were measured at 400x magnification (n = 6).

Accession	AD vs AB gs_{max} *P* values	
	Leaves	**Stipules**
Alaska	1.00	1.00
Cam	1.00	0.60
CamB	0.27	0.93
Cen	1.00	0.99
Elatius	0.50	**5.36E-05***
Eth	**1.10E-04***	0.49
Ji2822	1.00	0.99
KW	1.00	1.00
Met	0.59	0.09
Ni16	1.00	0.96
Ni11	0.11	NA
Pacco	NA	0.45
Torsdag	0.99	**2.97E-03**
Wando	**0.04***	0.25

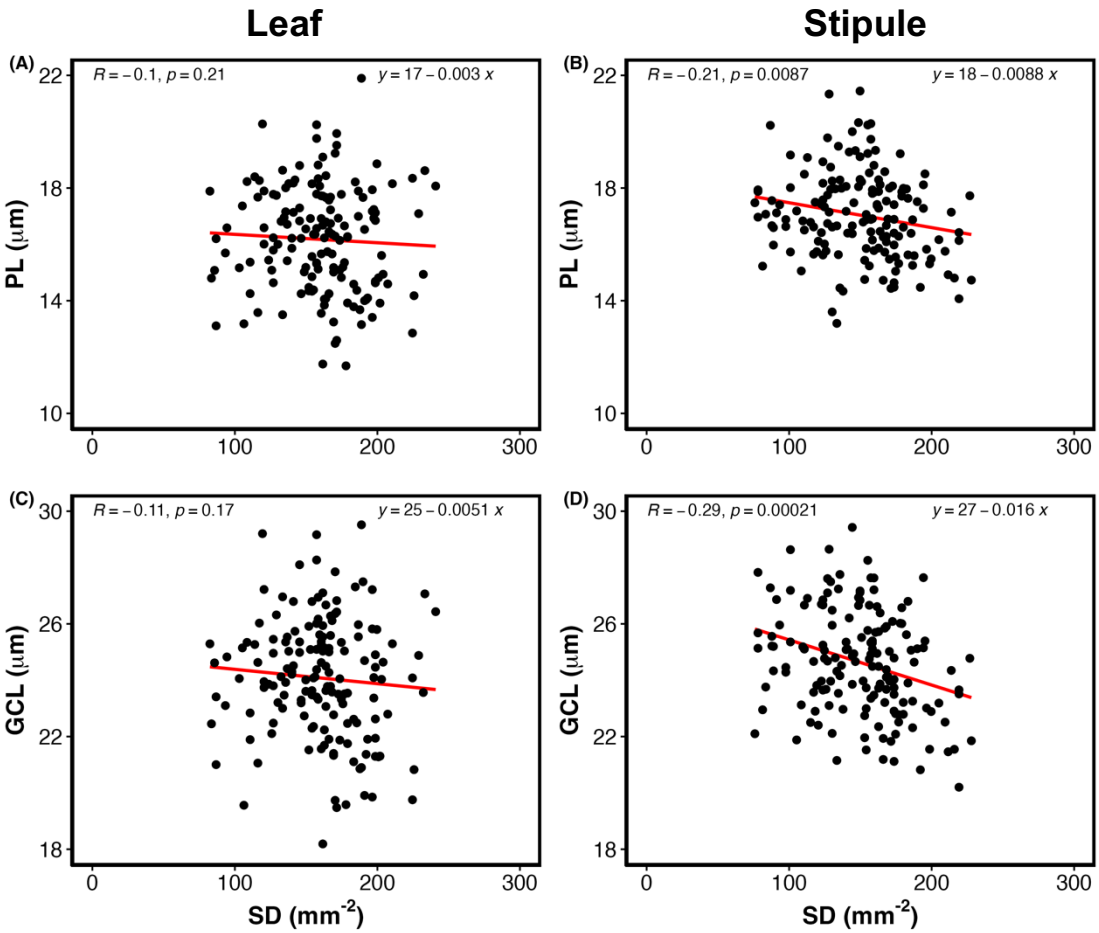

Figure 2.14. Spearmans correlation between stomatal densities and sizes in the leaves and stipules. Correlations between pore length (PL) and stomatal density (SD) in the **(A)** leaves and **(B)** stipules and correlations between guard cell length (GCL) and SD in the **(C)** leaves and **(D)** stipules. Stomatal sizes were measured at 400x magnification, whilst stomata were counted at 200x magnification in a 1 mm^2 grid (n = 6). Spearman's correlation coefficients (R) and linear regressions (represented as equations and red lines) were calculated for each anatomical component. $P < 0.05$ indicates a significant relationship.

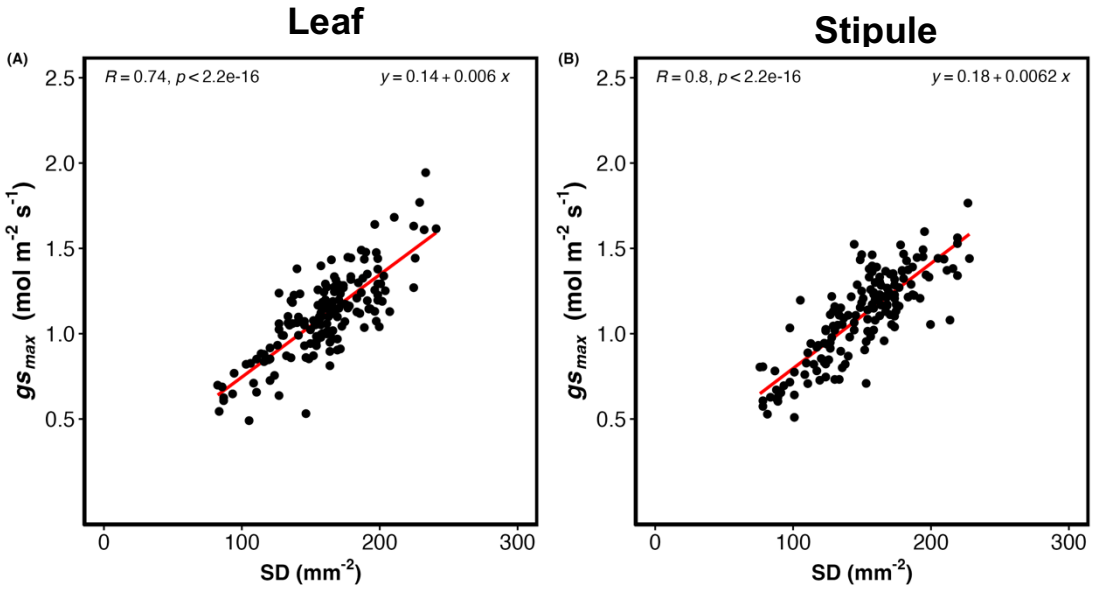

Figure 2.15. Spearmans correlation between stomatal densities and gs_{max} in the leaves and stipules. Correlation between stomatal densities (SD) and maximum anatomical g_s (gs_{max}) in the **(A)** leaves and **(B)** stipules. gs_{max} was calculated via the Dow et al. (2014a) method using stomatal densities and sizes. Stomata were counted at a 200x magnification in a 1 mm^2 grid, whilst stomatal sizes (pore and guard cell length) were measured at 400x magnification (n = 6). Spearman's correlation coefficients (R) and linear regressions (represented as equations and red lines) were calculated for each anatomical component. $P < 0.05$ indicates a significant relationship.

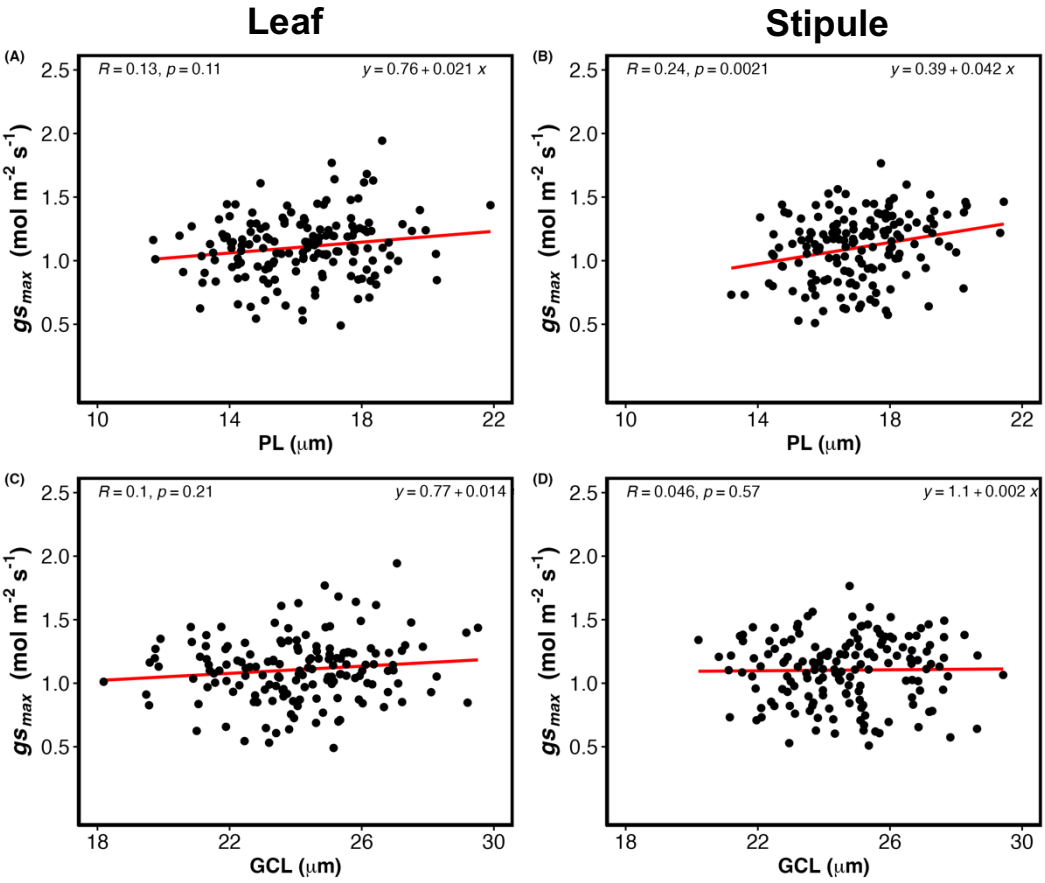

Figure 2.16. Spearmans correlation between stomatal sizes and gs_{max} in the leaves and stipules. Correlations between maximum anatomical g_s (gs_{max}) and stomatal pore length (PL) in the **(A)** leaves and **(B)** stipules and correlations between gs_{max} and stomatal guard cell length (GCL) in the **(C)** leaves and **(D)** stipules were generated. gs_{max} was calculated via the Dow et al. (2014a) method using stomatal densities and sizes. Stomata were counted at a 200x magnification in a 1 mm^2 grid, whilst stomatal sizes (pore and guard cell length) were measured at 400x magnification (n = 6). Spearman's correlation coefficients (R) and linear regressions (represented as equations and red lines) were calculated for each anatomical component. $P < 0.05$ indicates a significant relationship.

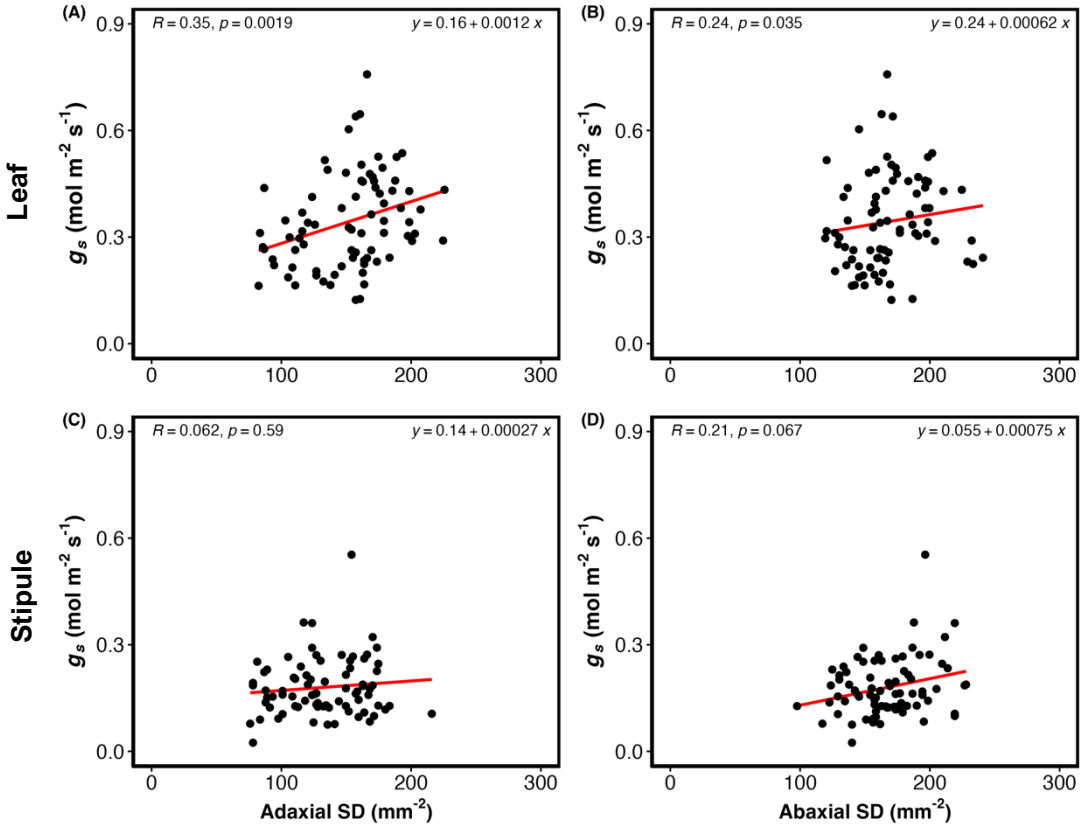

Figure 2.17. Spearmans correlation between stomatal densities and conductance in the leaves and stipules. Correlations between stomatal conductance (g_s) and the adaxial **(A)** leaves and **(C)** stipules stomatal densities (SD) and the abaxial **(B)** leaves and **(D)** stipules SD. Stomata were counted at 200x magnification in a 1 mm^2 grid (n = 6). g_s was measured at 400 µmol mol^{-1} intercellular CO_2 concentration within a Li-Cor 6800 at 23 ^oC and 1500 µmol m^{-2} s^{-1} photosynthetic photon flux density. Spearman's correlation coefficients (R) and linear regressions (represented as equations and red lines) were calculated for each SD against g_s. $P < 0.05$ indicates a significant relationship.

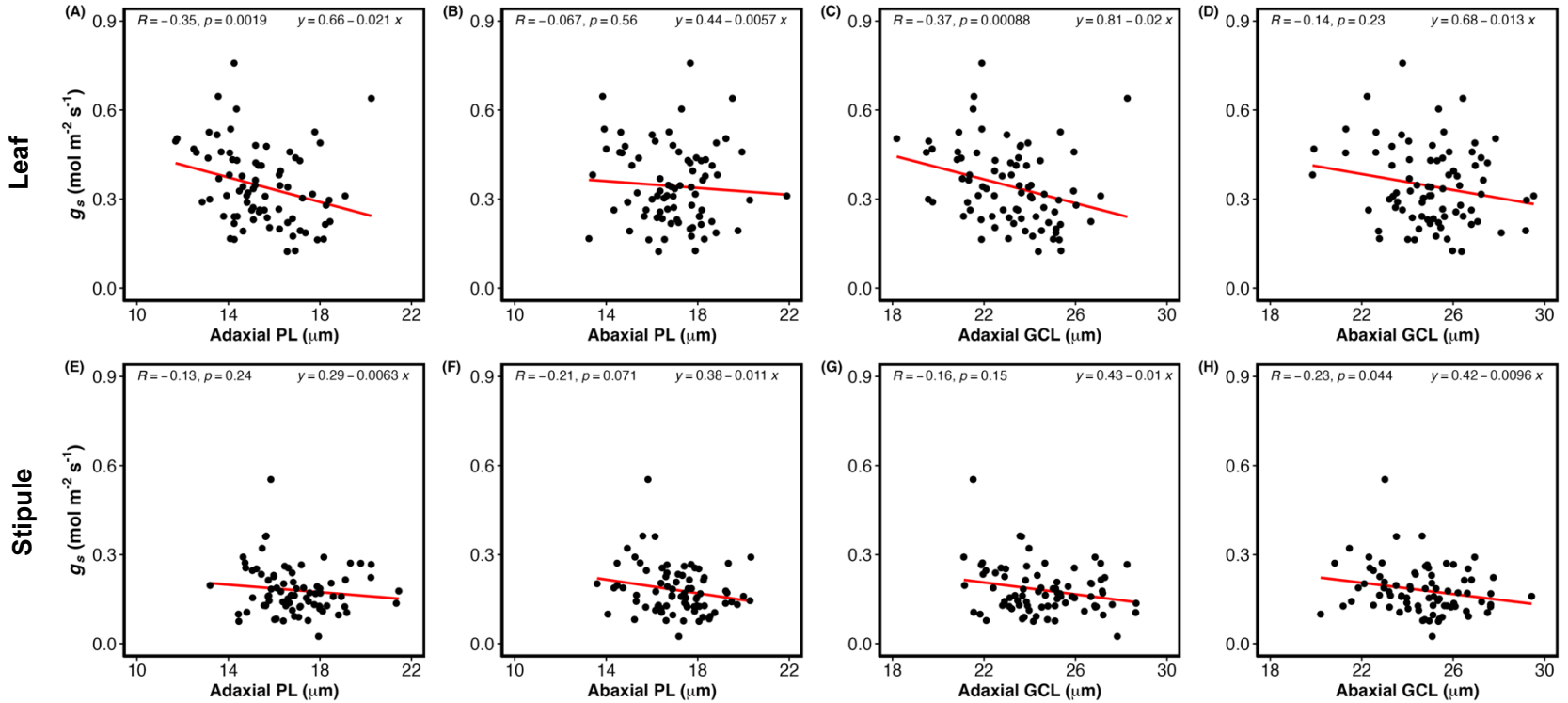

Figure 2.18. Spearmans correlation between stomatal sizes and conductance in the leaves and stipules. Correlations between stomatal conductance (g_s) and the adaxial **(A)** leaves and **(E)** stipules stomatal pore length (PL) and the abaxial **(B)** leaves and **(F)** stipules PL, and correlations between g_s and the adaxial **(C)** leaves and **(G)** stipules stomatal guard cell length (GCL) and the abaxial **(D)** leaves and **(H)** stipules GCL. Stomatal sizes were measured at 400x magnification (n = 6). g_s was measured at 400 µmol mol^{-1} intercellular CO_2 concentration within a Li-Cor 6800 at 23 ºC and 1500 µmol m^{-2} s^{-1} photosynthetic photon flux density. Spearman's correlation coefficients (R) and linear regressions (represented as equations and red lines) were calculated for each PL and GCL against g_s. $P < 0.05$ indicates a significant relationship.

2.3.5.5. Stomatal Kinetics

Leaf and stipule *A*, g_s and *i*WUE were observed following a step increase in light intensity across the *P. sativum* accessions (***Fig.2.19***). Steady state values at 100 and 1000 µmol m^{-2} s^{-1} PPFD were calculated for *A* (*A100* and *A1000*) and g_s (*gs100* and *gs1000*) respectively (***Fig.2.20***), and significant differences were found for *A100* ($F_{(11)}$ = 12.96, $P < 0.001$), *A1000* ($F_{(11)}$ = 26.34, $P < 0.001$), *gs100* ($F_{(11)}$ = 13.31, $P < 0.001$) and *gs1000* ($F_{(11)}$ = 26.92, $P < 0.001$), between the different accessions and foliar tissues (***Fig.2.20***).

Ji2822 exhibited a significantly higher leaf *A100* (5.05 ± 0.12 µmol m^{-2} s^{-1}) and leaf *gs100* (0.30 ± 0.01 mol m^{-2} s^{-1}), than the majority of accessions (TukeyHSD; $P < 0.05$), with the exception of Cam and CamB for leaf *A100* and Cam for leaf *gs100* (***Fig.2.20A&E***). The lowest leaf *A100* accession was Ni16 (3.61 ± 0.20 µmol m^{-2} s^{-1}), with a significantly lower *A100* to Cam, CamB, Ji2822 and Ni11 (TukeyHSD; $P < 0.05$) (***Fig.2.20A***). Whilst, KW had the lowest leaf *gs100* (0.16 ± 0.01 mol m^{-2} s^{-1}) and was significantly lower than Alaska, Cam, CamB, Elatius, Ji2822 and Met (TukeyHSD; $P < 0.05$) (***Fig.2.20E***). KW displayed a significantly greater stipule *A100* (4.45 ± 0.16 µmol m^{-2} s^{-1}) to all accessions (TukeyHSD; $P < 0.05$), excluding Cam, CamB and Pacco (***Fig.2.20B***). The lowest stipule *A100* was observed by Elatius (2.03 ± 0.05 µmol m^{-2} s^{-1}), with a significantly lower stipule *A100* to all accessions (TukeyHSD; $P < 0.05$), with the exception of Met (***Fig.2.20B***). Pacco displayed a significantly greater stipule *gs100* (0.24 ± 0.004 mol m^{-2} s^{-1}) to all accessions (TukeyHSD; $P < 0.05$) (***Fig.2.20F***). Whilst Elatius exhibited a significantly lower stipule *gs100* (0.08 ± 0.003 mol m^{-2} s^{-1}) to all accessions (TukeyHSD; $P < 0.05$) (***Fig.2.20F***).

At the higher light intensity, Cam leaves had a significantly higher *A1000* (22.60 ± 0.21 μmol m^{-2} s^{-1}) relative to all accessions (TukeyHSD; $P < 0.05$), excluding Ji2822 (***Fig.2.20C***). Whilst the lowest leaf *A1000* accession was Wando (13.83 ± 0.33 μmol m^{-2} s^{-1}), which was significantly lower (TukeyHSD; $P < 0.05$) to all accessions except Torsdag and Cen (***Fig.2.20C***). Ji2822 exhibited the greatest leaf *gs1000* (0.50 ± 0.01 mol m^{-2} s^{-1}) which was significantly greater than all the other accessions (TukeyHSD; $P < 0.05$), with the exception of Cam and Met (***Fig.2.20G***). Ni11 had a significantly lower leaf *gs1000* (0.27 ± 0.01 mol m^{-2} s^{-1}), compared with all accessions (TukeyHSD; $P < 0.05$), excluding Torsdag, Ni16, KW, Eth and Alaska (***Fig.2.20G***). The highest stipule *A1000* (18.19 ± 0.65 μmol m^{-2} s^{-1}) and *gs1000* (0.36 ± 0.02 mol m^{-2} s^{-1}) was found in KW, which were significantly greater than all accessions (TukeyHSD; $P < 0.05$), except from Cam and Pacco (***Fig.2.20D&H***). Whilst Elatius had a significantly lower stipule *A1000* (6.58 ± 0.07 μmol m^{-2} s^{-1}) and *gs1000* (0.12 ± 0.003 mol m^{-2} s^{-1}), to the other accessions (TukeyHSD; $P < 0.05$), exempting Wando (***Fig.2.20D&H***).

The maximum *i*WUE (*i*WUE_{max}) were calculated for both leaves and stipules, with a significant difference identified in *i*WUE_{max} between the *P. sativum* accessions and foliar tissues ($F_{(11)} = 3.86$, $P < 0.001$) (***Fig.2.21***). Ni11 was significantly greater in leaf *i*WUE_{max} (86.71 ± 2.64 μmol mol^{-1}) compared to the other accessions (TukeyHSD; $P < 0.05$), excluding KW (***Fig.2.21A***). Whilst Wando exhibited the lowest leaf *i*WUE_{max} (53.90 ± 1.17 μmol mol^{-1}) and was significantly different to Alaska, CamB, Eth, KW, Ni16 and Ni11 (TukeyHSD; $P < 0.05$) (***Fig.2.21A***). Within the stipules Ni16 had a significantly higher *i*WUE_{max} (78.87 ± 3.03 μmol mol^{-1}) than Cam, Ji2822, Met, Pacco, Torsdag and Wando (TukeyHSD; $P < 0.05$) (***Fig.2.21B***). Whilst Pacco had the lowest

stipule iWUE$_{max}$ (58.83 ± 1.69 µmol mol^{-1}) and was significantly lower than Alaska, CamB, Cen, Elatius, Eth, KW and Ni16 (TukeyHSD; $P < 0.05$) (***Fig.2.21B***).

The leaves generally exhibited a greater *A100*, *A1000*, *gs100* and *gs1000* than the stipules, with a significant difference identified between the leaves and stipules within each individual accession in *A100* (TukeyHSD; $P < 0.05$) and *gs100* (TukeyHSD; $P < 0.05$) respectively, excluding Alaska, Cen, KW, Ni16 and Torsdag for *A100* and KW and Eth for *gs100* (***Fig.2.20A,B,E&F***). A significant difference were also seen between the leaves and stipules within each individual accession in *A1000* (TukeyHSD; $P < 0.01$) and *gs1000* (TukeyHSD; $P < 0.001$) respectively, exempting Cen and KW in *A1000* and KW in *gs1000* (***Fig.2.20C,D,G&H***). In contrast, the stipules generally had a greater iWUE$_{max}$ than leaves, with a significant difference in iWUE$_{max}$ identified between the leaves and stipules within the individual accessions of Cen (TukeyHSD; $P < 0.001$) and Ni16 (TukeyHSD; $P < 0.05$) (***Fig.2.21***).

To determine differences in stomatal kinetics, leaf and stipule lag-times (initial temporal delay in the response of A and g_s to a light intensity change) and time constants (time taken for A and g_s to reach steady state) in A and g_s were calculated (***Fig.2.22***). Alaska exhibited a significantly higher leaf lag-time in A (0.55 ± 0.11 min) to Elatius and Torsdag (TukeyHSD; $P < 0.05$) (***Fig.2.22A***). The greatest time constant in A in the stipules was observed within Cen (4.02 ± 0.39 min) and was significantly different to Elatius and Torsdag (TukeyHSD; $P < 0.05$) (***Fig.2.22F***). Ni11 was significantly higher in leaf g_s time constant (18.57 ± 0.43 min) to Cam and Cen (TukeyHSD; $P < 0.05$) (***Fig.2.22G***). In contrast, Torsdag exhibited the lowest leaf A lag-time (0.27 ± 0.01 min) and was significantly different to Alaska (TukeyHSD; $P < 0.05$) (***Fig.2.22A***). Torsdag

was significantly lower in stipule *A* time constant (1.36 ± 0.15 min) to Cen (TukeyHSD; $P < 0.05$) (***Fig.2.22F***). Whilst Cam had the lowest leaf g_s time constant (12.86 ± 1.19 min) and was significantly lower than Alaska, KW, Met and Ni11 (TukeyHSD; $P < 0.05$) (***Fig.2.22G***). However, no significant differences were identified between the different *P. sativum* accessions in leaf g_s lag-time, leaf *A* time constant, stipule *A* lag-time, stipule g_s lag-time or stipule g_s time constant (TukeyHSD; $P > 0.05$) (***Fig.2.22B-E&H***). There were also no significant differences identified in *A* or g_s lag-times or time constants between the leaves and stipules within each individual accession (TukeyHSD; $P > 0.05$) (***Fig.2.22***).

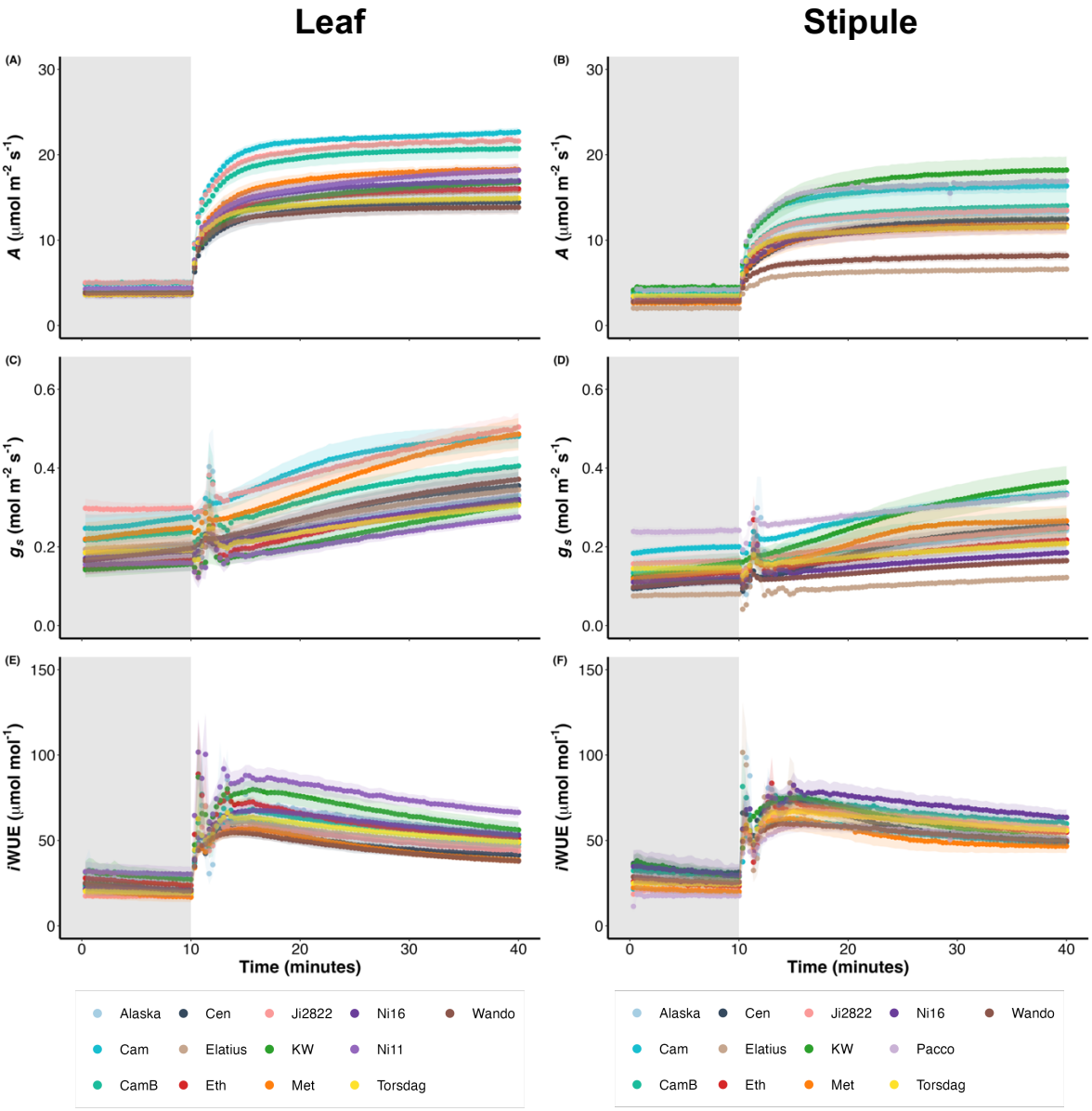

Figure 2.19. Variation in assimilation (A), stomatal conductance (g_s) and intrinsic water use efficiency (iWUE) in response to a step in light intensity across P. sativum accessions. **(A)** leaf *A*, **(B)** stipule *A*, **(C)** leaf g_s, **(D)** stipule g_s, **(E)** leaf *i*WUE and **(F)** stipule *i*WUE were monitored in response to an increase in light intensity from 100 to 1000 µmol m^{-2} s^{-1} photosynthetic photon flux density. Measured at 400 µmol mol^{-1} [CO_2] and 23 ^oC within a Li-Cor 6800 (n = 6). Error bars represent mean ± SE.

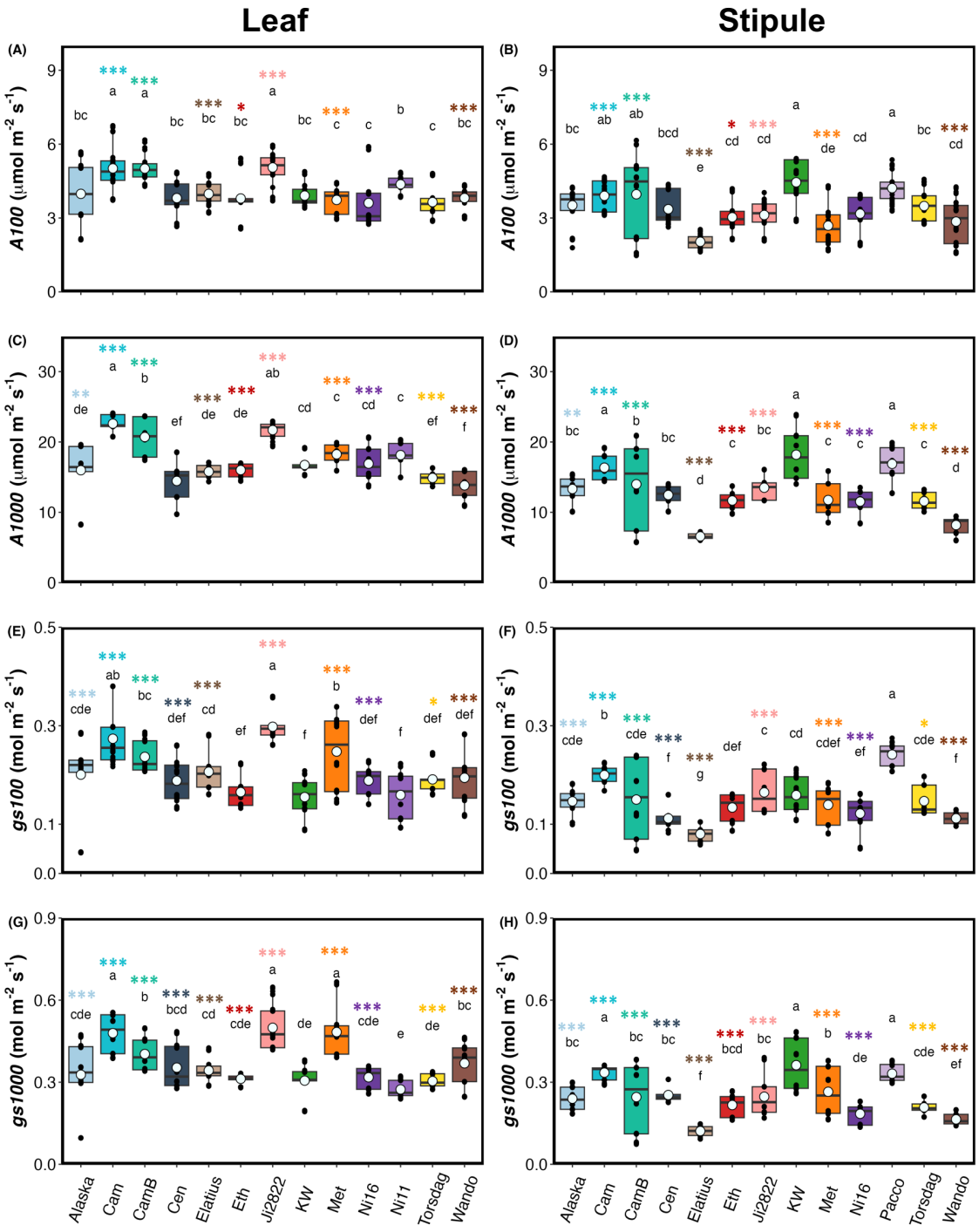

Figure 2.20. Variation in leaf and stipule steady state assimilation (A) and stomatal conductance (g_s) at 100 µmol m^{-2} s^{-1} and 1000 µmol m^{-2} s^{-1} photosynthetic photon flux density (PPFD) across P. sativum accessions. Steady state *A* at 100 µmol m^{-2} s^{-1} PPFD (*A100*) in the **(A)** leaves and **(B)** stipules, steady state *A* at 1000 µmol m^{-2} s^{-1} PPFD (*A1000*) in the **(C)** leaves and **(D)** stipules, steady state g_s at 100 µmol m^{-2} s^{-1} PPFD (*gs100*) in the **(E)** leaves and **(F)** stipules and steady state g_s at 1000 µmol m^{-2} s^{-1} PPFD (*gs1000*) in the **(G)** leaves and **(H)** stipules, were parameterised from data collected within a step in light intensity from 100 to 1000 µmol m^{-2} s^{-1} PPFD at 400 µmol mol^{-1} [CO_2] and 23 °C within a Li-Cor 6800 (n = 6). *A100* and *gs100* were calculated from the average of the last five data points before PPFD was increased to 1000 µmol m^{-2} s^{-1} PPFD. Whilst *A1000* and *gs1000* were calculated from the average of the last five data points at 1000 µmol m^{-2} s^{-1} PPFD. White dots symbolise the mean, whilst error bars represent mean ± SE. Different letters above each error bar represent significant differences in one of the steady state parameters between *P. sativum* accessions (P < 0.05; TukeyHSD). Whilst the presence of * of the same colour indicates a significant difference in one of the steady state parameters within an individual accession between the leaves and stipules, whereby * is P < 0.05, ** is P < 0.01 and *** is P < 0.001 (TukeyHSD).

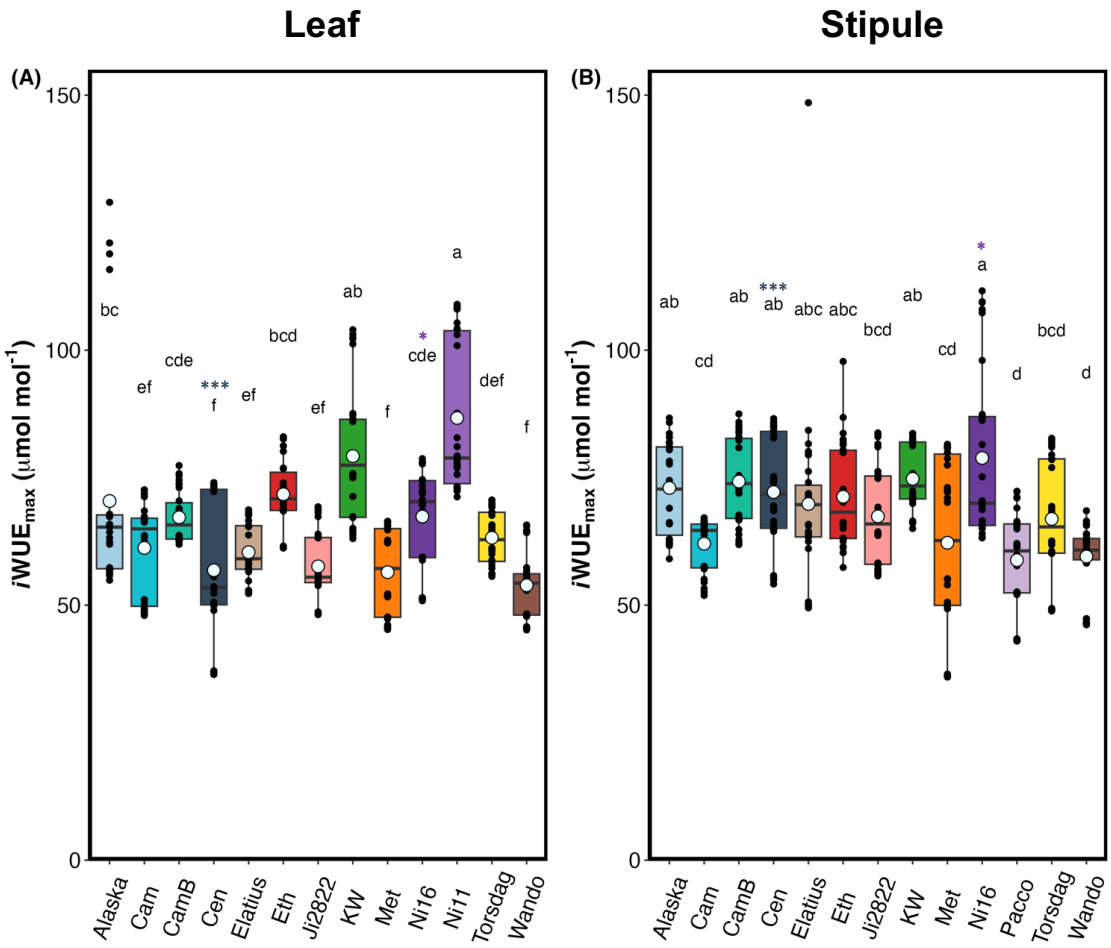

Figure 2.21. Variation in leaf and stipule maximum intrinsic water use efficiency (iWUE$_{max}$) across P. sativum accessions. **(A)** leaf and **(B)** stipule *i*WUE$_{max}$ were parameterised from data collected within a step in light intensity from 100 to 1000 µmol m^{-2} s^{-1} PPFD at 400 µmol mol^{-1} [CO_2] and 23 ºC within a Li-Cor 6800 (n = 6). *i*WUE$_{max}$ was calculated from the average of five data points (observations 45-49) after PPFD was increased to 1000 µmol m^{-2} s^{-1} PPFD, where *i*WUE was generally at the highest and most stable rate. White dots symbolise the mean, whilst error bars represent mean ± SE. Different letters above each error bar represent significant differences in *i*WUE$_{max}$ between *P. sativum* accessions ($P < 0.05$; TukeyHSD). Whilst the presence of * of the same colour indicates a significant difference in *i*WUE$_{max}$ within an individual accession between the leaves and stipules, whereby * is $P < 0.05$, ** is $P < 0.01$ and *** is $P < 0.001$ (TukeyHSD).

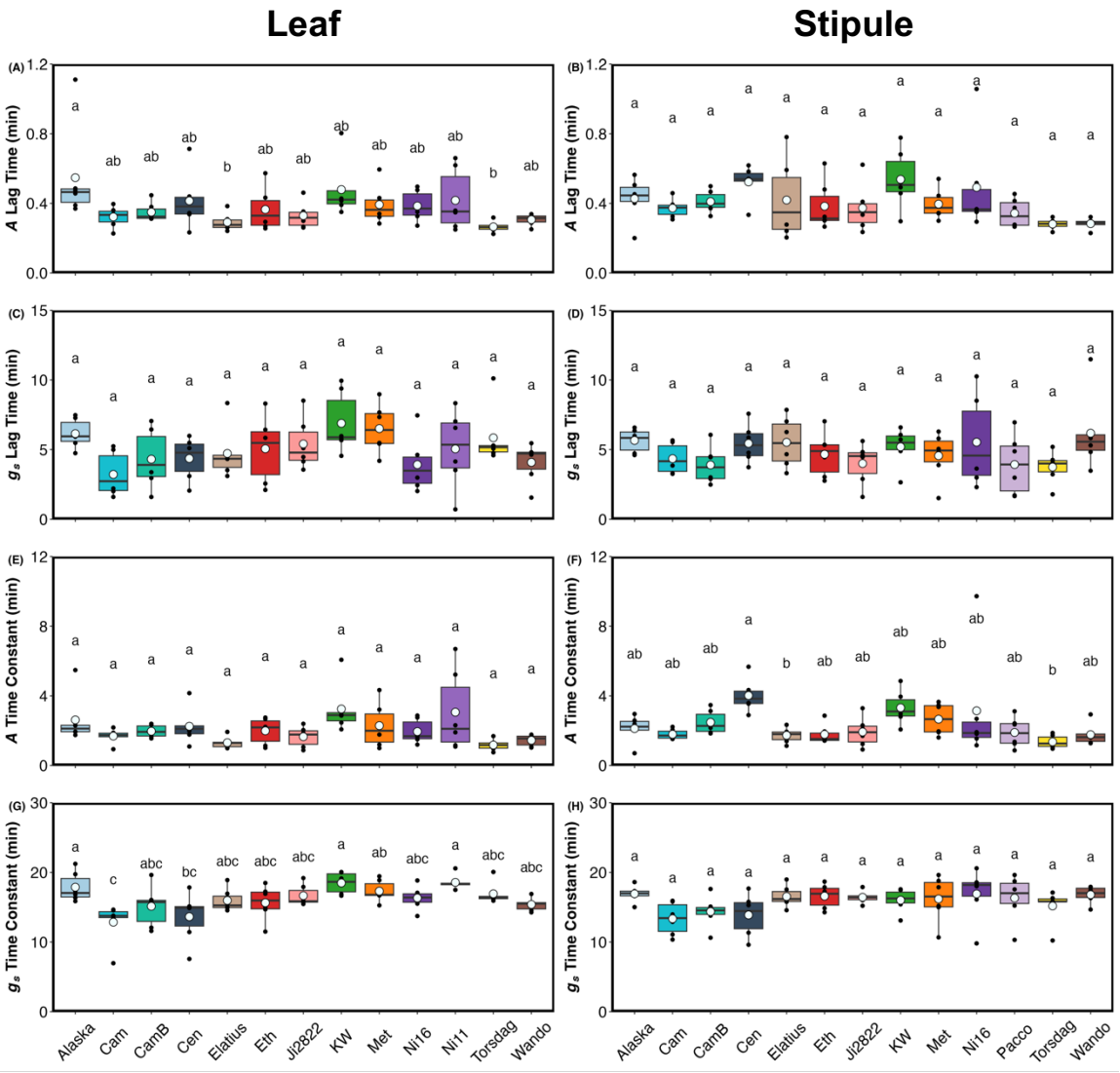

Figure 2.22. Variation in assimilation (A) and stomatal conductance (g_s) lag-times and time constants in response to a step in light intensity across P. sativum accessions. **(A)** leaf *A* lag-time, **(B)** stipule *A* lag-time, **(C)** leaf g_s lag-time, **(D)** stipule g_s lag-time, **(E)** leaf *A* time constant, **(F)** stipule *A* time constant, **(G)** leaf g_s time constant, and **(H)** stipule g_s time constant. Lag-time (initial temporal delay in the response of *A* and g_s to a light intensity change) and time constants (time taken for *A* and g_s to reach steady state) (calculated via the Vialet-Chabrand et al. (2013) model), were measured in response to an increase in light intensity from 100 to 1000 µmol m^{-2} s^{-1} photosynthetic photon flux density. Measured at 400 µmol mol^{-1} [CO_2] and 23 °C within a Li-Cor 6800 (n = 6). Error bars represent mean ± SE. Different letters above each error bar represent significant differences in either *A* or g_s lag-times or time constants between *P. sativum* accessions ($P < 0.05$; TukeyHSD). Whilst the presence of * of the same colour indicates a significant difference in either *A* or g_s lag-times or time constants within an individual accession between the leaves and stipules, whereby * is $P < 0.05$, ** is $P < 0.01$ and *** is $P < 0.001$ (TukeyHSD).

2.3.6. Variation in Foliar Anatomy and Yield

2.3.6.1. Foliar Anatomy

Significant variation were identified in both leaf mass per area; LMA ($F_{(12)} = 4.41$, $P < 0.001$) and stipule mass per area; SMA ($F_{(12)} = 3.21$, $P < 0.01$) between the *P. sativum* accessions (***Fig.2.23***). Cam had the greatest LMA (26.35 ± 2.72 g m^{-2}) and SMA (21.88 ± 2.90 g m^{-2}), with a significantly higher LMA than all accessions (TukeyHSD; $P < 0.05$), except from Cen, KW, Met, Ni16 and Ni11 and a significantly different SMA to Ji2822, Torsdag and Wando (TukeyHSD; $P < 0.05$) (***Fig.2.23***). In contrast, Wando had the smallest LMA (12.45 ± 1.01 g m^{-2}) and SMA (9.55 ± 0.72 g m^{-2}), with a significantly smaller LMA than Cam and KW (TukeyHSD; $P < 0.05$) and a significantly smaller SMA to Cam (TukeyHSD; $P < 0.05$) (***Fig.2.23***). However no significant differences were identified between leaf and stipule mass per area within each individual accession (TukeyHSD; $P > 0.05$) (***Fig.2.23***). A significant positive correlation was identified in leaf Vc_{max} (R = 0.36, $P < 0.01$) and leaf J_{max} (R = 0.31, $P < 0.01$) to LMA, as well as stipule Vc_{max} (R = 0.25, $P < 0.05$) to SMA (***Fig.2.24***).

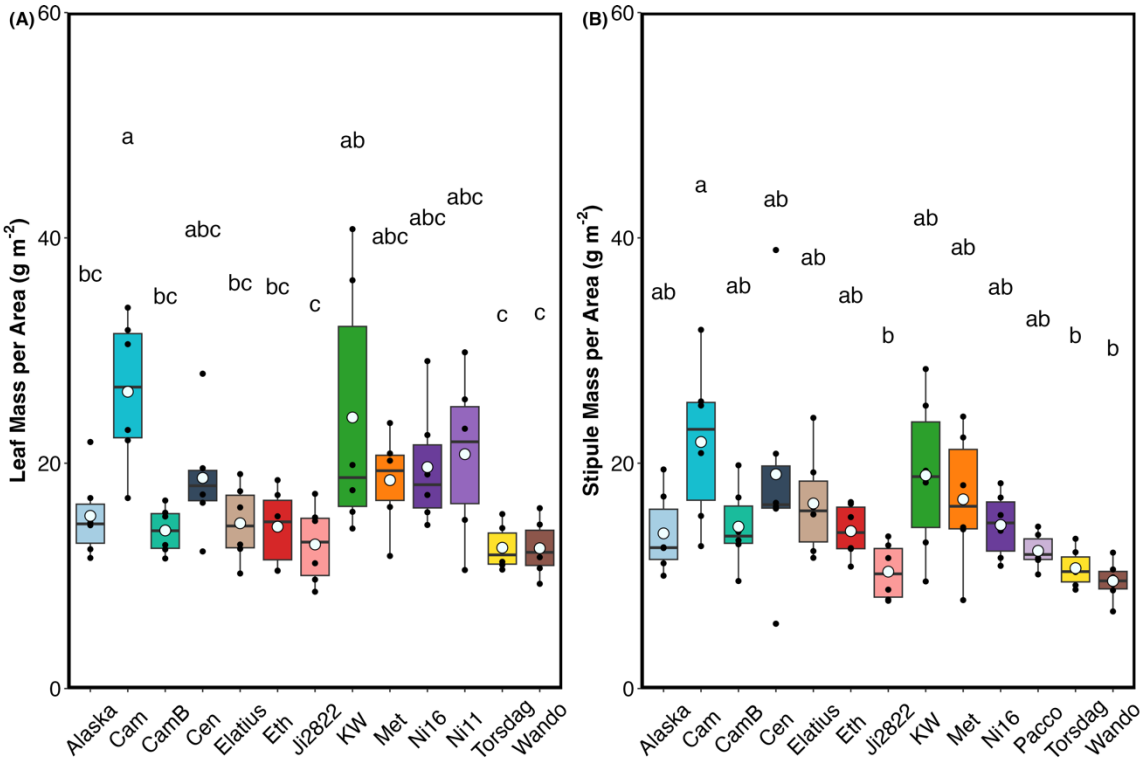

Figure 2.23. Variation in (A) leaf and (B) stipule mass per area across P. sativum accessions. Leaf/stipule areas were calculated using ImageJ (n = 6). Dry weights were measured after two weeks in a 60 °C oven (or until dried to a constant weight). White dots symbolise the mean, whilst error bars represent mean ± SE. Different letters above each error bar represent significant differences in either leaf or stipule mass per area between *P. sativum* accessions ($P < 0.05$; TukeyHSD). Whilst the presence of * of the same colour indicates a significant difference in leaf/stipule mass per area within an individual accession between the leaves and stipules, whereby * is $P < 0.05$, ** is $P < 0.01$ and *** is $P < 0.001$ (TukeyHSD).

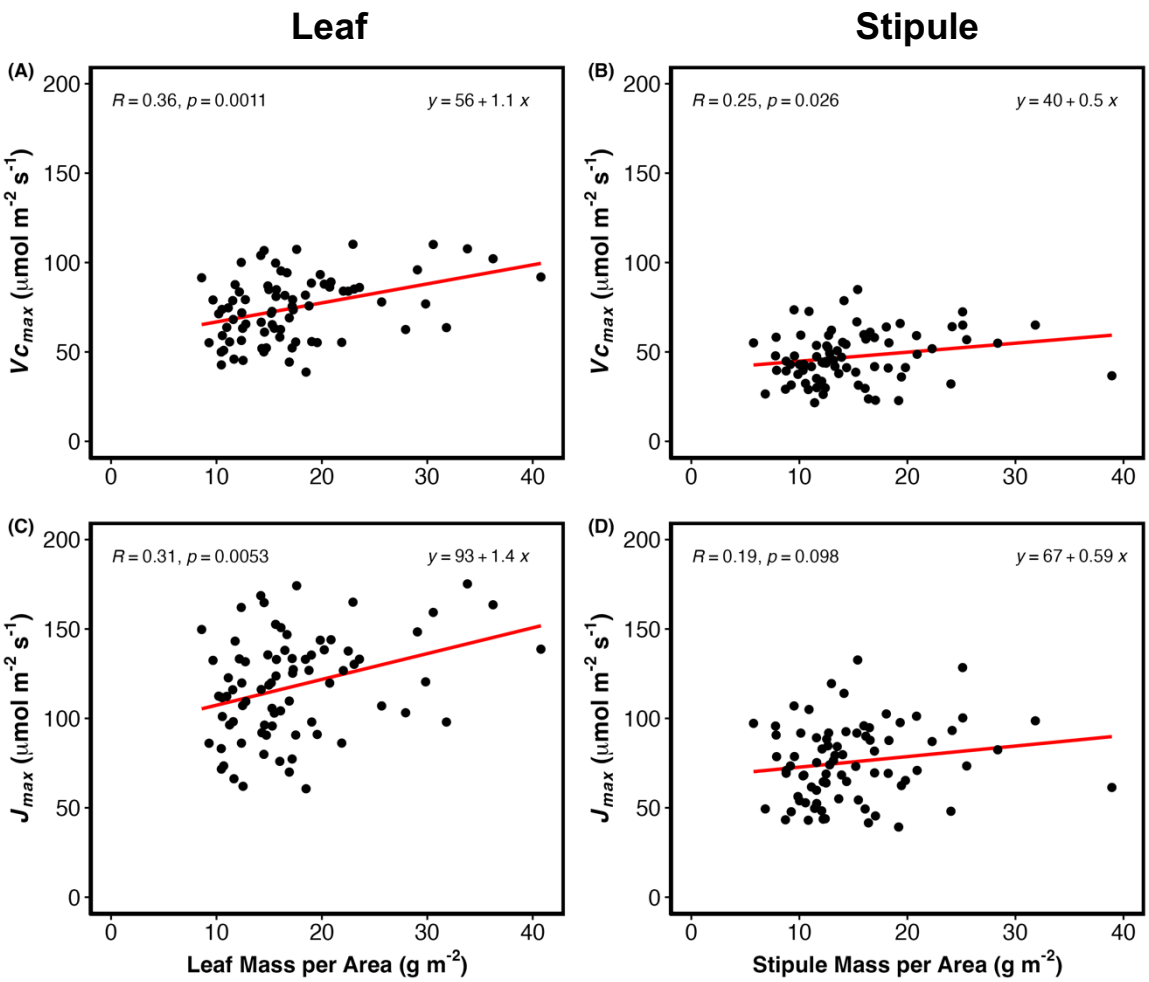

Figure 2.24. Spearmans correlation between leaf and stipule mass per area and photosynthetic capacity. Spearman's correlation coefficients (R) and linear regressions (represented as equations and red lines) were calculated between Vc_{max} (maximum rate of Rubisco activity) and **(A)** leaf mass per area (LMA) and **(B)** stipule mass per area (SMA), and between J_{max} (maximum rate of electron transport) and **(C)** LMA and **(D)** SMA. Gas exchange was measured within a Li-Cor 6800 at 1500 µmol m^{-2} s^{-1} photosynthetic photon flux density and 23 °C (n = 6). Leaf/stipule areas were calculated using ImageJ (n = 6). Dry weights were measured after two weeks in a 60 °C oven (or until dried to a constant weight). $P < 0.05$ indicates a significant relationship.

2.3.6.2. Yield

A significant difference were identified for all grain (mean number of pods, number of seeds, pod length, pod dry weight (DW), seed DW and total pod DW) and biomass (mean plant height, plant DW, mean number and DW of stems, leaves and stipules and mean tendril DW) yield parameters between the different *P. sativum* accessions ($P < 0.001$) (***Fig.2.25, Appendix Table.A1.1***).

Wando had a significantly greater seed DW (1.12 ± 0.11 g), pod DW (1.49 ± 0.13 g) and number of seeds (5.60 ± 0.45), than the other accessions (TukeyHSD; $P < 0.05$), excluding Ni11 and Met for seed DW, Met for pod DW and Ni11, Pacco and Met for the number of seeds (***Fig.2.25B,D&E***). Ni11 had a significantly longer pod length (8.39 ± 0.24 cm) and greater total pod DW (9.10 ± 3.08 g) to all accessions (TukeyHSD; $P < 0.05$) with the exception of Cam, CamB, Elatius and Pacco for total pod DW (***Fig.2.25C&F***). In contrast, Eth had a significantly lower seed DW (0.15 ± 0.01 g), pod length (3.28 ± 0.14 cm) and pod DW (0.21 ± 0.02 g) to all accessions (TukeyHSD; $P < 0.05$), excluding Elatius and Ji2822 for seed DW and Ji2822 for pod DW (***Fig.2.25B,E&F***). Whilst, Cen, Torsdag and Wando exhibited the smallest total pod DW (1.73 ± 0.32 g), number of seeds (1.60 ± 0.21) and number of pods (2.50 ± 0.29), respectively, which were significantly different to CamB and Ni11 for total pod DW (TukeyHSD; $P < 0.05$), to CamB and Elatius for the number of pods (TukeyHSD; $P < 0.05$) and to all accessions (with the exception of Alaska, Cam, CamB, Eth and Ji2822) for the number of seeds (TukeyHSD; $P < 0.05$) (***Fig.2.25A,C&D***).

The greatest overall biomass yield was attributed with Elatius, with a significantly greater plant (20.68 ± 1.03 g), stem (10.40 ± 0.30 g), leaf (1.16 ± 0.21 g), stipule (2.12

± 0.12 g) and tendril (0.84 ± 0.19 g) DW, as well as significantly higher number of leaves (154.3 ± 42.4), stipules (338.5 ± 22.7) and stems (6.75 ± 0.63) to all accessions (TukeyHSD; $P < 0.05$), except for CamB and Ni11 for leaf and plant DW and Eth for the number of leaves (***Fig.2.25H-O***). Elatius also had a higher number of pods (10 ± 1.87), with a significant difference to Alaska, Cen, KW, Met, Ni16, Torsdag and Wando (TukeyHSD; $P < 0.05$) (***Fig.2.25A***). Whilst Eth exhibited the tallest plants at harvest (115.3 ± 8.50 cm) and was significantly higher to all accessions (exempting Elatius) (TukeyHSD; $P < 0.05$) (***Fig.2.25G***). In contrast Ji2822 exhibited significantly smaller plants at harvest (14.83 ± 1.33 cm) to all accessions (par Cen) (TukeyHSD; $P < 0.05$) (***Fig.2.25G***). Cen had significantly lower plant DW (2.58 ± 0.41 g) to CamB, Elatius, Eth and Ni11 (TukeyHSD; $P < 0.05$), stem DW (0.38 ± 0.09 g) to CamB, Elatius, Eth, Ni11 and Torsdag (TukeyHSD; $P < 0.05$) and tendril DW (0 g) to Elatius, Eth, Ni11 and Pacco (TukeyHSD; $P < 0.05$) (***Fig.2.25H,I&M***). KW had the lowest number of leaves (19.67 ± 1.20), with a significant difference to Elatius and Eth (TukeyHSD; $P < 0.05$) (***Fig.2.25K***). Met and Wando exhibited the lowest number of stems (1 ± 0) and were significantly different to Elatius, Eth and Ni16 (TukeyHSD; $P < 0.05$) (***Fig.2.25J***). Met also had a significantly lower number of stipules (16.67 ± 1.23) than Elatius and Eth (TukeyHSD; $P < 0.05$) (***Fig.2.25L***). Alaska had a significantly lower leaf DW (0.19 ± 0.03 g) to CamB, Elatius and Ni11 (TukeyHSD; $P < 0.05$) and stipule DW (0.14 ± 0.01 g) to CamB, Elatius and Eth (TukeyHSD; $P < 0.05$) (***Fig.2.25N&O***).

2.3.6.3. Relationship Between Yield and Photosynthetic Capacity

To ascertain the impact of photosynthetic capacity on yield, relationships between each yield parameter and leaf and stipule Vc_{max} and J_{max} were established (***Table.2.10***), with a significant negative correlation identified between leaf and stipule Vc_{max} and J_{max} to plant height ($P < 0.001$), number of leaves ($P < 0.05$), number of stipules ($P < 0.05$) and tendril DW ($P < 0.01$) (***Table.2.10***). Whilst stipule Vc_{max} and J_{max} also had a significant negative correlation to the number of stems ($P < 0.01$) and pods ($P < 0.01$) and to stem ($P < 0.01$) and plant DW ($P < 0.05$) (***Table.2.10***). Significant negative correlations were identified between leaf and stipule Vc_{max} and stipule J_{max} to stipule DW ($P < 0.05$) (***Table.2.10***). Whilst significant positive correlations were identified between leaf and stipule Vc_{max} and stipule J_{max} to seed DW ($P < 0.05$) (***Table.2.10***). Stipule J_{max} were negatively correlated to leaf DW ($R = -0.27$, $P < 0.05$), whilst leaf Vc_{max} were positively correlated to pod length ($R = 0.28$, $P < 0.05$) (***Table.2.10***).

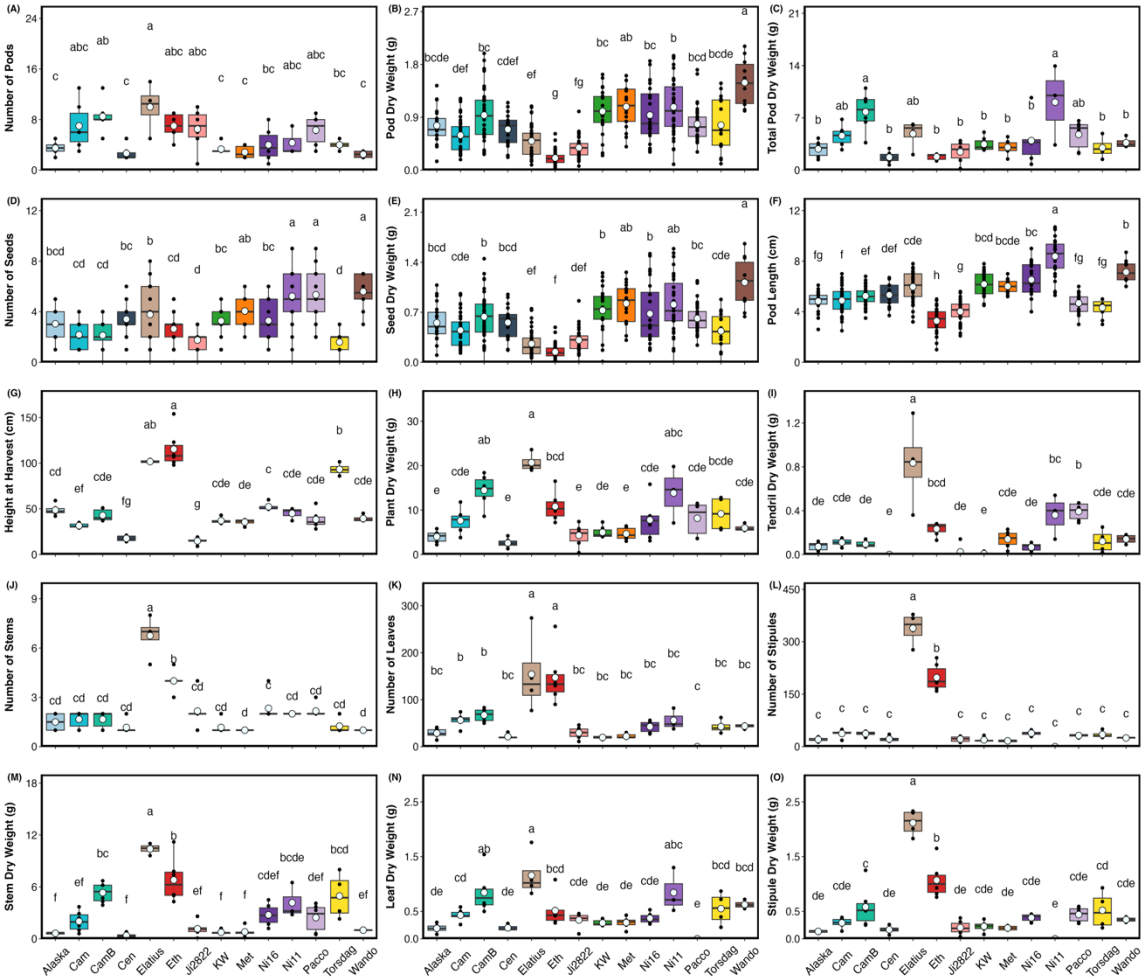

Figure 2.25. Variation in yield across P. sativum accessions. Mean **(A)** number of pods, **(B)** pod dry weight, **(C)** total pod dry weight, **(D)** number of seeds, **(E)** seed dry weight, **(F)** pod length, **(G)** plant height, **(H)** plant dry weight, **(I)** tendril dry weight, **(J)** number of stems, **(K)** number of leaves, **(L)** number of stipules, **(M)** stem dry weight, **(N)** leaf dry weight and **(O)** stipule dry weight. Averages were calculated from 3 to 6 reps per accession (n = 3-6), with pod lengths measured via ImageJ (version 1.53) and dry weights measured after a constant weight had been reached. White dots symbolise the mean, whilst error bars represent mean ± SE. Different letters above each error bar represent significant differences in one of the yield parameters between *P. sativum* accessions ($P < 0.05$; TukeyHSD).

Table 2.10. Spearmans correlation coefficient table showing the relationship between grain and biomass yield components and photosynthetic capacity. Whereby Vc_{max} (maximum rate of Rubisco activity), and J_{max} (maximum rate of electron transport) measurements (measured in µmol m^{-2} s^{-1}) were obtained at 1500 µmol m^{-2} s^{-1} photosynthetic photon flux density and 23 °C within a Li-Cor 6800. Grain yield parameters are represented by the number of pods, number of seeds, pod length, pod dry weight (DW), seed DW and total pod DW, whilst biomass yield parameters are represented by plant height, plant DW, number and DW of stems, leaves and stipules and tendril DW. Pod lengths were measured (in cm) via ImageJ (version 1.53), whilst dry weights (DW) were measured (in g) after a constant weight was reached. Spearman's correlation coefficients (R) were calculated for each yield component against capacity measurement, with the darker red boxes representing a strong negative correlation, whilst the dark green boxes represent a strong positive correlation. Statistical significance between yield parameters and capacity are illustrated as asterisks, whereby * is $P < 0.05$, ** is $P < 0.01$ and *** is $P < 0.001$ (n = 3-6).

Yield Parameter	Leaf		Stipule	
	Vc_{max}	J_{max}	Vc_{max}	J_{max}
Plant Height	*** -0.42	*** -0.42	*** -0.41	*** -0.49
Plant DW	-0.12	-0.14	* -0.3	*** -0.4
Number of Leaves	* -0.3	** -0.33	* -0.29	*** -0.38
Number of Stipules	* -0.28	* -0.24	** -0.32	*** -0.42
Number of Stems	-0.21	-0.21	** -0.33	*** -0.4
Leaf DW	-0.12	-0.16	-0.22	* -0.27
Stipule DW	* -0.25	-0.22	*** -0.41	*** -0.49
Stem DW	-0.19	-0.2	** -0.32	*** -0.4
Tendril DW	** -0.32	*** -0.39	*** -0.46	*** -0.55
Number of Pods	-0.14	-0.11	** -0.31	** -0.37
Pod DW	0.21	0.14	0.23	0.22
Number of Seeds	-0.07	-0.12	-0.079	-0.13
Seed DW	* 0.24	0.18	* 0.26	* 0.25
Pod Length	* 0.28	0.22	0.21	0.19
Total Pod DW	0.2	0.15	-0.063	-0.16

2.4. Discussion

As demand for pea production increases (*i.e.*, as an alternative protein source), identification of greater yielding pea varieties that are able to withstand future climatic conditions are required (Joseph et al., 2020; Rasskazova and Kirse-Ozolina, 2020; Pilorgé et al., 2021; Wu et al., 2023). Screening varieties for naturally varying traits have already been used in peas to identify beneficial pod shapes for reproduction (Ellis et al., 2021), seed nutritional qualities (Santos et al., 2019) and for investigation into genetic diversity (Burstin et al., 2015; Winther et al., 2023). However, exploration of natural variation in photosynthetic capacity in current pea germplasms remains an untapped and underutilised resource for crop improvements (Lawson et al., 2012; Ricroch et al., 2018; Faralli and Lawson, 2020; Burgess et al., 2023). This study utilised current physiological techniques (including chlorophyll fluorescence and gas exchange), to establish the extent of natural variation in photosynthetic capacity in pea populations, whilst determining differences in stomatal and photosynthetic responses to light intensity.

2.4.1. Variation in Photosynthetic Capacity

Significant variation existed between the different *P. sativum* accessions for the majority of physiological parameters measured (for both types of foliar tissues) (***Fig.2.2-2.25***), including photosynthetic capacity, whereby greater capacity were generally identified in elite accessions (KW) in comparison to landraces (Eth and Elatius) (***Fig.2.7&2.8***). Although such findings contradict recent studies in other crops, whereby landraces had greater photosynthetic capacity compared to elite varieties in wheat (Driever et al., 2014; McAusland et al., 2020), barley (Stevens et al., 2021),

soybean (Shamim et al., 2022) and cassava (De Souza and Long, 2018). However, despite the generally higher photosynthetic capacities in elite accessions, Wando exempted this trend by exhibiting a low leaf J_{max} (***Fig.2.8***), however elite accessions are not always bred for higher photosynthetic rates, as Wando is the offspring of two heirloom parent varieties developed for the purpose of drought/heat tolerance and potential ability to produce good yield under stress conditions (Yarnell, 1950; Baggett and Kean, 1987; Aggour, 1999).

Higher photosynthetic capacities can be linked to greater abundance of proteins, specifically Rubisco for enhanced carboxylation (Parry et al., 2011; Momayyezi et al., 2022). Yet, within this study there were no significant relationships identified between total protein content and capacity in either foliar tissue (***Fig.2.8-2.10***), this could be due to total protein content assays accounting for all proteins and not just Rubisco, leading to possible overestimations (Faisal et al., 2024). Whilst previous studies have identified that Rubisco activation and enzyme efficiency plays a more important role in enhancing photosynthetic capacity than Rubisco content (Parry et al., 2011; Driever et al., 2014). Thus, future studies could take into consideration Rubisco activity assays for a greater insight on the link between Rubisco and variations in photosynthetic capacity in pea populations (Faralli and Lawson, 2020; Faisal et al., 2024).

Despite many studies highlighting that foliar mass per area has a negative impact on photosynthetic capacity; with thicker leaves slowing the rate of CO_2 diffusion for carboxylation and restricting Vc_{max} (Wright et al., 2002; Poorter et al., 2009; Hikosaka and Shigeno, 2009; Lei et al., 2022), the present study identified a significant positive relationship between leaf photosynthetic capacity and LMA, whilst SMA also positively

impacted stipule Vc_{max} (***Fig.2.8&2.23-2.24***). However, these results are in alignment with studies within Walnut (Momayyezi et al., 2022), wheat (Silva-Pérez et al., 2020; McAusland et al., 2020) and beech trees (Wang et al., 2023) who found a positive link between LMA and photosynthetic capacity across genotypes. Whilst species in semi-arid climates have been shown to maintain a high photosynthetic capacity driven via a greater LMA, which prevents overheating when wind speeds decline (Dong et al., 2020). Subsequently, breeding crosses of higher LMA and photosynthetic capacity accessions (such as Cam and KW, respectively) may prove beneficial under future climatic conditions (Leigh et al., 2012; Dong et al., 2020).

Within this study, high photosynthetic capacity generally translated into a greater seed DW, supporting the findings of Yan et al. (2021) who identified that maize cultivars with higher yields (*i.e.*, 1000-kernal weight) exhibited a greater photosynthetic capacity (***Fig.2.8&2.25, Table.2.10***). Yet, within the present study there were also no significant relationships identified between photosynthetic capacity and seed number and pod DW (***Fig.2.8&2.25, Table.2.10***), consistent with the lack of correlations illustrated by Driever et al. (2014) and Silva-Pérez et al. (2020) in wheat and Stevens et al. (2021) in barley. Therefore, this study further adds to the complexity and ongoing debate on the relationship between photosynthetic capacity and yield (Driever et al., 2014; Faralli and Lawson, 2020; Yan et al., 2021). Although the positive impact on seed DW highlights the opportunity for further exploitation that could be beneficial for future breeding programmes (Stevens et al., 2021). Meanwhile the low photosynthetic capacities generally experienced by the landrace accessions could be explained by the negative relationship identified between photosynthetic capacity and plant height, with landrace accessions potentially putting more resources into biomass yield

parameters and creating a reduction in individual leaf and stipule capacity (***Fig.2.8&2.25, Table.2.10***) (Faralli et al., 2019; Acevedo-Siaca et al., 2020). Yet, more CO_2 uptake could have occurred in total throughout the landrace plants, equating to the greater pod output experienced by Elatius (***Fig.2.25***). Subsequently, measurements throughout the plant and not just on the youngest fully expanded leaf could also be considered (Acevedo-Siaca et al., 2020).

2.4.2. Variation in Stomatal and Photosynthetic Responses to Light Intensity Changes

Significant variation also existed between the different accessions in stomatal and photosynthetic responses to both light intensity changes and a step increase in light intensity, with three key accessions (Ji2822, KW and Ni16) generally exhibiting higher rates of F_q'/F_m', A and g_s (respectively) for both types of foliar tissues (***Fig.2.2-2.6,2.19-2.20***). Responses of A and g_s to light intensity changes are often the result of variations in stomatal anatomy and/or kinetics, with enhanced stomatal densities and sizes previously linked to g_s, maximum anatomical g_s (gs_{max}) and the rapidity of stomatal opening/closing (McAusland et al., 2016; Bertolino et al., 2019; Harrison et al., 2020; Faralli and Lawson, 2020; McAusland et al., 2020; Sakoda et al., 2020).

Within the present study, increases in g_{smax} were generally driven by stomatal densities rather than sizes in both foliar tissues (***Fig.2.11-2.13,2.15-2.16***), which are consistent with that of soybean (Tanaka et al., 2008) and wheat (Wall et al., 2023), although in the majority of cases improvements in gs_{max} are often generated through an increased density of smaller stomata (Dow et al., 2014a; Dow et al., 2014b; Bertolino et al., 2019;

Caine et al., 2023). In the current study, a greater abundance of smaller stomata potentially drove increases in g_s in the leaf tissues; as highlighted by the positive impact of increased stomatal density and negative impact of greater AD stomatal sizes on g_s in the leaves (***Fig.2.17&2.18***). These findings agree with Drake et al. (2013) in *Banksia* and McAusland et al. (2016) in dumbbell shaped stomata in wheat (Faralli et al., 2019). Greater densities of smaller stomata are often linked to faster stomatal responses to changes in light intensity and increased WUE, with smaller pore areas and greater surface area to volume ratios thought to generate quicker changes in guard cell turgidity due to rapid ion fluxes (Lawson and Blatt, 2014; Kardiman and Ræbild, 2018; Lawson and Vialet-Chabrand, 2019; Bertolino et al., 2019). However, within the present study, accessions with the highest *i*WUE$_{max}$ (Ni11 leaves and Ni16 stipules) did not convey faster responses in *A* or g_s lag-times or time constants, with the greater *i*WUE$_{max}$ seen by Ni11 potentially driven by low values of operational g_s rather than the slow g_s time constant, yet as debated by Elliott-Kingston et al. (2016), smaller stomata are not always quicker in stomatal responses (***Fig.2.19-2.22***) (Bertolino et al., 2019; Eyland et al., 2021). Whilst the impact of stomatal density or size on conductance were not generally apparent in the stipules (***Fig.2.17&2.18***), it highlights the potential for further variation to be explored between the different foliar tissue types (Faralli et al., 2019).

Interestingly the greatest *i*WUE$_{max}$ were observed within both the near isogenic lines (Ni11 and Ni16) for leaves and stipules, respectively (***Fig.2.21***). The near isogenic lines measured differ in their genotypic combinations of the stipules reduced (*ST*) gene (where Ni11 is recessive and Ni16 is dominant; *see* ***Table.2.1&2.2***), from this study the *stst* genotype (in conjunction with lower values of g_s), possibly generated the

greater *i*WUE$_{max}$ in the leaves of Ni11 in comparison to Ni16 (***Fig.2.21***) (Lafond et al., 1981; Snoad, 1981; Snoad et al., 1985; Mikic et al., 2011; Eyland et al., 2021; Tran et al., 2022). However, as Ni16 has both types of foliar tissues, it potentially put greater resources into maintaining a higher stipule *i*WUE$_{max}$ at the expense of levels in the leaves (***Fig.2.21***) (Sharma et al., 2012). In contrast, the semi-leafless afila variety (Pacco); which is recessive in the afila (*AF*) gene (*see* ***Table.2.1&2.2***), exhibited the lowest stipule *i*WUE$_{max}$ (***Fig.2.21***), possibly highlighting the significant variation that exists because of the different combination of the *ST* and *AF* genes and the potential to generate beneficial accessions from such combinations that are able to survive under future drought conditions (Moreau et al., 2018; Tran et al., 2022).

In alignment with Sharma et al. (2012), leaves and stipules were generally similar in terms of stomatal densities and sizes (***Fig.2.11&2.12***). Yet within the current study, the leaves were generally greater than the stipules for the majority of gas exchange parameters measured (***Fig.2.6,2.8&2.20***), which is consistent with previous research that identified that more compact mesophyll cells, reduced sugar exportation to sinks and increased respiration rates in the stipules, make the stipules less efficient than the leaves at gas exchange (Giovanardi et al., 2018). However, the stipules should not be ruled out, due to their potential to maintain carbon assimilation under stress conditions, as shown by the generally greater *i*WUE$_{max}$ identified in the stipules than the leaves (***Fig.2.21***). Reinforcing the potential for greater productivity by considering more than just normal leaf tissue (Tran et al., 2022).

2.4.3. Limitations

This study was limited by the fact that only 13 accessions were screened, with only two landrace and semi-leafless accessions utilised, which did not provide a fully representative analysis of the natural variation in the current pea germplasm. Therefore, future studies could utilise a greater pea screening population, which includes a greater diversity of accessions (*e.g.* more semi-leafless and landrace accessions). Such studies could also consider comparisons to field conditions to enable selection of accessions able to cope with dynamically changing environments (Faralli et al., 2019; Acevedo-Siaca et al., 2020). Furthermore, yield data was impacted by the onset of Powdery Mildew, with plants from accessions Elatius, Torsdag, Ni11 and Wando, dying before full yield could be taken, whilst disproportionate application of Rose Clear Ultra to only diseased plants may have additionally influenced final yield measurements, subsequently future experiments should maintain tighter regulation over disease onset and pesticide management.

2.4.4. Conclusions

In summary, the *P. sativum* accessions measured here exhibited significant variation for the majority of physiological parameters for both types of foliar tissues, with natural variation in photosynthetic capacity generally greater in elite than landrace accessions. Whilst LMA/SMA positive impact on photosynthetic capacity indicates potential for greater survival under future climatic conditions. The research presented here also adds to the complex relationship between photosynthetic capacity and yield, yet the positive impact on seed DW provides a potential area to exploit for greater productivity under future breeding programmes. The significant variation identified in

photosynthetic and stomatal responses to light intensity changes were possibly driven by smaller stomata of a higher density causing greater stomatal conductance. Meanwhile, the highest *i*WUE$_{max}$ accessions were both Near isogenic, whilst the lowest *i*WUE$_{max}$ was seen in the semi-leafless afila variety, highlighting the variation that exists in different leaf types and different combinations of the afila and stipules reduced genes. The leaves generally performed greater than the stipules for the majority of gas exchange parameters, however the stipules generally had a greater *i*WUE$_{max}$, subsequently other photosynthetically active tissues than leaves should be considered when evaluating naturally beneficial traits for future breeding programmes. The considerable variation presented within this study highlights great potential for enhanced photosynthetic capacity, stress-tolerant mechanisms and photosynthetic/stomatal responses for improved pea production under future climatic conditions (Lawson et al., 2012; Faralli and Lawson, 2020; Burgess et al., 2023).

2.4.5. Take Home Messages

- Significant variation was identified for the majority of measured physiological parameters between the *P. sativum* accessions, including photosynthetic capacity and stomatal and photosynthetic responses to light intensity changes.

- Elite accessions generally had a higher photosynthetic capacity in comparison to landraces, whilst three key accessions (Ji2822, KW and Ni16) illustrated greater stomatal and photosynthetic responses to light intensity changes and step increases in light intensity for both foliar tissues.

- Photosynthetic capacity was positively related to LMA/SMA, however no significant relationship were identified between photosynthetic capacity and protein content. Future studies could therefore utilise Rubisco activity assays to further test these relationships.

- Greater photosynthetic capacity translated to a higher seed DW, but no significant differences were identified to pod DW or seed number, further adding to the ongoing argument on whether photosynthetic capacity correlates to yield.

- A greater density of smaller stomata potentially drove increases in stomatal conductance in the leaves, however limited variation was identified in stomatal kinetics.

- The highest *i*WUE$_{max}$ accessions were both Near isogenic which differ in the stipules reduced gene, whilst the lowest was seen in the semi-leafless afila variety, highlighting the variation that exists in the different leaf types.

- Leaves generally performed greater than the stipules for the majority of gas exchange parameters, however stipules generally had a greater *i*WUE$_{max}$ and therefore more than just leaf tissues should be considered when evaluating naturally beneficial traits for future breeding programmes.

Chapter 3: Exploring Natural Variation in Response to Drought in Foliar Tissues of *P. sativum*

3.1. Introduction

The impacts of climate change are becoming ever more noticeable, with increased frequency and severity of droughts identified as one of the main abiotic factors impeding crop production and generating billions of dollars of agricultural losses worldwide (Singh and Reddy, 2011, Naim-Feil et al., 2017; Urban et al., 2017a; Mishra et al., 2021; Trivedi et al., 2022). Drought stress arises from reduced soil water availability and continued transpiration during a period of little to no precipitation, which can be generated through natural climatic events (such as El Niño and La Niña) but are heavily instigated and aggravated via anthropogenic activities (such as urbanisation, deforestation, river diversions, water overexploitation and increased global warming) (Zhao and Dai, 2015; Mathobo et al., 2017; Haile et al., 2019; Hellwig et al., 2021; Trivedi et al., 2022). Peas are particularly vulnerable to drought stress, especially during flowering and pod filling growth stages, causing both yield and protein quality to decline, with the drought experienced by the UK in 2022 triggering a 4% reduction in yield potentials from an increasingly dry harvest (Magyar-Tábori et al., 2011; Araújo et al., 2015; Bueckert et al., 2015; Osman, 2015; Couchoud et al., 2020; PGRO, 2022). Subsequently, identifying pea accessions that are able to withstand drought conditions may alleviate future yield losses and help secure production of an alternative source of protein for future generations (Magyar-Tábori et al., 2011; Sadras et al., 2013; Araújo et al., 2015; Annicchiarico et al., 2020; Bagheri et al., 2023).

Drought stress in pea plants (as with many other crop species) is characterised by both morphological and physiological changes, whereby plant growth (including height and biomass), leaf area (and number) and photosynthetic and transpiration rates are

often reported to decline (Araújo et al., 2015; Yang et al., 2021; Bagheri et al., 2023). Under mild drought, the reduction in plant height and leaf area is caused by the decrease in cell expansion through a drop in turgor pressure (Yang et al., 2021; Bagheri et al., 2023). Plant biomass partitioning also shifts with greater maintenance of root (to increase surface area for water uptake) over shoot growth, often leading to stunted plants (Couchoud et al., 2020; Tafesse et al., 2021). Whilst the fall in photosynthetic and transpiration rates are generated mainly by stomatal limitations, induced by abscisic acid (ABA) stomatal closure, which limits CO_2 uptake to prevent water loss from transpiration (Osman, 2015; Nemeskéri and Helyes, 2019; Couchoud et al., 2020; Ortiz and Salas-Fernandez, 2022; Bagheri et al., 2023). However, when drought becomes increasingly severe, photosynthetic and transportational losses are also driven by non-stomatal factors, including reductions in the activity and content of Ribulose Bisphosphate (RUBP), Rubisco, synthetic enzymes, chlorophyll content and the rates of phosphorylation and electron transport (ETR) (Yang et al., 2021; Ortiz and Salas-Fernandez, 2022; Bagheri et al., 2023). For both types of drought stress reactive oxidative species (ROS) are produced (including H_2O_2 and singlet oxygen free radicals) from the loss of homeostasis between light capture and carbon fixation for photosynthesis, leading to oxidative stress (including reductions in photosynthetic and enzymatic activity, increases in lipid and protein oxidation) and eventual cell death, with Moran et al. (1994) identifying a two-to-three-fold increase in the oxidation of lipids and proteins in drought-stressed pea plants (Moran et al., 1994; Araújo et al., 2015; Farooq et al., 2021; Khatun et al., 2021; Pandey et al., 2023; Bagheri et al., 2023). Although natural variation in photosynthetic rates and capacity under drought stress has been characterised within wheat (Sikder et al., 2015), Persian walnut (Arab et al.,

2023), rice (Lauteri et al., 2014) and olive (Golmohammadi et al., 2020), it has yet to be fully evaluated across different accessions and types of foliar tissues (such as leaves and stipules; *see* ***Chapter 2 Table.2.1***) in peas (Moran et al., 1994; Araújo et al., 2015).

In order to mitigate the effects of drought, pea plants have developed drought tolerant mechanisms, including the utilisation of antioxidants (*e.g.* catalase and superoxide dismutase) and osmolytes (such as proline and flavonoids), which remove ROS and/or maintain cell water potential (Farooq et al., 2021; Bagheri et al., 2023). A recent review by Lawson and Milliken (2023) also highlights the ability of non-foliar tissues to act as compensatory mechanisms for foliar tissues under stress environments (*e.g.* drought), further adding to the surplus of variation yet to be explored (as investigated in pea pods in ***Chapter 4***) (Lawson and Milliken, 2023). Whilst deep tap roots enable peas to discover water reserves deeper in the soil, as observed by Benjamin and Nielsen (2006) who found field peas under drought stress had a finer root system that grew further into the soil to obtain water (Benjamin and Nielsen, 2006; Araújo et al., 2015). The presence of epicuticular waxes on foliar tissues reduce transpiration rates to restrict water loss, however plants must mitigate the trade-off between reducing water loss and maintaining carbon assimilation for photosynthesis, in order to maintain high water use efficiency (WUE; rate of water lost compared to carbon gained) (Singh and Reddy, 2011; Blankenagel et al., 2018; Tafesse et al., 2022). Stomatal responses under drought conditions vary between species, with beans having a rapid and full closure of stomata, whilst cowpeas have a slower closure rate, remaining partially open to maintain photosynthesis and retain a high WUE (Singh and Reddy, 2011;

Nemeskéri and Helyes, 2019). Variation in stomatal responses and WUE are also believed to differ between varieties of peas, for instance the reduction in foliar area in leafless (which relies upon non-foliar material for photosynthesis; *see* ***Chapter 4***) and semi-leafless (*see* ***Chapter 2 Table.2.1***) pea varieties are thought to convey a greater WUE than conventional (WT) foliar dominant varieties (Baigorri et al., 1999; Araújo et al., 2015; Szablińska-Piernik and Lahuta, 2021; Bagheri et al., 2023). However, stomatal lags and kinetics are yet to be fully explored within peas (especially between accessions of different foliar morphology) therefore assessment of accessions with rapid stomatal responses and high WUE under drought stress, may help selection for breeding programmes under future climatic conditions (Lawson and Blatt, 2014; Couchoud et al., 2020; Tafesse et al., 2022).

This study determined the extent of natural variation in foliar photosynthetic capacity and yield in pea populations, whilst further examining stomatal and photosynthetic responses to light intensity changes under mild drought (henceforth called droughted conditions) and watered conditions and between different types of foliar pea morphology. Six accessions from the initial screening in ***Chapter 2*** were selected based on their photosynthetic, stomatal and intrinsic water use efficiency (*i*WUE) performances, as well as their variation in leaf structures/morphologies and heritage (*i.e.*, landrace), a leafless accession was additionally used for plant temperature and yield but is primarily utilised in ***Chapter 4*** (*see* ***Table. 3.1***). Foliar tissues were subjected to infra-red gas exchange analysis to determine the extent of natural variation in photosynthetic capacity, whilst step increases in light intensity and surface

impressions explored the variation in *i*WUE, stomatal kinetics and anatomy, as well as the impact of drought on functional traits.

Table 3.1. Description of the pea accessions utilised. Supplied by Professor Claire Domoney and Dr Noel Ellis, John Innes Centre Germplasm Resource Unit, Norwich; Thompson & Morgan, Ipswich, Suffolk; Accessions supplied by the John Innes Centre Germplasm Resource Unit have a JI coding. Stipules Reduced (*ST*), Afila (*AF*) and Tendriless (*TL*) genes.

Accession Name (Abbreviation)	Accession Type (Supplier)	Reason for Utilisation
Ethiopia (Eth)	Landrace (JI0281)	Landrace, low performance in ***Chapter 2*** (quicker growth rate than Elatius).
Filby	First Fully Leafless Cultivar; *stst*, *afaf*, *TLTL* (JI1768)	Leafless accession utilised mainly in ***Chapter 4*** for pod photosynthesis.
Kelvedon Wonder (KW)	Commercial Elite (*Thompson & Morgan* ©)	Elite, with high photosynthetic capacity in ***Chapter 2***.
Near isogenic line 11 (Ni11)	Near isogenic line Semi-leafless Stipules Reduced; *stst*, *AFAF*, *TLTL* (JI3310)	Semi-leafless, with high *i*WUE in ***Chapter 2***.
Near isogenic line 16 (Ni16)	Near isogenic line WT Dominant; *STST, AFAF, TLTL* (JI3315)	High *i*WUE in ***Chapter 2***.
Pacco	Commercial Semi-leafless Afila; *STST*, *afaf*, *TLTL* (*Thompson & Morgan* ©)	Semi-leafless, with low *i*WUE in ***Chapter 2***.
Wando	Elite Heat and Drought Tolerant (JI2483)	Potential drought tolerant accession with low photosynthetic capacity in ***Chapter 2***.

3.2. Material and Methods

3.2.1. Plant Materials and Growth

P. sativum accessions (Professor Claire Domoney and Dr Noel Ellis, John Innes Centre Germplasm Resource Unit, Norwich; Thompson & Morgan, Ipswich, Suffolk) were selected based on their initial screening in ***Chapter 2*** (*see* ***Table.3.1***). Seeds were potted and grown in the same soil type and conditions as per ***Chapter 2 Section 2.2.1***; however, after one week, plants of each accession were split into watered or mild drought (hereafter called droughted) treatments. Whereby, watered conditions corresponded to 80% of their relative soil water content (RSWC: mass moist soil (g) – mass of oven dried soil (g) / mass of oven dried soil (g) x 100) predetermined as optimal watering conditions. Whilst RSWC for droughted conditions was reduced to 50%, which was pre-established as the lowest RSWC plants could reach in order to have enough measurable pods for ***Chapter 4***. Plants were weighed twice a day (an hour before measurements in the morning and checked again after measurements) to maintain the correct weight and therefore RSWC; as calculated par Moisa et al. (2019) RSWC methodology (***Appendix Fig.A2.1***). Such conditions were maintained throughout the experiment. All *P. sativum* accessions were randomly sown at the same time and were regularly rotated within trays and around the growth room to prevent environmental heterogeneity. Unless stated otherwise, six plants were measured per accession between 21-30 days old and between 7 am and 4 pm.

3.2.2. Chlorophyll Fluorescence Imaging

Chlorophyll fluorescence imaging protocols were performed according to the methods in ***Chapter 2 Section 2.2.2***. Leaves and stipules were isolated using the Flourimager software.

3.2.3. Foliar Gas Exchange

All foliar gas exchange were performed in accordance with the methods in ***Chapter 2 Section 2.2.3*** for watered and droughted leaves and stipules. For A/C_i response and photosynthetic capacity measurements 5-6 reps were utilised.

3.2.4. Surface Impressions

Surface impressions were performed in accordance with the methods in ***Chapter 2 Section 2.2.5*** for watered and droughted leaves and stipules.

3.2.5. Thermal Imaging

Thermal images of whole plants were taken under standard growth conditions (*see* ***Chapter 2 Section 2.2.1***) using a ^{FLIR}T500-Series thermal camera (Wilsonville, Oregon, USA) to determine differences in mean whole plant temperature between watered and droughted conditions.

3.2.6. Foliar Anatomical Measurements

Leaf and stipule mass per area measurements were calculated as per the methods in ***Chapter 2 Section 2.2.6***.

3.2.7. Yield Calculations

Yield measurements for watered and droughted plants were performed according to ***Chapter 2 Section 2.2.7***.

3.2.8. Data Analysis/Statistics

Mean ± standard error (SE) were calculated for each measurement. A Shapiro-Wilk test and Levene's test were utilised (respectively) to check if data was normally distributed and had equal variance and thus met the assumptions of an ANOVA. A one-way ANOVA and TukeyHSD test were utilised between *P. sativum* accessions and yield parameters (***Appendix Table.A2.1***) and between experimental condition (watered and droughted) and yield parameters (***Appendix Table.A2.2***). Three-way and/or multi-way ANOVAs were also calculated for each measured physiological parameter between *P. sativum* accessions, foliar tissues (leaves and stipules) and experimental conditions, followed by TukeyHSD tests. A multi-way ANOVA was also performed for each chlorophyll fluorescence parameter between PPFD/time, foliar tissue, experimental condition and *P. sativum* accession, followed by TukeyHSD tests which were calculated on data at the end of the chlorophyll fluorescent protocol (*i.e.*, at 10 or 20 minutes of induction/relaxation or at 1500 μmol m^{-2} s^{-1} PPFD of the chlorophyll fluorescent light curve). TukeyHSD results for each physiological

parameter were compared between the leaves and stipules (for accessions that had both types of foliar tissues) of the same experimental condition to determine differences between leaf and stipule physiology within each individual accession. TukeyHSD results for each physiological parameter were also compared between watered and droughted conditions to determine the impact of drought within each individual accession. Whilst multi-way ANOVAs and TukeyHSD tests were also carried out for stomatal density (SD), size (SS) and maximum anatomical stomatal conductance (gs_{max}) between the adaxial (AD) and abaxial (AB) surface, foliar tissue, experimental condition and *P. sativum* accession, with TukeyHSD results compared between the leaves and stipules, between watered and droughted conditions and between the AD and AB surfaces to determine differences within each individual accession.

Spearman's correlation coefficients (R) and linear regression equations were run between A and g_s at 400 μmol mol^{-1} [CO_2] measured from the A/C_i data. Spearman's correlation coefficients and linear regression equations were additionally calculated between SD, SS, gs_{max} and against g_s (at 400 μmol mol^{-1} [CO_2] measured from the A/C_i data) to determine if stomatal anatomy impacted g_s and/or gs_{max}. Whilst Spearman's correlation coefficients and linear regression equations were additionally carried out between plant temperature and foliar iWUE$_{max}$, between photosynthetic capacity and leaf/stipule mass per area and between photosynthetic capacity and each yield parameter. Graphs and statistics were generated within RStudio (Mac version 2024.04.0+735).

3.3. Results

3.3.1. Variation in Chlorophyll Fluorescence Parameters in Response to Light Under Watered and Droughted Conditions

3.3.1.1. Variation in Response to an Induction and Relaxation in Light Intensity

Chlorophyll fluorescence parameters (F_q'/F_m', F_q'/F_v' and F_v'/F_m') were monitored during a light induction and relaxation (***Fig.3.1&3.2***). In the induction phase, significant variation were identified in F_q'/F_m' ($F_{(3)} = 15.12$, $P < 0.001$), F_q'/F_v' ($F_{(3)} = 11.91$, $P < 0.001$) and F_v'/F_m' ($F_{(3)} = 4.32$, $P < 0.01$) between the different accessions, foliar tissues and experimental conditions (***Fig.3.1&3.2***).

At the end of the 10 min induction, Eth displayed a significantly higher F_q'/F_m' for watered stipules (0.64 ± 0.005) to Ni16 and Pacco (TukeyHSD; $P < 0.05$) (***Fig.3.1C&Table.3.2C***). Whilst Pacco was significantly lower in watered stipule F_q'/F_m' at 10 min (0.6 ± 0.006) to KW and Eth (TukeyHSD; $P < 0.05$) (***Fig.3.1C&Table.3.2C***). Eth also exhibited the highest F_q'/F_m' at the end of the induction for watered (0.66 ± 0.008) and droughted (0.67 ± 0.007) leaves and droughted stipules (0.65 ± 0.006), whilst watered Ni11 (0.62 ± 0.01) and droughted KW (0.63 ± 0.02) leaves and droughted KW (0.63 ± 0.01) stipules had the lowest F_q'/F_m' (***Fig.3.1A,B&D***). However, no significant difference was identified in F_q'/F_m' in either watered or droughted leaves or droughted stipules (TukeyHSD; $P > 0.05$) (***Fig.3.1A,B&D&Table.3.2A,B&D***). Quenching parameters highlighted that the greater F_q'/F_m' at the end of the induction in Eth watered stipules was primarily driven by a significantly higher value of F_v'/F_m' to Wando, Pacco and Ni16 (TukeyHSD; $P < 0.05$) (***Fig.3.2G&Table.3.3C***). The high

F_q'/F_m' in Eth watered and droughted leaves at 10 min were potentially driven via F_v'/F_m' and F_q'/F_v' (although no significant difference were identified to the other accessions in either parameter (TukeyHSD; $P > 0.05$)) (***Fig.3.2A,B,E&F&Table.3.3A&B***). Whilst the significantly higher value of F_q'/F_v' to KW (TukeyHSD; $P < 0.05$) possibly drove the higher F_q'/F_m' in droughted Eth stipules (***Fig.3.2D&Table.3.3D***). The low F_q'/F_m' in Pacco watered stipules was primarily driven by a significantly lower value of F_v'/F_m' to KW and Eth (TukeyHSD; $P < 0.05$) (***Fig.3.2G&Table.3.3C***). Whilst the low F_q'/F_m' in droughted KW leaves and stipules were primarily driven by low values of F_q'/F_v', with a significant difference to Ni16 and Wando in droughted leaf F_q'/F_v' (TukeyHSD; $P < 0.05$) and to Eth, Ni16 and Wando in droughted stipule F_q'/F_v' (TukeyHSD; $P < 0.05$) (***Fig.3.2B&D&Table.3.3B&D***). Whereas the low F_q'/F_m' in Ni11 watered leaves at 10 min were potentially driven by both F_v'/F_m' and F_q'/F_v' (although no significant difference were identified to the other accessions in either parameter (TukeyHSD; $P > 0.05$) (***Fig.3.2A&E&Table.3.3A***)). After 10 mins of induction no significant differences were identified in F_q'/F_m' between the leaves and stipules in either experimental condition within each individual accession (TukeyHSD; $P > 0.05$) (***Fig.3.1***). Whilst there were also no significant difference identified in F_q'/F_m' at the end of the induction between watered and droughted conditions for either foliar tissue within each individual accession (TukeyHSD; $P > 0.05$) (***Fig.3.1***).

In the relaxation phase, significant variation existed in F_v/F_m ($F_{(3)} = 13.57$, $P < 0.001$) between the different accessions, foliar tissues and experimental conditions (***Fig.3.1***). At the end of the relaxation protocol, Eth exhibited the highest F_v/F_m in watered (0.82

± 0.002) and droughted (0.82 ± 0.002) leaves and watered (0.82 ± 0.002) and droughted (0.82 ± 0.002) stipules, with a significant difference to Wando, Pacco and Ni16 in watered stipules F_v/F_m (TukeyHSD; $P < 0.05$) and to Ni16, KW and Wando in droughted leaf (TukeyHSD; $P < 0.05$) and droughted stipule F_v/F_m (TukeyHSD; $P < 0.05$) respectively (***Fig.3.1&Table.3.2***). However, no significant difference were observed in F_v/F_m at the end of the relaxation protocol for watered leaves (TukeyHSD; $P > 0.05$) (***Fig.3.1&Table.3.2***). Ni16 exhibited significantly lower values of watered (0.79 ± 0.006) and droughted stipule (0.8 ± 0.003) F_v/F_m to KW and Eth in watered stipule F_v/F_m (TukeyHSD; $P < 0.05$) and to Eth in droughted stipule F_v/F_m (TukeyHSD; $P < 0.05$) (***Fig.3.1C&D&Table.3.2C&D***). Whilst Wando exhibited the lowest F_v/F_m for droughted leaves (0.79 ± 0.007), with a significant difference to Ni11 and Eth (***Fig.3.1B&Table.3.2B***). However at the end of the protocol no significant differences were identified in F_v/F_m between the leaves and stipules for either experimental condition within each individual accession (TukeyHSD; $P > 0.05$) (***Fig.3.1***). There were also no significant difference identified in F_v/F_m at the end of the protocol between watered and droughted conditions for either foliar tissue within each individual accession (TukeyHSD; $P > 0.05$) (***Fig.3.1***).

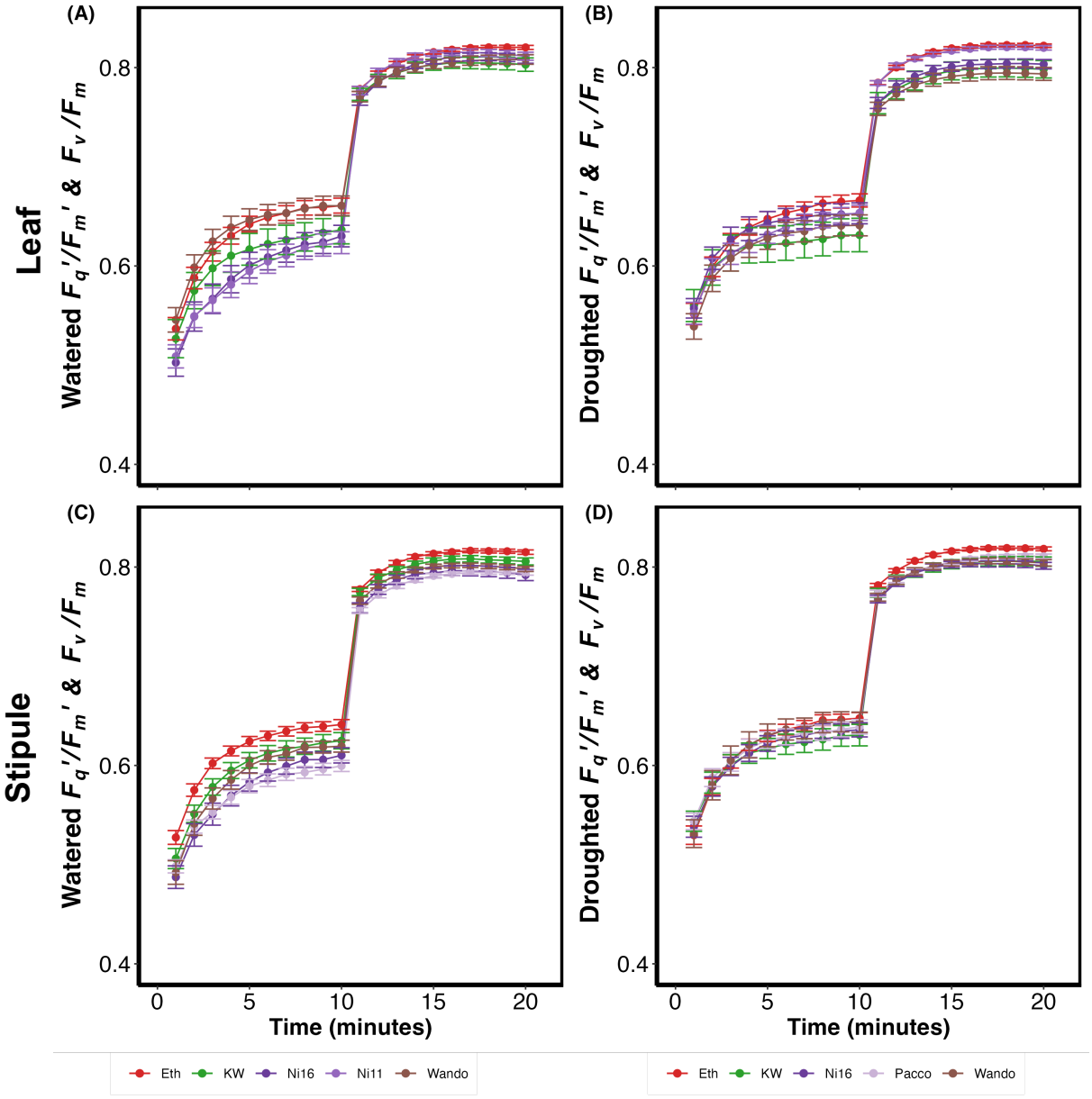

Figure 3.1. Variation in chlorophyll fluorescence induction and relaxation across P. sativum accessions under watered and droughted conditions. Induction responses were monitored as F_q'/F_m' (operating efficiency of photosystem II in the light) and recovery of F_v/F_m (photosystem II maximum efficiency in the dark) in both watered **(A)** leaves and **(C)** stipules and droughted **(B)** leaves and **(D)** stipules. Accessions were dark adapted for 30-min before being measured within a Fluorimager. Error bars represent mean ± SE (n = 6). Whilst the presence of * of the same colour indicates a significant difference in either F_q'/F_m' or F_v/F_m within an individual accession of the same experimental condition between the leaves and stipules, whereby * is $P < 0.05$, ** is $P < 0.01$ and *** is $P < 0.001$ (TukeyHSD). The presence of + of the same colour indicates a significant difference in either F_q'/F_m' or F_v/F_m within an individual accession of the same foliar tissue between watered and droughted conditions, whereby + is $P < 0.05$, ++ is $P < 0.01$ and +++ is $P < 0.001$ (TukeyHSD). Significant differences in either F_q'/F_m' at 10 minutes or F_v/F_m at 20 minutes between the *P. sativum* accessions can be found in ***Table.3.2***.

Table 3.2. Significant differences in chlorophyll fluorescence induction and relaxation parameters across P. sativum accessions under watered and droughted conditions. Induction responses were monitored as F_q'/F_m' (operating efficiency of photosystem II in the light) and recovery of F_v/F_m (photosystem II maximum efficiency in the dark) in ***Fig.3.1***. The different letters within the **(A)** watered leaf, **(B)** droughted leaf, **(C)** watered stipule and **(D)** droughted stipule tables indicate a significant difference in either F_q'/F_m' at 10 mins or F_v/F_m at 20 mins between the different *P. sativum* accessions ($P < 0.05$; TukeyHSD).

(A)

Accession	Watered Leaves	
	F_q'/F_m'	F_v/F_m
Eth	a	a
KW	a	a
Ni16	a	a
Ni11	a	a
Wando	a	a

(B)

Accession	Droughted Leaves	
	F_q'/F_m'	F_v/F_m
Eth	a	a
KW	a	c
Ni16	a	bc
Ni11	a	ab
Wando	a	c

(C)

Accession	Watered Stipules	
	F_q'/F_m'	F_v/F_m
Eth	a	a
KW	ab	ab
Ni16	bc	c
Pacco	c	bc
Wando	abc	bc

(D)

Accession	Droughted Stipules	
	F_q'/F_m'	F_v/F_m
Eth	a	a
KW	a	b
Ni16	a	b
Pacco	a	ab
Wando	a	b

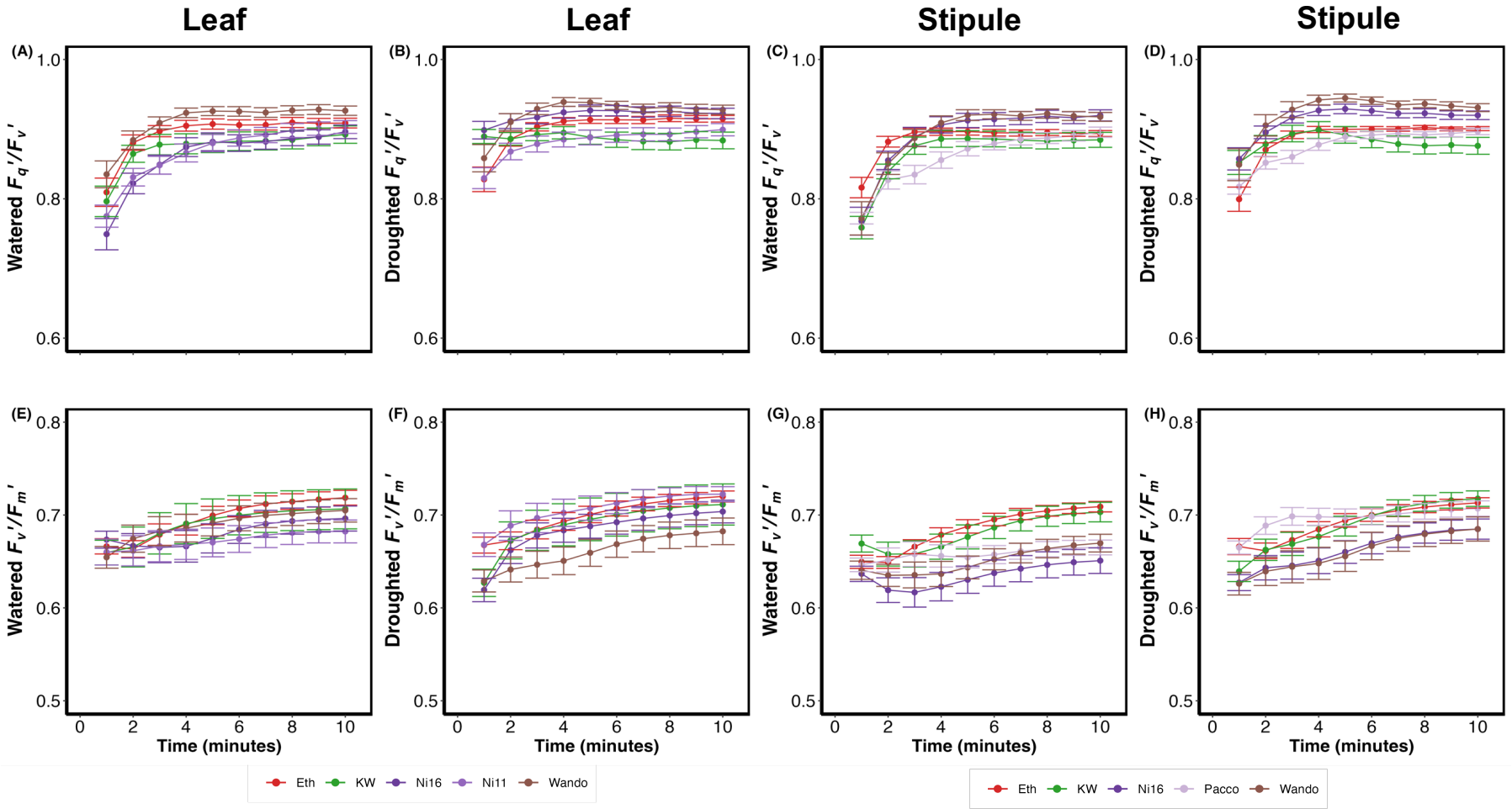

Figure 3.2. Variation in chlorophyll fluorescence induction parameters across P. sativum accessions under watered and droughted conditions. Induction responses were monitored as F_q'/F_v' (PSII photochemical quenching factor) in watered **(A)** leaves and **(C)** stipules and droughted **(B)** leaves and **(D)** stipules and as F_v'/F_m' (PSII maximum efficiency) in watered **(E)** leaves and **(G)** stipules and droughted **(F)** leaves and **(H)** stipules. Accessions were dark adapted for 30-minutes before being measured within a Fluorimager. Error bars represent mean ± SE (n = 6). Significant differences in either F_q'/F_v' or F_v'/F_m' at 10 minutes between the *P. sativum* accessions can be found in ***Table.3.3***.

Table 3.3. Significant differences in chlorophyll fluorescence induction parameters across P. sativum accessions under watered and droughted conditions. Induction responses were monitored as F_q'/F_v' (PSII photochemical quenching factor) and as F_v'/F_m' (PSII maximum efficiency) in ***Fig.3.2***. The different letters within the **(A)** watered leaf, **(B)** droughted leaf, **(C)** watered stipule and **(D)** droughted stipule tables indicate a significant difference in either F_q'/F_v' at 10 mins or F_v'/F_m' at 10 mins between the different *P. sativum* accessions ($P < 0.05$; TukeyHSD).

(A)

Accession	Watered Leaves	
	F_q'/F_v'	F_v'/F_m'
Eth	a	a
KW	a	a
Ni16	a	a
Ni11	a	a
Wando	a	a

(B)

Accession	Droughted Leaves	
	F_q'/F_v'	F_v'/F_m'
Eth	abc	a
KW	c	a
Ni16	ab	a
Ni11	bc	a
Wando	a	a

(C)

Accession	Watered Stipules	
	F_q'/F_v'	F_v'/F_m'
Eth	ab	a
KW	b	ab
Ni16	a	c
Pacco	ab	c
Wando	a	bc

(D)

Accession	Droughted Stipules	
	F_q'/F_v'	F_v'/F_m'
Eth	bc	a
KW	d	a
Ni16	ab	a
Pacco	cd	a
Wando	a	a

3.3.1.2. Photosynthetic Efficiency Light Response Curves

Chlorophyll fluorescence parameters (F_q'/F_m', F_q'/F_v', F_v'/F_m' and NPQ) were monitored as a function of irradiance, with significant variation identified in F_v'/F_m' ($F_{(3)}$ = 4.51, P < 0.01), F_q'/F_m' ($F_{(3)}$ = 7.90, P < 0.001) and NPQ ($F_{(3)}$ = 2.99, P < 0.05) between the different accessions, foliar tissues and experimental conditions (***Fig.3.3***). However, there were no significant difference observed in F_q'/F_v' ($F_{(3)}$ = 1.34, P = 0.25) or F_v/F_m (initial 0 µmol m^{-2} s^{-1} PPFD) ($F_{(3)}$ = 1.20, P = 0.31) between the different accessions, foliar tissues and experimental conditions (***Fig.3.3***).

At the highest light intensity (1500 µmol m^{-2} s^{-1} PPFD), Ni11 watered (0.28 ± 0.01) and KW droughted (0.28 ± 0.01) leaves and Pacco watered (0.26 ± 0.01) and Ni16 droughted (0.28 ± 0.01) stipules exhibited the lowest F_q'/F_m', with a significant difference identified to Eth in watered leaves (TukeyHSD; P < 0.05), watered stipules (TukeyHSD; P < 0.05) and droughted stipules (TukeyHSD; P < 0.05) respectively (***Fig.3.3A-D&Table.3.4***). Whereas Eth had the greatest F_q'/F_m' for watered (0.32 ± 0.008) and droughted (0.32 ± 0.007) leaves and watered (0.30 ± 0.005) and droughted (0.31 ± 0.006) stipules at 1500 µmol m^{-2} s^{-1} PPFD, with a significant difference in F_q'/F_m' to Ni16 and Ni11 in watered leaves (TukeyHSD; P < 0.05), Wando, Ni16 and Pacco in watered stipules (TukeyHSD; P < 0.05) and to Ni16 in droughted stipules (TukeyHSD; P < 0.05) F_q'/F_m' (***Fig.3.3A-D&Table.3.4***). However, no significant difference in F_q'/F_m' was identified in droughted leaves at the highest light intensity (***Fig.3.3B&Table.3.4B***).

Quenching parameters illustrated that the greater F_q'/F_m' in Eth watered leaves at 1500 µmol m^{-2} s^{-1} PPFD was primarily driven by a significantly higher value of F_q'/F_v' to Ni11 (TukeyHSD; $P < 0.05$) (***Fig.3.3I&Table.3.4A***). The greater F_q'/F_m' in Eth droughted leaves at the highest light intensity was potentially driven via significantly higher values of F_v'/F_m' to Wando (TukeyHSD; $P < 0.05$) and F_q'/F_v' to KW (TukeyHSD; $P < 0.05$) (***Fig.3.3F&J&Table.3.4B***). Whilst the higher F_q'/F_m' in Eth watered and droughted stipules were primarily driven by greater values of F_v'/F_m', with a significant difference identified to KW, Pacco, Ni16 and Wando in watered stipules F_v'/F_m' (TukeyHSD; $P < 0.05$) and to Ni16 and Wando in droughted stipules F_v'/F_m' (TukeyHSD; $P < 0.05$) (***Fig.3.3G,H,K&L&Table.3.4C&D***). The low F_q'/F_m' at 1500 µmol m^{-2} s^{-1} PPFD were primarily driven by low values of F_q'/F_v' for watered Ni11 and droughted KW leaves, with a significant difference identified to Eth in watered leaves (TukeyHSD; $P < 0.05$) and droughted leaves (TukeyHSD; $P < 0.05$) F_q'/F_v' respectively (***Fig.3.3I&J&Table.3.4A&B***). The low F_q'/F_m' in Pacco watered stipules at the highest light intensity was potentially driven via significantly lower values of F_v'/F_m' to Eth (TukeyHSD; $P < 0.05$) and F_q'/F_v' to Wando (TukeyHSD; $P < 0.05$) (***Fig.3.3G&K&Table.3.4C***). Whilst the low F_q'/F_m' at 1500 µmol m^{-2} s^{-1} PPFD in Ni16 droughted stipules were potentially driven by a significantly lower value of F_v'/F_m' to Pacco and Eth (TukeyHSD; $P < 0.05$) (***Fig.3.3H&Table.3.4D***). However, no significant differences were observed in F_q'/F_m' at 1500 µmol m^{-2} s^{-1} PPFD between the leaves and the stipules for either experimental condition within each individual accession (TukeyHSD; $P > 0.05$) (***Fig.3.3A-D***). There were also no significant difference identified in F_q'/F_m' at 1500 µmol m^{-2} s^{-1} PPFD between watered and droughted

conditions for either foliar tissue within each individual accession (TukeyHSD; $P > 0.05$) (***Fig.3.3A-D***).

Eth watered (2.46 ± 0.09) and Ni11 droughted (2.43 ± 0.13) leaves and Pacco watered (2.66 ± 0.07) and Eth droughted (2.61 ± 0.07) stipules exhibited the lowest NPQ at 1500 µmol m^{-2} s^{-1} PPFD, with a significant difference identified to Wando and Ni16 in droughted leaf (TukeyHSD; $P < 0.05$), watered stipule (TukeyHSD; $P < 0.05$) and droughted stipule (TukeyHSD; $P < 0.05$) NPQ respectively (***Fig.3.3M-P&Table.3.4***). Whereas Ni16 watered (2.79 ± 0.13) and droughted (2.93 ± 0.14) leaves and watered (3.05 ± 0.11) and droughted (3.09 ± 0.09) stipules had the highest NPQ at 1500 µmol m^{-2} s^{-1} PPFD, with a significant difference identified to Ni11 in droughted leaf NPQ (TukeyHSD; $P < 0.05$), to Pacco in watered stipule NPQ (TukeyHSD; $P < 0.05$) and to Pacco and Eth in droughted stipule NPQ (TukeyHSD; $P < 0.05$) (***Fig.3.3M-P&Table.3.4***). However, no significant difference in NPQ was identified in watered leaves at the highest light intensity (***Fig.3.3M&Table.3.4A***). Whilst there were no significant difference observed in NPQ at 1500 µmol m^{-2} s^{-1} PPFD between the leaves and the stipules for either experimental condition within each individual accession (TukeyHSD; $P > 0.05$) (***Fig.3.3M-P***). There were also no significant difference identified in NPQ at 1500 µmol m^{-2} s^{-1} PPFD between watered and droughted conditions for either foliar tissue within each individual accession (TukeyHSD; $P > 0.05$) (***Fig.3.3M-P***).

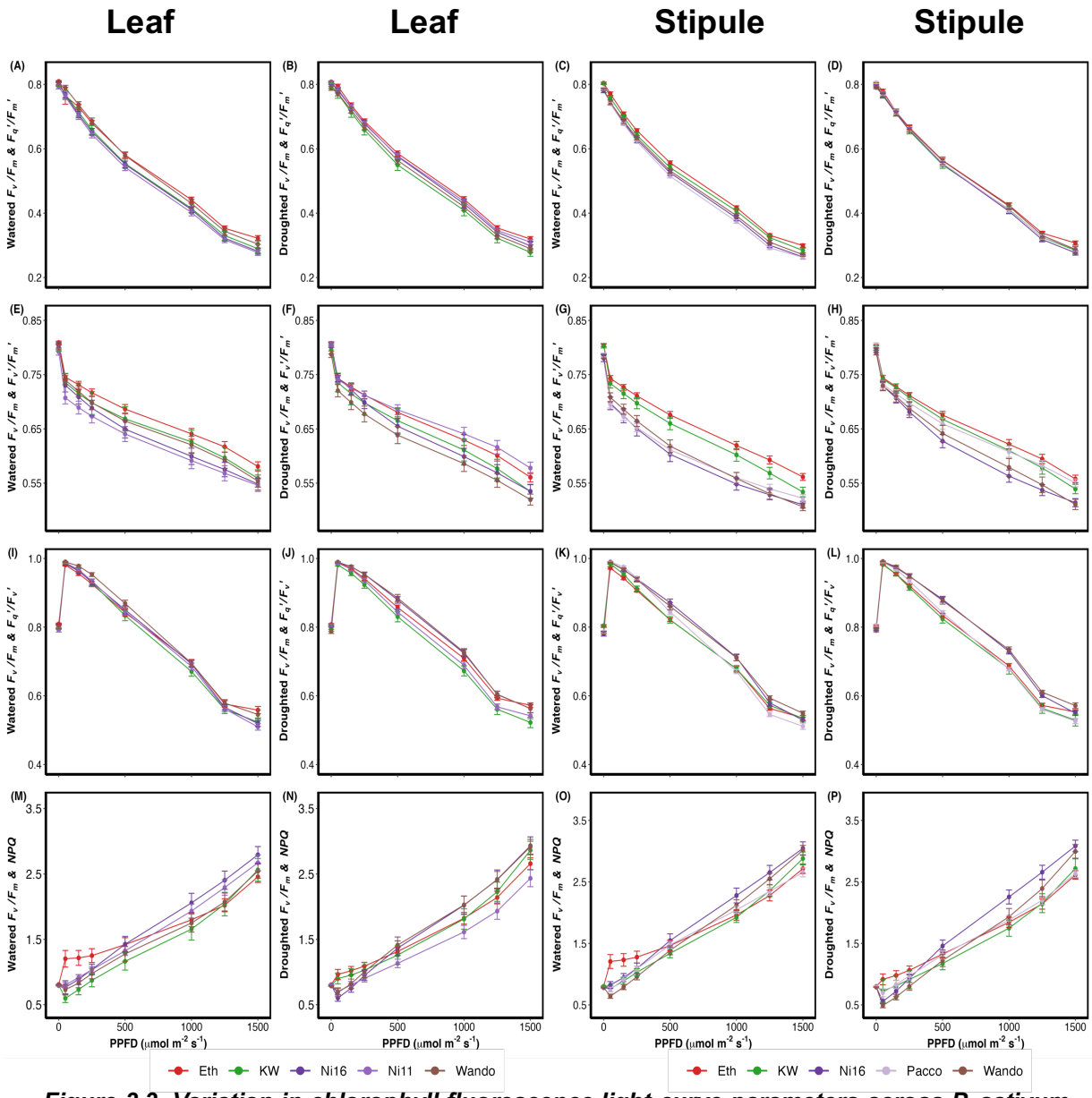

Figure 3.3. Variation in chlorophyll fluorescence light curve parameters across P. sativum accessions under watered and droughted conditions. Chlorophyll fluorescent responses to light intensity changes were monitored initially in the dark as F_v/F_m (photosystem II maximum efficiency in the dark) in all graphs, followed by measurements in the light monitored as F_q'/F_m' (operating efficiency of photosystem II; PSII) in watered **(A)** leaves and **(C)** stipules and droughted **(B)** leaves and **(D)** stipules, F_v'/F_m' (PSII maximum efficiency) in watered **(E)** leaves and **(G)** stipules and droughted **(F)** leaves and **(H)** stipules, F_q'/F_v' (PSII photochemical quenching factor) in watered **(I)** leaves and **(K)** stipules and droughted **(J)** leaves and **(L)** stipules and as NPQ (non-photochemical quenching) in watered **(M)** leaves and **(O)** stipules and droughted **(N)** leaves and **(P)** stipules. Accessions were dark adapted for 30-minutes before being measured at different photosynthetic photon flux densities (PPFD) within a Fluorimager. Error bars represent mean ± SE (n = 6). Whilst the presence of * of the same colour indicates a significant difference in either F_q'/F_m' or NPQ within an individual accession of the same experimental condition between the leaves and stipules, whereby * is $P < 0.05$, ** is $P < 0.01$ and *** is $P < 0.001$ (TukeyHSD). The presence of + of the same colour indicates a significant difference in either F_q'/F_m' or NPQ within an individual accession of the same foliar tissue between watered and droughted conditions, whereby + is $P < 0.05$, ++ is $P < 0.01$ and +++ is $P < 0.001$ (TukeyHSD). Significant differences in either F_q'/F_m', F_v'/F_m', F_q'/F_v' or NPQ at 1500 µmol m^{-2} s^{-1} PPFD between the *P. sativum* accessions can be found in ***Table.3.4***.

Table 3.4. Significant differences in chlorophyll fluorescence light curve parameters across P. sativum accessions under watered and droughted conditions. Chlorophyll fluorescent responses to light intensity changes were monitored in ***Fig.3.3*** as F_q'/F_m' (operating efficiency of photosystem II; PSII), F_v'/F_m' (PSII maximum efficiency), F_q'/F_v' (PSII photochemical quenching factor) and as NPQ (non-photochemical quenching). The different letters within the **(A)** watered leaf, **(B)** droughted leaf, **(C)** watered stipule and **(D)** droughted stipule tables indicate a significant difference in either F_q'/F_m', F_v'/F_m', F_q'/F_v' or NPQ at 1500 µmol m^{-2} s^{-1} photosynthetic photon flux density between the different *P. sativum* accessions ($P < 0.05$; TukeyHSD).

(A)

Accession	Watered Leaves			
	F_q'/F_m'	F_v'/F_m'	F_q'/F_v'	NPQ
Eth	a	a	a	a
KW	ab	a	ab	a
Ni16	b	a	ab	a
Ni11	b	a	b	a
Wando	ab	a	ab	a

(B)

Accession	Droughted Leaves			
	F_q'/F_m'	F_v'/F_m'	F_q'/F_v'	NPQ
Eth	a	a	a	ab
KW	a	ab	b	ab
Ni16	a	ab	ab	a
Ni11	a	a	ab	b
Wando	a	b	ab	a

(C)

Accession	Watered Stipules			
	F_q'/F_m'	F_v'/F_m'	F_q'/F_v'	NPQ
Eth	a	a	ab	ab
KW	ab	b	ab	ab
Ni16	b	b	ab	a
Pacco	b	b	b	b
Wando	b	b	a	a

(D)

Accession	Droughted Stipules			
	F_q'/F_m'	F_v'/F_m'	F_q'/F_v'	NPQ
Eth	a	a	ab	c
KW	ab	ab	b	abc
Ni16	b	b	ab	a
Pacco	ab	a	b	bc
Wando	ab	b	a	ab

3.3.2. Photosynthetic Rates in Response to Changing Light Intensity Under Watered and Droughted Conditions

A and g_s were monitored as a function of light intensity in watered and droughted leaves and stipules across the *P. sativum* accessions (***Fig.3.4***). For both conditions and foliar tissue types a typical hyperbolic response was observed in *A* with increasing light intensity, whilst little change in g_s was apparent (***Fig.3.4***). Significant variation was noted between the different accessions and foliar tissues in the light-saturated rate of *A*; A_{sat} ($F_{(3)} = 4.19$, $P < 0.01$) and g_s at 1500 µmol m^{-2} s^{-1} PPFD; gs_{1500} ($F_{(3)} = 4.91$, $P < 0.01$) (***Fig.3.5***). Significant variation was also identified between the different accessions and experimental conditions in A_{sat} ($F_{(5)} = 2.78$, $P < 0.05$) and gs_{1500} ($F_{(5)} = 4.96$, $P < 0.001$) (***Fig.3.5***).

KW exhibited the highest A_{sat} for watered leaves (25.3 ± 2.08 µmol m^{-2} s^{-1}) and watered (20.7 ± 1.46 µmol m^{-2} s^{-1}) and droughted stipules (14.9 ± 1.47 µmol m^{-2} s^{-1}) and was significantly different to Eth and Ni11 in watered leaf A_{sat} (TukeyHSD; $P < 0.05$), to Eth, Pacco and Wando in watered stipule A_{sat} (TukeyHSD; $P < 0.05$) and to Pacco in droughted stipule A_{sat} (TukeyHSD; $P < 0.05$) (***Fig.3.5A,C&D***). Whilst, Wando had a significantly higher A_{sat} for droughted leaves (18.5 ± 0.54 µmol m^{-2} s^{-1}) to Eth (TukeyHSD; $P < 0.05$) (***Fig.3.5B***). Eth exhibited the lowest A_{sat} for watered (14.6 ± 1.03 µmol m^{-2} s^{-1}) and droughted leaves (11.8 ± 0.5 µmol m^{-2} s^{-1}) and watered stipules (10.2 ± 0.77 µmol m^{-2} s^{-1}) with a significant difference to KW and Wando in watered leaf A_{sat} (TukeyHSD; $P < 0.05$), to KW and Ni16 in watered stipule A_{sat} (TukeyHSD; $P < 0.05$) and to KW, Ni11 and Wando in droughted leaf A_{sat} (TukeyHSD; $P < 0.05$)

(***Fig.3.5A-C***). Whilst Pacco had a significantly lower droughted stipule A_{sat} (8.57 ± 0.79 µmol m^{-2} s^{-1}) to KW and Ni16 (TukeyHSD; $P < 0.05$) (***Fig.3.5D***).

The highest gs_{1500} for droughted leaves and stipules were observed in Wando (0.44 ± 0.03 mol m^{-2} s^{-1}) and Ni16 (0.32 ± 0.04 mol m^{-2} s^{-1}), respectively, with a significant difference to Eth in droughted leaf gs_{1500} (TukeyHSD; $P < 0.05$) and to Eth and Pacco in droughted stipule gs_{1500} (TukeyHSD; $P < 0.05$) (***Fig.3.5F&H***). Whilst KW exhibited the highest watered leaf (0.64 ± 0.05 mol m^{-2} s^{-1}) and stipule (0.44 ± 0.07 mol m^{-2} s^{-1}) gs_{1500} and was significantly higher than Eth and Ni11 in watered leaf gs_{1500} (TukeyHSD; $P < 0.05$) and significantly greater than Eth in watered stipule gs_{1500} (TukeyHSD; $P < 0.05$) (***Fig.3.5E&G***). Whereas the lowest gs_{1500} for watered leaves and droughted stipules were observed in Ni11 (0.29 ± 0.03 mol m^{-2} s^{-1}) and Pacco (0.18 ± 0.02 mol m^{-2} s^{-1}), respectively, with a significant difference to KW, Ni16 and Wando in watered leaf gs_{1500} (TukeyHSD; $P < 0.05$) and to Ni16 in droughted stipule gs_{1500} (TukeyHSD; $P < 0.05$) (***Fig.3.5E&H***). Eth had the lowest droughted leaf (0.21 ± 0.01 mol m^{-2} s^{-1}) and watered stipule (0.17 ± 0.03 mol m^{-2} s^{-1}) gs_{1500} and was significantly different to Ni16, Ni11 and Wando in droughted leaf gs_{1500} (TukeyHSD; $P < 0.05$) and significantly lower than KW and Ni16 in watered stipule gs_{1500} (TukeyHSD; $P < 0.05$) (***Fig.3.5F&G***).

The leaves generally had a higher A_{sat} and gs_{1500} than the stipules for both watered and droughted conditions (***Fig.3.5***), with a significant difference identified in A_{sat} between the leaves and stipules of watered Wando (TukeyHSD; $P < 0.001$) and between the leaves and stipules of droughted Wando (TukeyHSD; $P < 0.05$)

(***Fig.3.5A-D***). A significant difference in gs_{1500} was also identified between watered Wando leaves and stipules (TukeyHSD; $P < 0.001$) and between droughted Wando leaves and stipules (TukeyHSD; $P < 0.05$) (***Fig.3.5E-H***). Watered conditions generally experienced a higher A_{sat} and gs_{1500} than droughted conditions, with a significant difference observed between KW watered and droughted leaves in gs_{1500} (TukeyHSD; $P < 0.001$) (***Fig.3.5E-H***). However, there were no significant difference seen in A_{sat} between watered and droughted conditions for either foliar tissue within each individual accession (TukeyHSD; $P > 0.05$) (***Fig.3.5A-D***).

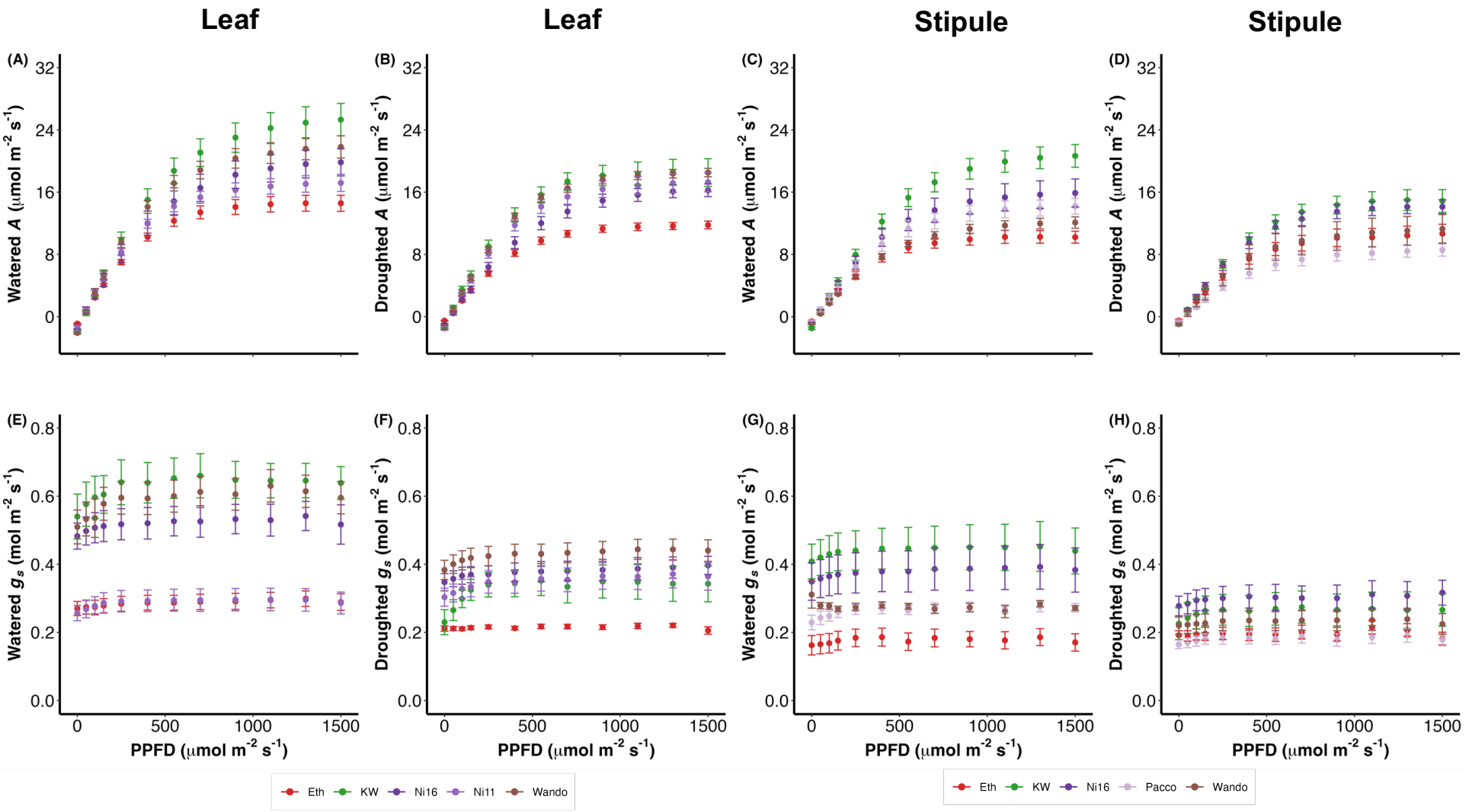

Figure 3.4. Variation in carbon assimilation (A) and stomatal conductance (g_s) in response to light across P. sativum accessions under watered and droughted conditions. Changes in watered **(A)** leaf and **(C)** stipule and droughted **(B)** leaf and **(D)** stipule assimilation as well as watered **(E)** leaf and **(G)** stipule and droughted **(F)** leaf and **(H)** stipule stomatal conductance were measured against increasing photosynthetic photon flux densities (PPFD) within in Li-Cor 6800 at 23°C and 400 μmol mol^{-1} [CO_2]. Error bars represent mean ± SE (n = 6).

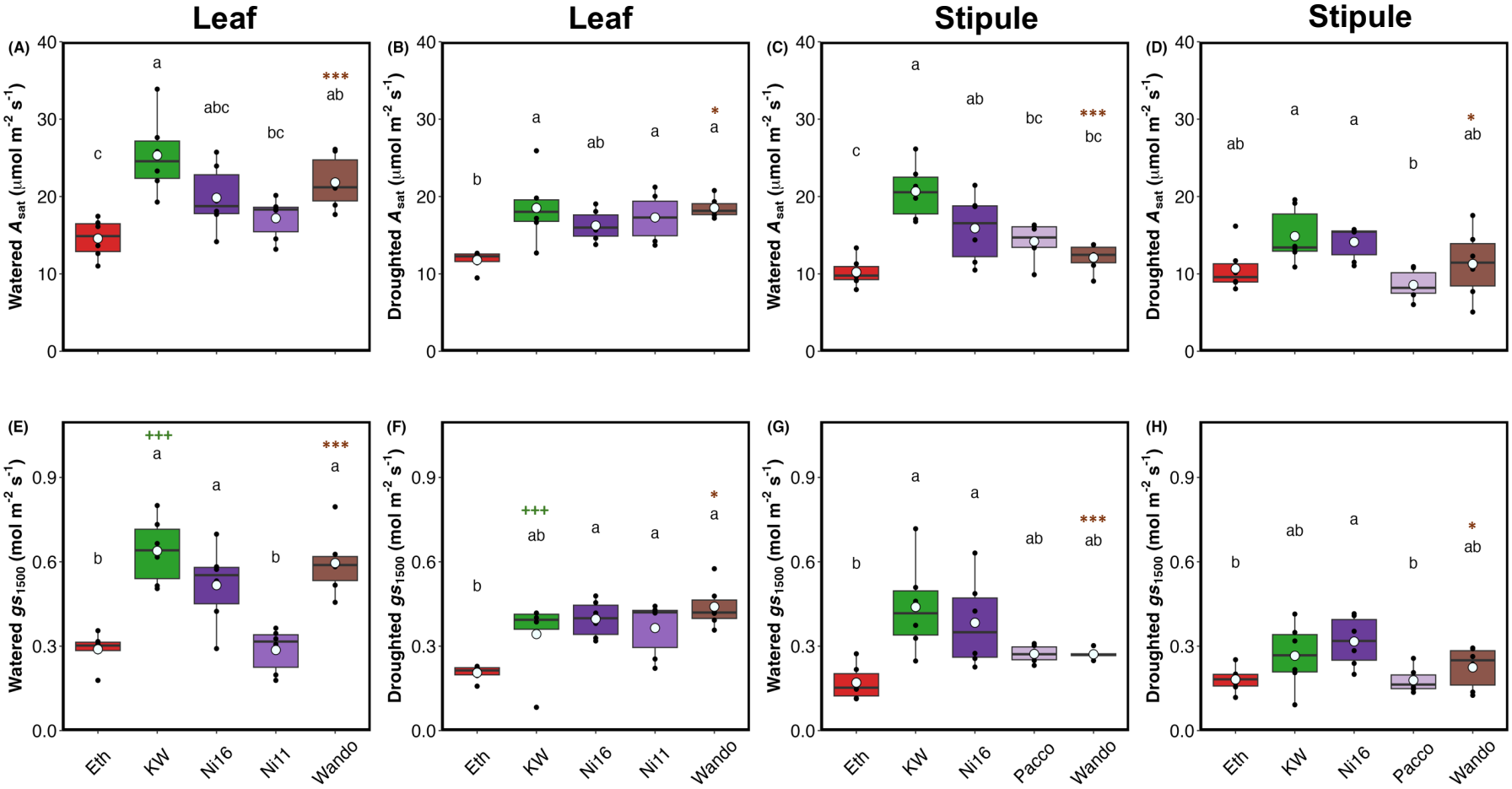

Figure 3.5. Variation in leaf and stipule light-saturated rate of A (A_{sat}) and g_s at 1500 µmol m^{-2} s^{-1} PPFD (gs_{1500}) across P. sativum accessions under watered and droughted conditions. Changes in watered **(A)** leaf and **(C)** stipule and droughted **(B)** leaf and **(D)** stipule light-saturated rate of assimilation (A_{sat}) and watered **(E)** leaf and **(G)** stipule and droughted **(F)** leaf and **(H)** stipule stomatal conductance at 1500 µmol m^{-2} s^{-1} photosynthetic photon flux density (gs_{1500}) were measured within a Li-Cor 6800 at 23 ºC and 400 µmol mol^{-1} [CO_2]. White dots symbolise the mean, whilst error bars represent mean ± SE (n = 6). Different letters above each error bar indicate a significant difference in either A_{sat} or gs_{1500} between *P. sativum* accessions ($P < 0.05$; TukeyHSD). Whilst the presence of * of the same colour indicates a significant difference in either A_{sat} or gs_{1500} within an individual accession of the same experimental condition between the leaves and stipules, whereby * is $P < 0.05$, ** is $P < 0.01$ and *** is $P < 0.001$ (TukeyHSD). The presence of + of the same colour indicates a significant difference in either A_{sat} or gs_{1500} within an individual accession of the same foliar tissue between watered and droughted conditions, whereby + is $P < 0.05$, ++ is $P < 0.01$ and +++ is $P < 0.001$ (TukeyHSD).

3.3.3. Variation in Photosynthetic Capacity Under Watered and Droughted Conditions

A was measured as a function of internal [CO_2] (C_i) in watered and droughted leaves and stipules, to determine differences in photosynthetic capacity across the *P. sativum* accessions (***Fig.3.6***). Both watered and droughted leaves and stipules exhibited a hyperbolic response in *A*, whilst as expected g_s remained relatively constant (***Fig.3.6***). KW generally had the greatest g_s, whilst Eth generally had the lowest g_s at the majority of measured C_i for both conditions and foliar tissue types (***Fig.3.6E-H***). A strong positive correlation was identified between leaf *A* and g_s (R = 0.88, $P < 0.001$) and between stipule *A* and g_s (R = 0.81, $P < 0.001$), with little observed difference between watered and droughted conditions for either correlation (***Fig.3.7***).

Significant variation in the maximum rate of Rubisco activity; Vc_{max} ($F_{(3)} = 2.97$, $P < 0.05$) and maximum rate of electron transport; J_{max} ($F_{(3)} = 4.86$, $P < 0.01$) was noted between the different accessions, foliar tissues and experimental conditions (***Fig.3.8***). KW exhibited the highest Vc_{max} (112 ± 7.86 µmol m^{-2} s^{-1}) and J_{max} (180.5 ± 12.12 µmol m^{-2} s^{-1}) for watered leaves and was significantly different in watered leaf Vc_{max} to Eth, Ni16 and Ni11 (TukeyHSD; $P < 0.05$) and significantly different in watered leaf J_{max} to the remaining accessions (TukeyHSD; $P < 0.05$) (***Fig.3.8A&E***). Whereas Eth had the lowest watered leaf Vc_{max} (61.6 ± 3.96 µmol m^{-2} s^{-1}) and J_{max} (108 ± 7.34 µmol m^{-2} s^{-1}), with a significant difference to KW and Wando in watered leaf Vc_{max} (TukeyHSD; $P < 0.05$) and to KW in watered leaf J_{max} (TukeyHSD; $P < 0.05$) (***Fig.3.8A&E***). KW also

had the highest droughted leaf Vc_{max} (109.3 ± 3.25 µmol m^{-2} s^{-1}) and J_{max} (179.6 ± 6.51 µmol m^{-2} s^{-1}), with a significant difference to the remaining accessions for droughted leaf Vc_{max} (TukeyHSD; $P < 0.05$) and J_{max} (TukeyHSD; $P < 0.05$) respectively (***Fig.3.8B&F***). The highest watered stipule Vc_{max} (91.1 ± 5.92 µmol m^{-2} s^{-1}) and J_{max} (148.4 ± 7.88 µmol m^{-2} s^{-1}) was also observed in KW, which was significantly higher than the remaining accessions in watered stipule Vc_{max} (TukeyHSD; $P < 0.05$) and J_{max} (TukeyHSD; $P < 0.05$), respectively (***Fig.3.8C&G***). In contrast, Eth exhibited a significantly lower droughted leaf Vc_{max} (57.1 ± 3.15 µmol m^{-2} s^{-1}) and J_{max} (98.22 ± 4.07 µmol m^{-2} s^{-1}) and watered stipule Vc_{max} (47.89 ± 3.82 µmol m^{-2} s^{-1}) to KW (TukeyHSD; $P < 0.05$) (***Fig.3.8B,C&F***). Whilst Wando was significantly lower in watered stipule J_{max} (73.22 ± 5.32 µmol m^{-2} s^{-1}) to KW (TukeyHSD; $P < 0.05$) (***Fig.3.8G***). However, no significant differences were identified in droughted stipule Vc_{max} or J_{max} between any of the accessions (TukeyHSD; $P > 0.05$) (***Fig.3.8D&H***).

The leaves generally had a higher Vc_{max} and J_{max} than the stipules for both watered and droughted conditions (***Fig.3.8***), with a significant difference identified in Vc_{max} between the leaves and stipules of watered Wando (TukeyHSD; $P < 0.001$) and between the leaves and stipules of droughted KW (TukeyHSD; $P < 0.001$) (***Fig.3.8A-D***). A significant difference in J_{max} was also identified between watered Wando leaves and stipules (TukeyHSD; $P < 0.001$) and between droughted KW leaves and stipules (TukeyHSD; $P < 0.001$) (***Fig.3.8E-H***). However, there were no significant difference seen in Vc_{max} or J_{max} between watered and droughted conditions for either foliar tissue within each individual accession (TukeyHSD; $P > 0.05$) (***Fig.3.8***).

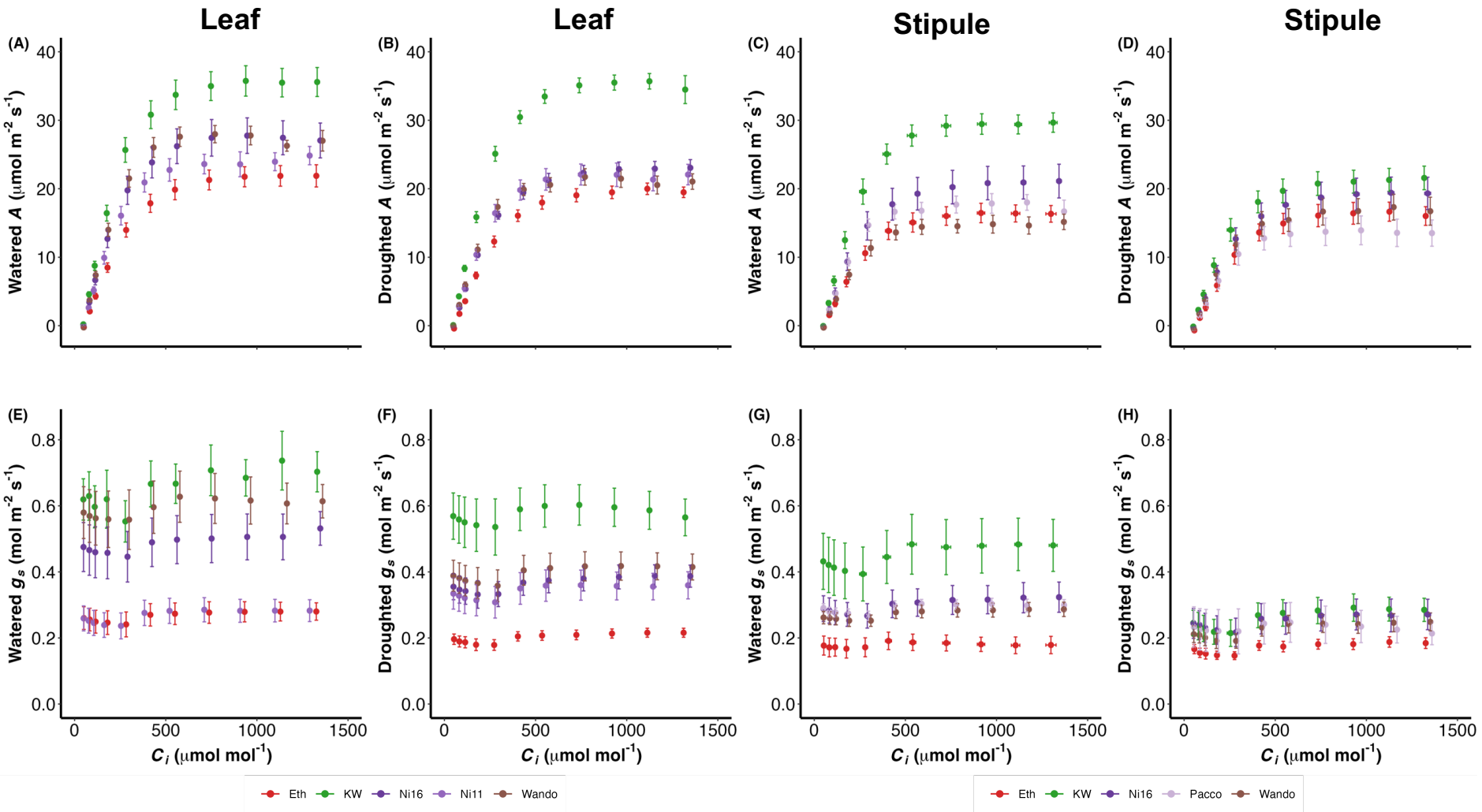

Figure 3.6. Variation in carbon assimilation (A) and stomatal conductance (g_s) in response to changing internal CO_2 concentration (C_i) across P. sativum accessions under watered and droughted conditions. Changes in watered **(A)** leaf and **(C)** stipule and droughted **(B)** leaf and **(D)** stipule assimilation and watered **(E)** leaf and **(G)** stipule and droughted **(F)** leaf and **(H)** stipule stomatal conductance were measured against increasing C_i within a Li-Cor 6800 at 23 ºC and 1500 µmol m^{-2} s^{-1} photosynthetic photon flux density. Error bars represent mean ± SE (n = 5-6).

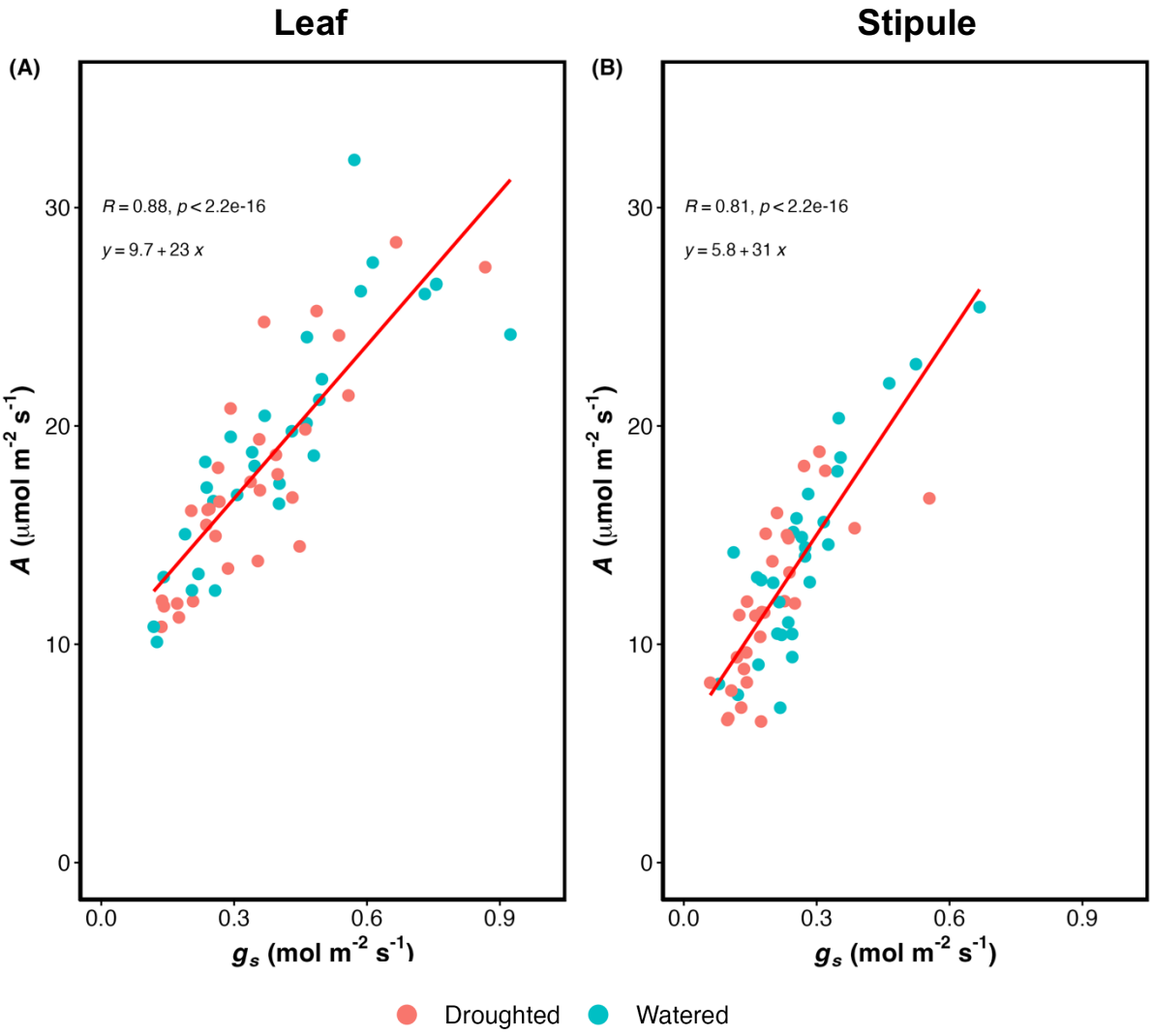

Figure 3.7. Spearmans correlation between Assimilation (A) and stomatal conductance (g_s) for leaves and stipules under watered and droughted conditions. Correlations between *A* and g_s for the **(A)** leaves and **(B)** stipules, red dots indicate droughted whilst blue dots represent watered conditions. *A* and g_s were measured at 400 µmol mol^{-1} intercellular CO_2 concentration within a Li-Cor 6800 at 23 °C and 1500 µmol m^{-2} s^{-1} photosynthetic photon flux density. Spearman's correlation coefficients (R) and linear regressions (represented as equations and red lines) were calculated for each *A* against g_s. $P < 0.05$ indicates a significant relationship (n=5-6).

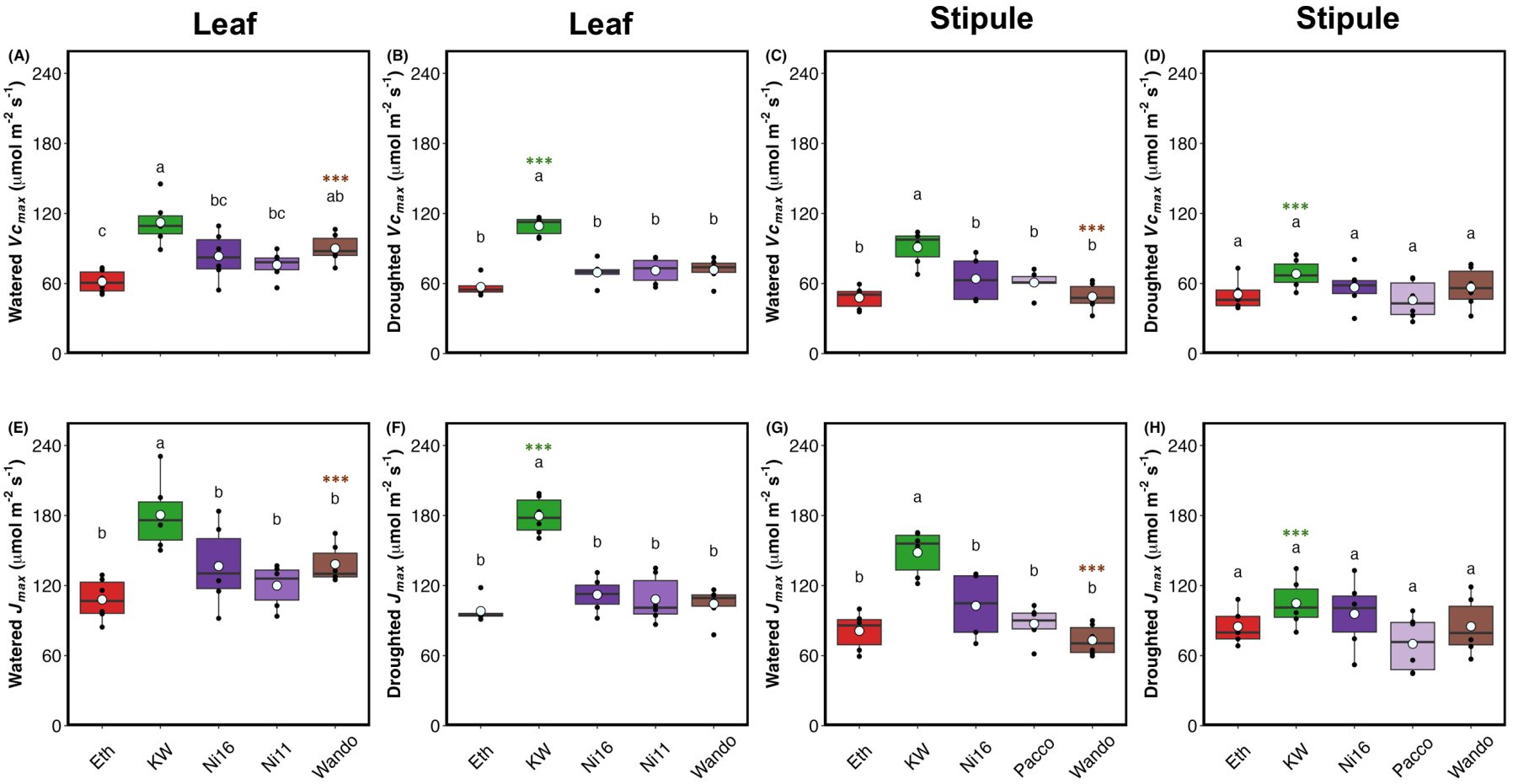

Figure 3.8. Variation in photosynthetic capacity across P. sativum accessions under watered and droughted conditions. Photosynthetic capacity were monitored as Vc_{max} (maximum rate of Rubisco activity) in watered **(A)** leaves and **(C)** stipules and droughted **(B)** leaves and **(D)** stipules and as J_{max} (maximum rate of electron transport) in watered **(E)** leaves and **(G)** stipules and droughted **(F)** leaves and **(H)** stipules. Measured within a Li-Cor 6800 at 1500 µmol m^{-2} s^{-1} photosynthetic photon flux density and 23 ºC (n = 5-6). White dots symbolise the mean, whilst error bars represent mean ± SE. Different letters above each error bar represent significant differences in either Vc_{max} or J_{max} between *P. sativum* accessions ($P < 0.05$; TukeyHSD). Whilst the presence of * of the same colour indicates a significant difference in either Vc_{max} or J_{max} within an individual accession of the same experimental condition between the leaves and stipules, whereby * is $P < 0.05$, ** is $P < 0.01$ and *** is $P < 0.001$ (TukeyHSD). The presence of + of the same colour indicates a significant difference in either Vc_{max} or J_{max} within an individual accession of the same foliar tissue between watered and droughted conditions, whereby + is $P < 0.05$, ++ is $P < 0.01$ and +++ is $P < 0.001$ (TukeyHSD).

3.3.4. Variation in Stomatal Characteristics Under Watered and Droughted Conditions

3.3.4.1. Stomatal Densities

Variation in stomatal densities (SD) were determined in watered and droughted leaves and stipules for the adaxial (AD) and abaxial (AB) surfaces across the *P. sativum* accessions (***Fig.3.9***). Significant variation were apparent in SD between the different *P. sativum* accessions for the AD ($F_{(4)}$ = 12.41, P < 0.001) and AB ($F_{(4)}$ = 9.56, P < 0.001) watered leaves, AD ($F_{(4)}$ = 5.52, P < 0.01) and AB ($F_{(4)}$ = 4.30, P < 0.01) droughted leaves, AD ($F_{(4)}$ = 20.72, P < 0.001) and AB ($F_{(4)}$ = 24.34, P < 0.001) watered stipules and AD ($F_{(4)}$ = 9.99, P < 0.001) and AB ($F_{(4)}$ = 16.31, P < 0.001) droughted stipules (***Fig.3.9***). An overall significant difference was also noted in SD between the different accessions, foliar tissues and experimental conditions ($F_{(3)}$ = 8.42, P < 0.001) (***Fig.3.9***).

The lowest AD SD was observed within Eth for watered (88.61 ± 3.71 mm^{-2}) and droughted (98.74 ± 6.19 mm^{-2}) leaves and watered (74.87 ± 3.17 mm^{-2}) and droughted (90.78 ± 6.44 mm^{-2}) stipules, with a significant difference to KW, Ni16, Ni11 and Wando in watered leaf AD SD (TukeyHSD; P < 0.05), to KW, Ni11 and Ni16 in droughted leaf AD SD (TukeyHSD; P < 0.05), to KW, Ni16, Pacco and Wando in watered stipule AD SD and to KW and Ni16 in droughted stipule AD SD (TukeyHSD; P < 0.05) (***Fig.3.9A-D***). Whilst Ni16 exhibited the highest AD SD for watered (158.8 ± 8.44 mm^{-2}) and droughted (136.9 ± 8.45 mm^{-2}) leaves and watered (122.6 ± 4.68 mm^{-2}) and droughted (130 ± 4.36 mm^{-2}) stipules and was significantly different to Eth and KW in watered

leaf AD SD (TukeyHSD; $P < 0.05$), to Eth in droughted leaf AD SD (TukeyHSD; $P < 0.05$), to Pacco and Eth in watered stipule AD SD (TukeyHSD; $P < 0.05$) and to Eth, Pacco and Wando in droughted stipule AD SD (TukeyHSD; $P < 0.05$) (***Fig.3.9A-D***). The lowest AB SD were also observed within Eth for watered (118.5 ± 3.25 mm^{-2}) and droughted (122.1 ± 4.23 mm^{-2}) leaves and watered (106.9 ± 2.56 mm^{-2}) and droughted (110 ± 8.34 mm^{-2}) stipules, which were significantly different in watered leaf AB SD to Ni16 and Wando (TukeyHSD; $P < 0.05$), in droughted leaf AB SD to KW (TukeyHSD; $P < 0.05$), and to KW, Ni16 and Wando in watered stipule (TukeyHSD; $P < 0.05$) and droughted stipule (TukeyHSD; $P < 0.05$) AB SD, respectively (***Fig.3.9E-H***). In contrast, Ni16 had the highest watered leaf AB (195.5 ± 17.14 mm^{-2}) and droughted stipule AB (147.57 ± 2.73 mm^{-2}) SD, with a significant difference to Eth, KW and Ni11 for watered AB leaves (TukeyHSD; $P < 0.05$) and to Eth and Pacco for droughted AB stipules (TukeyHSD; $P < 0.05$) (***Fig.3.9E&H***). Whilst KW and Wando had the greatest droughted leaf (156.6 ± 8.80 mm^{-2}) and watered stipules (164.39 ± 5.57 mm^{-2}) AB SD respectively, which were significantly different in droughted leaf AB SD to Eth (TukeyHSD; $P < 0.05$) and in watered stipule AB SD to Eth, Ni16 and Pacco (TukeyHSD; $P < 0.05$) (***Fig.3.9F&G***).

AB surfaces generally exhibited higher SD for both watered and droughted leaves and stipules than the AD surfaces (***Fig.3.9***), with a significant difference identified in SD between the AD and AB surfaces within the individual accession of watered Ni16 leaves (TukeyHSD; $P < 0.05$), watered Wando leaves (TukeyHSD; $P < 0.05$) and watered Wando stipules (TukeyHSD; $P < 0.001$) (***Table.3.5&Fig.3.9A,C,E&G***). The leaves were generally higher in SD than the stipules for watered AD and AB and

droughted AD surfaces (***Fig.3.9***), with a significant difference identified in SD between the leaves and stipules within the individual accession of watered Ni16 AD (TukeyHSD; $P < 0.05$) and watered Ni16 AB (TukeyHSD; $P < 0.001$) (***Fig.3.9A,C,E&G***). Watered conditions generally had a greater SD than droughted conditions for AD and AB leaves and AD stipules, whereas droughted conditions generally exhibited higher SD for AB stipules than watered conditions (***Fig.3.9***), with a significant difference identified in SD between watered and droughted conditions within the individual accession of Ni16 AB leaves (TukeyHSD; $P < 0.001$) and Wando AB leaves (TukeyHSD; $P < 0.01$) (***Fig.3.9E&F***).

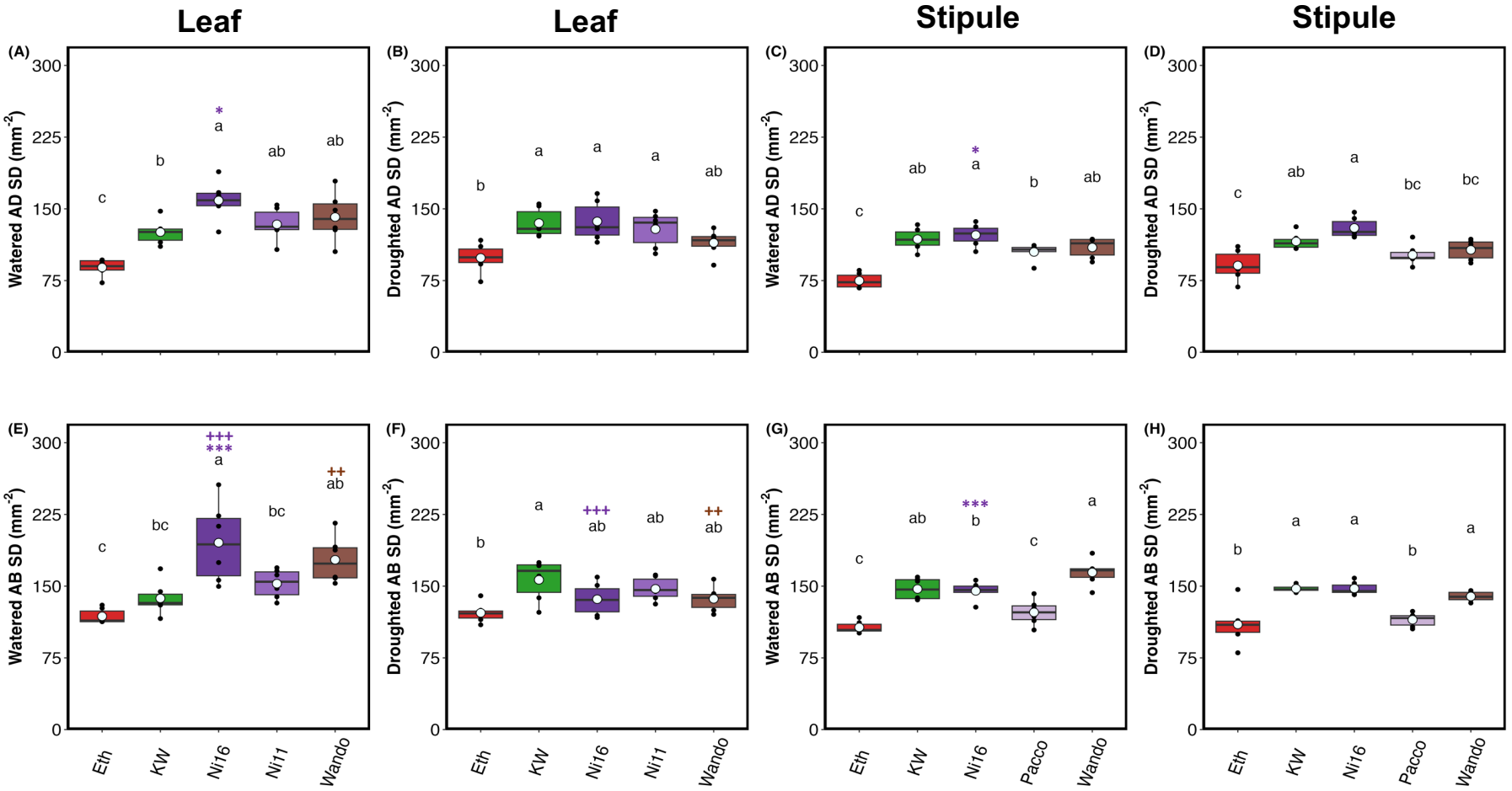

Figure 3.9. Variation in adaxial and abaxial leaf and stipule stomatal densities across P. sativum accessions under watered and droughted conditions. Stomatal densities (SD) were calculated for the adaxial (AD) watered **(A)** leaves and **(C)** stipules and droughted **(B)** leaves and **(D)** stipules and for the abaxial (AB) watered **(E)** leaves and **(G)** stipules and droughted **(F)** leaves and **(H)** stipules. Stomata were counted at 200x magnification in a 1 mm^2 grid (n = 6). White dots symbolise the mean, whilst error bars represent mean ± SE. Different letters above each error bar represent significant differences in either AD or AB SD between *P. sativum* accessions ($P < 0.05$; TukeyHSD). Whilst the presence of * of the same colour indicates a significant difference in either AD or AB SD within an individual accession of the same experimental condition between the leaves and stipules, whereby * is $P < 0.05$, ** is $P < 0.01$ and *** is $P < 0.001$ (TukeyHSD). The presence of + of the same colour indicates a significant difference in either AD or AB SD within an individual accession of the same foliar tissue between watered and droughted conditions, whereby + is $P < 0.05$, ++ is $P < 0.01$ and +++ is $P < 0.001$ (TukeyHSD). Significant differences in SD between the AD and AB surfaces can be found in ***Table.3.5***.

Table 3.5. Statistical P values between adaxial (AD) and abaxial (AB) stomatal densities (SD). Statistical differences were generated from ***Fig.3.9*** via TukeyHSD comparisons of AD vs AB SD of the same foliar tissue and same experimental condition for each individual accession, whereby * is $P < 0.05$, ** is $P < 0.01$ and *** is $P < 0.001$ (TukeyHSD). Stomata were counted at 200x magnification in a 1 mm^2 grid (n = 6).

Accession	AD vs AB SD *P* values			
	Watered		Droughted	
	Leaves	Stipules	Leaves	Stipules
Eth	0.34	0.19	0.88	0.99
KW	1.00	0.43	0.96	0.22
Ni16	**0.04***	0.93	1.00	1.00
Ni11	0.99	NA	1.00	NA
Pacco	NA	1.00	NA	1.00
Wando	**4.89E-02***	**5.01E-06*****	0.93	0.18

3.3.4.2. Stomatal Sizes

Variation in stomatal sizes (SS: consisting of pore length; PL and guard cell length; GCL) were assessed in watered and droughted leaves and stipules for the adaxial (AD) and abaxial (AB) surfaces across the *P. sativum* accessions (***Fig.3.10***). Significant variation were identified between the different surfaces and *P. sativum* accessions for PL ($F_{(5)} = 4.22$, $P < 0.01$) and GCL ($F_{(5)} = 3.32$, $P < 0.01$) and between the different accessions and foliar regions for PL ($F_{(3)} = 4.65$, $P < 0.01$) and GCL ($F_{(3)} = 5.26$, $P < 0.01$) (***Fig.3.10***). Significant variation was also observed for PL between the different accessions and experimental conditions ($F_{(5)} = 5.31$, $P < 0.001$) (***Fig.3.10***).

Eth exhibited the largest watered stipule AD PL (18.18 ± 0.19 µm) and GCL (29.15 ± 0.43 µm) and AB PL (18.11 ± 0.79 µm) and GCL (29.14 ± 0.77 µm), with a significant difference in watered stipule AD PL to Ni16, Pacco and Wando (TukeyHSD; $P < 0.05$), a significant difference to all accessions in watered stipule AD GCL (TukeyHSD; $P < 0.05$) and a significant difference to Pacco and Wando in watered stipule AB PL (TukeyHSD; $P < 0.05$) and AB GCL (TukeyHSD; $P < 0.05$) respectively (***Fig.3.10C,G,K&O***). In contrast, Pacco had the smallest watered stipule AD PL (14.77 ± 0.37 µm) and GCL (23.34 ± 0.38 µm) and AB PL (14.35 ± 0.45 µm), which were significantly different to Eth, KW and Ni16 in watered stipule AD PL (TukeyHSD; $P < 0.05$), AB PL (TukeyHSD; $P < 0.05$) and AD GCL (TukeyHSD; $P < 0.05$) respectively (***Fig.3.10C,G&K***). Whilst Wando had a significantly lower watered stipule AB GCL (24.2 ± 0.87 µm) to Eth, KW and Ni16 (TukeyHSD; $P < 0.05$) (***Fig.3.10O***). Eth also had a significantly larger AB PL in droughted stipules (18.21 ± 0.33 µm) than Pacco

and Wando (TukeyHSD; $P < 0.05$) and a significantly larger AB GCL in droughted stipules (28.74 ± 0.34 µm) to Wando (TukeyHSD; $P < 0.05$) (***Fig.3.10H&P***). Whereas Wando exhibited significantly smaller AB PL in droughted stipules (15.30 ± 0.30 µm) to Eth and KW (TukeyHSD; $P < 0.05$) and significantly smaller AB GCL in droughted stipules (24.13 ± 0.62 µm) to Eth (TukeyHSD; $P < 0.05$) (***Fig.3.10H&P***). The largest AB GCL for droughted leaves was observed within KW (28.56 ± 0.94 µm), which was significantly different in AB GCL to Ni11 and Wando droughted leaves (TukeyHSD; $P < 0.05$) (***Fig.3.10N***). Whilst Ni11 droughted leaves had a significantly smaller AB GCL (23.86 ± 0.78 µm) to KW, Ni16 and Eth droughted leaves (TukeyHSD; $P < 0.05$) (***Fig.3.10N***). However no significant differences were identified between any of the accessions in watered leaves for AD or AB PL or GCL, in droughted leaves for AD or AB PL or AD GCL, or in droughted stipules for AD PL or GCL (TukeyHSD; $P > 0.05$) (***Fig.3.10A,B,D,E,F, I,J,L&M***).

There were no significant difference identified in PL or GCL between the AD and AB surfaces for either foliar tissues or experimental condition within each individual accession (TukeyHSD; $P > 0.05$) (***Table.3.6&Fig.3.10***). There were also no significant difference identified in PL or GCL between the leaves and stipules for either surface or experimental condition within each individual accession (TukeyHSD; $P > 0.05$) (***Fig.3.10***). Whilst there were no significant difference identified in PL or GCL between watered and droughted conditions for either surface or foliar tissues within each individual accession (TukeyHSD; $P > 0.05$) (***Fig.3.10***).

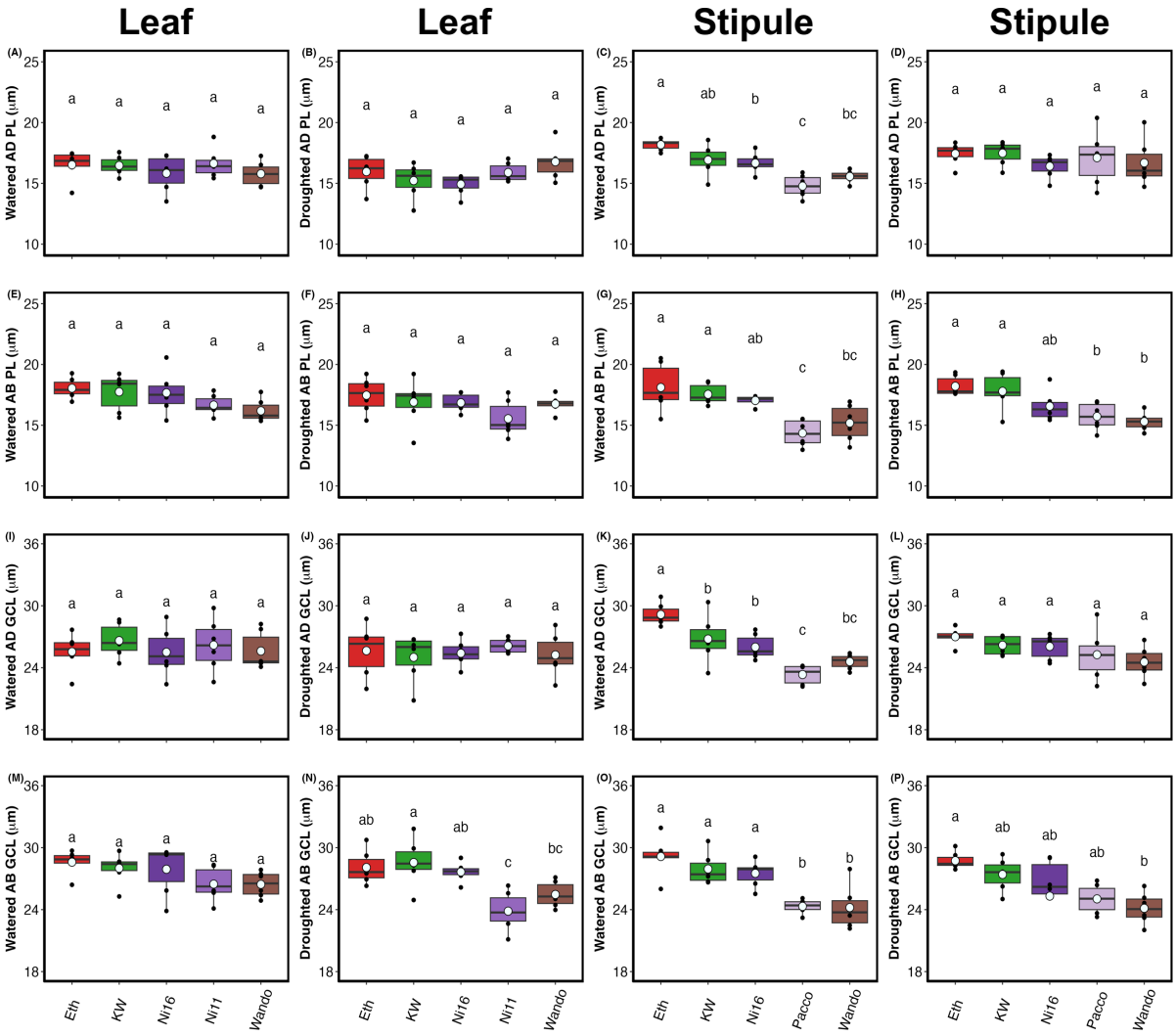

Figure 3.10. Variation in leaf and stipule adaxial and abaxial stomatal sizes across P. sativum accessions under watered and droughted conditions. Stomatal sizes were calculated as pore length (PL) for the adaxial (AD) watered **(A)** leaves and **(C)** stipules and droughted AD **(B)** leaves and **(D)** stipules and as PL for the abaxial (AB) watered **(E)** leaves and **(G)** stipules and droughted AB **(F)** leaves and **(H)** stipules and as guard cell length (GCL) for the AD watered **(I)** leaves and **(K)** stipules and droughted AD **(J)** leaves and **(L)** stipules and as GCL for the AB watered **(M)** leaves and **(O)** stipules and AB droughted **(N)** leaves and **(P)** stipules. Stomatal sizes were measured at 400x magnification (n = 6). White dots symbolise the mean, whilst error bars represent mean ± SE. Different letters above each error bar represent significant differences in either AD or AB PL or GCL between *P. sativum* accessions ($P < 0.05$; TukeyHSD). Whilst the presence of * of the same colour indicates a significant difference in either AD or AB PL or GCL within an individual accession of the same experimental condition between the leaves and stipules, whereby * is $P < 0.05$, ** is $P < 0.01$ and *** is $P < 0.001$ (TukeyHSD). The presence of + of the same colour indicates a significant difference in either AD or AB PL or GCL within an individual accession of the same foliar tissue between watered and droughted conditions, whereby + is $P < 0.05$, ++ is $P < 0.01$ and +++ is $P < 0.001$ (TukeyHSD). Significant differences in stomatal size between the AD and AB surfaces can be found in ***Table.3.6***.

Table 3.6. Statistical P values between adaxial (AD) and abaxial (AB) stomatal sizes. Stomatal sizes were calculated as pore length (PL) and guard cell length (GCL). Statistical differences were generated from ***Fig.3.10*** via TukeyHSD comparisons of AD vs AB for either **(A)** PL or **(B)** GCL of the same foliar tissue and same experimental condition for each individual accession, whereby * is $P < 0.05$, ** is $P < 0.01$ and *** is $P < 0.001$ (TukeyHSD). Stomatal sizes were measured at 400x magnification (n = 6).

(A)

Accession	AD vs AB PL *P* values			
	Watered		Droughted	
	Leaves	Stipules	Leaves	Stipules
Eth	0.99	1.00	0.99	1.00
KW	1.00	1.00	0.96	1.00
Ni16	0.88	1.00	0.82	1.00
Ni11	1.00	NA	1.00	NA
Pacco	NA	1.00	NA	1.00
Wando	1.00	1.00	1.00	1.00

(B)

Accession	AD vs AB GCL *P* values			
	Watered		Droughted	
	Leaves	Stipules	Leaves	Stipules
Eth	0.67	1.00	0.97	1.00
KW	1.00	1.00	0.29	1.00
Ni16	0.98	1.00	0.99	1.00
Ni11	1.00	NA	0.99	NA
Pacco	NA	1.00	NA	1.00
Wando	1.00	1.00	1.00	1.00

3.3.4.3. Maximum Anatomical g_s

Significant variation in the maximum anatomical stomatal conductance (gs_{max}; calculated using SD and SS) were identified between the different *P. sativum* accessions for the AD ($F_{(4)} = 6.46$, $P < 0.01$) and AB ($F_{(4)} = 6.89$, $P < 0.001$) watered leaves, AD ($F_{(4)} = 14.23$, $P < 0.001$) and AB ($F_{(4)} = 7.73$, $P < 0.001$) watered stipules and AD ($F_{(4)} = 4.75$, $P < 0.01$) and AB ($F_{(4)} = 10.72$, $P < 0.001$) droughted stipules (***Fig.3.11***). A significant difference was also apparent in gs_{max} between the different accessions, foliar tissues and experimental conditions ($F_{(3)} = 4.69$, $P < 0.01$) (***Fig.3.11***).

Ni16 had the greatest gs_{max} for watered leaf AD (1.05 ± 0.08 mol m^{-2} s^{-1}) and AB (1.45 ± 0.14 mol m^{-2} s^{-1}) and for watered (0.86 ± 0.05 mol m^{-2} s^{-1}) and droughted (0.89 ± 0.05 mol m^{-2} s^{-1}) stipule AD, with a significant difference to Eth in watered leaf AD (TukeyHSD; $P < 0.05$) and droughted stipule AD (TukeyHSD; $P < 0.05$) respectively, to Eth, KW and Ni11 in watered leaf AB (TukeyHSD; $P < 0.05$) and to Eth, Pacco and Wando in watered stipule AD (TukeyHSD; $P < 0.05$) gs_{max} (***Fig.3.11A,C,D,E***). In contrast, Eth exhibited the lowest gs_{max} for watered leaf AD (0.62 ± 0.04 mol m^{-2} s^{-1}) and AB (0.9 ± 0.05 mol m^{-2} s^{-1}) and for watered (0.57 ± 0.03 mol m^{-2} s^{-1}) and droughted (0.67 ± 0.05 mol m^{-2} s^{-1}) stipule AD, which were significantly lower in gs_{max} than Ni16, Ni11 and Wando in watered leaf AD (TukeyHSD; $P < 0.05$), Ni16 in watered leaf AB (TukeyHSD; $P < 0.05$), KW, Ni16 and Wando in watered stipule AD (TukeyHSD; $P < 0.05$) and to KW and Ni16 in droughted stipule AD (TukeyHSD; $P < 0.05$) (***Fig.3.11A,C,D,E***). Whilst the highest AB stipule gs_{max} was observed within watered (1.08 ± 0.06 mol m^{-2} s^{-1}) and droughted (1.11 ± 0.03 mol m^{-2} s^{-1}) KW and significantly different to Eth and Pacco for watered stipule AB (TukeyHSD; $P < 0.05$) and to Eth,

Pacco and Wando for droughted stipule AB gs_{max} (TukeyHSD; $P < 0.05$) (***Fig.3.11G&H***). Whereas Pacco exhibited the lowest watered (0.72 ± 0.05 mol m^{-2} s^{-1}) and droughted (0.75 ± 0.01 mol m^{-2} s^{-1}) AB stipule gs_{max}, with a significant difference to KW, Ni16 and Wando in watered stipule AB (TukeyHSD; $P < 0.05$) and to KW and Ni16 in droughted stipule AB gs_{max} (TukeyHSD; $P < 0.05$) (***Fig.3.11G&H***). However no significant difference in gs_{max} were identified between any of the accessions for AD or AB droughted leaves (TukeyHSD; $P < 0.05$) (***Fig.3.11B&F***).

AB surfaces generally exhibited higher gs_{max} for both watered and droughted leaves and stipules than the AD surfaces (***Fig.3.11***), with a significant difference identified in gs_{max} between the AD and AB surfaces within the individual accession of watered Ni16 leaves (TukeyHSD; $P < 0.01$) and watered Wando stipules (TukeyHSD; $P < 0.05$) (***Table.3.7&Fig.3.11A,C,E&G***). The leaves were generally higher than the stipules in gs_{max} for watered AD and AB surfaces, whilst the stipules generally exhibited a higher gs_{max} than the leaves for droughted AD surfaces (***Fig.3.11***), with a significant difference observed in gs_{max} between the leaves and stipules within the individual accession of watered Ni16 AB (TukeyHSD; $P < 0.001$) (***Fig.3.11E&G***). Watered conditions generally had a greater gs_{max} than droughted for AD and AB leaves, whereas droughted conditions generally experienced a higher gs_{max} for AD and AB stipules (***Fig.3.11***), with a significant difference identified in gs_{max} between watered and droughted conditions within the individual accession of Ni16 AB leaves (TukeyHSD; $P < 0.001$) (***Fig.3.11E&F***).

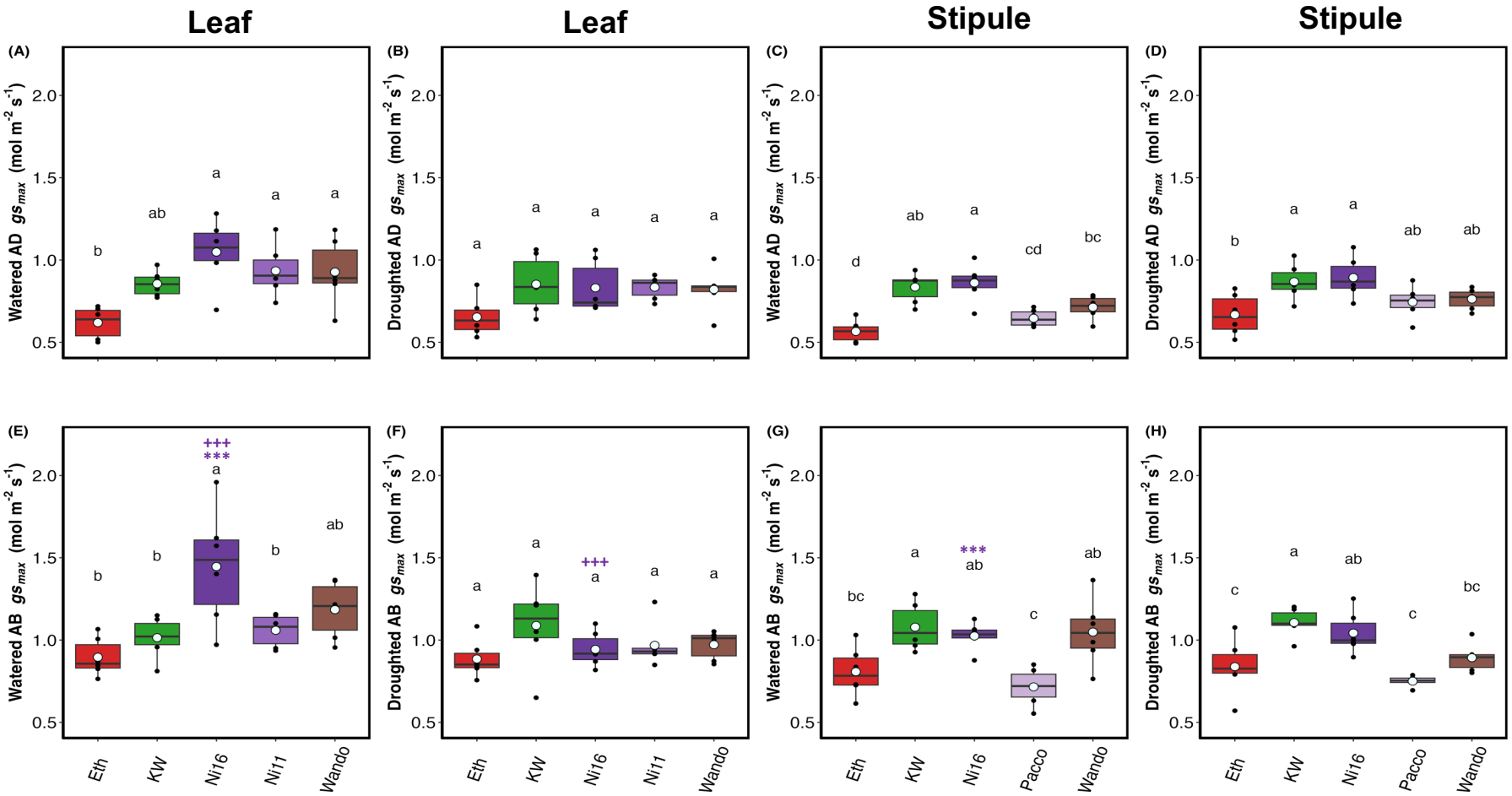

Figure 3.11. Variation in leaf and stipule adaxial and abaxial gs_{max} across P. sativum accessions under watered and droughted conditions. Mean maximum anatomical g_s (gs_{max}) were generated for the adaxial (AD) watered **(A)** leaves and **(C)** stipules and droughted **(B)** leaves and **(D)** stipules and for the abaxial (AB) watered **(E)** leaves and **(G)** stipules and droughted **(F)** leaves and **(H)** stipules. gs_{max} was calculated via the Dow et al. (2014a) method using stomatal densities and sizes from the AD and AB surfaces. Stomata were counted at a 200x magnification in a 1 mm^2 grid, whilst stomatal sizes (pore and guard cell length) were measured at 400x magnification (n = 6). White dots symbolise the mean, whilst error bars represent mean ± SE. Different letters above each error bar represent significant differences in either AD or AB gs_{max} between *P. sativum* accessions ($P < 0.05$; TukeyHSD). Whilst the presence of * of the same colour indicates a significant difference in either AD or AB gs_{max} within an individual accession of the same experimental condition between the leaves and stipules, whereby * is $P < 0.05$, ** is $P < 0.01$ and *** is $P < 0.001$ (TukeyHSD). The presence of + of the same colour indicates a significant difference in either AD or AB gs_{max} within an individual accession of the same foliar tissue between watered and droughted conditions, whereby + is $P < 0.05$, ++ is $P < 0.01$ and +++ is $P < 0.001$ (TukeyHSD). Significant differences in gs_{max} between the AD and AB surfaces can be found in ***Table.3.7***.

Table 3.7. Statistical P values between adaxial (AD) and abaxial (AB) maximum anatomical stomatal conductance (gs_{max}). Statistical differences were generated from ***Fig.3.11*** via TukeyHSD comparisons of AD vs AB gs_{max} of the same foliar tissue and same experimental condition for each individual accession, whereby * is $P < 0.05$, ** is $P < 0.01$ and *** is $P < 0.001$ (TukeyHSD). gs_{max} was calculated via the Dow et al. (2014a) method using stomatal densities and sizes from the AD and AB surfaces. Stomata were counted at a 200x magnification in a 1 mm^2 grid, whilst stomatal sizes (pore and guard cell length) were measured at 400x magnification (n = 6).

Accession	AD vs AB gs_{max} *P* values			
	Watered		Droughted	
	Leaves	Stipules	Leaves	Stipules
Eth	0.26	0.59	0.69	0.99
KW	1.00	0.58	0.65	0.63
Ni16	**1.30E-03****	1.00	1.00	1.00
Ni11	1.00	NA	1.00	NA
Pacco	NA	1.00	NA	1.00
Wando	0.42	**0.03***	1.00	1.00

3.3.4.4. Relationship Between Stomatal Densities, Sizes and Conductance

Although there were no significant correlations identified between SD and SS (PL or GCL) for either foliar tissue or condition ($P > 0.05$) (***Fig.3.12***), significant positive correlations were observed between gs_{max} and SD in both watered ($R = 0.92$, $P < 0.001$) and droughted ($R = 0.83$, $P < 0.001$) leaves and watered ($R = 0.87$, $P < 0.001$) and droughted ($R = 0.80$, $P < 0.001$) stipules (***Fig.3.13***). Significant positive correlations between gs_{max} and PL were noted in watered ($R = 0.28$, $P < 0.05$) and droughted ($R = 0.46$, $P < 0.001$) leaves and watered ($R = 0.31$, $P < 0.05$) and droughted ($R = 0.31$, $P < 0.05$) stipules, and additionally seen between gs_{max} and GCL in watered ($R = 0.26$, $P < 0.05$) and droughted ($R = 0.31$, $P < 0.05$) leaves and droughted stipules ($R = 0.36$, $P < 0.01$) (***Fig.3.14***). A significant positive correlation was also identified between g_s and AB SD in droughted leaves ($R = 0.43$, $P < 0.05$) (***Fig.3.15***). However, there were no significant correlations identified between g_s and SS (PL or GCL) for either surface, foliar tissue or condition ($P > 0.05$) (***Fig.3.16***).

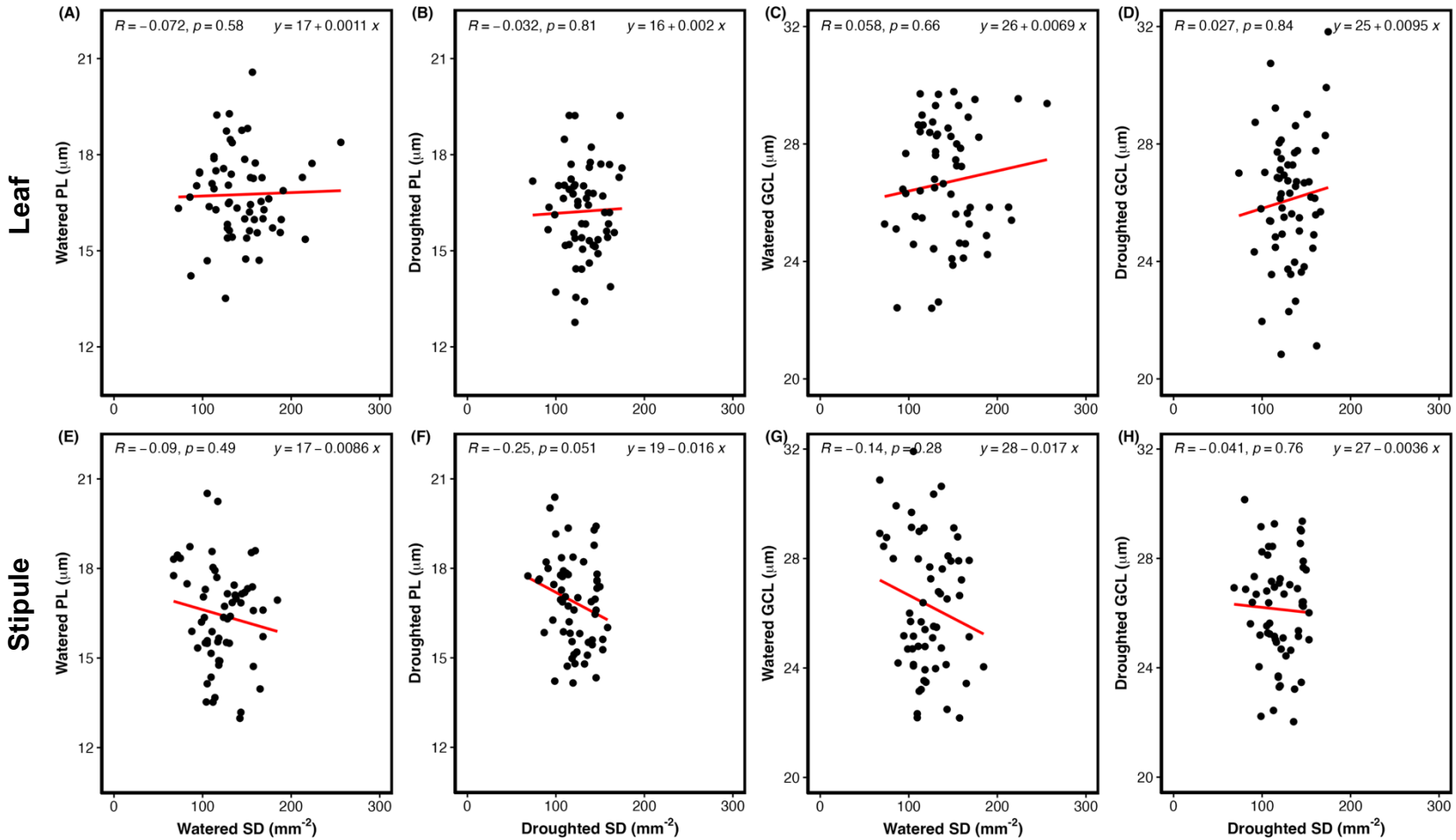

Figure 3.12. Spearmans correlation between stomatal densities and sizes in the leaves and stipules under watered and droughted conditions. Correlations between pore length (PL) and stomatal density (SD) in watered **(A)** leaves and **(E)** stipules and droughted **(B)** leaves and **(F)** stipules and correlations between guard cell length (GCL) and SD in watered **(C)** leaves and **(G)** stipules and droughted **(D)** leaves and **(H)** stipules. Stomatal sizes were measured at 400x magnification, whilst stomata were counted at 200x magnification in a 1 mm^2 grid (n = 6). Spearman's correlation coefficients (R) and linear regressions (represented as equations and red lines) were calculated for each anatomical component. $P < 0.05$ indicates a significant relationship.

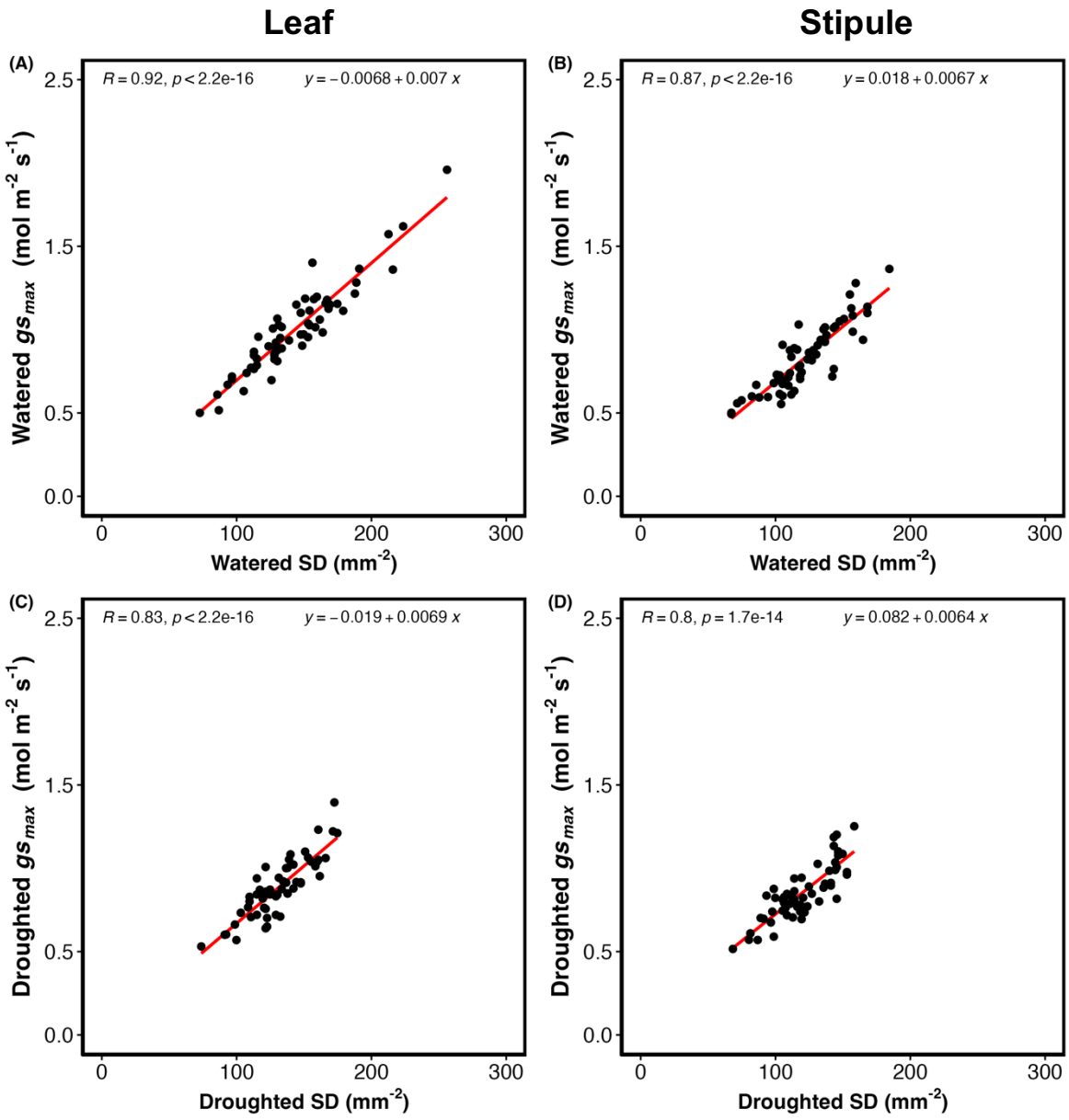

Figure 3.13. Spearmans correlation between stomatal densities and gs_{max} in the leaves and stipules under watered and droughted conditions. Correlation between stomatal densities (SD) and maximum anatomical g_s (gs_{max}) in watered **(A)** leaves and **(B)** stipules and droughted **(C)** leaves and **(D)** stipules. gs_{max} was calculated via the Dow et al. (2014a) method using stomatal densities and sizes. Stomata were counted at a 200x magnification in a 1 mm^2 grid, whilst stomatal sizes (pore and guard cell length) were measured at 400x magnification. Spearman's correlation coefficients (R) and linear regressions (represented as equations and red lines) were calculated for each anatomical component. $P < 0.05$ indicates a significant relationship (n = 6).

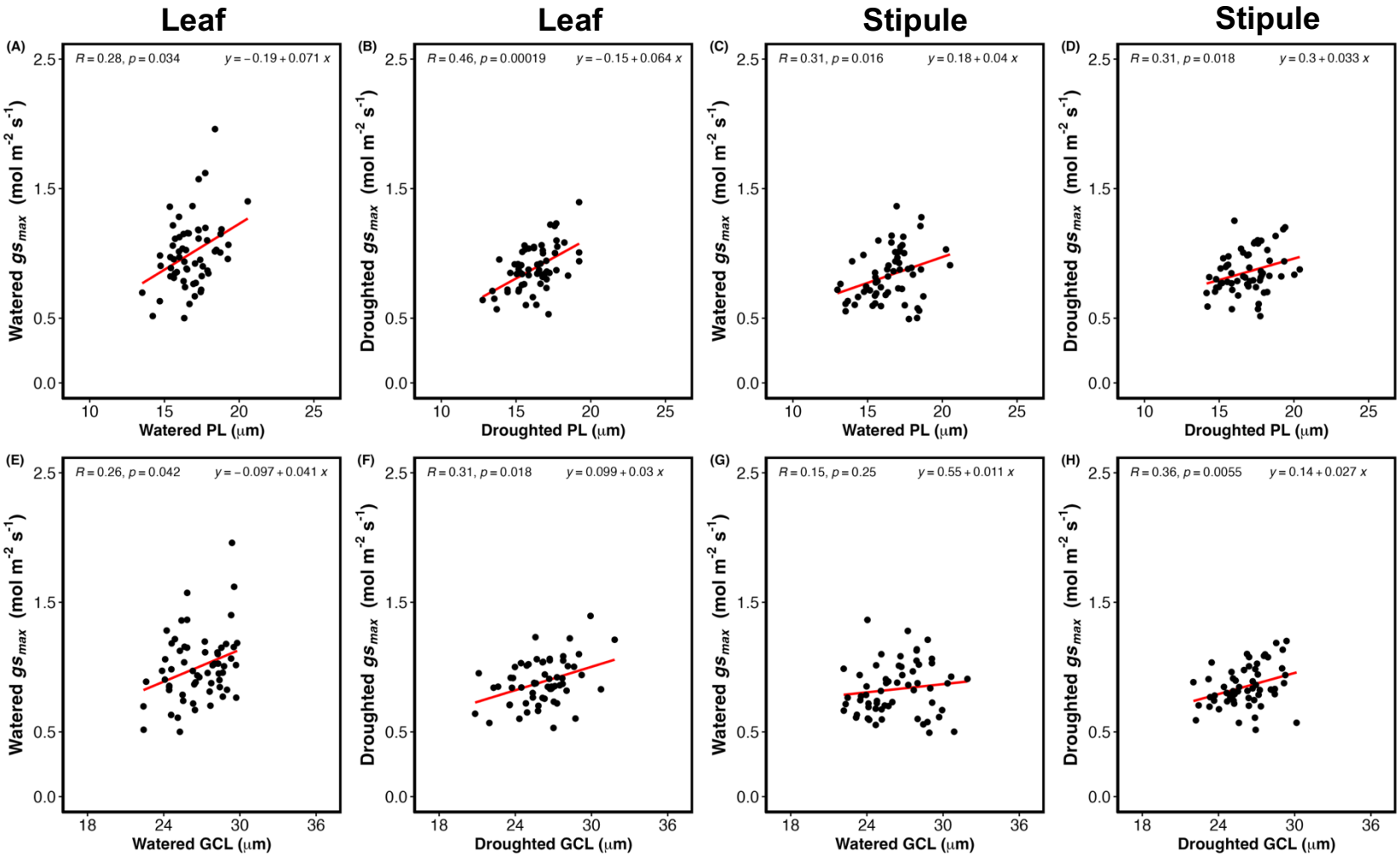

Figure 3.14. Spearmans correlation between stomatal sizes and gs_{max} in the leaves and stipules under watered and droughted conditions. Correlations between maximum anatomical g_s (gs_{max}) and stomatal pore length (PL) in watered **(A)** leaves and **(C)** stipules and droughted **(B)** leaves and **(D)** stipules and correlations between gs_{max} and stomatal guard cell length (GCL) in watered **(E)** leaves and **(G)** stipules and droughted **(F)** leaves and **(H)** stipules. gs_{max} was calculated via the Dow et al. (2014a) method using stomatal densities and sizes. Stomata were counted at a 200x magnification in a 1 mm^2 grid, whilst stomatal sizes (pore and guard cell length) were measured at 400x magnification. Spearman's correlation coefficients (R) and linear regressions (represented as equations and red lines) were calculated for each anatomical component. $P < 0.05$ indicates a significant relationship (n=6).

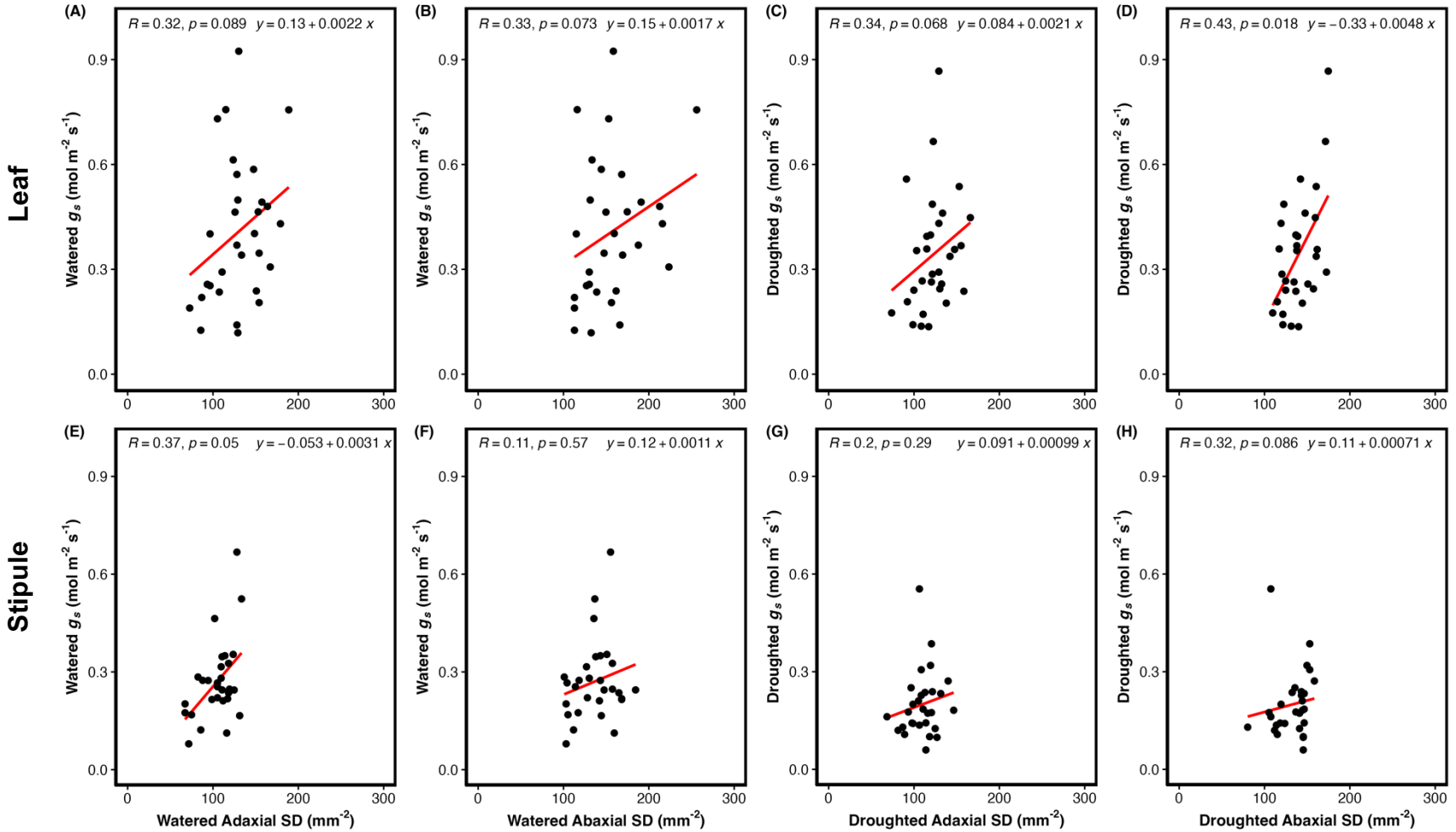

Figure 3.15. Spearmans correlation between stomatal densities and conductance in the leaves and stipules under watered and droughted conditions. Correlations between stomatal conductance (g_s) and watered **(A)** adaxial leaves, **(B)** abaxial leaves, **(E)** adaxial stipules and **(F)** abaxial stipules stomatal densities (SD) and droughted **(C)** adaxial leaves, **(D)** abaxial leaves, **(G)** adaxial stipules and **(H)** abaxial stipules SD. Stomata were counted at 200x magnification in a 1 mm^2 grid. g_s was measured at 400 µmol mol^{-1} intercellular CO_2 concentration within a Li-Cor 6800 at 23 °C and 1500 µmol m^{-2} s^{-1} photosynthetic photon flux density. Spearman's correlation coefficients (R) and linear regressions (represented as equations and red lines) were calculated for each SD against g_s. $P < 0.05$ indicates a significant relationship (n=5-6).

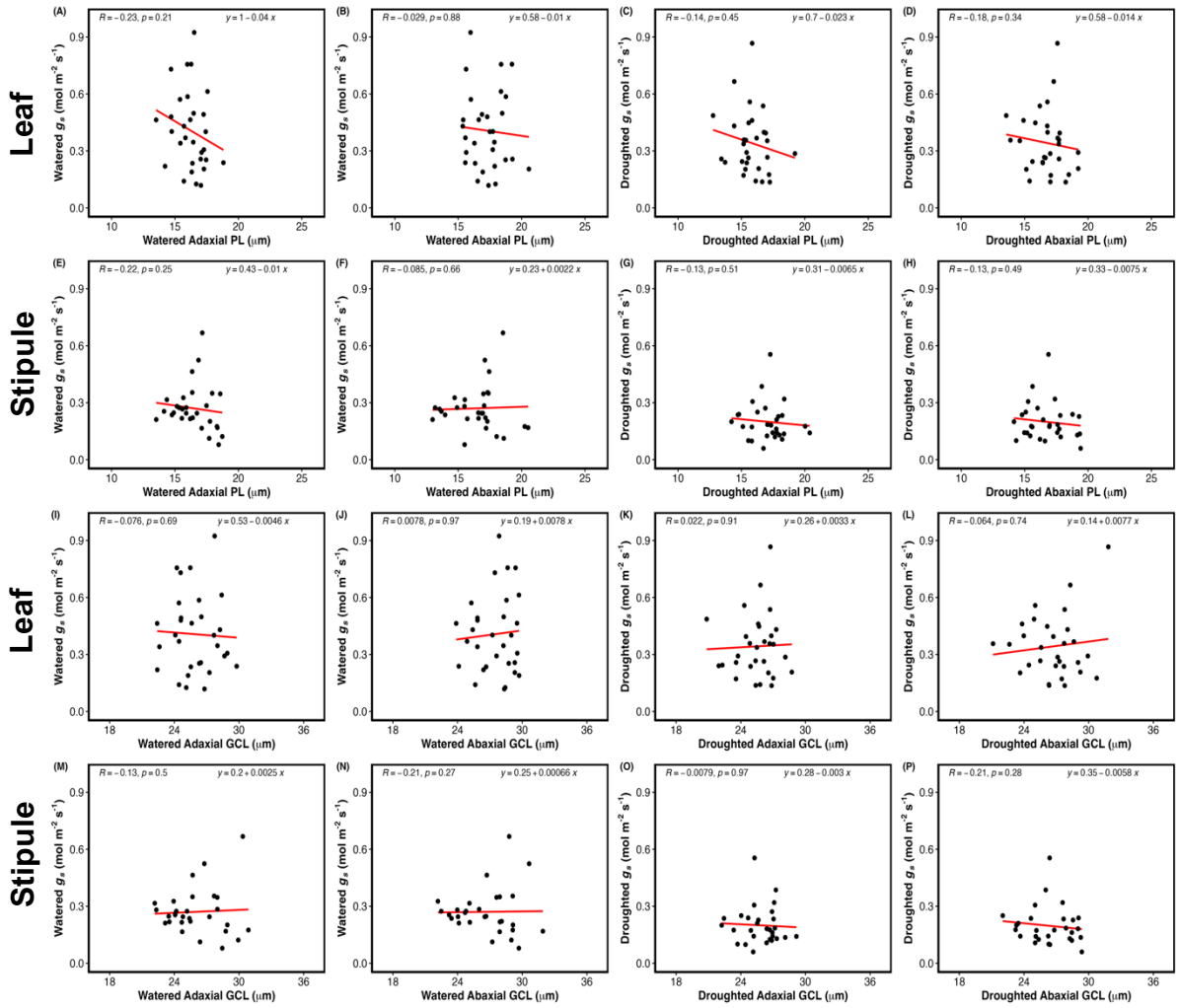

Figure 3.16. Spearmans correlation between stomatal sizes and conductance in the leaves and stipules under watered and droughted conditions. Correlations between stomatal conductance (g_s) and watered **(A)** adaxial leaf pore length (PL), **(B)** abaxial leaf PL, **(E)** adaxial stipule PL, **(F)** abaxial stipule PL, **(I)** adaxial leaf guard cell length (GCL), **(J)** abaxial leaf GCL, **(M)** adaxial stipule GCL and **(N)** abaxial stipule GCL and between g_s and droughted **(C)** adaxial leaf PL, **(D)** abaxial leaf PL, **(G)** adaxial stipule PL, **(H)** abaxial stipule PL, **(K)** adaxial leaf GCL, **(L)** abaxial leaf GCL, **(O)** adaxial stipule GCL and **(P)** abaxial stipule GCL. Stomatal sizes were measured at 400x magnification. g_s was measured at 400 μmol mol^{-1} intercellular CO_2 concentration within a Li-Cor 6800 at 23 °C and 1500 μmol m^{-2} s^{-1} photosynthetic photon flux density. Spearman's correlation coefficients (R) and linear regressions (represented as equations and red lines) were calculated for each PL and GCL against g_s. $P < 0.05$ indicates a significant relationship (n=5-6).

3.3.4.5. Stomatal Kinetics

A, g_s and *i*WUE were monitored following a step increase in light intensity in watered and droughted leaves and stipules across the *P. sativum* accessions (***Fig.3.17***). Steady state values at 100 and 1000 µmol m^{-2} s^{-1} PPFD were calculated for *A* (*A100* and *A1000*) and g_s (*gs100* and *gs1000*) respectively (***Fig.3.18***), with significant variation identified in *A100* ($F_{(3)}$ = 18.87, P < 0.001), *A1000* ($F_{(3)}$ = 16.53, P < 0.001), *gs100* ($F_{(3)}$ = 2.30, P < 0.05) and *gs1000* ($F_{(3)}$ = 4.72, P < 0.01) between the different accessions, foliar tissues and experimental conditions (***Fig.3.18***).

Ni16 exhibited the highest watered (3.99 ± 0.13 µmol m^{-2} s^{-1}) and droughted (4.10 ± 0.12 µmol m^{-2} s^{-1}) leaf *A100* and watered (0.31 ± 0.02 mol m^{-2} s^{-1}) and droughted (0.26 ± 0.01 mol m^{-2} s^{-1}) leaf *gs100*, with a significant difference to all accessions par KW and Wando in watered leaf *A100* (TukeyHSD; P < 0.05), to all accessions par Ni11 in droughted leaf *A100* (TukeyHSD; P < 0.05) and to all accessions in watered (TukeyHSD; P < 0.05) and droughted (TukeyHSD; P < 0.05) leaf *gs100* respectively (***Fig.3.18A,B,I&J***). In contrast, KW had a significantly lower watered leaf *A100* (3.25 ± 0.10 µmol m^{-2} s^{-1}) to Ni16 (TukeyHSD; P < 0.05), whilst Eth had a significantly lower droughted leaf *A100* (2.58 ± 0.13 µmol m^{-2} s^{-1}) to the remaining droughted leaf accessions (excluding Wando) (TukeyHSD; P < 0.05) (***Fig.3.18A&B***). Ni11 had the lowest watered (0.16 ± 0.01 mol m^{-2} s^{-1}) and droughted (0.13 ± 0.01 mol m^{-2} s^{-1}) leaf *gs100*, with a significant difference to all accessions in watered leaf *gs100* (par Eth) (TukeyHSD; P < 0.05) and a significant difference in droughted leaf *gs100* to the remaining accessions (TukeyHSD; P < 0.05) (***Fig.3.18I&J***). KW had the highest watered (3.6 ± 0.13 µmol m^{-2} s^{-1}) and droughted (3.9 ± 0.17 µmol m^{-2} s^{-1}) stipule *A100*

and watered (0.23 ± 0.01 mol m^{-2} s^{-1}) and droughted (0.19 ± 0.01 mol m^{-2} s^{-1}) stipule *gs100*, which was significantly different to all accessions in watered stipule *A100* (TukeyHSD; $P < 0.05$), to all accessions in droughted stipule *A100* (TukeyHSD; $P < 0.05$), to all accessions in watered stipule *gs100* (TukeyHSD; $P < 0.05$) and to all accessions in droughted stipule *gs100* (TukeyHSD; $P < 0.05$), respectively (***Fig.3.18C,D,K&L***). Whereas Wando exhibited the lowest watered *A100* (2.1 ± 0.17 µmol m^{-2} s^{-1}) and *gs100* (0.11 ± 0.01 mol m^{-2} s^{-1}) in the stipules, with a significant difference identified to Eth and KW in watered stipule *A100* (TukeyHSD; $P < 0.05$) and to KW in watered stipule *gs100* (TukeyHSD; $P < 0.05$) (***Fig.3.18C&K***). Whilst the lowest droughted stipule *A100* (1.16 ± 0.09 µmol m^{-2} s^{-1}) and *gs100* (0.07 ± 0.002 mol m^{-2} s^{-1}) was noted in Ni16, with a significant difference identified to all accessions (excluding Eth) in droughted stipule *A100* (TukeyHSD; $P < 0.05$) and to all accessions in droughted stipule *gs100* (TukeyHSD; $P < 0.05$) (***Fig.3.18D&L***).

At the higher light intensity, Ni16 exhibited the highest watered (21.06 ± 0.43 µmol m^{-2} s^{-1}) and droughted (18.6 ± 0.24 µmol m^{-2} s^{-1}) leaf *A1000* and watered (0.46 ± 0.02 mol m^{-2} s^{-1}) and droughted (0.39 ± 0.01 mol m^{-2} s^{-1}) leaf *gs1000*, with a significant difference to Eth, Ni11 and Wando in watered leaf *A1000* (TukeyHSD; $P < 0.05$), to all accessions in droughted leaf *A1000* (TukeyHSD; $P < 0.05$) and to all accessions (exempting KW) in watered leaf *gs1000* (TukeyHSD; $P < 0.05$) and in droughted leaf *gs1000* (TukeyHSD; $P < 0.05$), respectively (***Fig.3.18E,F,M&N***). In contrast, the lowest *A1000* was observed within watered Ni11 (16.19 ± 0.43 µmol m^{-2} s^{-1}) and droughted Wando (13.1 ± 0.41 µmol m^{-2} s^{-1}) leaves, which were significantly lower in watered leaf *A1000* to KW and Ni16 (TukeyHSD; $P < 0.05$) and significantly lower to all accessions

(par Eth) in droughted leaf *A1000* (TukeyHSD; $P < 0.05$) (***Fig.3.18E&F***). Whilst the lowest *gs1000* were noted within watered Eth (0.26 ± 0.01 mol m^{-2} s^{-1}) and droughted Ni11 (0.23 ± 0.01 mol m^{-2} s^{-1}) leaves, with a significant difference in watered leaf *gs1000* to all accessions (excluding Ni11) (TukeyHSD; $P < 0.05$) and a significant difference in droughted leaf *gs1000* to KW and Ni16 (TukeyHSD; $P < 0.05$) (***Fig.3.18M&N***). KW had the highest watered (18.55 ± 0.35 µmol m^{-2} s^{-1}) and droughted (17.01 ± 0.47 µmol m^{-2} s^{-1}) stipule *A1000* and watered (0.35 ± 0.01 mol m^{-2} s^{-1}) and droughted (0.32 ± 0.01 mol m^{-2} s^{-1}) stipule *gs1000*, which was significantly different to all accessions in watered stipule *A1000* (TukeyHSD; $P < 0.05$), to all accessions in droughted stipule *A1000* (TukeyHSD; $P < 0.05$), to all accessions in watered stipule *gs1000* (TukeyHSD; $P < 0.05$) and to all accessions in droughted stipule *gs1000* (TukeyHSD; $P < 0.05$), respectively (***Fig.3.18G,H,O&P***). Whereas Wando exhibited the lowest watered *A1000* (10.27 ± 0.38 µmol m^{-2} s^{-1}) and *gs1000* (0.17 ± 0.01 mol m^{-2} s^{-1}) in the stipules, with a significant difference identified to all accessions (par Ni16) in watered stipule *A1000* (TukeyHSD; $P < 0.05$) and to KW and Pacco in watered stipule *gs1000* (TukeyHSD; $P < 0.05$) (***Fig.3.18G&O***). Whilst the lowest droughted stipule *A1000* (5.39 ± 0.1 µmol m^{-2} s^{-1}) and *gs1000* (0.10 ± 0.004 mol m^{-2} s^{-1}) was noted in Ni16, with a significant difference identified to all accessions in droughted stipule *A1000* (TukeyHSD; $P < 0.05$) and to all accessions in droughted stipule *gs1000* (TukeyHSD; $P < 0.05$) (***Fig.3.18H&P***).

The maximum *i*WUE (*i*WUE_{max}) were calculated for watered and droughted leaves and stipules, with significant variation identified in *i*WUE_{max} between the different accessions, foliar tissues and experimental conditions ($F_{(3)} = 4.79$, $P < 0.01$)

(***Fig.3.19***). Ni11 exhibited the greatest *i*WUE$_{max}$ in watered (83.29 ± 3.27 µmol mol^{-1}) and droughted (87.86 ± 2.45 µmol mol^{-1}) leaves, which were significantly different to the remaining accessions in watered leaf *i*WUE$_{max}$ (TukeyHSD; $P < 0.05$) and in droughted leaf *i*WUE$_{max}$ (TukeyHSD; $P < 0.05$), respectively (***Fig.3.19A&C***). Whilst Ni16 had the lowest leaf *i*WUE$_{max}$ for watered (57.12 ± 1.22 µmol mol^{-1}) and droughted (60.47 ± 1.32 µmol mol^{-1}) conditions, with a significant difference in watered leaf *i*WUE$_{max}$ to all accessions (excluding Wando) (TukeyHSD; $P < 0.05$) and a significant difference to Ni11 and Eth in droughted leaf *i*WUE$_{max}$ (TukeyHSD; $P < 0.05$) (***Fig.3.19A&C***). The highest stipule *i*WUE$_{max}$ was observed in watered Eth (80.38 ± 1.68 µmol mol^{-1}) and droughted Pacco (82.33 ± 2.05 µmol mol^{-1}), which were significantly different to KW and Ni16 in watered stipule *i*WUE$_{max}$ (TukeyHSD; $P < 0.05$) and to all accessions in droughted stipule *i*WUE$_{max}$ (TukeyHSD; $P < 0.05$) (***Fig.3.19B&D***). Whereas watered KW (64.36 ± 1.80 µmol mol^{-1}) and droughted Eth (64.62 ± 2.30 µmol mol^{-1}) exhibited the lowest stipule *i*WUE$_{max}$ and were significantly different to all accessions (par Ni16) in watered stipule *i*WUE$_{max}$ (TukeyHSD; $P < 0.05$) and to Pacco in droughted stipule *i*WUE$_{max}$ (TukeyHSD; $P < 0.05$) (***Fig.3.19B&D***).

The leaves generally had a higher *A100*, *A1000*, *gs100* and *gs1000* than the stipules for both watered and droughted conditions (***Fig.3.18***), with a significant difference in *A100* between the leaves and stipules within the individual accession of droughted Eth (TukeyHSD; $P < 0.001$), watered Ni16 (TukeyHSD; $P < 0.001$), droughted Ni16 (TukeyHSD; $P < 0.001$) and watered Wando (TukeyHSD; $P < 0.001$) (***Fig.3.18A-D***). A significant difference was also identified in *A1000*, *gs100* and *gs1000* (respectively) between the leaves and stipules within the individual accession of watered Eth

(TukeyHSD; $P < 0.05$), droughted Eth (TukeyHSD; $P < 0.001$), watered Ni16 (TukeyHSD; $P < 0.001$), droughted Ni16 (TukeyHSD; $P < 0.001$), watered Wando (TukeyHSD; $P < 0.001$) and droughted Wando (TukeyHSD; $P < 0.001$) (***Fig.3.18E-P***). Whereas the stipules generally had a greater $iWUE_{max}$ than the leaves for both watered and droughted conditions, with a significant difference identified the between leaves and stipules within the individual accession of watered Ni16 (TukeyHSD; $P < 0.01$) and droughted Ni16 (TukeyHSD; $P < 0.05$) (***Fig.3.19***).

Watered conditions were significantly higher than droughted conditions in *A100* within the individual accessions of Eth leaves (TukeyHSD; $P < 0.001$), Eth stipules (TukeyHSD; $P < 0.001$) and Ni16 stipules (TukeyHSD; $P < 0.001$) (***Fig.3.18A-D***). Watered conditions were also generally higher than droughted conditions in *A1000*, *gs100* and *gs1000* (***Fig.3.18E-P***). A significant difference was identified in *A1000* between watered and droughted conditions within the individual accession of Eth leaves (TukeyHSD; $P < 0.001$), Eth stipules (TukeyHSD; $P < 0.001$), KW leaves (TukeyHSD; $P < 0.001$), Ni16 leaves (TukeyHSD; $P < 0.01$), Ni16 stipules (TukeyHSD; $P < 0.001$) and Wando leaves (TukeyHSD; $P < 0.001$) (***Fig.3.18E-H***). A significant difference was also identified in *gs100* between watered and droughted conditions within the individual accession of Eth stipules (TukeyHSD; $P < 0.05$), Ni16 leaves (TukeyHSD; $P < 0.05$) and Ni16 stipules (TukeyHSD; $P < 0.001$) (***Fig.3.18I-L***). Whilst a significant difference was additionally seen in *gs1000* between watered and droughted conditions within the individual accession of Eth stipules (TukeyHSD; $P < 0.05$), Ni16 leaves (TukeyHSD; $P < 0.01$), Ni16 stipules (TukeyHSD; $P < 0.001$) and Wando leaves (TukeyHSD; $P < 0.001$) (***Fig.3.18M-P***). Watered conditions were

significantly higher than and droughted conditions in iWUE$_{max}$ within the individual accession of Eth stipules (TukeyHSD; $P < 0.001$) (***Fig.3.19B&D***). However, there were no significant difference identified in iWUE$_{max}$ between watered and droughted conditions for the leaves within each individual accession (TukeyHSD; $P > 0.05$) (***Fig.3.19A&C***).

To determine differences in stomatal kinetics, lag-times (initial temporal delay in the response of A and g_s to a light intensity change) and time constants (time taken for A and g_s to reach steady state) in A and g_s were calculated for watered and droughted leaves and stipules across the *P. sativum* accessions (***Fig.3.20***). Significant variation were identified in g_s time constant ($F_{(3)} = 3.12$, $P < 0.05$) between the different accessions, foliar tissues and experimental conditions (***Fig.3.20***). Ni11 exhibited a significantly higher time constant in g_s for droughted leaves (18.34 ± 0.74 min) in comparison to Wando (quickest droughted leaf g_s time constant; 14.96 ± 1.10 min) (TukeyHSD; $P < 0.05$) (***Fig.3.20N***). However, no significant differences were identified between any of the accessions in A or g_s lag-time or time constants for watered leaves, watered stipules or droughted stipules (TukeyHSD; $P > 0.05$), whilst no significant difference was seen for droughted leaves in A or g_s lag-times or in A time constants (TukeyHSD; $P > 0.05$) (***Fig.3.20A-M&O-P***). Droughted A lag-time was significantly longer in the stipules than the leaves within the individual accession of droughted Eth (TukeyHSD; $P < 0.05$) (***Fig.3.20B&D***). However there were no significant differences identified between the leaves and stipules within each individual accession in watered A lag-time, watered or droughted g_s lag-time or watered or droughted A or g_s time constants (TukeyHSD; $P > 0.05$) (***Fig.3.20A,C&E-P***). There were also no significant

differences identified in *A* or g_s lag-times or time constants between watered and droughted conditions for either foliar tissues within each individual accession (TukeyHSD; $P > 0.05$) (***Fig.3.20***).

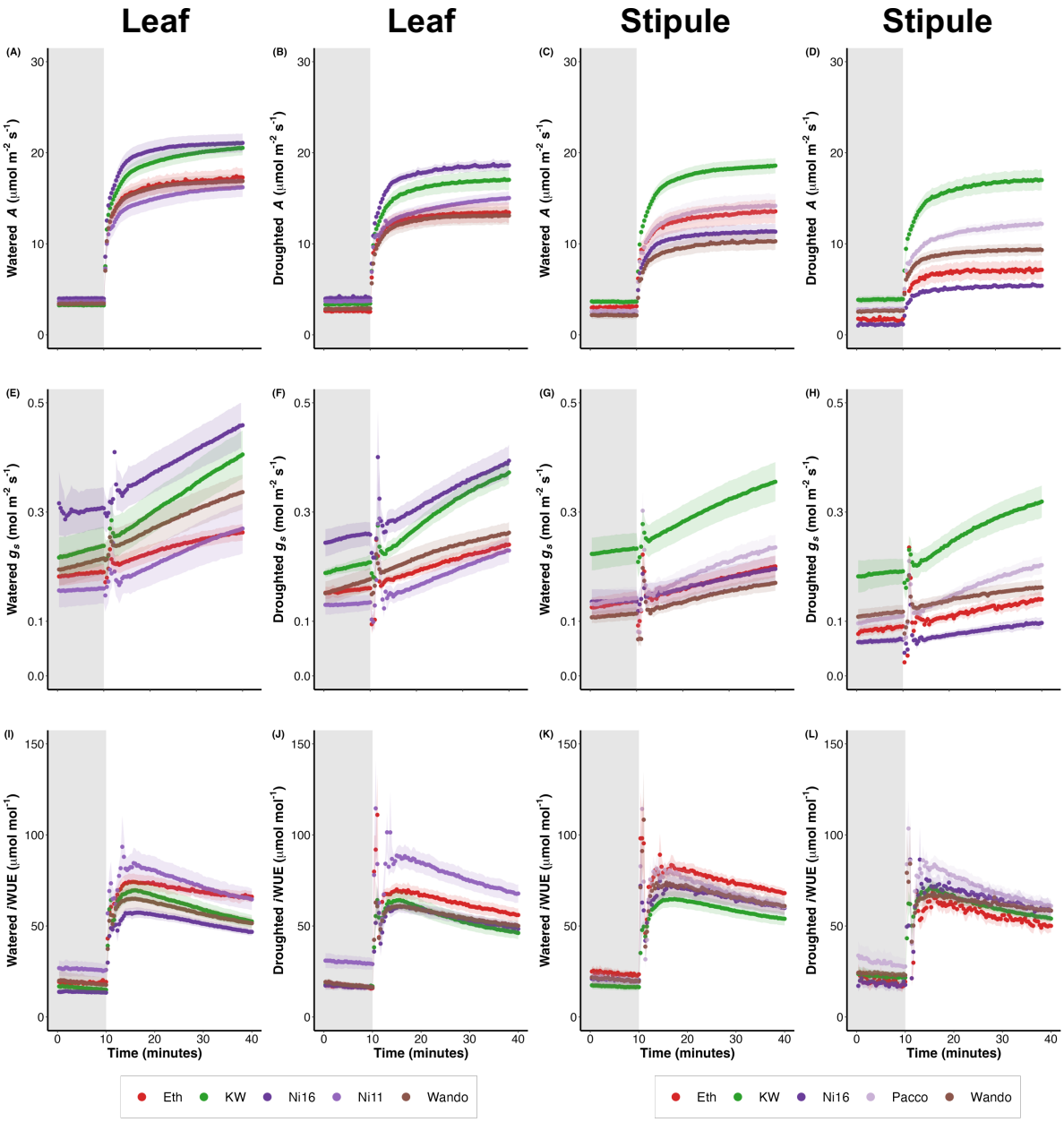

Figure 3.17. Variation in assimilation (A), stomatal conductance (g_s) and intrinsic water use efficiency (iWUE) in response to a step in light intensity across P. sativum accessions under watered and droughted conditions. Assimilation in watered **(A)** leaves and **(C)** stipules and droughted **(B)** leaves and **(D)** stipules and stomatal conductance in watered **(E)** leaves and **(G)** stipules and droughted **(F)** leaves and **(H)** stipules and *i*WUE in watered **(I)** leaves and **(K)** stipules and droughted **(J)** leaves and **(L)** stipules were monitored in response to an increase in light intensity from 100 to 1000 µmol m^{-2} s^{-1} photosynthetic photon flux density. Measured at 400 µmol mol^{-1} [CO_2] and 23 ºC within a Li-Cor 6800 (n = 6). Error bars represent mean ± SE.

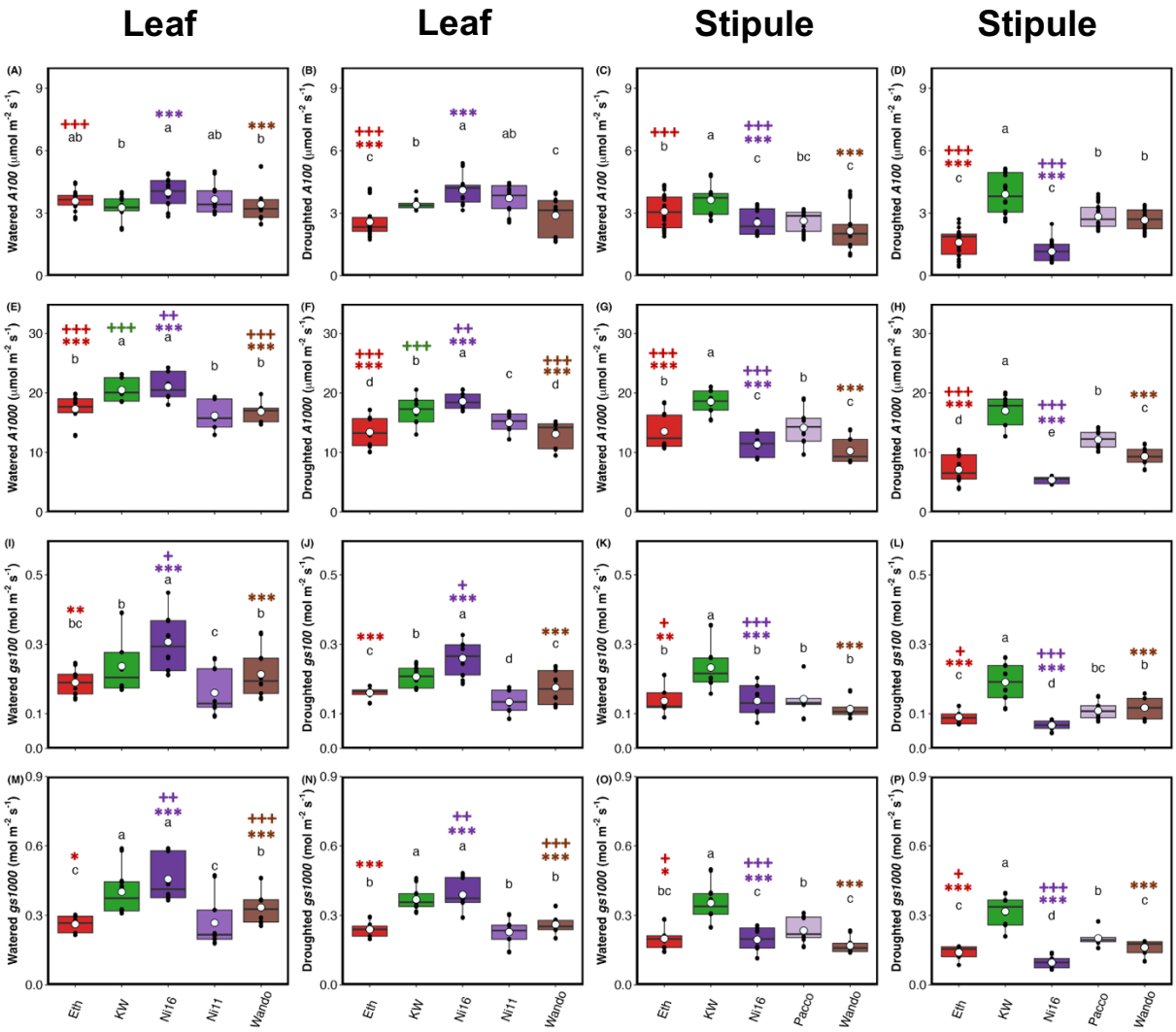

Figure 3.18. Variation in leaf and stipule steady state assimilation (A) and stomatal conductance (g_s) at 100 µmol m^{-2} s^{-1} and 1000 µmol m^{-2} s^{-1} photosynthetic photon flux density (PPFD) across P. sativum accessions under watered and droughted conditions. Steady state *A* at 100 µmol m^{-2} s^{-1} PPFD (*A100*) in watered **(A)** leaves and **(C)** stipules and droughted **(B)** leaves and **(D)** stipules and steady state *A* at 1000 µmol m^{-2} s^{-1} PPFD (*A1000*) in watered **(E)** leaves and **(G)** stipules and droughted **(F)** leaves and **(H)** stipules and steady state g_s at 100 µmol m^{-2} s^{-1} PPFD (*gs100*) in watered **(I)** leaves and **(K)** stipules and droughted **(J)** leaves and **(L)** stipules as well as steady state g_s at 1000 µmol m^{-2} s^{-1} PPFD (*gs1000*) in watered **(M)** leaves and **(O)** stipules and droughted **(N)** leaves and **(P)** stipules were parameterised from data collected within a step in light intensity from 100 to 1000 µmol m^{-2} s^{-1} PPFD at 400 µmol mol^{-1} [CO_2] and 23 °C within a Li-Cor 6800 (n = 6). *A100* and *gs100* were calculated from the average of the last five data points before PPFD was increased to 1000 µmol m^{-2} s^{-1}. Whilst *A1000* and *gs1000* were calculated from the average of the last five data points at 1000 µmol m^{-2} s^{-1} PPFD. White dots symbolise the mean, whilst error bars represent mean ± SE. Different letters above each error bar represent significant differences in one of the steady state parameters between the *P. sativum* accessions ($P < 0.05$; TukeyHSD). Whilst the presence of * of the same colour indicates a significant difference in one of the steady state parameters within an individual accession of the same experimental condition between the leaves and stipules, whereby * is $P < 0.05$, ** is $P < 0.01$ and *** is $P < 0.001$ (TukeyHSD). The presence of + of the same colour indicates a significant difference in one of the steady state parameters within an individual accession of the same foliar tissue between watered and droughted conditions, whereby + is $P < 0.05$, ++ is $P < 0.01$ and +++ is $P < 0.001$ (TukeyHSD).

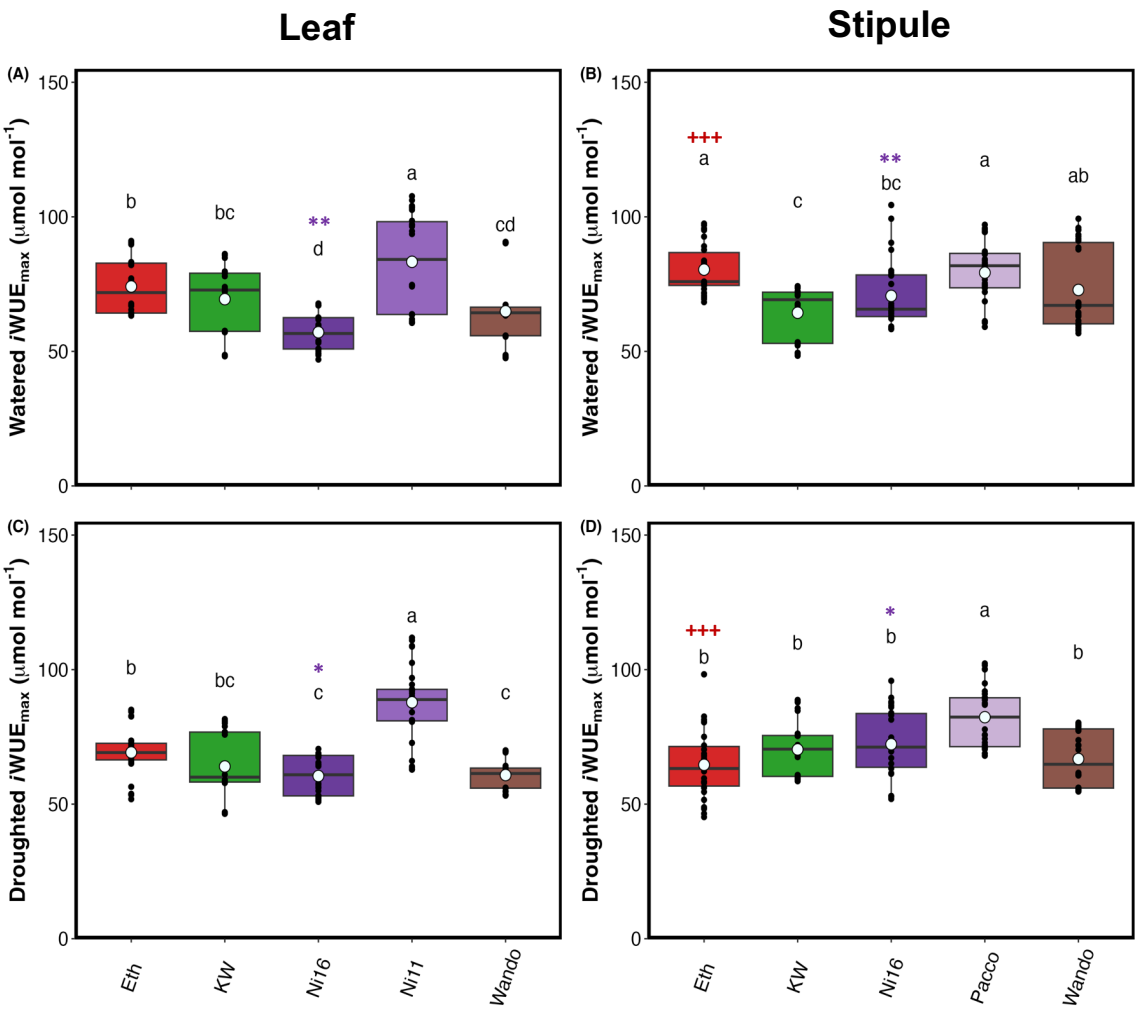

Figure 3.19. Variation in leaf and stipule maximum intrinsic water use efficiency (iWUE$_{max}$) across P. sativum accessions under watered and droughted conditions. *i*WUE$_{max}$ in watered **(A)** leaves and **(B)** stipules and droughted **(C)** leaves and **(D)** stipules were parameterised from data collected within a step in light intensity from 100 to 1000 µmol m^{-2} s^{-1} PPFD at 400 µmol mol^{-1} [CO_2] and 23 °C within a Li-Cor 6800 (n = 6). *i*WUE$_{max}$ was calculated from the average of five data points (observations 45-49) after PPFD was increased to 1000 µmol m^{-2} s^{-1}, where *i*WUE was generally at the highest and most stable rate. White dots symbolise the mean, whilst error bars represent mean ± SE. Different letters above each error bar represent significant differences in *i*WUE$_{max}$ between the *P. sativum* accessions ($P < 0.05$; TukeyHSD). Whilst the presence of * of the same colour indicates a significant difference in *i*WUE$_{max}$ within an individual accession of the same experimental condition between the leaves and stipules, whereby * is $P < 0.05$, ** is $P < 0.01$ and *** is $P < 0.001$ (TukeyHSD). The presence of + of the same colour indicates a significant difference in *i*WUE$_{max}$ within an individual accession of the same foliar tissue between watered and droughted conditions, whereby + is $P < 0.05$, ++ is $P < 0.01$ and +++ is $P < 0.001$ (TukeyHSD).

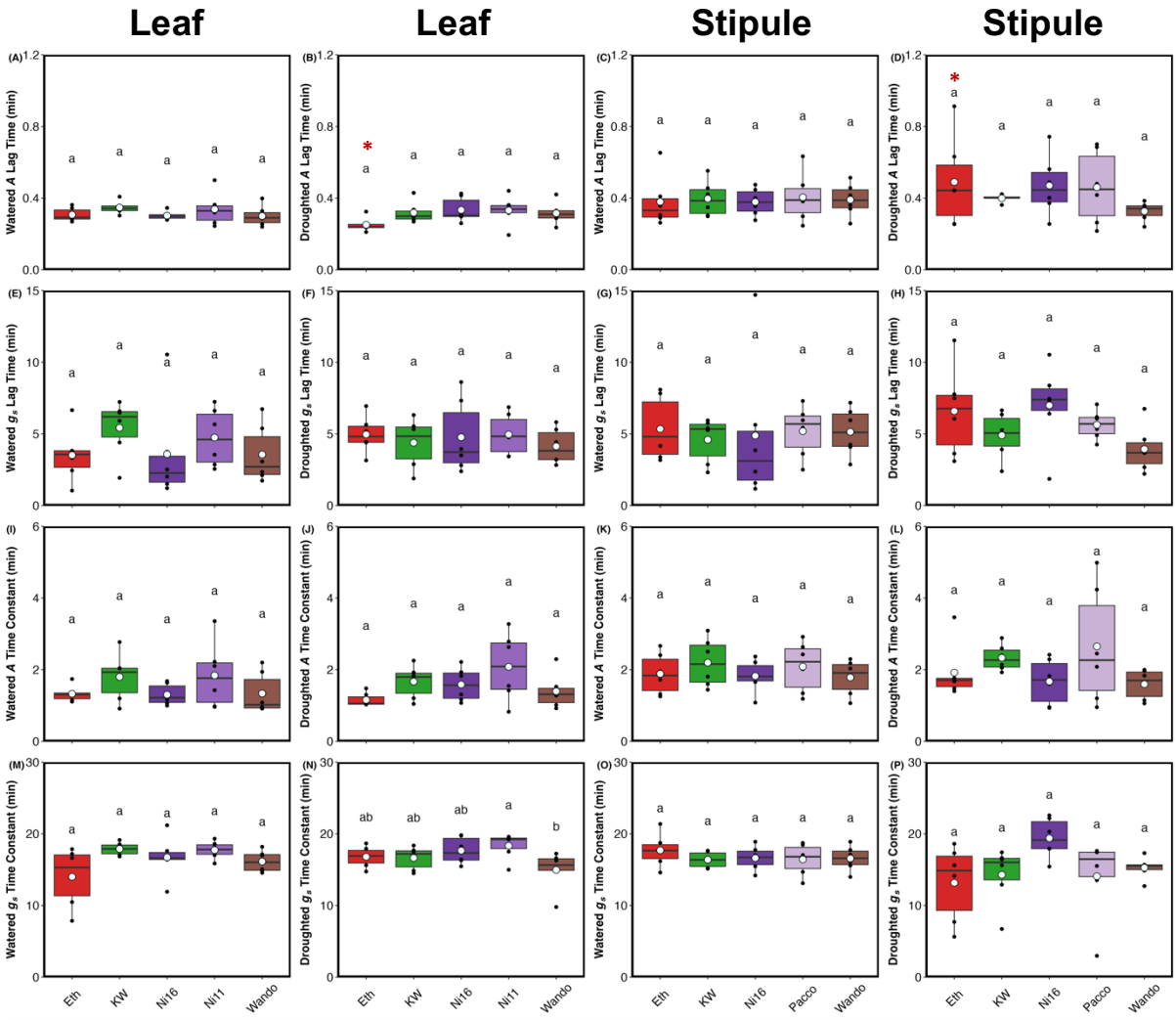

Figure 3.20. Variation in assimilation (A) and stomatal conductance (g_s) lag-time and time constants in response to a step in light intensity across P. sativum accessions under watered and droughted conditions. Lag-time (initial temporal delay in the response of *A* and g_s to a light intensity change) in assimilation in watered **(A)** leaves and **(C)** stipules and droughted **(B)** leaves and **(D)** stipules and lag-time in stomatal conductance in watered **(E)** leaves and **(G)** stipules and droughted **(F)** leaves and **(H)** stipules as well as time constants (time taken for *A* and g_s to reach steady state) in assimilation in watered **(I)** leaves and **(K)** stipules and droughted **(J)** leaves and **(L)** stipules and time constants in stomatal conductance in watered **(M)** leaves and **(O)** stipules and droughted **(N)** leaves and **(P)** stipules were measured in response to an increase in light intensity from 100 to 1000 µmol m^{-2} s^{-1} photosynthetic photon flux density at 400 µmol mol^{-1} [CO_2] and 23 ºC within a Li-Cor 6800 (n = 6). Calculated via the Vialet-Chabrand et al. (2013) model. Error bars represent mean ± SE. Different letters above each error bar represent significant differences in either *A* or g_s lag-times or time constants between the *P. sativum* accessions ($P < 0.05$; TukeyHSD). Whilst the presence of * of the same colour indicates a significant difference in either *A* or g_s lag-times or time constants within an individual accession of the same experimental condition between the leaves and stipules, whereby * is $P < 0.05$, ** is $P < 0.01$ and *** is $P < 0.001$ (TukeyHSD). The presence of + of the same colour indicates a significant difference in either *A* or g_s lag-times or time constants within an individual accession of the same foliar tissue between watered and droughted conditions, whereby + is $P < 0.05$, ++ is $P < 0.01$ and +++ is $P < 0.001$ (TukeyHSD).

3.3.4.6. Variation in Whole Plant Temperature Under Watered and Droughted Conditions

Significant variation were observed in whole plant temperature between the different accessions ($F_{(6)} = 41.09$, $P < 0.001$) and between the different experimental conditions ($F_{(1)} = 36.52$, $P < 0.001$) (***Fig.3.21***).

Filby exhibited the highest watered (22.2 ± 0.22 ^{o}C) and droughted (23.03 ± 0.22 ^{o}C) whole plant temperature and was significantly higher than the remaining watered (TukeyHSD; $P < 0.05$) and droughted accessions (TukeyHSD; $P < 0.05$), respectively (***Fig.3.21***). In contrast, Wando had the lowest watered whole plant temperature (18.75 ± 0.23 ^{o}C), with a significant difference to Ni11 and Filby watered plants (TukeyHSD; $P < 0.05$) (***Fig.3.21A***). Whilst, KW had the lowest droughted whole plant temperature (19.72 ± 0.32 ^{o}C), which was significantly lower than Filby, Eth and Ni11 droughted plants (TukeyHSD; $P < 0.05$) (***Fig.3.21B***). Interestingly, semi-leafless accession Pacco exhibited a significantly cooler watered whole plant temperature (18.75 ± 0.23 ^{o}C) to Ni11 and Filby (TukeyHSD; $P < 0.05$) (***Fig.3.21A***) and a significantly lower droughted whole plant temperature (19.73 ± 0.19 ^{o}C) to Filby, Eth and Ni11 (TukeyHSD; $P < 0.05$) (***Fig.3.21B***). Whilst semi-leafless accession Ni11 was significantly warmer in watered whole plant temperature (20.87 ± 0.19 ^{o}C) to the remaining accessions (par Filby) and significantly higher in droughted whole plant temperature (21.82 ± 0.23 ^{o}C) to the remaining accessions (excluding Eth and Filby) (TukeyHSD; $P < 0.05$) (***Fig.3.21***). Droughted plants generally had a higher temperature than watered plants, with a

significant difference in whole plant temperature identified between watered and droughted Eth plants (TukeyHSD; $P < 0.05$) (***Fig.3.21***).

A significant positive correlation was identified between droughted leaf *i*WUE$_{max}$ and droughted whole plant temperatures (R = 0.69, $P < 0.001$) (***Fig.3.22***). Although the remaining correlations between whole plant temperatures and foliar *i*WUE$_{max}$ were not significantly different, it is interesting to note that the leaves had positive correlations to *i*WUE$_{max}$ (watered: R = 0.26, $P = 0.17$) whilst the stipules exhibited negative correlations (watered: R = -0.067, $P = 0.73$; droughted: R = -0.16 $P = 0.4$) (***Fig.3.22***).

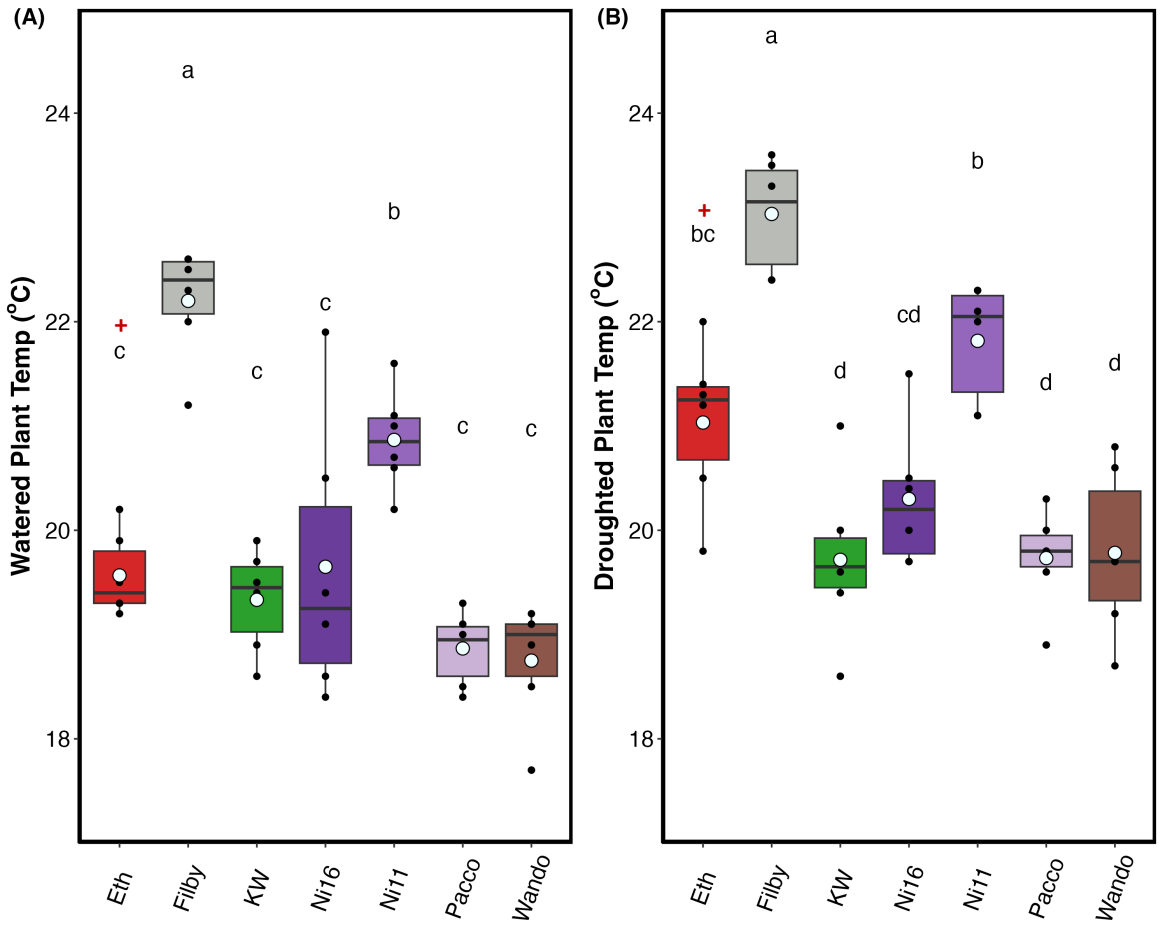

Figure 3.21. Variation in watered and droughted whole plant temperatures across P. sativum accessions. Temperature was observed in **(A)** watered and **(B)** droughted plants using a ^{FLIR}T500-Series thermal camera under standard growth conditions (300 µmol m^{-2} s^{-1} ± 10 µmol m^{-2} s^{-1} photosynthetic photon flux density and 23°C). White dots symbolise the mean, whilst error bars represent mean ± SE (n = 6). Different letters above each error bar represent significant differences in whole plant temperature between the *P. sativum* accessions ($P < 0.05$; TukeyHSD). Whilst the presence of + of the same colour indicates a significant difference in whole plant temperature within an individual accession between watered and droughted conditions, whereby + is $P < 0.05$, ++ is $P < 0.01$ and +++ is $P < 0.001$ (TukeyHSD).

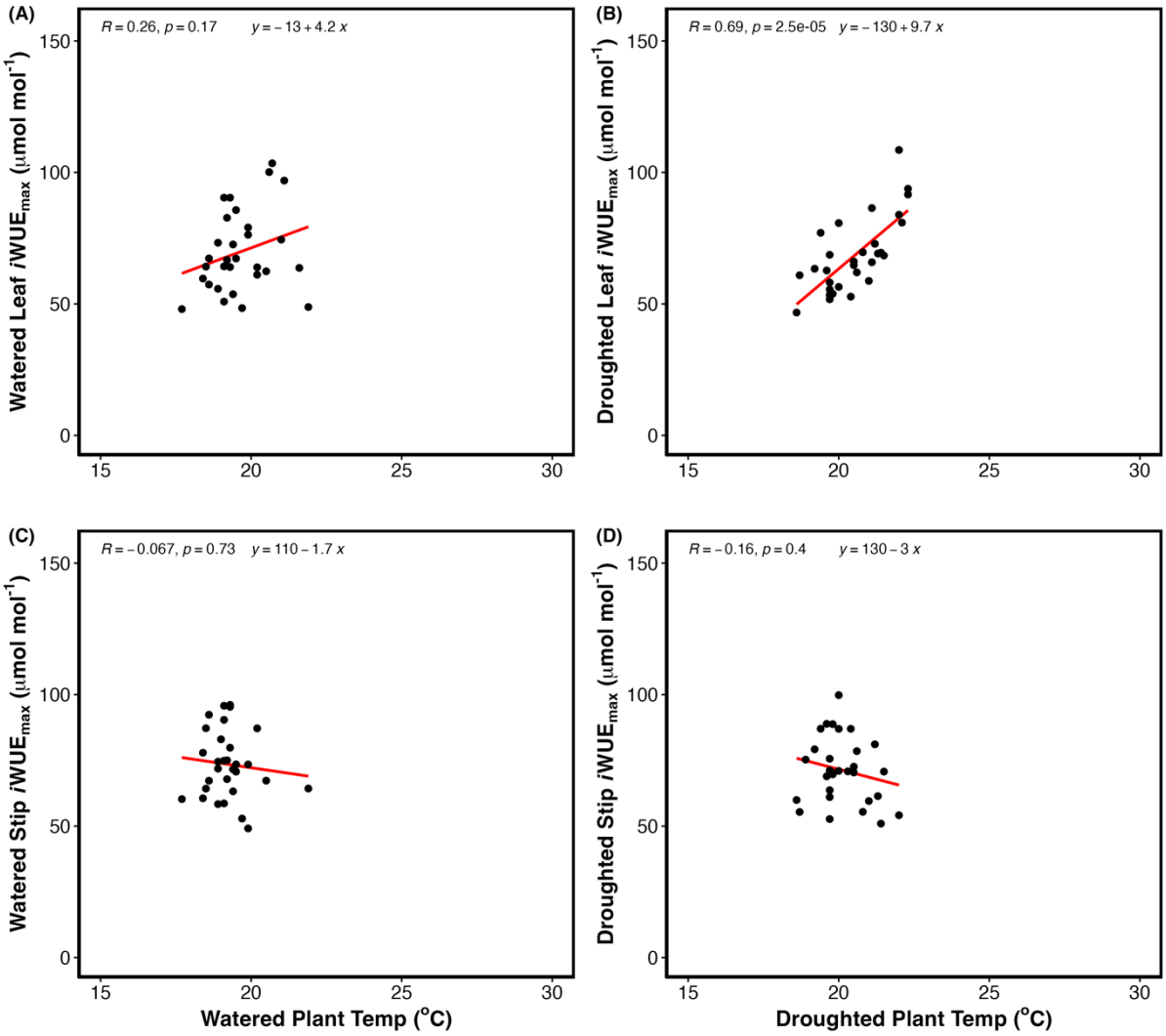

Figure 3.22. Spearmans correlation between foliar iWUE$_{max}$ and plant temperature under watered and droughted conditions. Spearman's correlation coefficients (R) and linear regressions (represented as equations and red lines) were calculated between watered plant temperature and **(A)** watered leaf *i*WUE$_{max}$ (maximum rate *i*WUE; A/g_s) and **(C)** watered stipule (stip) *i*WUE$_{max}$ and between droughted plant temperature and **(B)** droughted leaf *i*WUE$_{max}$ and **(D)** droughted stipule *i*WUE$_{max}$. A ^{FLIR}T500-Series thermal camera was used under standard growth conditions (300 µmol m^{-2} s^{-1} ± 10 µmol m^{-2} s^{-1} photosynthetic photon flux density (PPFD) and 23°C) to generate plant temperatures. Whilst *i*WUE$_{max}$ was calculated from the average of five data points (observations 45-49) after PPFD was increased to 1000 µmol m^{-2} s^{-1}, where *i*WUE was around the highest and most stable rate. Measured at 400 µmol mol^{-1} [CO_2] and 23 °C within a Li-Cor 6800. $P < 0.05$ indicates a significant relationship (n = 6).

3.3.5. Variation in Foliar Anatomy and Yield Under Watered and Droughted Conditions

3.3.5.1. Foliar Anatomy

Significant variation were identified in watered ($F_{(4)}$ = 22.8, P < 0.001) and droughted ($F_{(4)}$ = 12.6, P < 0.001) leaf mass per area (LMA) and in watered ($F_{(4)}$ = 33.6, P < 0.001) and droughted ($F_{(4)}$ = 10.4, P < 0.001) stipule mass per area (SMA) between the different *P. sativum* accessions (***Fig.3.23***).

KW had the greatest watered (33.6 ± 2.63 g m^{-2}) and droughted (30.5 ± 2.91 g m^{-2}) LMA, which was significantly higher than the remaining watered (TukeyHSD; P < 0.05) and droughted (TukeyHSD; P < 0.05) leaf accessions, respectively (***Fig.3.23A&C***). In contrast, Eth exhibited a significantly lower watered (15.6 ± 0.93 g m^{-2}) and droughted (16.7 ± 1.2 g m^{-2}) LMA to KW (TukeyHSD; P < 0.05) respectively (***Fig.3.23A&C***). KW also had the highest watered (30.3 ± 1.59 g m^{-2}) and droughted (27.1 ± 2.66 g m^{-2}) SMA and was significantly different to the remaining watered (TukeyHSD; P < 0.05) and droughted (TukeyHSD; P < 0.05) stipule accessions (***Fig.3.23B&D***). Whilst the lowest SMA was observed in watered Eth (12.7 ± 0.64 g m^{-2}) and droughted Pacco (12.8 ± 0.90 g m^{-2}), respectively, with a significant difference to KW, Ni16 and Wando in watered SMA (TukeyHSD; P < 0.05) and to KW in droughted SMA (TukeyHSD; P < 0.05) (***Fig.3.23B&D***). There were no significant difference identified between leaf and stipule mass per area for either condition within each individual accession (TukeyHSD; P > 0.05) (***Fig.3.23***). Whilst there were also no significant difference identified in either

leaf or stipule mass per area between watered and droughted conditions for either foliar tissue within each individual accession (TukeyHSD; $P > 0.05$) (***Fig.3.23***).

Significant positive correlations were identified between watered LMA and watered leaf Vc_{max} (R = 0.62, $P < 0.001$) and watered leaf J_{max} (R = 0.56, $P < 0.01$) and between droughted LMA and droughted leaf Vc_{max} (R = 0.44, $P < 0.05$) and droughted leaf J_{max} (R = 0.48, $P < 0.01$) (***Fig.3.24***). Significant positive correlations were also observed between watered SMA and watered stipule Vc_{max} (R = 0.47, $P < 0.05$) and watered stipule J_{max} (R = 0.44, $P < 0.05$) and between droughted SMA and droughted stipule Vc_{max} (R = 0.45, $P < 0.05$) and droughted stipule J_{max} (R = 0.42, $P < 0.05$) (***Fig.3.24***).

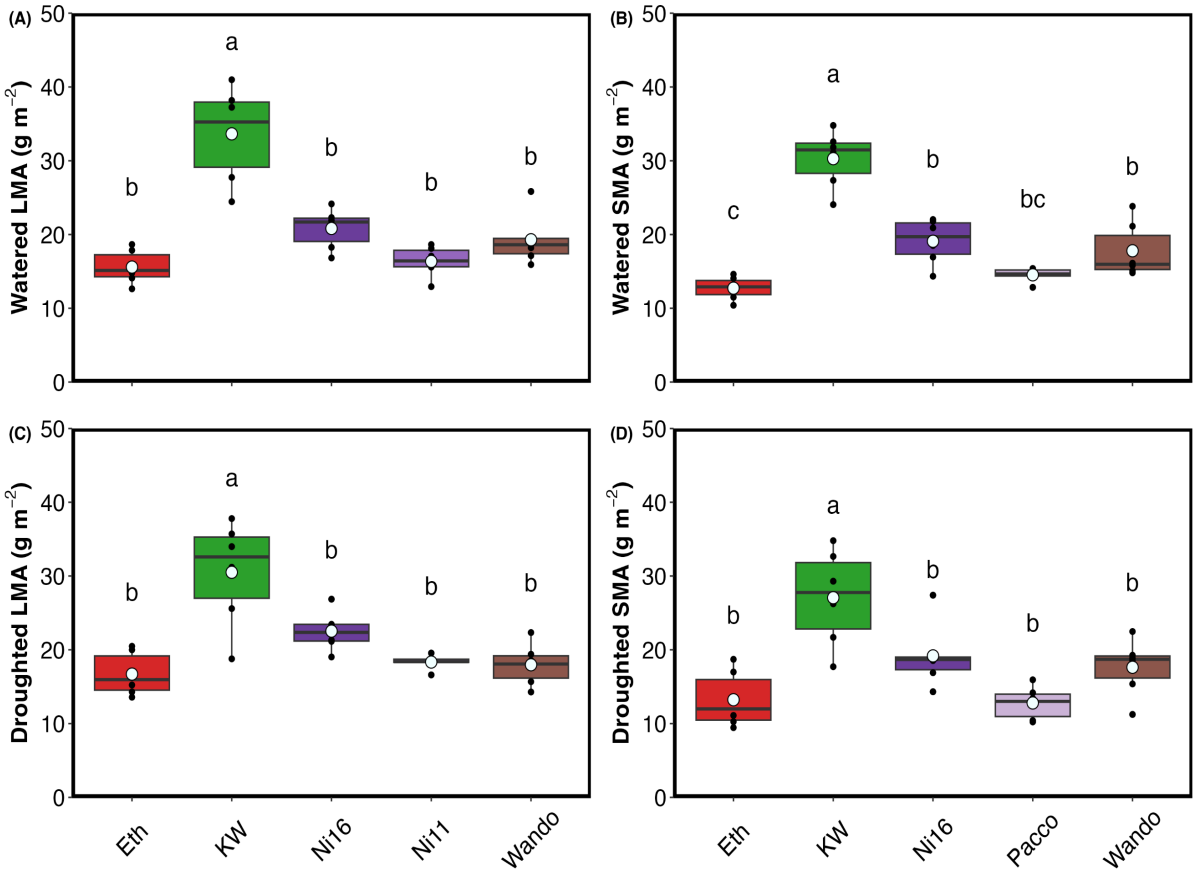

Figure 3.23. Variation in leaf and stipule mass per area across P. sativum accessions under watered and droughted conditions. Watered **(A)** leaf mass per area (LMA) and **(B)** stipule mass per area (SMA) and droughted **(C)** LMA and **(D)** SMA were monitored between the *P. sativum* accessions. Leaf/stipule areas were calculated using ImageJ (n = 6). Dry weights were measured after two weeks in a 60 ºC oven (or until dried to a constant weight). White dots symbolise the mean, whilst error bars represent mean ± SE. Different letters above each error bar represent significant differences in either leaf or stipule mass per area between the *P. sativum* accessions ($P < 0.05$; TukeyHSD). Whilst the presence of * of the same colour indicates a significant difference in leaf/stipule mass per area within an individual accession of the same experimental condition between the leaves and stipules, whereby * is $P < 0.05$, ** is $P < 0.01$ and *** is $P < 0.001$ (TukeyHSD). The presence of + of the same colour indicates a significant difference in leaf/stipule mass per area within an individual accession of the same foliar tissue between watered and droughted conditions, whereby + is $P < 0.05$, ++ is $P < 0.01$ and +++ is $P < 0.001$ (TukeyHSD).

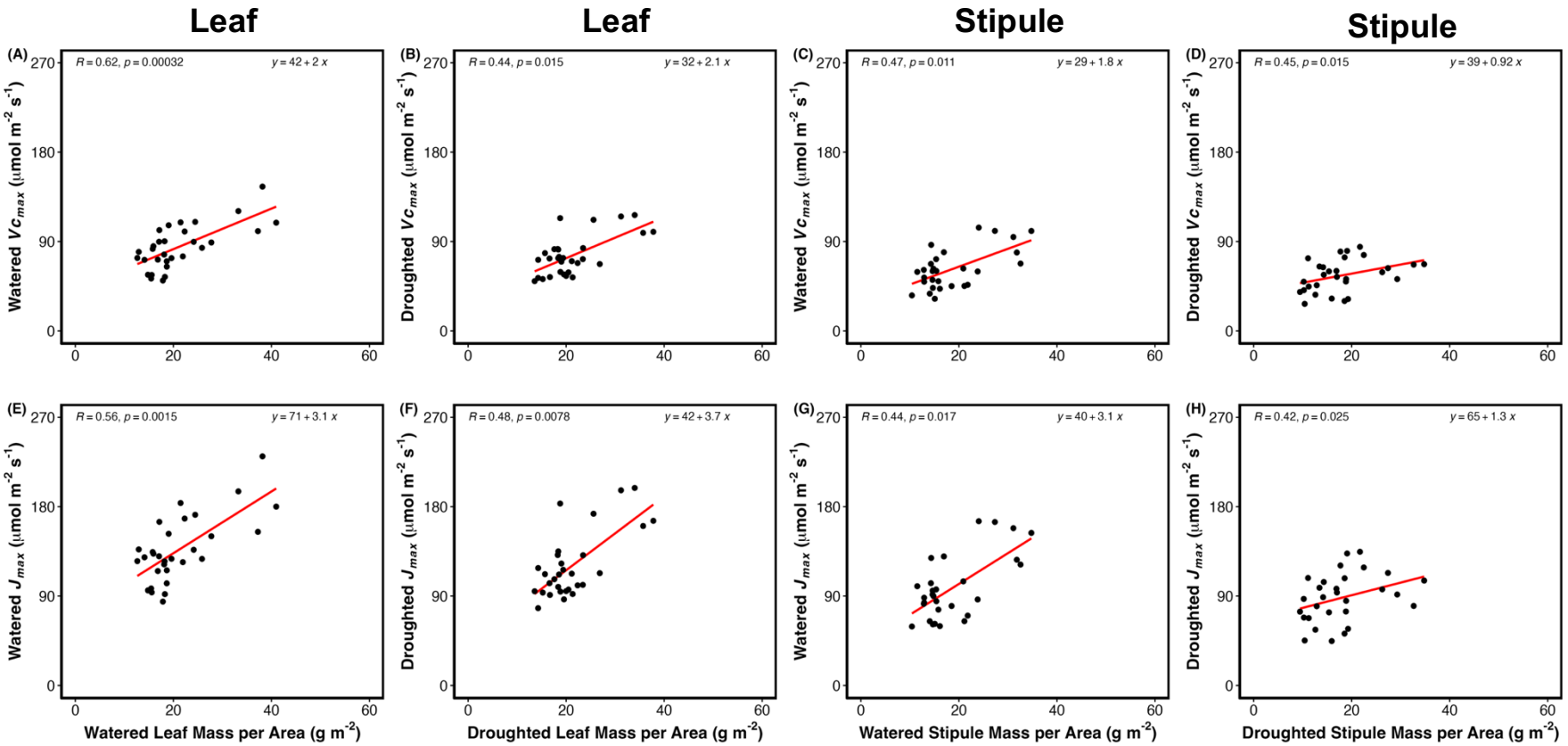

Figure 3.24. Spearmans correlation between leaf and stipule mass per area and photosynthetic capacity under watered and droughted conditions. Spearman's correlation coefficients (R) and linear regressions (represented as equations and red lines) were calculated between watered Vc_{max} (maximum rate of Rubisco activity) and watered **(A)** leaf mass per area (LMA) and **(C)** stipule mass per area (SMA) and between droughted Vc_{max} and droughted **(B)** LMA and **(D)** SMA, as well as between watered J_{max} (maximum rate of electron transport) and watered **(E)** LMA and **(G)** SMA and droughted J_{max} and droughted **(F)** LMA and **(H)** SMA. Gas exchange was measured within a Li-Cor 6800 at 1500 μmol m^{-2} s^{-1} photosynthetic photon flux density and 23 °C. Leaf/stipule areas were calculated using ImageJ. Dry weights were measured after two weeks in a 60 °C oven (or until dried to a constant weight). $P < 0.05$ indicates a significant relationship (n=5-6).

3.3.5.2. Biomass Yield

Significant variation were identified in leaf dry weight (DW) ($F_{(6)}$ = 14.18, P < 0.001), stem DW ($F_{(6)}$ = 2.37, P < 0.05) and in the number of leaves ($F_{(6)}$ = 3.35, P < 0.01), stipules ($F_{(6)}$ = 2.24, P < 0.05) and stems ($F_{(6)}$ = 5.18, P < 0.001) between the different *P. sativum* accessions and experimental conditions (***Fig.3.25***). Whilst a significant difference was observed in all biomass yield parameters (plant height, plant DW, tendril DW and number and DW of stems, leaves and stipules) between the different *P. sativum* accessions (P < 0.001) and in all biomass yield parameters (excluding plant height) between the different experimental conditions (P < 0.01) (***Fig.3.25, Appendix Table.A2.1&A2.2***). For grain yield parameter results please *see* ***Chapter 4 Section 4.3.5.1***.

KW had a significantly lower watered number of leaves (23.67 ± 1.74) to Eth, Ni11 and Wando (TukeyHSD; P < 0.05) and droughted number of leaves (14.3 ± 1.61) to all accessions (TukeyHSD; P < 0.05), as well as a significantly lower watered leaf DW (0.41 ± 0.05 g) to Eth, Ni11 and Wando (TukeyHSD; P < 0.05) and droughted leaf DW (0.217 ± 0.03 g) to all accessions (TukeyHSD; P < 0.05) (***Fig.3.25E-H***). KW was also significantly lower in watered tendril DW (0.17 ± 0.01 g) to Filby, Ni11 and Pacco (TukeyHSD; P < 0.05) and to Filby and Pacco in droughted tendril DW (0.07 ± 0.02 g) (TukeyHSD; P < 0.05) (***Fig.3.25Q&R***). The lowest watered (23 ± 2.28) and droughted (17.3 ± 0.80) number of stipules and watered (0.318 ± 0.03 g) and droughted (0.18 ± 0.02 g) stipule DW was also observed within KW, with a significant difference to Eth and Pacco in watered (TukeyHSD; P < 0.05) and droughted number of stipules

(TukeyHSD; $P < 0.05$) and in watered stipule DW (TukeyHSD; $P < 0.05$) respectively and to Eth, Ni16 and Pacco in droughted stipule DW (TukeyHSD; $P < 0.05$) (***Fig.3.25I-L***). Whilst KW was also significantly lower in droughted plant DW (3.95 ± 0.19 g) to Eth and Ni16 (TukeyHSD; $P < 0.05$), droughted stem DW (0.5 ± 0.03 g) to Eth, Ni16 and Ni11 (TukeyHSD; $P < 0.05$) and watered number of stems (1 ± 0) to Eth, Filby, Ni11, Ni16 and Pacco (TukeyHSD; $P < 0.05$) (***Fig.3.25D,M&P***). Pacco exhibited the lowest watered (29.5 ± 1.82 cm) and droughted (27.83 ± 1.9 cm) plant height and droughted number of stems (1 ± 0), with a significant difference to Eth in watered plant height (TukeyHSD; $P < 0.05$), to Eth, Filby, Ni16 and Ni11 in droughted plant height (TukeyHSD; $P < 0.05$) and to Eth and Filby in droughted number of stems (TukeyHSD; $P < 0.05$) (***Fig.3.25A,B&N***). Whilst Filby had a significantly lower watered plant DW (4.97 ± 0.54 g) to Eth, Ni11 and Wando and significantly lower watered stem DW (0.87 ± 0.09 g) to Eth, Ni16, Ni11 and Wando (***Fig.3.25C&O***).

The greatest overall biomass yield was attributed with Eth, with a significantly greater watered (W) and droughted (D) plant height (W: 80.83 ± 8.18 cm, D: 73.75 ± 3.66 cm), plant DW (W:11.68 ± 0.88 g, D: 9.35 ± 0.92 g), stem (W: 4.93 ± 0.29 g, D: 4.22 ± 0.27 g) and stipule (W: 1.23 ± 0.09 g, D: 1.10 ±. 0.09 g) DW and the number of leaves (W: 99.83 ± 6.37, D: 94.67 ± 3.07), stems (W: 5 ± 0, D: 4 ± 0.37) and stipules (W: 168.33 ± 10.93, D: 142.5 ± 6.85) in comparison to all accessions (except for Ni16 in droughted plant DW) (TukeyHSD; $P < 0.05$) (***Fig.3.25A-F&I-P***). Ni11 exhibited the greatest overall watered (1.29 ± 0.07 g) and droughted (0.63 ± 0.04 g) leaf DW, with a significant difference to all accessions in watered leaf DW (TukeyHSD; $P < 0.05$) and to all accessions (par Eth) in droughted leaf DW (TukeyHSD; $P < 0.05$) (***Fig.3.25G&H***).

Whilst Filby had the highest watered (1.8 ± 0.18 g) and droughted (1.65 ± 0.25 g) tendril DW and was significantly different to all accessions in watered tendril DW (TukeyHSD; $P < 0.05$) and to all accessions in droughted tendril DW (TukeyHSD; $P < 0.05$) respectively (***Fig.3.25Q&R***).

Watered conditions were generally higher than droughted conditions for all yield parameters (***Fig.3.25***), with a significant difference identified between watered and droughted conditions within the individual accessions of Ni11 for plant DW (TukeyHSD; $P < 0.05$) and number of leaves (TukeyHSD; $P < 0.001$), Eth (TukeyHSD; $P < 0.05$) and Pacco (TukeyHSD; $P < 0.001$) for number of stems, Eth for number of stipules (TukeyHSD; $P < 0.01$), Wando (TukeyHSD; $P < 0.05$), Eth (TukeyHSD; $P < 0.05$) and Ni11 (TukeyHSD; $P < 0.05$) for stem DW, Wando (TukeyHSD; $P < 0.01$) and Ni11 (TukeyHSD; $P < 0.001$) for leaf DW and Pacco for stipule DW (TukeyHSD; $P < 0.01$) (***Fig.3.25C-P***). However no significant difference were identified in plant height or tendril DW between watered and droughted conditions within each individual accession (TukeyHSD; $P > 0.05$) (***Fig.3.25A-B&Q-R***).

3.3.5.3. Relationship Between Yield and Photosynthetic Capacity

To determine the impact of photosynthetic capacity on yield, biomass and grain (from ***Chapter 4 Section 4.3.5.1***) yield parameters were correlated against leaf and stipule Vc_{max} and J_{max} for watered and droughted conditions (***Table.3.8***). Significant negative correlations were identified in plant height, stem DW, number of leaves and number of stems to watered leaf Vc_{max} and J_{max}, droughted leaf Vc_{max} and J_{max} and watered stipule Vc_{max} ($P < 0.05$) (***Table.3.8***). Significant negative correlations were also seen in plant DW to watered and droughted leaf Vc_{max} and J_{max} and to watered stipule Vc_{max} and J_{max} ($P < 0.05$) (***Table.3.8***). Whilst the number of stipules negatively correlated with watered (R = -0.36, $P < 0.05$) and droughted (R = -0.51, $P < 0.01$) leaf Vc_{max} and with watered stipule Vc_{max} (R = -0.45, $P < 0.05$) and J_{max} (R = -0.38, $P < 0.05$) (***Table.3.8***). Leaf DW had a significant negative correlation with watered leaf (R = -0.38, $P < 0.05$) and stipule (R = -0.41, $P < 0.05$) Vc_{max} and droughted leaf Vc_{max} (R = -0.43, P < 0.05) and J_{max} (R = -0.44, $P < 0.05$) (***Table.3.8***). Whilst stipule DW had a significant negative correlation to droughted leaf Vc_{max} (R = -0.58, $P < 0.001$) and J_{max} (R = -0.43, $P < 0.05$), watered stipule Vc_{max} (R = -0.52, $P < 0.01$) and J_{max} (R = -0.43, $P < 0.05$) and watered leaf Vc_{max} (R = -0.36, $P < 0.05$) (***Table.3.8***). Tendril DW was significantly negatively correlated to droughted leaf Vc_{max} (R = -0.49, $P < 0.01$) and J_{max} (R = -0.4, $P < 0.05$), whilst watered leaf Vc_{max} also had a significant negative correlation to the number of pods (R = -0.46, $P < 0.05$) (***Table.3.8***).

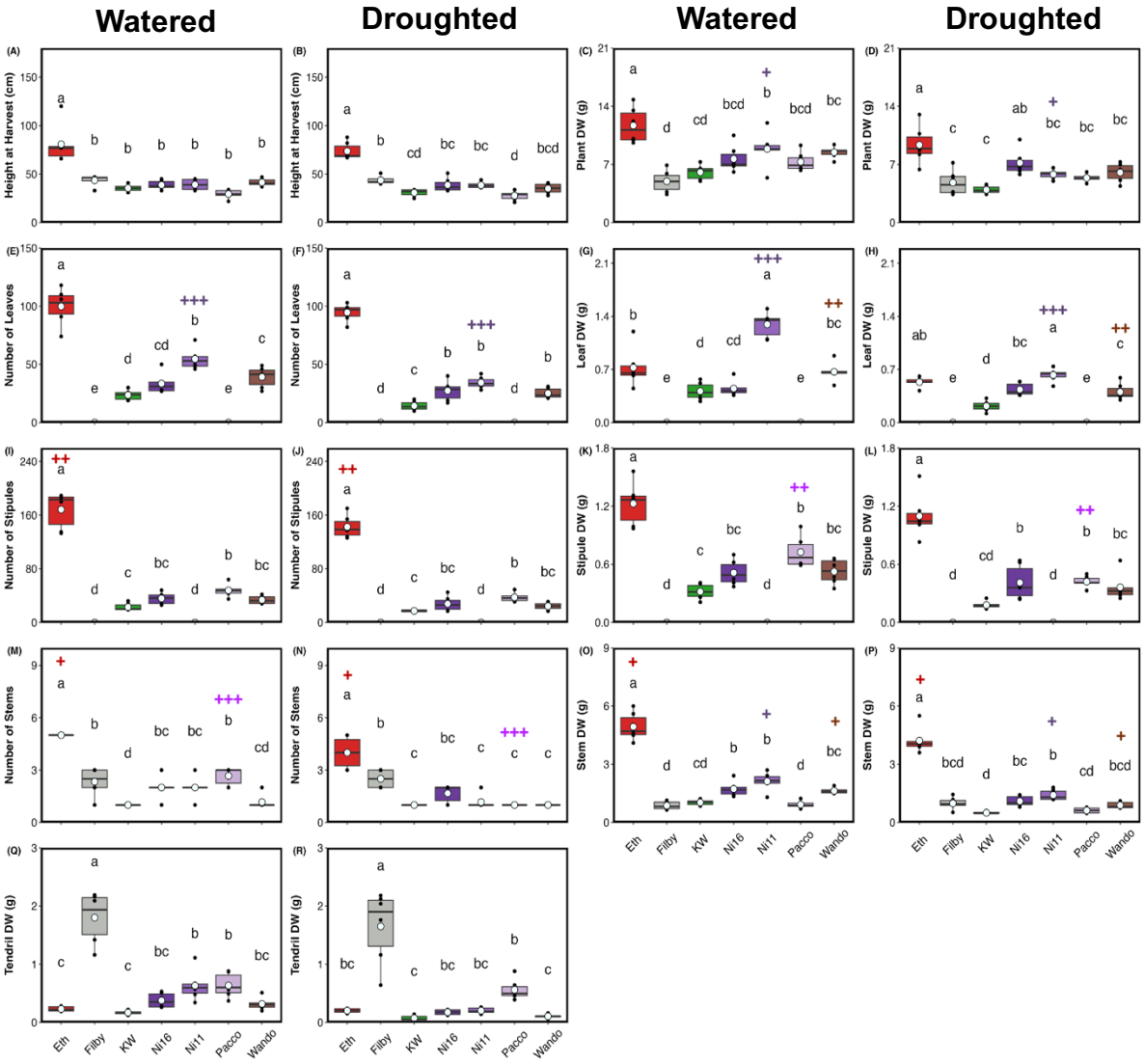

Figure 3.25. Variation in biomass yield parameters across P. sativum accessions under watered and droughted conditions. Biomass yield parameters are represented by watered **(A)** plant height at harvest, **(C)** plant dry weight (DW), **(E)** number of leaves, **(G)** leaf DW, **(I)** number of stipules, **(K)** stipule DW, **(M)** number of stems, **(O)** stem DW and **(Q)** tendril DW, as well as droughted **(B)** plant height at harvest, **(D)** plant DW, **(F)** number of leaves, **(H)** leaf DW, **(J)** number of stipules, **(L)** stipule DW, **(N)** number of stems, **(P)** stem DW and **(R)** tendril DW. Dry weights were measured after a constant weight had been reached. White dots symbolise the mean, whilst error bars represent mean ± SE. Different letters above each error bar represent significant differences in one of the biomass yield parameters between the *P. sativum* accessions ($P < 0.05$; TukeyHSD) (n = 6). Whilst the presence of + of the same colour indicates a significant difference in a biomass yield parameter within an individual accession between watered and droughted conditions, whereby + is $P < 0.05$, ++ is $P < 0.01$ and +++ is $P < 0.001$ (TukeyHSD).

Table 3.8. Spearmans correlation coefficient table showing the relationship between grain and biomass yield components and photosynthetic capacity under watered and droughted conditions. Whereby Vc_{max} (maximum rate of Rubisco activity), and J_{max} (maximum rate of electron transport) measurements (measured in µmol m^{-2} s^{-1}) were obtained at 1500 µmol m^{-2} s^{-1} photosynthetic photon flux density and 23 °C within a Li-Cor 6800. Grain yield parameters are represented by the number of pods, number of seeds, pod length, pod dry weight (DW), seed DW and total pod DW, whilst biomass yield parameters are represented by plant height, plant DW, number and DW of stems, leaves and stipules and tendril DW. Pod lengths were measured (in cm) via ImageJ (version 1.53), whilst dry weights (DW) were measured (in g) after a constant weight was reached. Spearman's correlation coefficients (R) were calculated for each yield component against capacity measurement for both watered and droughted conditions, with the darker red boxes representing a strong negative correlation, whilst the dark green boxes represent a strong positive correlation. Statistical significance between yield parameters and capacity are illustrated as asterisks, whereby * is $P < 0.05$, ** is $P < 0.01$ and *** is $P < 0.001$ (n = 5-6).

Yield Parameters	Watered Leaf		Droughted Leaf		Watered Stipule		Droughted Stipule	
	Vc_{max}	J_{max}	Vc_{max}	J_{max}	Vc_{max}	J_{max}	Vc_{max}	J_{max}
Plant Height	*** -0.58	** -0.49	** -0.54	* -0.39	* -0.45	-0.28	-0.043	0.11
Plant DW	** -0.56	** -0.5	** -0.57	** -0.49	** -0.55	* -0.41	-0.15	-0.055
Number of Leaves	*** -0.73	*** -0.66	*** -0.62	** -0.56	* -0.43	-0.26	-0.07	0.02
Number of Stipules	* -0.36	-0.34	** -0.51	-0.34	* -0.45	* -0.38	-0.32	-0.25
Number of Stems	*** -0.74	*** -0.66	*** -0.61	* -0.38	* -0.37	-0.32	-0.13	0.04
Leaf DW	* -0.38	-0.34	* -0.43	* -0.44	* -0.41	-0.29	0.0099	0.089
Stipule DW	* -0.36	-0.3	*** -0.58	* -0.43	** -0.52	* -0.43	-0.18	-0.13
Stem DW	*** -0.73	*** -0.68	*** -0.64	** -0.55	* -0.42	-0.25	-0.16	-0.093
Tendril DW	-0.26	-0.3	** -0.49	* -0.4	-0.19	-0.33	-0.3	-0.23
Number of Pods	* -0.46	-0.31	-0.34	-0.25	-0.22	-0.15	-0.16	-0.13
Pod DW	0.33	0.18	0.16	0.095	0.17	0.11	0.11	0.17
Number of Seeds	0.053	-0.065	0.0087	-0.044	-0.057	-0.17	-0.23	-0.16
Seed DW	0.32	0.17	0.17	0.094	0.2	0.13	0.077	0.14
Pod Length	0.12	0.04	0.13	0.099	0.25	0.2	0.14	0.21
Total Pod DW	0.12	0.071	-0.02	-0.069	-0.019	-0.074	-0.077	-0.056

3.4. Discussion

The frequency and severity of droughts are increasing and threatening current global pea productivity, subsequently identifying accessions that are able to tolerate drought conditions is an increasingly important way to alleviate yield loss and secure future food production (Moran et al., 1994; Magyar-Tábori et al., 2011; Araújo et al., 2015; Bagheri et al., 2023; Jiang et al., 2023). Screening lines under drought/water-limited environments have already been used to determine genetic diversity in drought responses of *P. fulvum* (wild pea) (Naim-Feil et al., 2017; Hellwig et al., 2021), variation in yield of *L. sativus* (grass pea) (Jafarinasab et al., 2022) and *P. sativum* (Sadras et al., 2013) and variation in spectral traits in *P. sativum* (Nemeskéri et al., 2015). Yet exploration of natural variation in photosynthetic capacity and stomatal responses in current pea germplasms was yet to be fully evaluated under drought stress in different foliar tissues (Faralli and Lawson, 2020; Bagheri et al., 2023; Burgess et al., 2023). This study utilised current physiological techniques to assess natural variation in photosynthetic capacity in pea populations, whilst establishing differences in stomatal and photosynthetic responses to light intensity changes under watered and droughted conditions in the different foliar tissues. Whereby significant variation existed between the different *P. sativum* accessions for the majority of measured parameters under both watered and droughted conditions and for both types of foliar tissues (leaves and stipules) (***Fig.3.1-3.25***).

3.4.1. Variation in Photosynthetic Rates and Capacity Under Drought

Significant variation existed within photosynthetic capacity, whereby greater capacity was identified within an elite variety (KW) in comparison to a landrace accession (Eth) (***Fig.3.6&3.8***). Unexpectedly elite accession Wando exempted this trend with a lower watered stipule J_{max} and did not perform as efficiently under drought stress environments, despite being bred for drought/heat tolerance, however heat stress was not studied within this experiment and therefore Wando may still have the potential for higher photosynthetic capacity and yield when subjected to elevated heat (Yarnell, 1950; Pallas and Michel, 1971; Baggett and Kean, 1987; Aggour, 1999). Interestingly drought did not influence photosynthetic capacity for either foliar tissue (***Fig.3.8***). Such findings contradict that of Du et al. (2024) in soybean, Moran et al. (1994) in pea, Limousin et al. (2010) in Holm Oak and Sherrard et al. (2009) in slender wild oat. Subsequently the level of drought utilised (50% relative soil water content; RSWC) may not have been sufficient to trigger non-stomatal drought factors (*e.g.* reductions in Rubisco and other Calvin cycle enzyme activity) (Liang et al., 2020; Yang et al., 2021; Ortiz and Salas-Fernandez, 2022). Thus future experiments could incorporate different levels of RSWC to further explore the impact of drought on photosynthetic capacity in peas (Bagheri et al., 2023). Although discrepancies to Moran et al. (1994) in pea may arise from the different cultivars utilised, the present study potentially highlights pea accessions with less susceptibility to mild drought stress, as reinforced by the negligible impact of drought on the relationship between A and g_s, which suggested that A was significantly influenced by stomatal regulation regardless of experimental condition (***Fig.3.7***) (Zhao et al., 2020b; Bagheri et al., 2023).

The positive relationships identified between LMA/SMA and photosynthetic capacity (***Fig.3.8,3.23&3.24***) indicated that LMA/SMA may have driven the differences in photosynthetic capacity between elite and landrace accessions (Poorter et al., 2009; Ren et al., 2019). Positive relationships between LMA and photosynthesis are often associated with increased development of palisade parenchyma, mesophyll cell surface area and thicker mesophyll structures to facilitate greater photosynthetic capacity and has been seen as an adaptive mechanism to drought stress, with Damour et al. (2008) reporting that LMA increased by around 30% when water potential declined in Lychee (Damour et al., 2008; Poorter et al., 2009; Ren et al., 2019; Nardini, 2022). However, within the present study neither LMA nor SMA was significantly influenced by drought stress, further reinforcing that the level of drought utilised was not enough to trigger certain morphological changes (***Fig.3.23***) (Damour et al., 2008).

Generally foliar photosynthetic capacity had little to no effect upon grain yield (for either condition or foliar tissue), supporting findings in wheat (Driever et al., 2014; Silva-Pérez et al., 2020) barley (Stevens et al., 2021) and rice (Priyadarsini et al., 2022) where no correlations were identified under standard watering conditions (***Table.3.8***). Photosynthetic capacity was also negatively correlated with some biomass yield parameters, such as plant height and weight for both watered and droughted conditions (***Table.3.8***), yet these relationships may explain the physiological properties of the landrace accession. Whereby the lower photosynthetic capacity observed within the landrace accession could be attributed to its higher biomass yield, with resources being partitioned more into growth and in turn

generating a reduction in individual leaf and stipule capacity (***Fig.3.8&3.25, Table.3.8***) (Faralli et al., 2019; Acevedo-Siaca et al., 2020). The high biomass yield experienced by the landrace accession may have additionally been driven by its greater operational efficiency of PSII (F_q'/F_m') (***Fig.3.1-3.3***), which has previously been identified to have a positive relationship with dry matter accumulation in wheat (Sherstneva et al., 2021) and grain yield in hybrid rice (Huang et al., 2016) and thus chlorophyll fluorescence may provide a beneficial tool for uncovering the drivers of greater yield (Murchie and Lawson, 2013; Pszczółkowski et al., 2023). Yet, it is curious whether the landrace accession would exhibit greater photosynthetic capacity if measurements were taken on a total leaf area basis and thus future experiments could also take this into consideration (Acevedo-Siaca et al., 2020). Nonetheless photosynthetic capacity measurements are not always representative of dynamic environments (such as those in the field), often leading to disconnections between capacity and yield, therefore future studies could additionally utilise comparisons to field experiments (Lawson et al., 2012; Faralli and Lawson, 2020).

Drought did lead to a decrease in the majority of biomass yield parameters (although only within certain accessions) in comparison to watered conditions (for the impact of drought on grain yield please *see* ***Chapter 4 Section 4.4***) (***Fig.3.25***). Such findings were expected as drought causes reductions in foliar tissues through senescence, whilst reductions in biomass within different tissues is associated with redistribution of resources, with root biomass often increasing for enhanced water uptake whereas foliar and stem biomass decrease to limit above ground water loss (Nemeskéri et al., 2015; Yang et al., 2021; Yan et al., 2023).

3.4.2. Variation in Stomatal and Photosynthetic Responses to Light Intensity Changes Under Drought

Significant variation was also identified in stomatal and photosynthetic responses to light intensity changes, as well as in a step increase in light intensity, with elite accessions (KW and Ni16) generally exhibiting higher rates of *A* and/or g_s (respectively) (***Fig.3.4-3.5&3.17-3.18***). Whilst drought generally had a negative impact on g_s with changes in light intensity and on *A* and g_s with a step increase in light intensity, such responses may suggest that the level of drought utilised triggered stomatal limitations which restricted CO_2 diffusion for photosynthesis (***Fig.3.4-3.5&3.17-3.18***) (Yang et al., 2021; Ortiz and Salas-Fernandez, 2022).

Differences in stomatal anatomy (including stomatal densities (SD) and sizes (SS)) often influence *A* and g_s responses to fluctuations in light intensity, especially under drought stress (Ouyang et al., 2017; Bertolino et al., 2019; Conesa et al., 2020; Caine et al., 2023; Hasanuzzaman et al., 2023). Whereby ABA can reduce stomatal aperture through declines in turgor pressure in the guard cell, whilst restricted cell expansion (also driven by reductions in turgor pressure) limit leaf area, which is often complemented by an increase in SD (Xu and Zhou, 2008; Sherrard et al., 2009; Bertolino et al., 2019; Conesa et al., 2020; Hasanuzzaman et al., 2023). SD has been previously seen to increase in maize (Zhao et al., 2015), olive (Ennajeh et al., 2010), slender wild oat (Sherrard et al., 2009) and bluebunch wheatgrass (Fraser et al., 2009), whilst SS has been seen to decrease in false wheatgrass (*L. chinensis*) (Xu and Zhou, 2008), rice (Ouyang et al., 2017) and maize (Zhao et al., 2015) under drought stress. Yet within the present study only SD was seen to significantly decrease

under drought conditions (***Fig.3.9&3.10***), which supports Nemeskéri et al. (2015) who found that drought negatively impacted SD of certain pea varieties (*i.e.*, Milor), but had no impact on SS (Nemeskéri et al., 2015; Nemeskéri and Helyes, 2019). However within the present study SD and SS generally had no impact upon g_s for either condition (***Fig.3.15&3.16***), although it has previously been established that amongst some angiosperm species there is a general lack of relationship between SD/SS and operational g_s often suggesting that other unknown factors may be regulating g_s (McElwain et al., 2016; Xiong and Flexas, 2020).

Maximum anatomical g_s (gs_{max}) was generally impacted by both SD and SS (for the majority of experimental conditions and foliar tissues), with increases in gs_{max} occurring from both a higher density of stomata and greater SS (***Fig.3.13&3.14***). Such findings do not agree with the majority of studies, whereby increases in gs_{max} are generally driven from a greater density of smaller stomata (Dow et al., 2014a; Bertolino et al., 2019; Caine et al., 2023). Whilst a higher density of larger stomata would often be considered damaging under drought, due to greater transportational losses, drought generally had no impact on gs_{max} within this study (***Fig.3.11***) (Bertolino et al., 2019; Caine et al., 2023). Declines in gs_{max} are frequently associated with greater *i*WUE, yet within the present study accessions with high $i\text{WUE}_{max}$ did not generally have the lowest gs_{max} (***Fig.3.11&3.19***) (Dow et al., 2014a; Bertolino et al., 2019). Greater drought tolerance through high *i*WUE can also be influenced by stomatal kinetics, with rapid responses often more efficient at mitigating water loss, however within the present study, the accession (Ni11) with the longest g_s time constant also conveyed the highest $i\text{WUE}_{max}$ in the leaves under drought stress (***Fig.3.19&3.20***),

similar to that of Eyland et al. (2021) in Banana. Yet in the remaining cases stomatal kinetics did not vary significantly between accessions and thus differences in *i*WUE$_{max}$ may instead be attributed with the low values of operational g_s experienced by Ni11 (***Fig.3.18-3.20***) (Lawson and Blatt, 2014; Eyland et al., 2021; Lv et al., 2023; Nguyen et al., 2023).

Intriguingly the highest *i*WUE$_{max}$ accessions were mainly semi-leafless, which confers with prior studies whereby semi-leafless varieties had greater WUE than conventional leafed varieties (Wilson et al., 1981; Baigorri et al., 1999; Nemeskéri et al., 2015; Checa et al., 2020), although these results oppose that of Armstrong et al. (1994) and Nguyen et al. (2018), yet these studies derived WUE as a function of estimated biomass per water supplied in contrast to the present study (***Fig.3.17&3.19***) (Armstrong et al.,1994; Nguyen et al., 2018). Greater WUE of semi-leafless varieties are often attributed to their reduced foliar surface areas and subsequent reductions in transpiration, however this can generate increased plant/leaf temperatures due to restricted heat dissipation (Nemeskéri et al., 2015; Perez and Feeley, 2018; Bagheri et al., 2023). Although the present study did not highlight significant relationships between *i*WUE$_{max}$ and plant temperature (***Fig.3.22***), the semi-leafless afila variety (Pacco) remained cooler than the semi-leafless stipule reduced (Ni11) and the fully leafless accession (Filby), suggesting that transformation of leaves into tendrils, but not total loss of foliar tissues may prevent overheating and therefore could be a beneficial trait for future climatic conditions (***Fig.3.21***) (Checa et al., 2020). Such findings may be supported by the stipules generally exhibiting a greater *i*WUE$_{max}$ than the leaves (***Fig.3.19***), which may have generated the cooler plant temperatures seen

within the semi-leafless afila variety, potentially driven by the greater osmolarity and better response to water deficit previously reported in semi-leafless pea stipules by Gonzalez et al. (2002). Reinforcing the potential for greater productivity and survival under future climatic conditions by considering more than just conventional leaf tissues (Tran et al., 2022). However as only one semi-leafless afila accession was utilised within this study further experiments with a greater number of varieties are required to confirm this (Checa et al., 2020).

When comparing the different types of foliar tissues, it was identified that the leaves were generally greater than the stipules for the majority of gas exchange parameters measured under both experimental conditions (***Fig.3.4-3.8,3.17&3.18***), which aligns with Giovanardi et al. (2018), who found that stipules were less efficient at gas exchange due to increased respiration rates, lower photosynthetic conversion capacities and compact mesophyll cells (Giovanardi et al., 2018). It was also noted within the present study that the leaves generally exhibited greater SD and gs_{max} than stipules (***Fig.3.9&3.11***), unlike the findings of Sharma et al. (2012), who found stomatal anatomy was similar between the leaves and stipules, yet such discrepancies may be due to differences in the varieties utilised between studies (Sharma et al., 2012). Although drought negatively impacted some physiological parameters, it appears that on an overall scale the influence of drought within this experiment was limited (***Fig.3.1-3.25***) reinforcing that the level of drought utilised may not have been enough to initiate large scale physiological impacts, however such findings may also indicate that the accessions utilised may be less susceptible to mild drought and therefore may provide untapped genes for drought tolerance yet to be explored (Yang et al., 2021).

3.4.3. Limitations

A limitation to this study was that only six-seven accessions were screened, with only one type of semi-leafless afila, semi-leafless stipules reduced, fully leafless and landrace accession utilised, which was not fully representative of the natural variation in the current pea germplasm, thus future experiments could screen a more diverse population of peas. As mentioned in ***Sections 3.4.1*** and ***3.4.2*** these studies could also utilise a more severe level of drought to fully explore the ability of different pea accessions to survive under future climatic conditions. Whilst future studies could also consider utilisation of nitrogen fixing bacteria and/or comparisons to field conditions to provide a more accurate representation of pea performances under natural/agricultural settings (Faralli et al., 2019; Acevedo-Siaca et al., 2020, Yang et al., 2021).

3.4.4. Conclusions

In summary, natural variation existed for the majority of measured parameters under both watered and droughted conditions and for both foliar tissue types. The greater photosynthetic capacity experienced by elite accessions were potentially driven through differences in LMA/SMA. Yet despite the low capacity of the landrace, the greater operational efficiency of PSII may have translated into a higher biomass yield, indicating that chlorophyll fluorescence may provide a more accurate tool of uncovering the drivers of greater biomass yield. Although stomatal density and size had little impact on g_s, they did influence gs_{max} through a greater density of larger

stomata which further contributes to the debate of how stomatal anatomy influences conductance. Although *i*WUE$_{max}$ did not generally impact plant temperature, the semi-leafless afila variety remained cooler than the semi-leafless stipules reduced and fully leafless accessions, highlighting that transformation of leaves into tendrils, but not a total loss of foliar tissues may be a beneficial trait under future climatic conditions. The leaves generally performed greater than the stipules for the majority of gas exchange parameters, as well as SD and gs_{max}, however the stipules generally had a greater *i*WUE$_{max}$ reinforcing the need to consider more than just conventional leaf tissues for the identification of beneficial drought tolerant traits for future breeding programmes. Although drought negatively impacted some physiological parameters, the overall influence was limited, potentially indicating that the level of droughted utilised may not have been severe enough, yet may also indicate that the accessions measured are possibly less susceptible to mild drought stress and may provide untapped genes for drought tolerance yet to be fully investigated. Nevertheless, the considerable variation presented within this study highlights potentially beneficial accessions and traits for improved pea production under future climatic conditions (Faralli and Lawson, 2020; Bagheri et al., 2023; Burgess et al., 2023).

3.4.5. Take Home Messages

- Significant variation existed for the majority of measured physiological parameters between the different *P. sativum* accessions, the different foliar tissues and the different experimental conditions including photosynthetic capacity and stomatal and photosynthetic responses to light intensity changes.

- Elite accession KW generally had greater photosynthetic capacity than the landrace, whilst elite accessions (KW and Ni16) also illustrated the greater responses of A and/or g_s to light intensity changes and a step increase in light intensity.

- Differences in photosynthetic capacities were potentially driven by differences in LMA/SMA. However limited/no relationships were identified between photosynthetic capacities and grain yield.

- The negative relationship between photosynthetic capacity and biomass yield parameters could be due to the landrace accession putting more resources into growth, reducing individual leaf and stipule photosynthetic capacities. Yet the greater operational efficiency of PSII observed within the landrace potentially translated into a higher biomass yield.

- Stomatal anatomy generally had no impact on g_s, however a greater density of larger stomata potentially drove increases in gs_{max}.

- The highest *i*WUE$_{max}$ accessions were mainly semi-leafless. Whilst the semi-leafless afila variety was cooler than the semi-leafless stipules reduced and fully leafless accessions, thus conversion of leaves into tendrils (but not loss of all foliar tissues) may be a beneficial trait under future climatic conditions.

- Leaves generally performed greater than the stipules for the majority of gas exchange parameters, as well as SD and gs_{max}, however the stipules generally had a greater *i*WUE$_{max}$. Subsequently more than just conventional leaf tissues should be considered when screening accessions for future breeding programmes.

- The overall impact of drought on physiological parameters was limited (although some parameters were negatively affected), possibly suggesting the level of drought utilised within this experiment was not severe enough to induce physiological impacts, however, it may indicate that the accessions utilised may not be susceptible to mild drought stress.

Chapter 4: Investigating Natural Variation in Response to Drought in Non-Foliar Tissues of *P. sativum*

4.1. Introduction

The frequency of droughts are increasing and having detrimental impacts upon global crop yields, with an average global loss of 0.8% calculated per drought event in agricultural gross domestic production (Urban et al., 2017a; Kim et al., 2019). However, crops have developed a multitude of strategies to try and overcome/tolerate the impacts of drought, including utilisation of antioxidants, osmoregulation, deep tap roots and development of rapid stomatal characteristics (*see* ***Chapter 3 Section 3.1***) (Singh and Reddy, 2011; Araújo et al., 2015; Farooq et al., 2021). Within peas the development of semi-leafless and leafless varieties limit detrimental water loss by reducing foliar area (Gonzalez et al., 2002; Araújo et al., 2015; Szablińska-Piernik and Lahuta, 2021; Bagheri et al., 2023). Varieties that are fully leafless are thought to be solely reliant on the ability of non-foliar tissues (such as the pods) to provide photo-assimilates for growth/survival (Heath and Hebblethwaite, 1985, Heath et al., 1994; Lawson and Milliken, 2023). Although variation in foliar photosynthesis under drought stress has been examined in numerous species (as explored in ***Chapter 3***), little research has investigated natural variation in non-foliar photosynthesis and the implications on yield in response to drought, especially within peas (Simkin et al., 2020; Lawson and Milliken, 2023).

Under stress environments (such as drought), non-foliar photosynthesis is believed to act as a compensatory mechanism when foliar photosynthesis is compromised, as reported by Tambussi et al. (2005) who found that photosynthetic rates in wheat ears were less impacted by water limitations than the flag leaf and further established by Zhang et al. (2011) who identified that the green non-foliar area in wheat increased

when drought was induced (Ma et al., 2001; Tambussi et al., 2005; Zhang et al., 2011; Li et al., 2017; Hu et al., 2019; Simkin et al., 2020; Antonietta et al., 2024). The ability of non-foliar tissues to act as a compensatory mechanism and have higher photosynthetic rates under drought stress is thought to be the result of multiple drought tolerant mechanisms, including osmotic adjustments (difference in osmotic potential between water-stressed and non-stressed plants), which have been identified in the glumes (40%), lemmas (46%) and awns (28%) of wheat in comparison to the flag leaf (6%) (Tambussi et al., 2005; Hu et al., 2019), whilst similar results have been conferred in barley spike tissues in comparison to the fifth leaf (Hein et al., 2016). Higher levels of ROS scavengers such as antioxidant enzymes have also been reported at a higher concentration in non-foliar tissues than the leaves, with stable photosynthetic rates in spike bracts in winter wheat attributed to an increase in antioxidant activity which alleviated ROS damage under drought stress (Lou et al., 2018). Although the presence of xeromorphic anatomy in non-foliar tissues; including sclerenchyma tissues, epicuticular waxes and thicker cell walls can restrict gas exchange, they also limit water loss and prevent desiccation often resulting in greater water use efficiency (WUE) and drought tolerance (Hu et al., 2019; Simkin et al., 2020; Garrido et al., 2023). The possibility of C_4 photosynthesis in non-foliar tissues is still being debated, yet the presence of C_4 enzymes; such as phosphoenolpyruvate carboxylase (PEPC) and NAD-dependent malic enzyme (NAD-ME) and molecules including malate and oxaloacetate, have been established in numerous non-foliar tissues including wheat and barley spikes, whereby activity and expression of such enzymes and molecules have been shown to heighten under water deficit, further suggesting that non-foliar photosynthesis increases under drought stress (Macnicol and Jacobsen, 1992;

Rangan et al., 2016; Zhang et al., 2019b; Henry et al., 2020; Simkin et al., 2020; Garrido et al., 2023).

It is well established that non-foliar tissues have two potential sources of CO_2 for carbon fixation; atmospheric CO_2 that enters via the stomata and refixed CO_2 supplied by internal respiration (such as embryonic respiration) (Henry et al., 2020; Simkin et al., 2020; Garrido et al., 2023; Lawson and Milliken, 2023). Utilisation of refixed CO_2 prevents water loss from the stomata and maintains a high WUE, as photosynthesis still occurs regardless of closed stomata, with soybean pod and seed photosynthesis able to compensate for 81% of carbon loss by using respiratory CO_2 (Hu et al., 2019; Henry et al., 2020; Cho et al., 2023). Within legumes, the pod walls are believed to be one of the main sites of non-foliar carbon fixation, with over 80% of CO_2 found in the pod walls of chickpeas, whilst alfalfa pod walls have been reported to contribute 25.6-48.1% to seed weight per pod (Ma et al., 2001; Wang et al., 2016). The pod walls of peas have been illustrated by Atkins et al. (1977) to consist of two distinct photosynthetic layers (***Fig.4.1***); the outer layer made up mesocarp chlorenchyma (chlorophyll containing tissue) which have a thick cuticle and contain stomata (reported to have a stomatal density of 25% of that of nearby leaves/stipules) for atmospheric CO_2 fixation, and the inner layer consisting of epidermis that line the pod gas cavities and are reported to have high levels of PEPC activity and contain 20% pod chlorophyll content capable of refixing 66% respiratory CO_2 (Atkins et al., 1977, Wang et al., 2016, Basu et al., 2022; Garrido et al., 2023). Differences in pod wall thickness, stomatal anatomy, PEPC activity, pod sizes/shapes and differing drought tolerance mechanisms (mentioned above) are all thought to generate variation in non-

foliar photosynthesis and WUE (as explored in ***Chapter 1 Section 1.4.3***) (Wang et al., 2016; Hu et al., 2019; Simkin et al., 2020; Garrido et al., 2023; Lawson and Milliken, 2023). Whilst the different leaf morphologies that exist across peas varieties (*see* ***Chapter 2*** and ***3***) are also believed to contribute to variation in pod photosynthetic rates, with conventional WT leafed varieties associated with greater shading, restricted irradiance and reduced photosynthetic activity of lower plant tissues (such as the pods) in comparison to leafless and semi-leafless varieties (Heath and Hebblethwaite, 1985; Bianculli et al., 2016; Tran et al., 2022). However, it is yet to be fully evaluated whether natural variation in non-foliar photosynthesis exists in peas and if differences in foliar morphology, stomatal anatomy and kinetics play a key role in maintaining non-foliar photosynthesis under drought stress (Simkin et al., 2020; Lawson and Milliken, 2023).

This study determined the extent of natural variation in pea non-foliar tissues under mild drought (hereafter called droughted conditions) and watered conditions, whilst further examining stomatal responses for drought tolerance in peas. Accessions from ***Chapter 3*** were utilised, with pod non-foliar tissues subjected to infra-red gas exchange analysis to determine the extent of natural variation in pod assimilation, whilst step increases in light intensity and surface impressions explored the variation in *i*WUE, stomatal kinetics and anatomy.

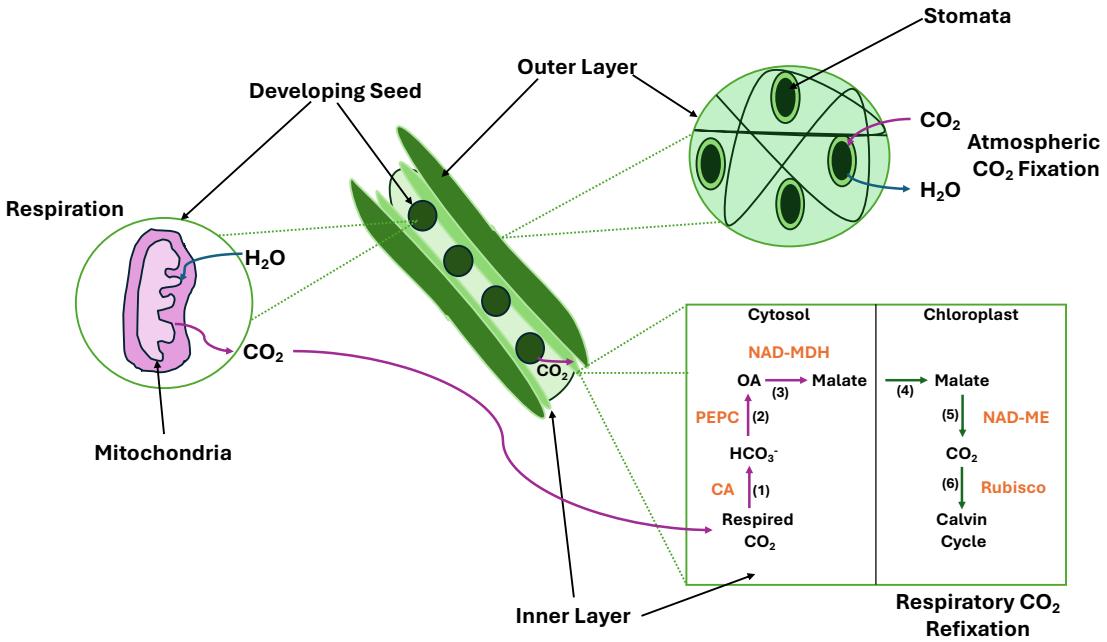

Figure 4.1. Schematic of a legume pod. Showing the inner and outer layers of pea pod walls as described by Atkins et al. (1977). The outer layer contains chlorenchyma that contain stomata allowing CO_2 to enter from the atmosphere. Whilst the inner layer contains chloroplasts capable of refixing respiratory CO_2 from internal sources such as the respiring seed. It has been reported that phosphoenolpyruvate carboxylase (PEPC) has high activity in the inner pod layer and therefore maybe involved in refixing respiratory CO_2 via C_4 mechanisms. With Blanke and Lenz (1989) suggesting a malate-CO_2 shuttle, whereby **(1)** respiratory CO_2 is converted into HCO_3^- via carbonic anhydrase (CA), with **(2)** the β-carboxylation step of HCO_3^- with PEP catalysed via PEPC generating oxaloacetate (OA), which **(3)** in turn is converted into malate via NAD-dependent malate dehydrogenase (NAD-MDH) in the cytosol. **(4)** Malate is translocated into the chloroplast, where **(5)** it is decarboxylated by NAD-dependent malic enzyme (NAD-ME) to provide CO_2 to **(6)** Rubisco and the Calvin cycle (Atkins et al., 1977; Blanke and Lenz, 1989; Henry et al., 2020; Garrido et al., 2023). Figure has been generated based on the descriptions found in Atkins et al. (1977), Blanke and Lenz (1989) and Garrido et al. (2023).

4.2. Material and Methods

4.2.1. Plant Materials and Growth

The same growth conditions and seven *P. sativum* accessions (Professor Claire Domoney and Dr Noel Ellis, John Innes Centre Germplasm Resource Unit, Norwich; Thompson & Morgan, Ipswich, Suffolk) as ***Chapter 3*** were utilised (*see* ***Chapter 3 Table 3.1***). Unless stated otherwise, five pods (before the pod-filling stage, which were randomly chosen from different plant heights) were used for each non-foliar measurement.

4.2.2. Chlorophyll Fluorescence Imaging

Chlorophyll fluorescence imaging protocols were performed according to the methods in ***Chapter 2 Section 2.2.2***. Pods were isolated using the Flourimager software (n = 6).

4.2.3. Non-Foliar Gas Exchange

Non-foliar photosynthetic gas exchange analysis was conducted via a conifer cuvette chamber (PLC3, PP Systems Inc, MA, USA) in accordance with Milliken et al. (2024). A Li-Cor 6400 portable gas exchange system (Li-Cor, Lincoln, Nebraska, USA) calculated assimilation (A), stomatal conductance (g_s) and respiration from differentials in CO_2 and H_2O concentrations from the sample air (from the conifer cuvette) and the known IRGA reference air (***Fig.4.2***). Neoprene gaskets lined/sealed the conifer cuvette to minimise leaks. A dew point generator (Li610, Li-Cor) controlled

vapour pressure deficit (VPD) within the Li-6400. White LEDs (Luxeon Stars, Rapid Electronics, UK) enabled pod bi-illumination (with lights calibrated via a quantum light sensor (US-SQS/L, Walz, Germany)), attached to a TLC programmable driver (TLC, Technologica, UK). Non-Foliar temperatures were maintained via a water chiller (BC20; Fisher Scientific, UK) connected to the cuvette by an integral water jacket and monitored by type-E thermocouples (Omega Engineering, Manchester, UK) placed internally and externally to the cuvette to measure pod and air temperatures. Two digital flow meters (FLIR1000, Omega Engineering, Manchester, UK) analysed if flow to and from the cuvette were equal in order to monitor gas leaks within the cuvette. A previously calculated boundary layer resistance of 0.32 $m^2\ mol^{-1}\ s^{-1}$ was used for all calculations. The non-foliar gas exchange system utilised will henceforth be referred to as the bespoke Lawson Lab non-foliar gas exchange chamber. Pod areas were calculated via ImageJ (version 1.53) using scaled images of the illuminated pod surfaces. Unless stated otherwise all non-foliar gas exchange measurements were carried out at 23 ^oC, 400-500 µmol s^{-1} flow rate, 400 µmol mol^{-1} CO_2 concentration and 1.2 (± 0.2) kPa VPD.

4.2.3.1. Pod Dark Respiration Measurements

Pods were dark adapted for 20-minutes before being placed into the non-foliar cuvette. Cuvette conditions were set to that in ***Section 4.2.3***, with the lights remaining off. Measurements were recorded every 10 seconds for two minutes to obtain a stable rate of pod dark respiration (negative inverse of *A*). The average dark respiration rate

for each accession was taken from three observations per rep where the dark respiration rate was most stable.

4.2.3.2. Pod A/C_a Response Curves

Pods were stabilised to the conditions in ***Section 4.2.3*** with the lights set to 1000 µmol m^{-2} s^{-1} PPFD, after waiting 20-30 minutes for stabilisation of A and g_s, responses of A and g_s were measured in response to changes in CO_2 concentrations (400, 250, 150, 100, 50, 400, 550, 700, 900, 1100, 1300, 1500, 1800, 2000 and 400 µmol mol^{-1}). Measurements were taken after A had stabilised to each new CO_2 concentration (2-5 min). Only the first 400 µmol mol^{-1} CO_2 concentration value was used in data analysis, as this was representative of the true stabilised value. Mean A/C_a curves were generated by plotting A as a function of atmospheric CO_2 concentration (C_a). The CO_2-saturated rate of A (A_{sat400}) and mean g_s (gs_{400}) at 400 µmol mol^{-1} C_a were also calculated, by averaging the A and g_s measured for each accession at 400 µmol mol^{-1} CO_2 concentration.

4.2.3.3. Pod Step Increases in Light Intensity

Pods were acclimated to the conditions described in ***Section 4.2.3***, but with a lower light intensity of 100 µmol m^{-2} s^{-1} PPFD. When both A and g_s were stable, measurements were taken every 10 s at 100 µmol m^{-2} s^{-1} PPFD for 10-minutes, before PPFD was increased to 1000 µmol m^{-2} s^{-1} for 40-minutes, with cuvette temperature maintained at 23 °C via the water chiller. Parameterisation of A, g_s and iWUE and kinetic responses of the pods to a light induction, were carried out as per ***Chapter 2***

Section 2.2.3.3, but utilising observations 115-119 to calculate the maximum *i*WUE ($iWUE_{max}$) where *i*WUE was generally highest and most stable.

4.2.4. Pod Surface Impressions

Surface impressions were performed in accordance with the methods in ***Chapter 2 Section 2.2.5*** for all watered and droughted pods, however only one surface (upper surface facing the light for gas exchange) was utilised to limit negative impacts on final yield.

4.2.5. Pod Thermal Imaging

Thermal imaging were performed as per the methods in ***Chapter 3 Section 3.2.5*** to determine differences in mean pod temperature between watered and droughted conditions (n = 6).

4.2.6. Yield Calculations

Yield measurements for all watered and droughted plants were performed according to ***Chapter 2 Section 2.2.7*** (n = 6).

4.2.7. Data Analysis/Statistics

Mean ± standard error (SE) were calculated for each measurement. A Shapiro-Wilk test and Levene's test were utilised (respectively) to check if data was normally distributed and had equal variance and thus met the assumptions of an ANOVA. A

one-way ANOVA and TukeyHSD test were utilised between *P. sativum* accessions and yield parameters (***Appendix Table.A2.1***) and between experimental condition (watered and droughted) and yield parameters (***Appendix Table.A2.2***). Two-way and/or multi-way ANOVAs were also calculated for each measured physiological parameter between *P. sativum* accession and experimental condition, followed by TukeyHSD tests. A multi-way ANOVA was also performed for each chlorophyll fluorescence parameter between PPFD/time, experimental condition and *P. sativum* accession, followed by TukeyHSD tests which were calculated on data at the end of the chlorophyll fluorescent protocol (*i.e.,* at 10 or 20 minutes of induction/relaxation or at 1500 µmol m^{-2} s^{-1} PPFD of the chlorophyll fluorescent light curve). TukeyHSD results for each physiological parameter were also compared between watered and droughted conditions to determine the impact of drought within each individual accession. Spearman's correlation coefficients (R) and linear regression equations were run between pod *A* and g_s at 400 µmol mol^{-1} [CO_2] measured from the A/C_a data. Spearman's correlation coefficients and linear regression equations were run between pod SD, SS, gs_{max} and against g_s (at 400 µmol mol^{-1} [CO_2] measured from the A/C_a data) to determine if pod stomatal anatomy impacted g_s and/or gs_{max}. Whilst Spearman's correlation coefficients and linear regression equations were additionally carried out between pod temperature and pod $i\text{WUE}_{max}$ and between each yield parameter and pod A_{sat400}. Graphs and statistics were generated within RStudio (Mac version 2024.04.0+735).

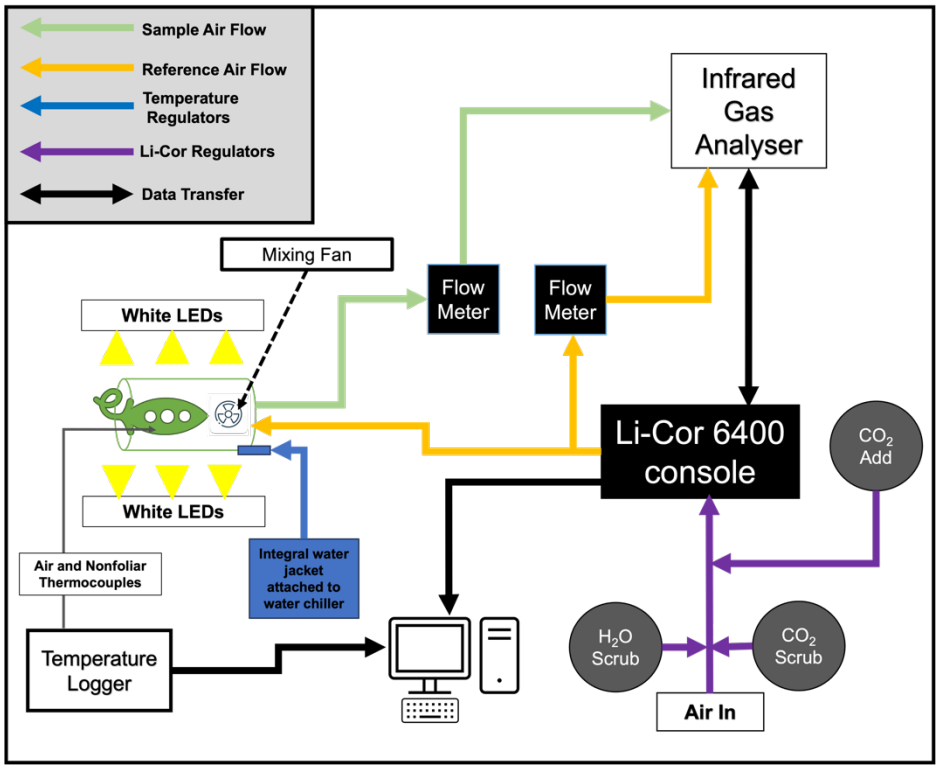

Figure 4.2. Schematic of the non-foliar gas exchange system known as the bespoke Lawson Lab chamber. Pods were placed inside the cuvette chamber, with the cuvette chamber sealed with neoprene gaskets to minimise leaks, as a mixing fan inside the cuvette chamber prevented air stagnation. An integral water jacket placed on the external surface of the cuvette chamber enabled temperature regulation via a water chiller, with pod temperatures monitored via internally placed thermocouples. White LEDs provided bi-illumination to the pods. Reference air flow (yellow) was supplied from the Li-Cor 6400 console to the non-foliar cuvette chamber and to the infra-red gas analyser. The sample air flow (green) generated within the cuvette chamber would travel to the infra-red gas analyser. Both sample and reference air flows would travel through flow meters to check for leaks and ensure air flow was constant. Differentials in CO_2 and H_2O were calculated by the Li-Cor 6400 console to generate the rates of assimilation and stomatal conductance. Figure has been adapted from Milliken et al. (2024).

4.3. Results

4.3.1. Variation in Chlorophyll Fluorescence Parameters in the Pods in Response to Light Under Watered and Droughted Conditions

4.3.1.1. Variation in Response to an Induction and Relaxation in Light Intensity

Chlorophyll fluorescent parameters (F_q'/F_m', F_q'/F_v' and F_v'/F_m') were monitored within the pods during a light induction and relaxation (***Fig.4.3&4.4***). In the induction phase, significant variation was identified in F_q'/F_m' ($F_{(6)}$ = 21.76, P < 0.001), F_q'/F_v' ($F_{(6)}$ = 38.02, P < 0.001) and F_v'/F_m' ($F_{(6)}$ = 17.17, P < 0.001) between the different *P. sativum* accessions and experimental conditions (***Fig.4.3&4.4***).

At the end of the 10 min induction, Wando exhibited a significantly greater watered F_q'/F_m' (0.64 ± 0.006) to Eth and Filby (TukeyHSD; P < 0.05) and a significantly higher droughted F_q'/F_m' (0.64 ± 0.02) to Ni16, Eth and Filby (TukeyHSD; P < 0.05) (***Fig.4.3&Table.4.1***). In contrast Eth had the lowest watered (0.42 ± 0.004) and droughted (0.46 ± 0.01) pod F_q'/F_m', with a significant difference in watered F_q'/F_m' to all watered accessions (TukeyHSD; P < 0.05) and in droughted F_q'/F_m' to all droughted accessions (TukeyHSD; P < 0.05) (***Fig.4.3&Table.4.1***). When quenching parameters were observed to identify what was driving the differences in F_q'/F_m', it was highlighted that the low F_q'/F_m' in Eth watered pods at the end of the induction was potentially driven by significantly lower values of F_q'/F_v' to all watered accessions (TukeyHSD; P < 0.05) and F_v'/F_m' to watered Wando (TukeyHSD; P < 0.05) (***Fig.4.3A,4.4A&4.4C&Table.4.2A***). The high F_q'/F_m' experienced by watered Wando pods at the end of the induction may have been driven by both F_v'/F_m' and F_q'/F_v', with

significant differences in watered F_v'/F_m' identified to Filby, Ni16, Eth and Pacco (TukeyHSD; $P < 0.05$) and in watered F_q'/F_v' to Eth and Filby (TukeyHSD; $P < 0.05$) (***Fig.4.3A,4.4A&4.4C&Table.4.2A***). The low F_q'/F_m' observed by droughted Eth pods at the end of the induction were primarily driven by significantly lower values of F_q'/F_v' to all droughted accessions (excluding Filby) (TukeyHSD; $P < 0.05$), as no significant differences were seen in droughted F_v'/F_m' (TukeyHSD; $P > 0.05$) (***Fig.4.3B,4.4B&4.4D&Table.4.2B***). Whilst the high F_q'/F_m' observed by droughted Wando pods at the end of the induction were potentially driven via significantly higher values of F_q'/F_v' to Eth and Filby (TukeyHSD; $P < 0.05$) and F_v'/F_m' to Pacco (TukeyHSD; $P < 0.05$) (***Fig.4.3B,4.4B&4.4D&Table.4.2B***). After 10 mins of the induction protocol no significant difference were observed in F_q'/F_m' between watered and droughted conditions within each individual accession (TukeyHSD; $P > 0.05$) (***Fig.4.3***).

Significant variation also existed within the relaxation phase in F_v/F_m between the different accessions and experimental conditions ($F_{(6)} = 10.67$, $P < 0.001$) (***Fig.4.3***). At the end of the relaxation protocol Eth exhibited a significantly lower watered F_v/F_m (0.76 ± 0.007) to all watered accessions (excluding Filby) (TukeyHSD; $P < 0.05$) and droughted F_v/F_m (0.74 ± 0.02) to all droughted accessions (TukeyHSD; $P < 0.05$) (***Fig.4.3&Table.4.1***). Whilst watered Pacco (0.82 ± 0.003) and droughted Wando (0.82 ± 0.003) had the highest F_v/F_m at the end of the relaxation protocol, with a significant difference to Eth, Filby and Ni16 in watered F_v/F_m (TukeyHSD; $P < 0.05$) and to Eth in droughted F_v/F_m (TukeyHSD; $P < 0.05$) (***Fig.4.3&Table.4.1***). There were no significant

difference identified in F_v/F_m at the end of the relaxation protocol between watered and droughted conditions within each induvial accession (TukeyHSD; $P > 0.05$) (***Fig.4.3***).

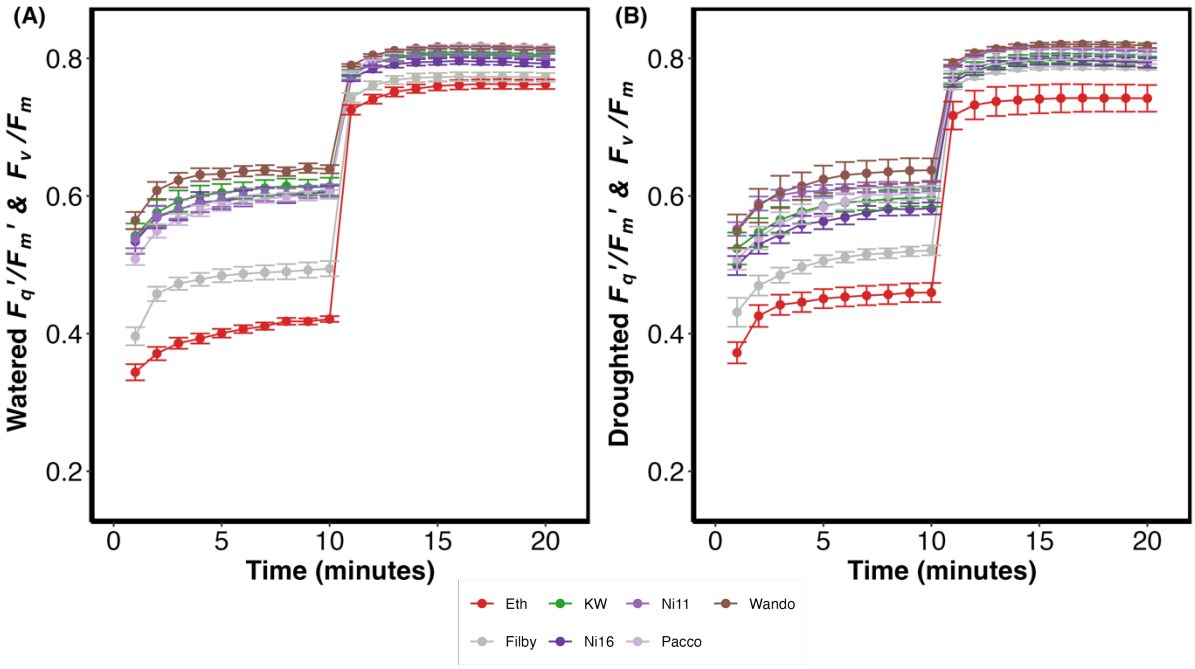

Figure 4.3. Variation in pod chlorophyll fluorescence induction and relaxation across P. sativum accessions under watered and droughted conditions. Induction responses were monitored as F_q'/F_m' (operating efficiency of photosystem II in the light) and recovery of F_v/F_m (photosystem II maximum efficiency in the dark) in both **(A)** watered and **(B)** droughted pods. Accessions were dark adapted for 30-min before being measured within a Fluorimager. Error bars represent mean ± SE (n = 6). The presence of + of the same colour indicates a significant difference in either F_q'/F_m' or F_v/F_m within an individual accession between watered and droughted conditions, whereby + is $P < 0.05$, ++ is $P < 0.01$ and +++ is $P < 0.001$ (TukeyHSD). Significant differences in either F_q'/F_m' at 10 minutes or F_v/F_m at 20 minutes between the *P. sativum* accessions can be found in ***Table.4.1***.

Table 4.1. Significant differences in pod chlorophyll fluorescence induction and relaxation parameters across P. sativum accessions under watered and droughted conditions. Induction responses were monitored as F_q'/F_m' (operating efficiency of photosystem II in the light) and recovery of F_v/F_m (photosystem II maximum efficiency in the dark) in ***Fig.4.3***. The different letters within the **(A)** watered and **(B)** droughted pod tables indicate a significant difference in either F_q'/F_m' at 10 mins or F_v/F_m at 20 mins between the different *P. sativum* accessions ($P < 0.05$; TukeyHSD).

(A)

Accession	Watered	
	F_q'/F_m'	F_v/F_m
Eth	c	d
Filby	b	cd
KW	a	ab
Ni16	a	bc
Ni11	a	ab
Pacco	a	a
Wando	a	ab

(B)

Accession	Droughted	
	F_q'/F_m'	F_v/F_m
Eth	d	b
Filby	c	a
KW	ab	a
Ni16	b	a
Ni11	ab	a
Pacco	ab	a
Wando	a	a

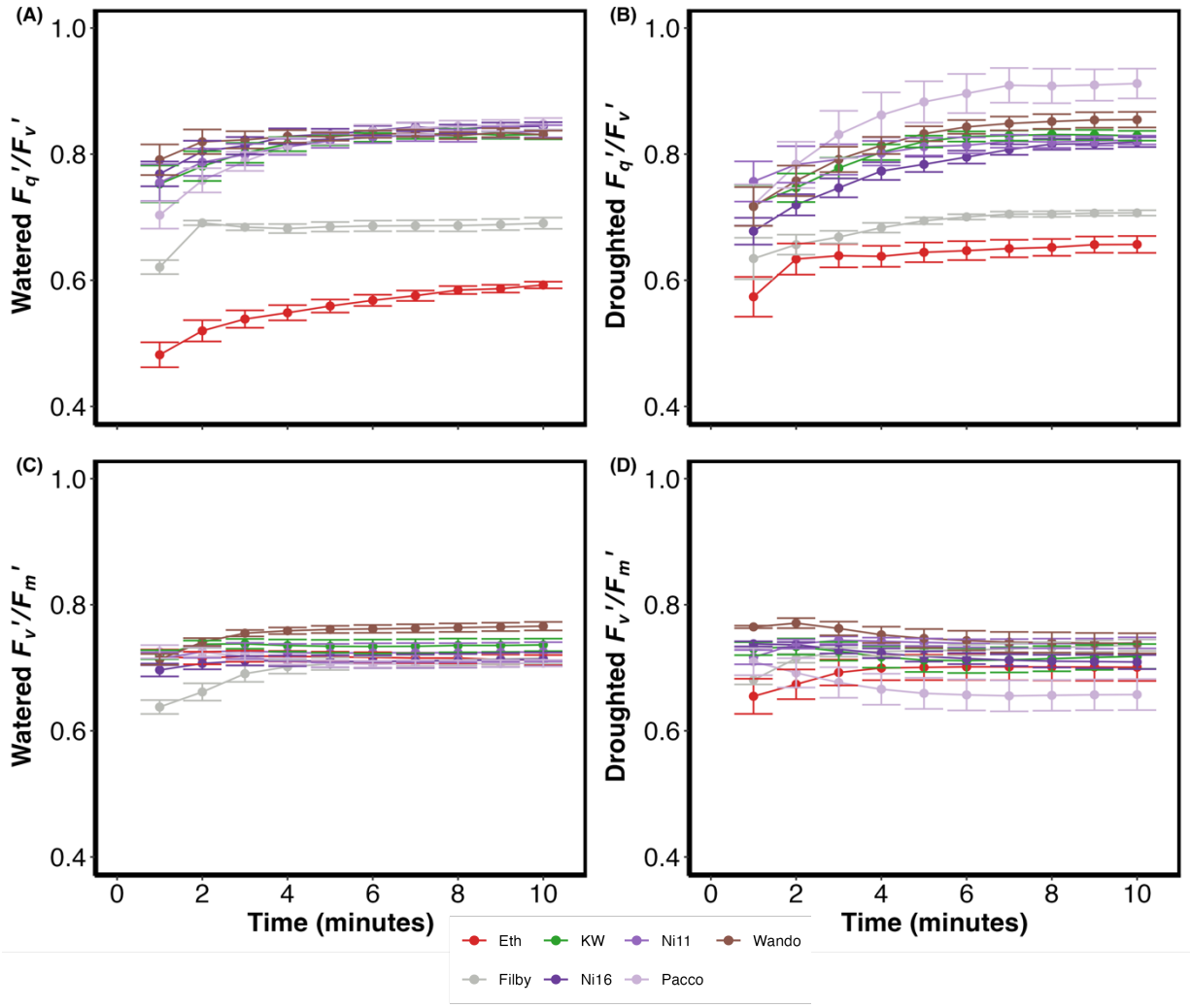

Figure 4.4. Variation in pod chlorophyll fluorescence induction parameters across P. sativum accessions under watered and droughted conditions. Induction responses were monitored as F_q'/F_v' (PSII photochemical quenching factor) in **(A)** watered and **(B)** droughted pods and as F_v'/F_m' (PSII maximum efficiency) in **(C)** watered and **(D)** droughted pods. Accessions were dark adapted for 30-minutes before being measured within a Fluorimager. Error bars represent mean ± SE (n = 6). Significant differences in either F_q'/F_v' or F_v'/F_m' at 10 minutes between the *P. sativum* accessions can be found in ***Table.4.2***.

Table 4.2. Significant differences in pod chlorophyll fluorescence induction parameters across P. sativum accessions under watered and droughted conditions. Induction responses were monitored as F_q'/F_v' (PSII photochemical quenching factor) and as F_v'/F_m' (PSII maximum efficiency) in ***Fig.4.4***. The different letters within the **(A)** watered and **(B)** droughted pod tables indicate a significant difference in either F_q'/F_v' at 10 mins or F_v'/F_m' at 10 mins between the different *P. sativum* accessions ($P < 0.05$; TukeyHSD).

(A)

Accession	Watered	
	F_q'/F_v'	F_v'/F_m'
Eth	c	b
Filby	b	b
KW	a	ab
Ni16	a	b
Ni11	a	ab
Pacco	a	b
Wando	a	a

(B)

Accession	Droughted	
	F_q'/F_v'	F_v'/F_m'
Eth	c	ab
Filby	c	a
KW	b	ab
Ni16	b	ab
Ni11	b	a
Pacco	a	b
Wando	b	a

4.3.1.2. Photosynthetic Efficiency Light Response Curves

Chlorophyll fluorescence parameters (F_q'/F_m', F_q'/F_v', F_v'/F_m' and NPQ) were monitored in the pods as a function of irradiance, with significant variation identified in F_q'/F_m' ($F_{(6)} = 7.79$, $P < 0.001$), F_q'/F_v' ($F_{(6)} = 19.36$, $P < 0.001$), F_v'/F_m' ($F_{(6)} = 11.32$, $P < 0.001$) and NPQ ($F_{(6)} = 4.54$, $P < 0.001$), between the different *P. sativum* accessions and experimental conditions (***Fig.4.5***). An additional overall significant variation was also identified in F_q'/F_v' ($F_{(42)} = 1.60$, $P < 0.05$) between the different accessions, experimental conditions and light intensities (***Fig.4.5E&F***). However, there were no significant differences observed in F_v/F_m (initial 0 µmol m^{-2} s^{-1} PPFD) ($F_{(6)} = 1.22$, $P = 0.31$) between the different accessions and experimental conditions (***Fig.4.5***).

At the highest light intensity (1500 µmol m^{-2} s^{-1} PPFD), Wando exhibited a significantly greater watered F_q'/F_m' (0.29 ± 0.006) to Ni16, Eth and Filby (TukeyHSD; $P < 0.05$) and a significantly higher droughted F_q'/F_m' (0.28 ± 0.02) to Eth and Filby (TukeyHSD; $P < 0.05$) (***Fig.4.5A&B&Table.4.3***). In contrast Eth had the lowest watered (0.18 ± 0.005) and droughted (0.19 ± 0.007) F_q'/F_m', with a significant difference in watered F_q'/F_m' to all watered accessions (TukeyHSD; $P < 0.05$) and in droughted F_q'/F_m' to all droughted accessions (excluding Filby) (TukeyHSD; $P < 0.05$) (***Fig.4.5A&B&Table.4.3***). Observation of quenching parameters highlighted that the low F_q'/F_m' exhibited by watered Eth at the highest light intensity was potentially driven by significantly lower values of watered F_q'/F_v' to all watered accessions (TukeyHSD; $P < 0.05$) and watered F_v'/F_m' to Wando (TukeyHSD; $P < 0.05$) (***Fig.4.5A,C&E&Table.4.3A***). The low F_q'/F_m' in droughted Eth at 1500 µmol m^{-2} s^{-1} PPFD may have been driven by both F_q'/F_v' and F_v'/F_m', with significantly lower

droughted F_q'/F_v' to Ni11, Pacco and Wando (TukeyHSD; $P < 0.05$) and significantly lower droughted F_v'/F_m' to KW and Wando (TukeyHSD; $P < 0.05$) (***Fig.4.5B,D&F&Table.4.3B***). The greater F_q'/F_m' in droughted Wando at the highest light intensity was potentially driven by significantly higher values of droughted F_v'/F_m' to Pacco and Eth (TukeyHSD; $P < 0.05$) and droughted F_q'/F_v' to Filby and Eth (TukeyHSD; $P < 0.05$) (***Fig.4.5B,D&F&Table.4.3B***). Whilst the higher F_q'/F_m' in watered Wando was potentially driven by both F_v'/F_m' and F_q'/F_v', with significant differences identified to all watered accessions (excluding KW) in watered F_v'/F_m' (TukeyHSD; $P < 0.05$) and to Filby and Eth in watered F_q'/F_v' (TukeyHSD; $P < 0.05$) (***Fig.4.5A,C&E&Table.4.3A***). At the highest light intensity no significant difference were observed in F_q'/F_m' between watered and droughted conditions within each individual accession (TukeyHSD; $P > 0.05$) (***Fig.4.5A&B***).

Watered (3.05 ± 0.07) and droughted (3.20 ± 0.16) Pacco exhibited the highest NPQ at 1500 µmol m^{-2} s^{-1} PPFD, with a significant difference to KW, Wando and Eth for watered NPQ (TukeyHSD; $P < 0.05$) and to all droughted accessions (exempting Ni11) in droughted NPQ (TukeyHSD; $P < 0.05$) (***Fig.4.5G&H&Table.4.3***). Whilst Eth at 1500 µmol m^{-2} s^{-1} PPFD was significantly lower in watered NPQ (1.76 ± 0.06) to all watered accessions (TukeyHSD; $P < 0.05$) and in droughted NPQ (2.22 ± 0.1) to Ni11 and Pacco (TukeyHSD; $P < 0.05$) (***Fig.4.5G&H&Table.4.3***). However, no significant difference were observed in NPQ at the highest light intensity between watered and droughted conditions within each individual accession (TukeyHSD; $P > 0.05$) (***Fig.4.5G&H***).

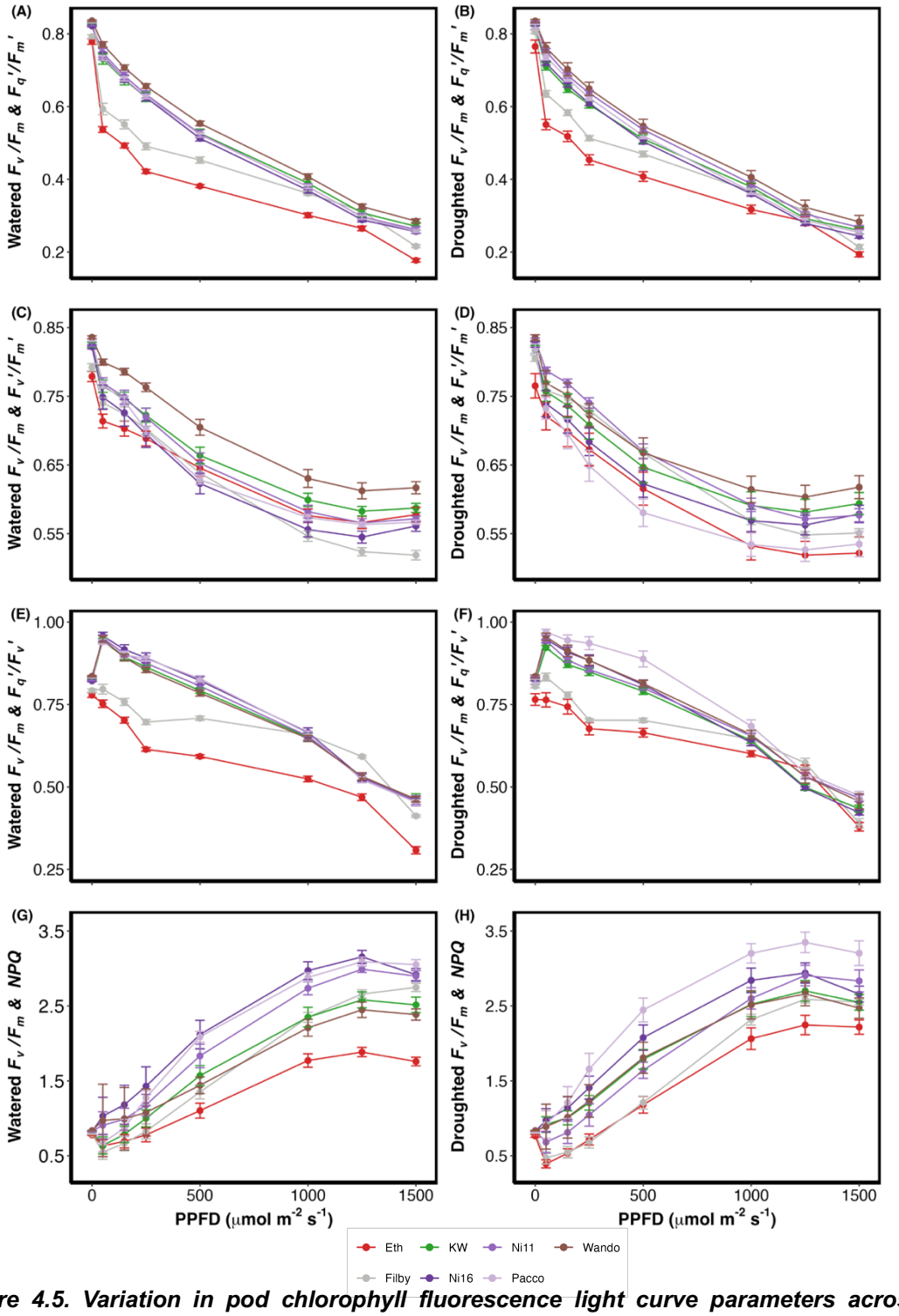

Figure 4.5. Variation in pod chlorophyll fluorescence light curve parameters across P. sativum accessions under watered and droughted conditions. Chlorophyll fluorescent responses to light intensity changes were monitored initially in the dark as F_v/F_m (photosystem II maximum efficiency in the dark) in all graphs, followed by measurements in the light monitored as F_q'/F_m' (operating efficiency of photosystem II; PSII) in **(A)** watered and **(B)** droughted pods, F_v'/F_m' (PSII maximum efficiency) in **(C)** watered and **(D)** droughted pods, F_q'/F_v' (PSII photochemical quenching factor) in **(E)** watered and **(F)** droughted pods and as NPQ (non-photochemical quenching) in **(G)** watered and **(H)** droughted pods. Accessions were dark adapted for 30-minutes before being measured at different photosynthetic photon flux densities (PPFD) within a Fluorimager. Error bars represent mean ± SE (n = 6). The presence of + of the same colour indicates a significant difference in either F_q'/F_m' or NPQ within an individual accession between watered and droughted conditions, whereby + is $P < 0.05$, ++ is $P < 0.01$ and +++ is $P < 0.001$ (TukeyHSD). Significant differences in either F_q'/F_m', F_v'/F_m', F_q'/F_v' or NPQ at 1500 µmol m^{-2} s^{-1} PPFD between the *P. sativum* accessions can be found in ***Table.4.3***.

Table 4.3. Significant differences in pod chlorophyll fluorescence light curve parameters across P. sativum accessions under watered and droughted conditions. Chlorophyll fluorescent responses to light intensity changes were monitored in ***Fig.4.5*** as F_q'/F_m' (operating efficiency of photosystem II; PSII), F_v'/F_m' (PSII maximum efficiency), F_q'/F_v' (PSII photochemical quenching factor) and as NPQ (non-photochemical quenching). The different letters within the **(A)** watered and **(B)** droughted pod tables indicate a significant difference in either F_q'/F_m', F_v'/F_m', F_q'/F_v' or NPQ at 1500 µmol m^{-2} s^{-1} photosynthetic photon flux density between the different *P. sativum* accessions ($P < 0.05$; TukeyHSD).

(A)

Accession	Watered			
	F_q'/F_m'	F_v'/F_m'	F_q'/F_v'	NPQ
Eth	d	b	c	d
Filby	c	c	b	ab
KW	ab	ab	a	bc
Ni16	b	b	ab	a
Ni11	ab	b	ab	a
Pacco	ab	b	ab	a
Wando	a	a	a	c

(B)

Accession	Droughted			
	F_q'/F_m'	F_v'/F_m'	F_q'/F_v'	NPQ
Eth	c	c	b	c
Filby	bc	abc	b	bc
KW	a	ab	ab	bc
Ni16	ab	abc	ab	bc
Ni11	a	abc	a	ab
Pacco	a	bc	a	a
Wando	a	a	a	bc

4.3.2. Pod Photosynthetic Rates in Response to Changing CO_2 Concentration Under Watered and Droughted Conditions

Assimilation (*A*) was measured as a function of atmospheric [CO_2] (C_a) in watered and droughted pods, with *A* exhibiting a linear response, whilst limited change in stomatal conductance (g_s) was noted with increasing C_a for both watered and droughted conditions (***Fig.4.6***). Pacco generally had the greatest g_s for all C_a in both watered and droughted pods (***Fig.4.6C&D***). A positive correlation was identified between *A* and g_s (R = 0.57, $P < 0.001$), with droughted conditions observed to have a greater range whilst watered conditions remained centralised (***Fig.4.7***).

Significant variation was apparent between the different accessions and experimental conditions in the CO_2-saturated rate of *A* at 400 µmol mol^{-1} C_a; A_{sat400} ($F_{(6)} = 7.65$, $P < 0.001$) and g_s at 400 µmol mol^{-1} C_a; gs_{400} ($F_{(6)} = 5.34$, $P < 0.001$) (***Fig.4.8***). Ni16 exhibited a significantly lower A_{sat400} under watered conditions (1.53 ± 0.11 µmol m^{-2} s^{-1}) to Eth, Filby, KW and Pacco (TukeyHSD; $P < 0.05$) and under droughted conditions (1.62 ± 0.08 µmol m^{-2} s^{-1}) to KW, Ni11 and Pacco (TukeyHSD; $P < 0.05$) (***Fig.4.8A&B***). The highest droughted A_{sat400} was observed within KW (3.41 ± 0.22 µmol m^{-2} s^{-1}), which was significantly different to Eth, Filby, Ni16 and Wando (TukeyHSD; $P < 0.05$) (***Fig.4.8B***). Whilst Filby had a significantly greater watered A_{sat400} (3.03 ± 0.17 µmol m^{-2} s^{-1}) to Ni16, Ni11 and Wando (TukeyHSD; $P < 0.05$) (***Fig.4.8A***). Pacco exhibited the highest gs_{400} in both watered (0.11 ± 0.001 mol m^{-2} s^{-1}) and droughted (0.11 ± 0.005 mol m^{-2} s^{-1}) pods, with a significant difference identified to all watered accessions in watered gs_{400} (TukeyHSD; $P < 0.05$) and to Eth, Filby, Ni16 and Wando in droughted gs_{400} (TukeyHSD; $P < 0.05$) (***Fig.4.8C&D***). Whilst watered Filby (0.06 ±

0.004 mol m^{-2} s^{-1}) and droughted Eth (0.04 ± 0.006 mol m^{-2} s^{-1}) had the lowest gs_{400}, with a significant difference identified to KW, Ni11 and Pacco in both watered (TukeyHSD; $P < 0.05$) and droughted (TukeyHSD; $P < 0.05$) gs_{400} respectively (***Fig.4.8C&D***).

Droughted conditions were generally greater in A_{sat400} compared to watered conditions, with a significant difference identified between watered and droughted KW (TukeyHSD; $P < 0.05$), although Filby had a significantly greater watered A_{sat400} compared to droughted conditions (TukeyHSD; $P < 0.05$) (***Fig.4.8A&B***). In contrast, watered conditions were generally higher in gs_{400} compared to droughted conditions, with a significant difference observed in gs_{400} between watered and droughted Eth (TukeyHSD; $P < 0.01$) (***Fig.4.8C&D***).

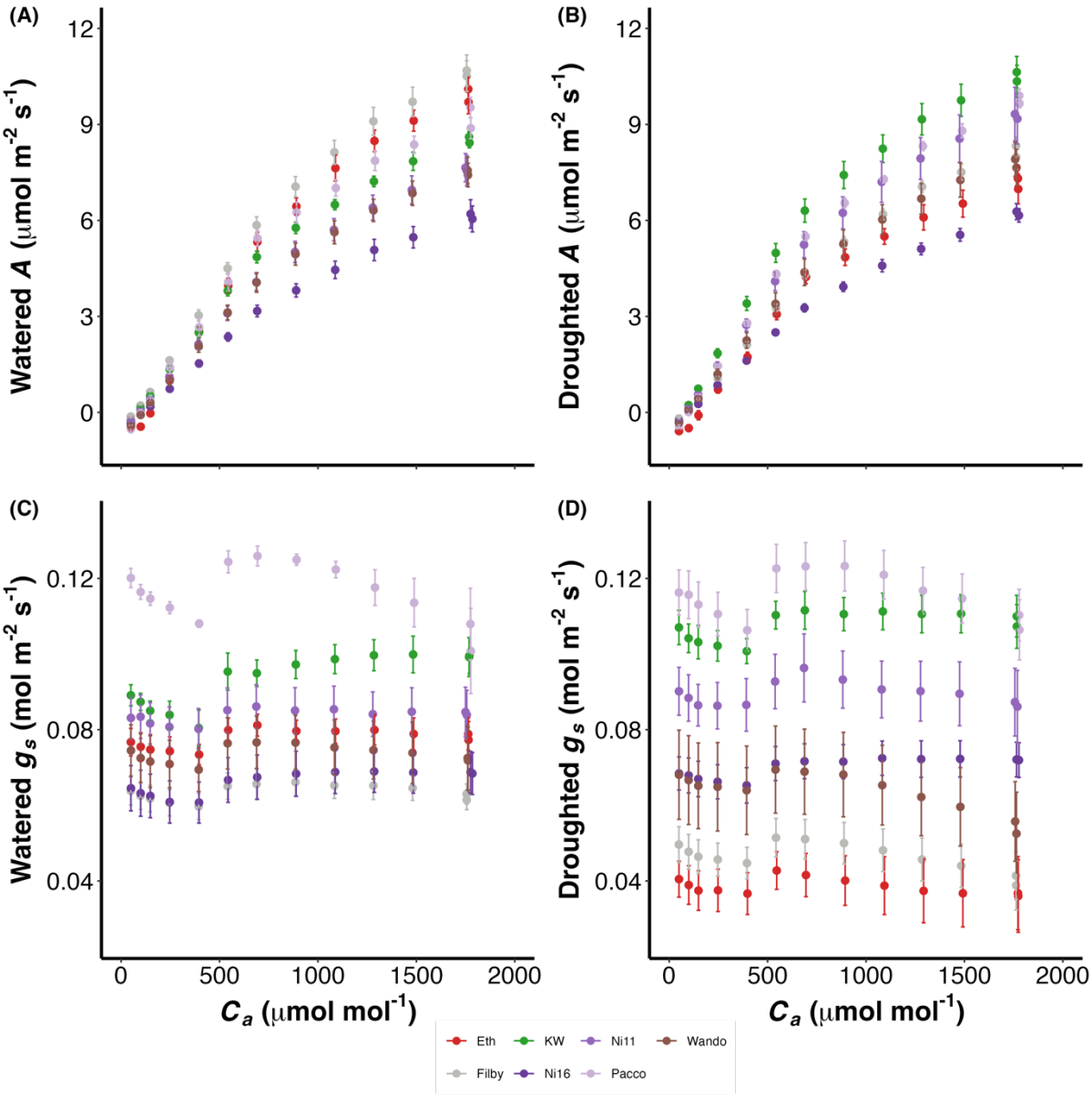

Figure 4.6. Variation in pod carbon assimilation (A) and stomatal conductance (g_s) in response to changing atmospheric CO_2 concentration (C_a) across P. sativum accessions under watered and droughted conditions. Changes in **(A)** watered and **(B)** droughted pod assimilation and **(C)** watered and **(D)** droughted pod stomatal conductance was measured against increasing C_a within a bespoke Lawson Lab non-foliar gas exchange chamber at 23 °C and 1000 µmol m^{-2} s^{-1} photosynthetic photon flux density. Error bars represent mean ± SE (n = 5).

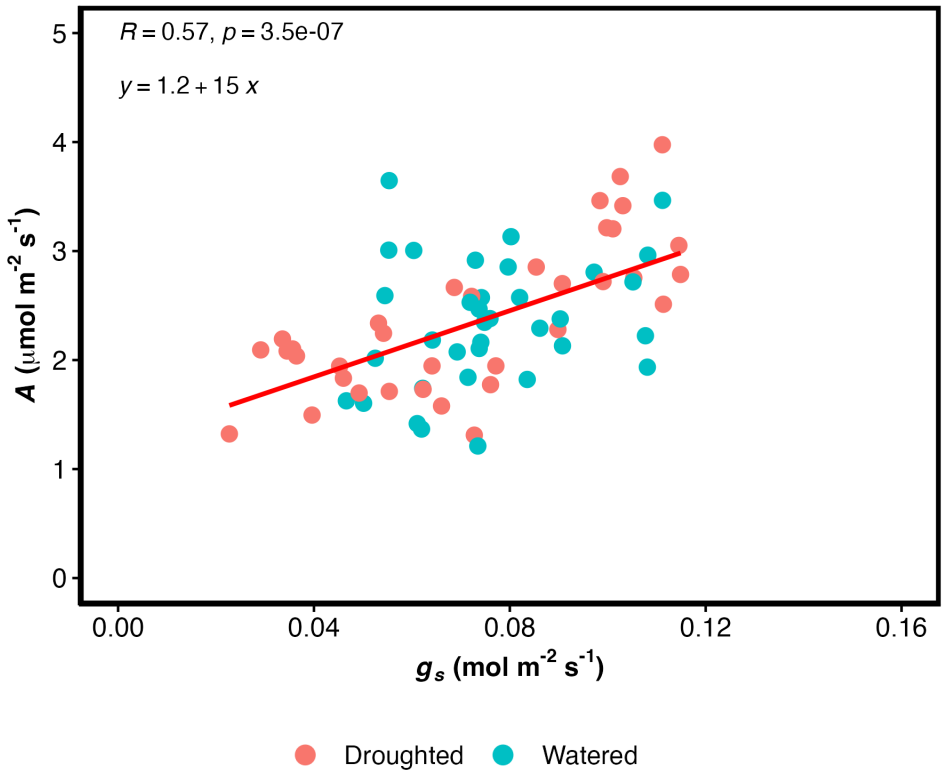

Figure 4.7. Spearmans correlation between pod Assimilation (A) and stomatal conductance (g_s) under watered and droughted conditions. Red dots indicate droughted whilst blue dots represent watered conditions. *A* and g_s were measured at 400 µmol mol^{-1} atmospheric CO_2 concentration within a bespoke Lawson Lab non-foliar gas exchange chamber at 23 °C and 1000 µmol m^{-2} s^{-1} photosynthetic photon flux density. Spearman's correlation coefficients (R) and linear regressions (represented as equations and red lines) were calculated for *A* against g_s. $P < 0.05$ indicates a significant relationship (n = 5).

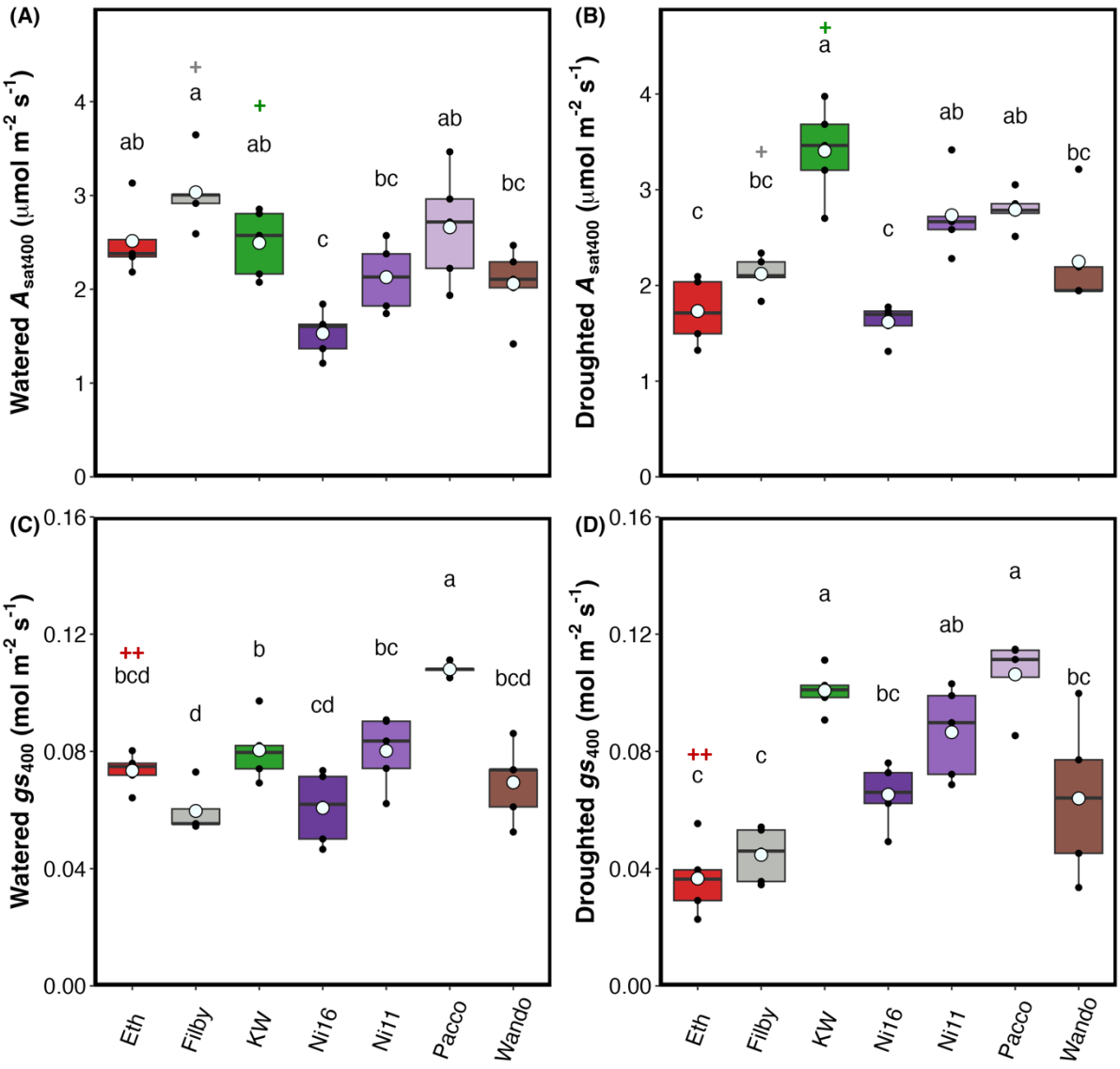

Figure 4.8. Variation in pod A_{sat400} and gs_{400} across P. sativum accessions under watered and droughted conditions. Changes in **(A)** watered and **(B)** droughted pod CO_2-saturated rate of *A* at 400 µmol mol^{-1} atmospheric CO_2; C_a (A_{sat400}) and **(C)** watered and **(D)** droughted pod g_s at 400 µmol mol^{-1} C_a (gs_{400}). Measured within a bespoke Lawson Lab non-foliar gas exchange chamber at 23 °C and 1000 µmol m^{-2} s^{-1} photosynthetic photon flux density. White dots symbolise the mean, whilst error bars represent mean ± SE (n = 5). Different letters above each error bar indicate a significant difference in either A_{sat400} or gs_{400} between the different *P. sativum* accessions ($P < 0.05$; TukeyHSD). The presence of + of the same colour indicates a significant difference within an individual accession between watered and droughted conditions in either A_{sat400} or gs_{400}, whereby + is $P < 0.05$, ++ is $P < 0.01$ and +++ is $P < 0.001$ (TukeyHSD).

4.3.3. Pod Dark Respiration Rates Under Watered and Droughted Conditions

Significant variation in dark respiration was identified between the different *P. sativum* accessions and experimental conditions ($F_{(6)} = 54.14$, $P < 0.001$) (***Fig.4.9***). The lowest dark respiration was observed within watered (2.91 ± 0.15 µmol m^{-2} s^{-1}) and droughted (2.19 ± 0.14 µmol m^{-2} s^{-1}) Ni16, with a significant difference identified in watered dark respiration to Eth, Filby, KW and Ni11 (TukeyHSD; $P < 0.05$) and in droughted dark respiration to all droughted accessions (excluding Filby) (TukeyHSD; $P < 0.05$) (***Fig.4.9***). Watered KW (5.27 ± 0.3 µmol m^{-2} s^{-1}) had a significantly higher dark respiration to all watered accessions (TukeyHSD; $P < 0.05$) (***Fig.4.9A***). Whilst droughted Pacco (8.36 ± 0.53 µmol m^{-2} s^{-1}) exhibited a significantly higher dark respiration to all droughted accessions (excluding Eth) (TukeyHSD; $P < 0.05$) (***Fig.4.9B***). Although watered conditions generally exhibited greater dark respiration rates than droughted conditions; with a significant difference observed in dark respiration between watered and droughted Filby (TukeyHSD; $P < 0.05$), droughted conditions were significantly higher than watered conditions in dark respiration rates within the individual accessions of Eth (TukeyHSD; $P < 0.001$) and Pacco (TukeyHSD; $P < 0.001$) (***Fig.4.9***).

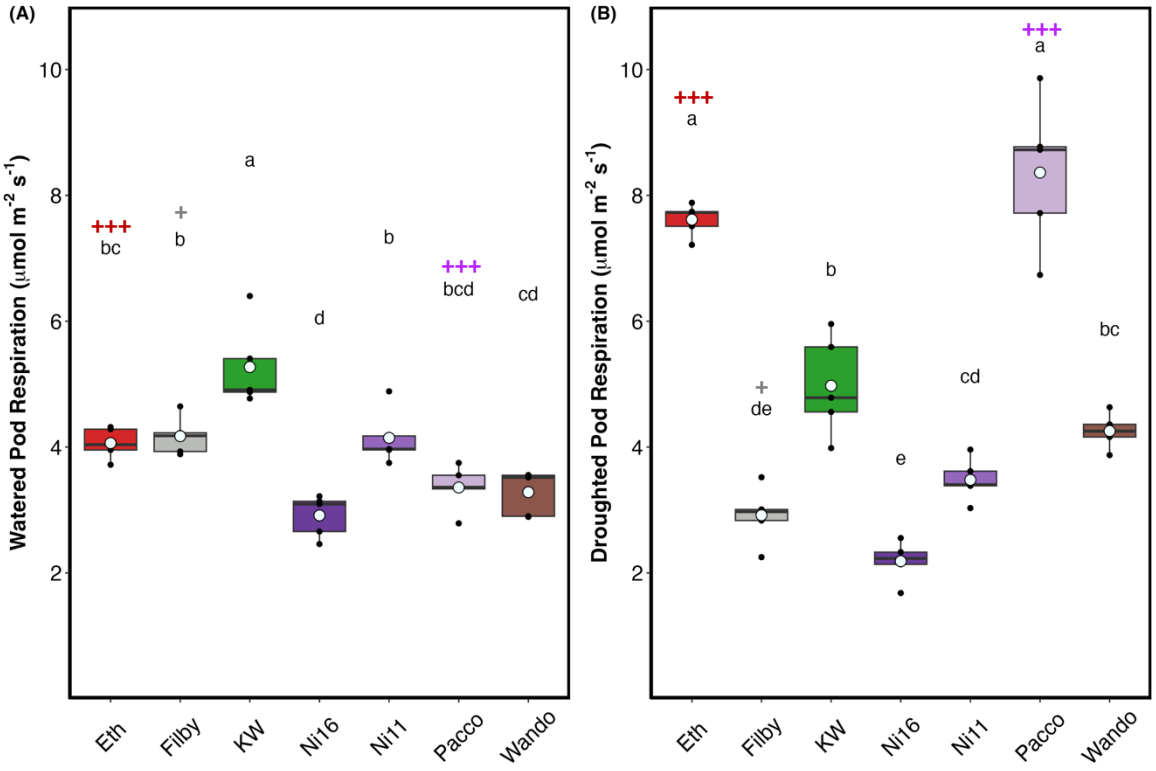

Figure 4.9. Variation in pod dark respiration across P. sativum accessions under watered and droughted conditions. Changes in **(A)** watered and **(B)** droughted pod dark respiration were measured within a bespoke Lawson Lab non-foliar gas exchange chamber at 23 ºC and 400 µmol mol^{-1} CO_2 concentration in the dark. Pods were dark-adapted for 20-minutes before measurements were taken. White dots symbolise the mean, whilst error bars represent mean ± SE (n = 5). Different letters above each error bar indicate a significant difference in dark respiration between the different *P. sativum* accessions ($P < 0.05$; TukeyHSD). The presence of + of the same colour indicates a significant difference within an individual accession between watered and droughted conditions in dark respiration, whereby + is $P < 0.05$, ++ is $P < 0.01$ and +++ is $P < 0.001$ (TukeyHSD).

4.3.4. Variation in Pod Stomatal Characteristics Under Watered and Droughted Conditions

4.3.4.1. Stomatal Densities

Significant variation was identified in stomatal densities (SD) between the different *P. sativum* accessions ($F_{(6)} = 2.80$, $P < 0.05$) and between the different experimental conditions ($F_{(1)} = 9.51$, $P < 0.01$) (***Fig.4.10***). Pacco exhibited the greatest watered (24.74 ± 6.65 mm^{-2}) and droughted (16.06 ± 4.30 mm^{-2}) SD, whilst watered Ni16 (9.77 ± 2.54 mm^{-2}) and droughted KW (9.77 ± 1.53 mm^{-2}) had the lowest SD, however no significant differences were observed in watered SD to any of the watered accessions (TukeyHSD; $P > 0.05$) or in droughted SD to any of the droughted accessions (TukeyHSD; $P > 0.05$) (***Fig.4.10***). There was also no significant difference identified in SD between watered and droughted conditions within each individual accession (TukeyHSD; $P > 0.05$) (***Fig.4.10***).

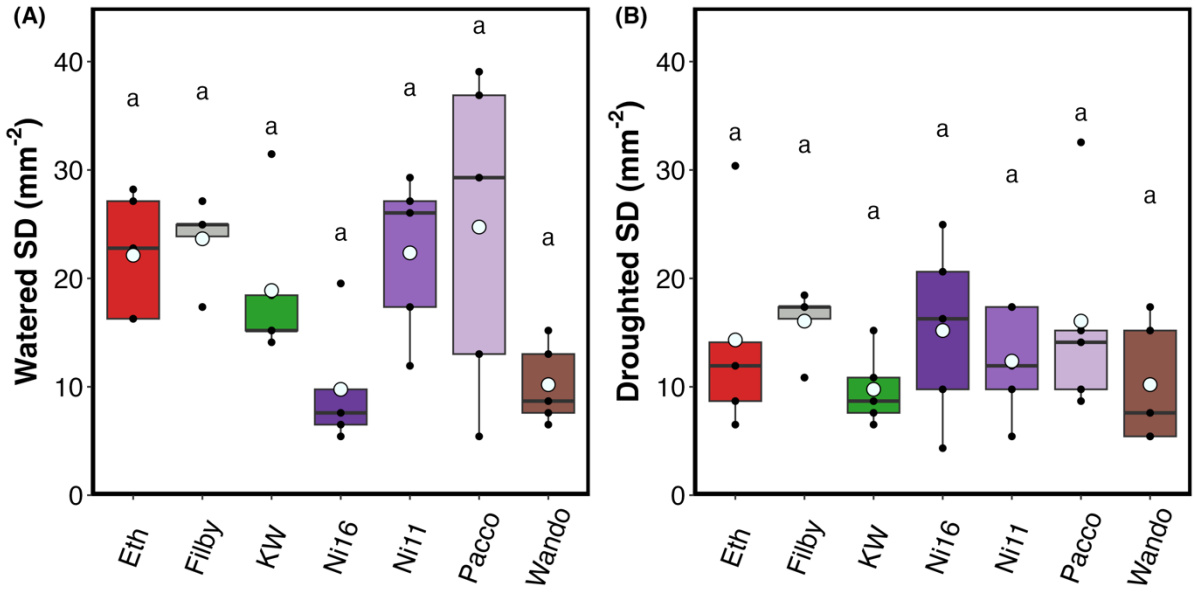

Figure 4.10. Variation in pod stomatal densities across P. sativum accessions under watered and droughted conditions. Stomatal densities were calculated for **(A)** watered and **(B)** droughted pods. Stomata were counted on the upper pod surface (facing the light in gas exchange) at 200x magnification in a 1 mm^2 grid (n = 5). White dots symbolise the mean, whilst error bars represent mean ± SE. Different letters above each error bar represent significant differences in stomatal densities between the different *P. sativum* accessions ($P < 0.05$; TukeyHSD). The presence of + of the same colour indicates a significant difference within an individual accession between watered and droughted conditions in SD, whereby + is $P < 0.05$, ++ is $P < 0.01$ and +++ is $P < 0.001$ (TukeyHSD).

4.3.4.2. Stomatal Sizes

Significant variation was observed in stomatal sizes (SS: consisting of pore length; PL and guard cell length; GCL) between the different *P. sativum* accessions for PL ($F_{(6)}$ = 11.27, P < 0.001) and GCL ($F_{(6)}$ = 8.94, P < 0.001) (***Fig.4.11***).

KW exhibited a significantly larger watered PL (20.53 ± 1.06 µm) to Eth, Filby, Ni16 and Ni11 (TukeyHSD; P < 0.05) and a significantly greater droughted PL (20.25 ± 0.99 µm) to Filby, Ni16 and Ni11 (TukeyHSD; P < 0.05) (***Fig.4.11A&B***). Whereas watered Filby (16.07 ± 0.46 µm) and droughted Ni11 (16.90 ± 0.48 µm) had the lowest PL, with a significant difference in watered PL to KW and Wando (TukeyHSD; P < 0.05) and in droughted PL to KW and Pacco (TukeyHSD; P < 0.05) (***Fig.4.11A&B***). The greatest GCL was observed within watered Wando (28.20 ± 1.16 µm) and droughted Pacco (27.90 ± 0.38 µm), with a significant difference to Filby in watered GCL (TukeyHSD; P < 0.05) and to Filby, Ni16 and Ni11 in droughted GCL (TukeyHSD; P < 0.05) (***Fig.4.11C&D***). In contrast Filby was significantly lower in watered GCL (22.99 ± 0.69 µm) to Wando (TukeyHSD; P < 0.05), whilst Ni16 was significantly lower in droughted GCL (22.92 ± 0.78 µm) to KW, Pacco and Wando (TukeyHSD; P < 0.05) (***Fig.4.11C&D***). However, no significant difference in PL or GCL was identified between watered and droughted conditions within each individual accession (TukeyHSD; P > 0.05) (***Fig.4.11***).

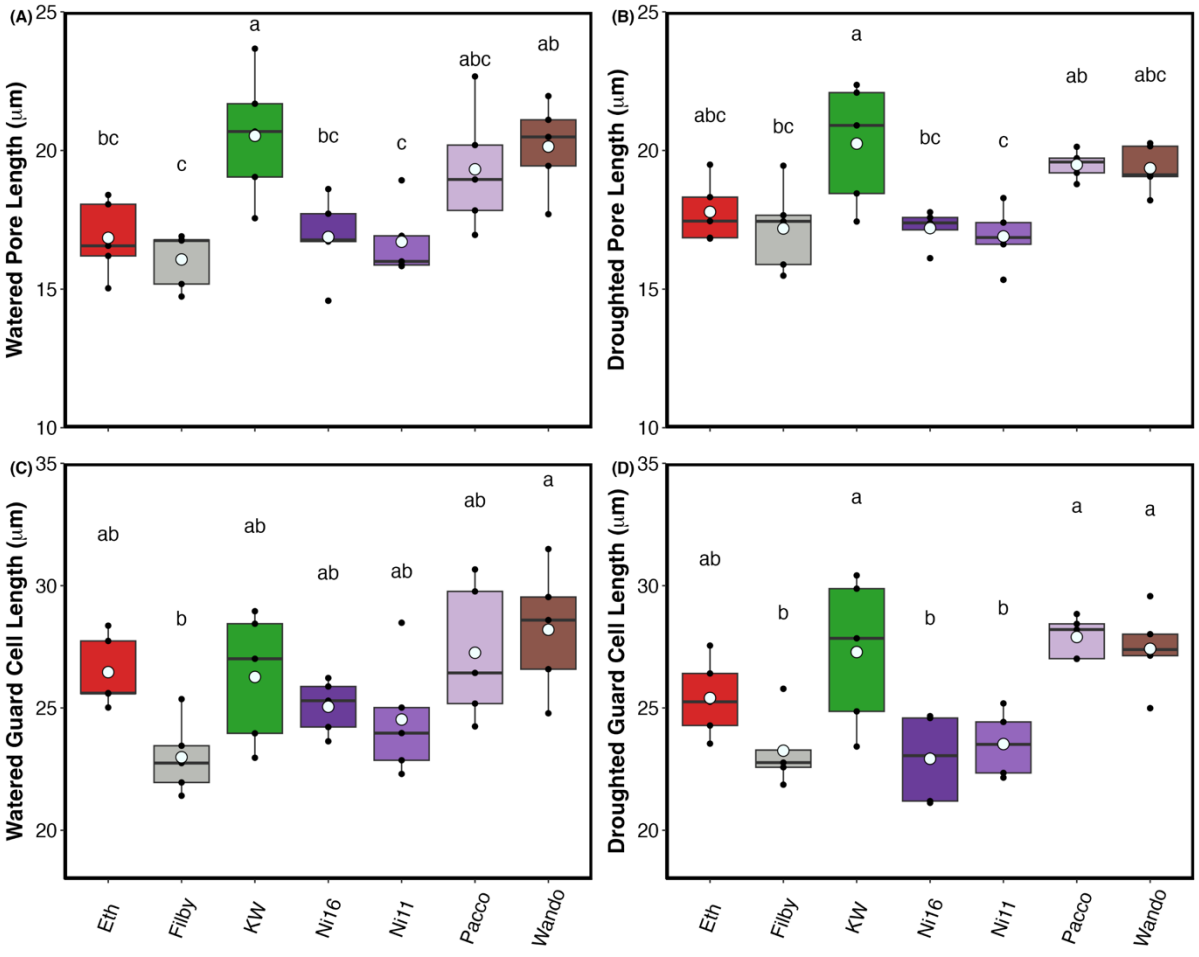

Figure 4.11. Variation in pod stomatal sizes across P. sativum accessions under watered and droughted conditions. Stomatal sizes were calculated as pore length (PL) for **(A)** watered and **(B)** droughted pods, and as guard cell length (GCL) for **(C)** watered and **(D)** droughted pods. Stomatal sizes were measured on the upper pod surface (facing the light in gas exchange) at 400x magnification (n = 5). White dots symbolise the mean, whilst error bars represent mean ± SE. Different letters above each error bar represent significant differences in either PL or GCL between the different *P. sativum* accessions ($P < 0.05$; TukeyHSD). The presence of + of the same colour indicates a significant difference within an individual accession between watered and droughted conditions in either PL or GCL, whereby + is $P < 0.05$, ++ is $P < 0.01$ and +++ is $P < 0.001$ (TukeyHSD).

4.3.4.3. Maximum Anatomical g_s

Significant variation in the maximum anatomical g_s (gs_{max}; calculated using SD and SS) was identified between the different *P. sativum* accessions for watered conditions ($F_{(6)} = 2.67$, $P < 0.05$), however no significant variation was identified in gs_{max} between the different *P. sativum* accessions for droughted conditions ($F_{(6)} = 0.63$, $P = 0.71$) (***Fig.4.12***). Pacco (0.21 ± 0.06 mol m^{-2} s^{-1}) had a significantly greater watered gs_{max} to Ni16 (the lowest watered gs_{max} accession; 0.07 ± 0.02 mol m^{-2} s^{-1}) (TukeyHSD; $P < 0.05$) (***Fig.4.12A***). However, there was no significant difference in gs_{max} identified between watered and droughted conditions within each individual accession (TukeyHSD; $P > 0.05$) (***Fig.4.12***).

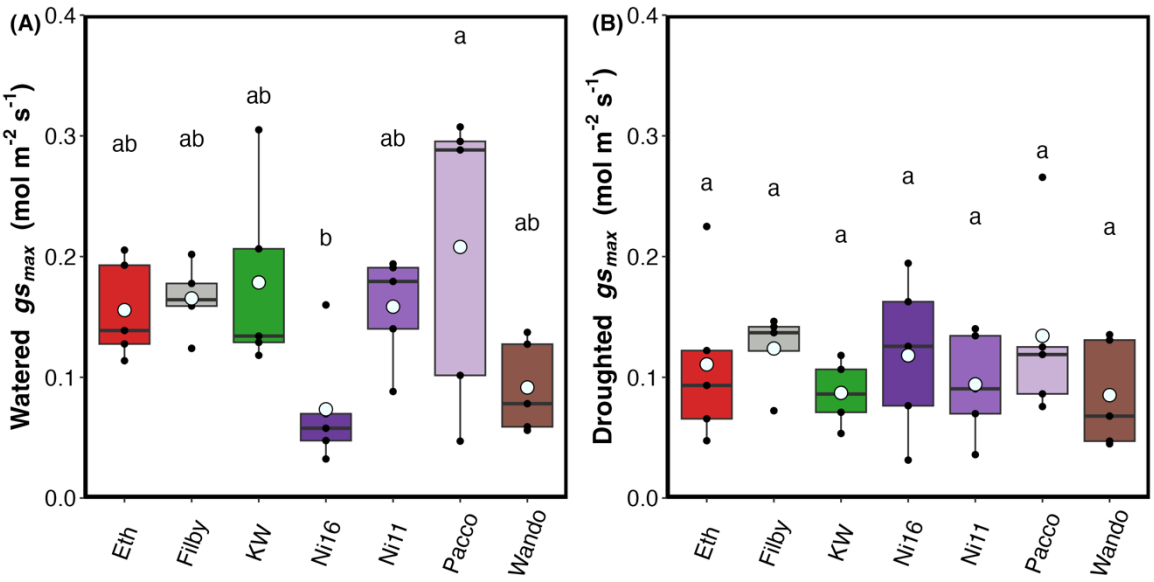

Figure 4.12. Variation in pod gs_{max} across P. sativum accessions under watered and droughted conditions. Mean maximum anatomical g_s (gs_{max}) were generated for **(A)** watered and **(B)** droughted pods via the Dow et al. (2014a) method using stomatal densities and sizes. Stomata were counted at a 200x magnification in a 1 mm^2 grid, whilst stomatal sizes (pore and guard cell length) were measured at 400x magnification (n = 5) using the upper pod surface (facing the light in gas exchange). White dots symbolise the mean, whilst error bars represent mean ± SE. Different letters above each error bar represent significant differences in gs_{max} between the different *P. sativum* accessions ($P < 0.05$; TukeyHSD). The presence of + of the same colour indicates a significant difference within an individual accession between watered and droughted conditions in gs_{max}, whereby + is $P < 0.05$, ++ is $P < 0.01$ and +++ is $P < 0.001$ (TukeyHSD).

4.3.4.4. Relationship Between Stomatal Densities, Sizes and Conductance

Despite the lack of significant correlations between SD and SS (PL or GCL) ($P > 0.05$) for either experimental condition (***Fig.4.13***), significant positive correlations were identified between SD and gs_{max} for both watered (R = 0.96, $P < 0.001$) and droughted (R = 0.97, $P < 0.001$) conditions (***Fig.4.14***). There were no significant correlations identified between SS and gs_{max} ($P > 0.1$) (***Fig.4.15***) or between SD and g_s ($P > 0.1$) (***Fig.4.16***) for either experimental condition. A significant positive correlation was identified between droughted PL and g_s (R = 0.34, $P < 0.05$), however there were no significant correlations between watered g_s and PL (R = 0.32, $P = 0.06$) or GCL (R = 0.33, $P = 0.05$) or between droughted g_s and GCL (R = 0.30, $P = 0.08$) (***Fig.4.17***).

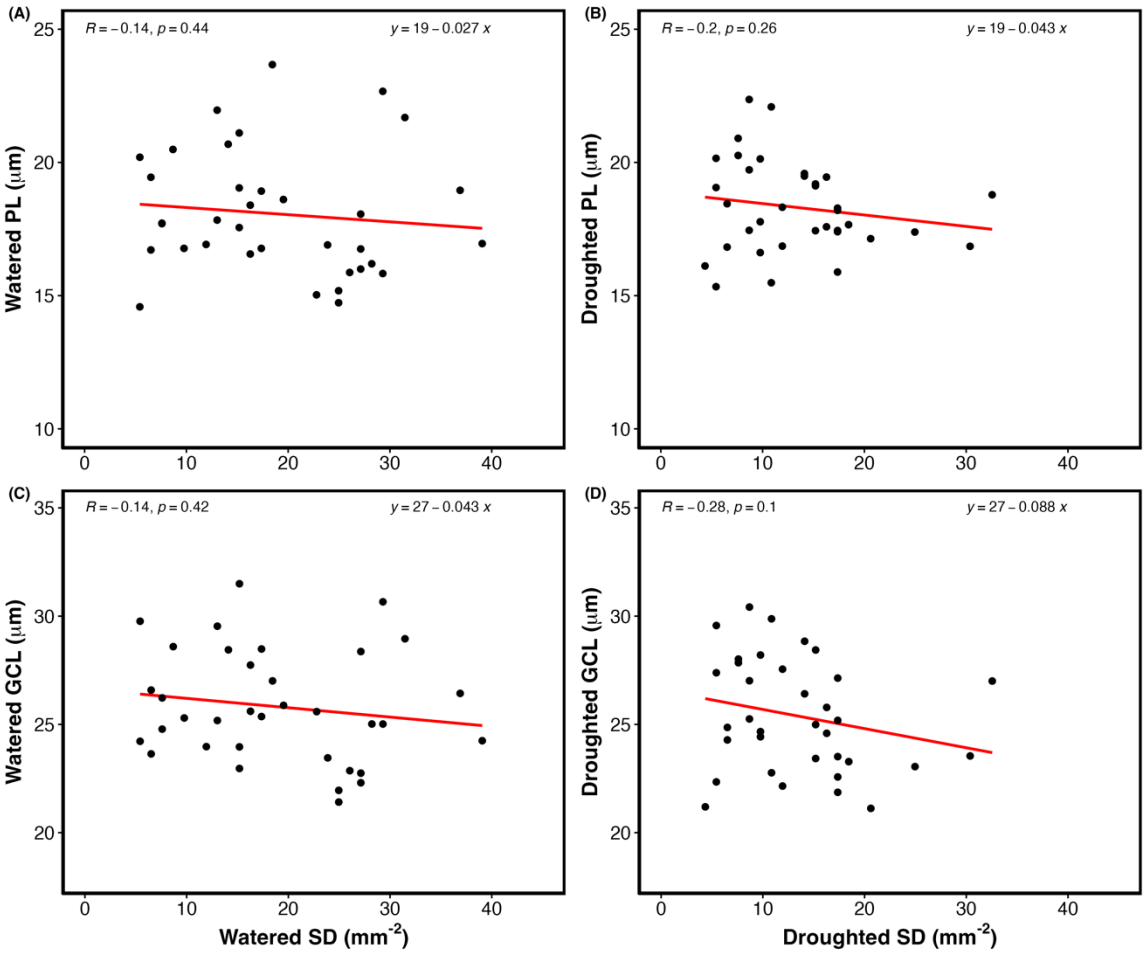

Figure 4.13. Spearmans correlation between stomatal densities and sizes in the pods under watered and droughted conditions. Correlations between pore length (PL) and stomatal density (SD) in **(A)** watered and **(B)** droughted pods and correlations between guard cell length (GCL) and SD in **(C)** watered and **(D)** droughted pods. Stomatal sizes were measured at 400x magnification, whilst stomata were counted at 200x magnification in a 1mm^2 grid using the upper pod surface (facing the light in gas exchange) (n = 5). Spearman's correlation coefficients (R) and linear regressions (represented as equations and red lines) were calculated for each anatomical component. $P < 0.05$ indicates a significant relationship.

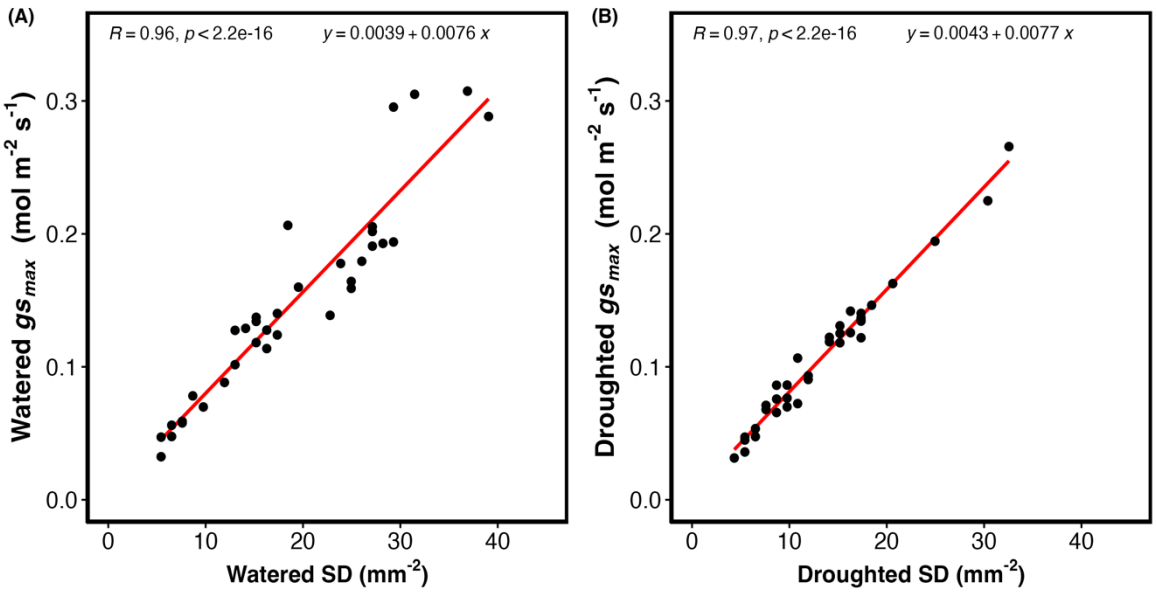

Figure 4.14. Spearmans correlation between stomatal densities and gs_{max} in the pods under watered and droughted conditions. Correlation between stomatal densities (SD) and maximum anatomical g_s (gs_{max}) in **(A)** watered and **(B)** droughted pods. gs_{max} was calculated via the Dow et al. (2014a) method using stomatal densities and sizes. Stomata were counted at a 200x magnification in a 1 mm^2 grid, whilst stomatal sizes (pore and guard cell length) were measured at 400x magnification using the upper pod surface (facing the light in gas exchange). Spearman's correlation coefficients (R) and linear regressions (represented as equations and red lines) were calculated for each anatomical component. $P < 0.05$ indicates a significant relationship (n = 5).

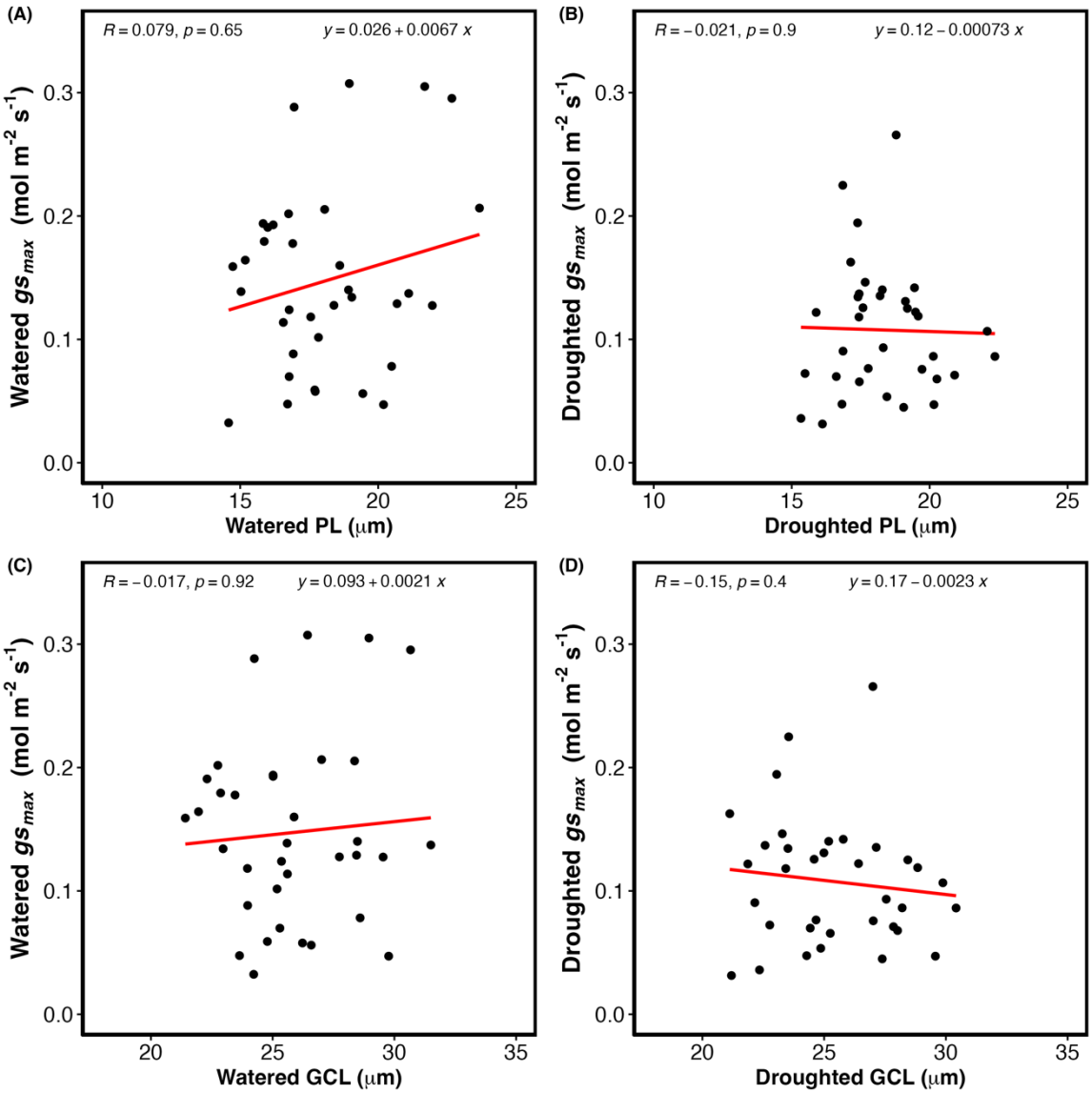

Figure 4.15. Spearmans correlation between stomatal sizes and gs_{max} in the pods under watered and droughted conditions. Correlations between maximum anatomical g_s (gs_{max}) and stomatal pore length (PL) in **(A)** watered and **(B)** droughted pods and correlations between gs_{max} and stomatal guard cell length (GCL) in **(C)** watered and **(D)** droughted pods. gs_{max} was calculated via the Dow et al. (2014a) method using stomatal densities and sizes. Stomata were counted at a 200x magnification in a 1 mm^2 grid, whilst stomatal sizes (pore and guard cell length) were measured at 400x magnification using the upper pod surface (facing the light in gas exchange). Spearman's correlation coefficients (R) and linear regressions (represented as equations and red lines) were calculated for each anatomical component. $P < 0.05$ indicates a significant relationship (n = 5).

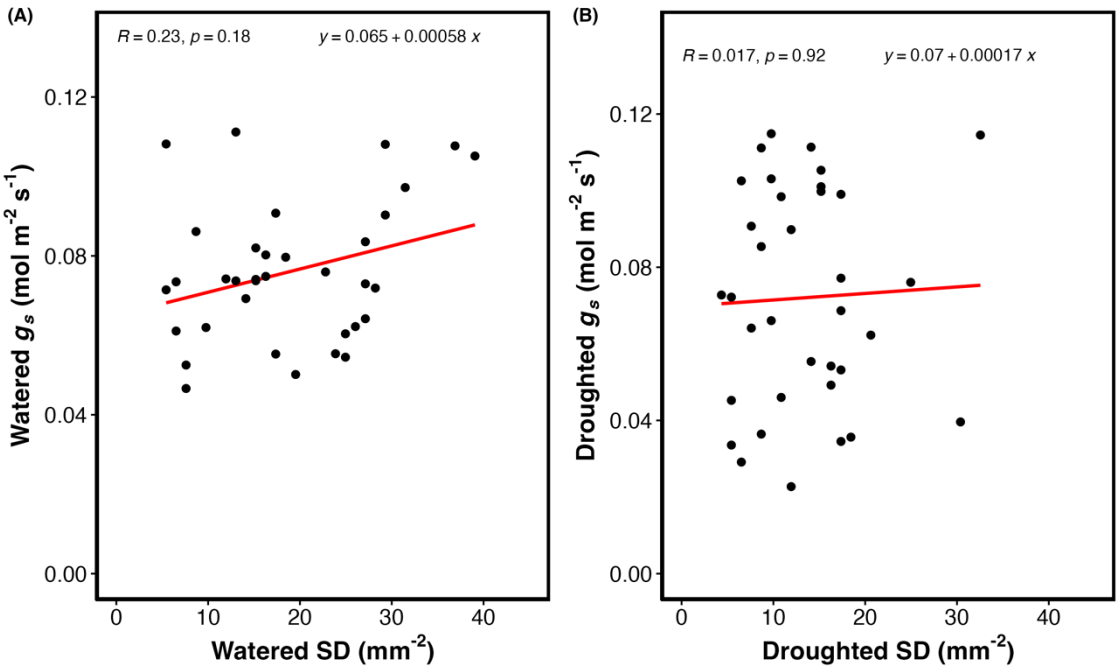

Figure 4.16. Spearmans correlation between stomatal densities and conductance in the pods under watered and droughted conditions. Correlations between stomatal conductance (g_s) and stomatal densities (SD) in **(A)** watered and **(B)** droughted pods. Stomata were counted at 200x magnification in a 1 mm^2 grid using the upper pod surface (facing the light in gas exchange). g_s was measured at 400 µmol mol^{-1} atmospheric CO_2 concentration within a bespoke Lawson Lab non-foliar gas exchange chamber at 23 °C and 1000 µmol m^{-2} s^{-1} photosynthetic photon flux density. Spearman's correlation coefficients (R) and linear regressions (represented as equations and red lines) were calculated for each SD against g_s. $P < 0.05$ indicates a significant relationship (n = 5).

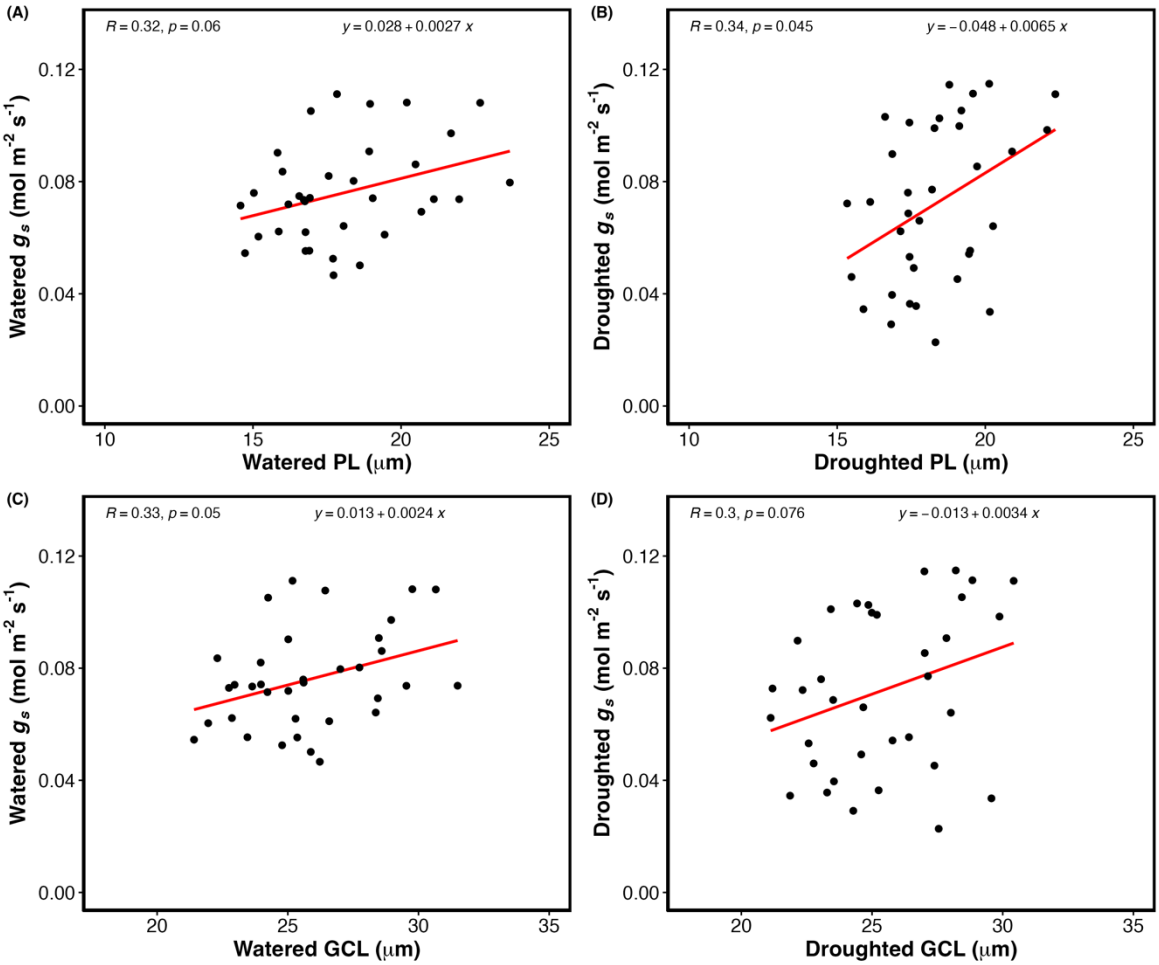

Figure 4.17. Spearmans correlation between stomatal sizes and conductance in the pods under watered and droughted conditions. Correlations between stomatal conductance (g_s) and pore length (PL) in **(A)** watered and **(B)** droughted pods, and correlations between g_s and guard cell length (GCL) in **(C)** watered and **(D)** droughted pods. Stomatal sizes were measured at 400x magnification using the upper pod surface (facing the light in gas exchange). g_s was measured at 400 µmol mol^{-1} atmospheric CO_2 concentration within a bespoke Lawson Lab non-foliar gas exchange chamber at 23 °C and 1000 µmol m^{-2} s^{-1} photosynthetic photon flux density. Spearman's correlation coefficients (R) and linear regressions (represented as equations and red lines) were calculated for each PL and GCL against g_s. $P < 0.05$ indicates a significant relationship (n = 5).

4.3.4.5. Stomatal Kinetics

Following a step increase in light intensity, *A*, g_s and *i*WUE were monitored in watered and droughted pods across the *P. sativum* accessions (***Fig.4.18***). Steady state values at 100 and 1000 µmol m^{-2} s^{-1} PPFD were calculated for *A* (*A100* and *A1000*) and g_s (*gs100* and *gs1000*) respectively (***Fig.4.19***), whereby significant variation was observed in *A100* ($F_{(6)}$ = 17.36, P < 0.001), *A1000* ($F_{(6)}$ = 31.61, P < 0.001), *gs100* ($F_{(6)}$ = 11.14, P < 0.001) and *gs1000* ($F_{(6)}$ = 4.42, P < 0.001) between the different *P. sativum* accessions and experimental conditions (***Fig.4.19***).

Pacco exhibited a significantly higher watered *A100* (0.64 ± 0.08 µmol m^{-2} s^{-1}) to Ni16 and Wando (TukeyHSD; P < 0.05) and significantly greater droughted *A100* (0.78 ± 0.11 µmol m^{-2} s^{-1}) to all droughted accessions (exempting KW) (TukeyHSD; P < 0.05) (***Fig.4.19A&B***). In contrast the lowest *A100* was observed within watered Wando (-0.40 ± 0.15 µmol m^{-2} s^{-1}) and droughted Eth (-1.10 ± 0.09 µmol m^{-2} s^{-1}), with a significant difference to all watered accessions in watered *A100* (TukeyHSD; P < 0.05) and to all droughted accessions in droughted *A100* (TukeyHSD; P < 0.05) (***Fig.4.19A&B***). KW had a significantly higher watered (0.04 ± 0.003 mol m^{-2} s^{-1}) and droughted (0.05 ± 0.002 mol m^{-2} s^{-1}) *gs100* to Eth, Filby, Ni16 and Wando in both watered (TukeyHSD; P < 0.05) and droughted *gs100* (TukeyHSD; P < 0.05), respectively (***Fig.4.19E&F***). Whilst watered (0.03 ± 0.001 mol m^{-2} s^{-1}) and droughted (0.01 ± 0.001 mol m^{-2} s^{-1}) Eth exhibited the lowest *gs100* and was significantly different in watered *gs100* to KW, Ni11 and Pacco (TukeyHSD; P < 0.05) and in droughted *gs100* to all droughted accessions (exempting Filby) (TukeyHSD; P < 0.05) (***Fig.4.19E&F***).

At the higher light intensity, the greatest *A1000* was observed within watered Filby (3.25 ± 0.08 μmol m^{-2} s^{-1}) and droughted KW (3.39 ± 0.05 μmol m^{-2} s^{-1}), with a significant difference in watered *A1000* to all watered accessions (TukeyHSD; $P < 0.05$) and in droughted *A1000* to all droughted accessions (exempting Pacco) (TukeyHSD; $P < 0.05$) (***Fig.4.19C&D***). Whilst watered Ni16 (1.59 ± 0.06 μmol m^{-2} s^{-1}) and droughted Eth (1.45 ± 0.15 μmol m^{-2} s^{-1}) exhibited the lowest *A1000* and was significantly different to all watered accessions in watered *A1000* (TukeyHSD; $P < 0.05$) and to all droughted accessions (excluding Ni16) in droughted *A1000* (TukeyHSD; $P < 0.05$) (***Fig.4.19C&D***). Pacco had a significantly greater watered *gs1000* (0.10 ± 0.001 mol m^{-2} s^{-1}) to all watered accessions (TukeyHSD; $P < 0.05$) and a significantly higher droughted *gs1000* (0.09 ± 0.004 mol m^{-2} s^{-1}) to all droughted accessions (par KW) (TukeyHSD; $P < 0.05$) (***Fig.4.19G&H***). Whereas watered Filby (0.05 ± 0.001 mol m^{-2} s^{-1}) and droughted Eth (0.04 ± 0.002 mol m^{-2} s^{-1}) exhibited the lowest *gs1000*, with a significant difference in watered *gs1000* to KW, Ni11, Pacco and Wando (TukeyHSD; $P < 0.05$) and in droughted *gs1000* to all droughted accessions (exempting Filby) (TukeyHSD; $P < 0.05$) (***Fig.4.19G&H***).

The maximum *i*WUE (*i*WUE_{max}) was calculated for watered and droughted pods to assess the responses of *i*WUE, with significant variation identified in *i*WUE_{max} between the different *P. sativum* accessions and experimental conditions ($F_{(6)} = 4.25$, $P < 0.001$) (***Fig.4.20***). Filby had a significantly higher watered *i*WUE_{max} (78.68 ± 2.54 μmol mol^{-1}) to all watered accessions (TukeyHSD; $P < 0.05$) and significantly greater droughted *i*WUE_{max} (81.22 ± 1.86 μmol mol^{-1}) to all droughted accessions (TukeyHSD; $P < 0.05$) (***Fig.4.20***). Whilst the lowest *i*WUE_{max} were observed in watered Ni11 (33.05 ± 1.54

μmol mol^{-1}) and droughted Ni16 (35.43 ± 2.38 μmol mol^{-1}), with a significant difference to Eth, Filby and KW in both watered (TukeyHSD; $P < 0.05$) and droughted $iWUE_{max}$ (TukeyHSD; $P < 0.05$), respectively (***Fig.4.20***).

Watered *A100* were generally higher than droughted conditions, with a significant difference identified in *A100* between watered and droughted Eth pods (TukeyHSD; $P < 0.001$) (***Fig.4.19A&B***). Although droughted *A1000* were generally higher than watered conditions; with a significant difference in *A1000* identified between watered and droughted pods within the individual accession of KW (TukeyHSD; $P < 0.001$) and Ni11 (TukeyHSD; $P < 0.001$), watered *A1000* was identified to be significantly higher than droughted conditions within the individual accession of Eth (TukeyHSD; $P < 0.001$) and Filby (TukeyHSD; $P < 0.001$) (***Fig.4.19C&D***). Whilst watered *gs1000* were generally higher than droughted conditions, with a significant difference identified in *gs1000* between watered and droughted Eth pods (TukeyHSD; $P < 0.001$) (***Fig.4.19G&H***). Although droughted *gs100* were generally higher than watered conditions; with a significant difference identified in *gs100* between watered and droughted Ni11 (TukeyHSD; $P < 0.05$), watered *gs100* was significantly greater than droughted conditions within the individual accession of Eth (TukeyHSD; $P < 0.001$) and Filby (TukeyHSD; $P < 0.001$) (***Fig.4.19E&F***). Whilst watered $iWUE_{max}$ was significantly higher than droughted conditions within Eth pods (TukeyHSD; $P < 0.01$) (***Fig.4.20***).

To examine the differences in stomatal kinetics, lag-times (initial temporal delay in the response of A and g_s to a light intensity change) and time constants (time taken for A

and g_s to reach steady state) in *A* and g_s were calculated for watered and droughted pods across the *P. sativum* accessions (***Fig.4.21***). Whereby significant variation between the different *P. sativum* accessions was identified in watered *A* ($F_{(6)} = 3.17$, $P < 0.05$) and g_s ($F_{(6)} = 2.68$, $P < 0.05$) time constants and in droughted *A* ($F_{(6)} = 3.75$, $P < 0.01$) and g_s ($F_{(6)} = 4.18$, $P < 0.01$) time constants, whilst an overall significant difference was also identified in *A* lag-time ($F_{(6)} = 2.32$, $P < 0.05$) between the different *P. sativum* accessions and experimental conditions (***Fig.4.21***). The longest watered *A* time constant was exhibited by Pacco (10.13 ± 2.73 min) and was significantly different to Filby, Ni16 (lowest watered *A* time constant; 2.51 ± 0.17 min) and Ni11 (TukeyHSD; $P < 0.05$) (***Fig.4.21E***). Whilst KW (22.99 ± 2.16 min) was significantly longer in watered g_s time constant than Ni11 (quickest accession; 14.65 ± 1.71 min) (TukeyHSD; $P < 0.05$) (***Fig.4.21G***). Eth exhibited the longest *A* (13.89 ± 3.60 min) and g_s (26.85 ± 2.30 min) time constant under droughted conditions, with a significant difference to Filby, Ni11, Ni16 and Wando in droughted *A* time constant (TukeyHSD; $P < 0.05$) and to Ni11, Ni16 and Wando in droughted g_s time constant (TukeyHSD; $P < 0.05$) (***Fig.4.21F&H***). Whilst Ni16 had the quickest *A* (2.62 ± 0.11 min) and g_s (14.81 ± 1.49 min) time constants under drought stress, with a significant difference to Eth for both droughted *A* time constant (TukeyHSD; $P < 0.05$) and droughted g_s time constant (TukeyHSD; $P < 0.05$) (***Fig.4.21F&H***). Droughted *A* lag-times were generally longer than watered conditions, with a significant difference identified between watered and droughted Eth pods (TukeyHSD; $P < 0.05$) (***Fig.4.21A&B***). However, there were no significant differences between watered and droughted conditions within each individual accession for g_s lag-times, *A* time constants or g_s time constants (TukeyHSD; $P > 0.05$) (***Fig.4.21C-H***).

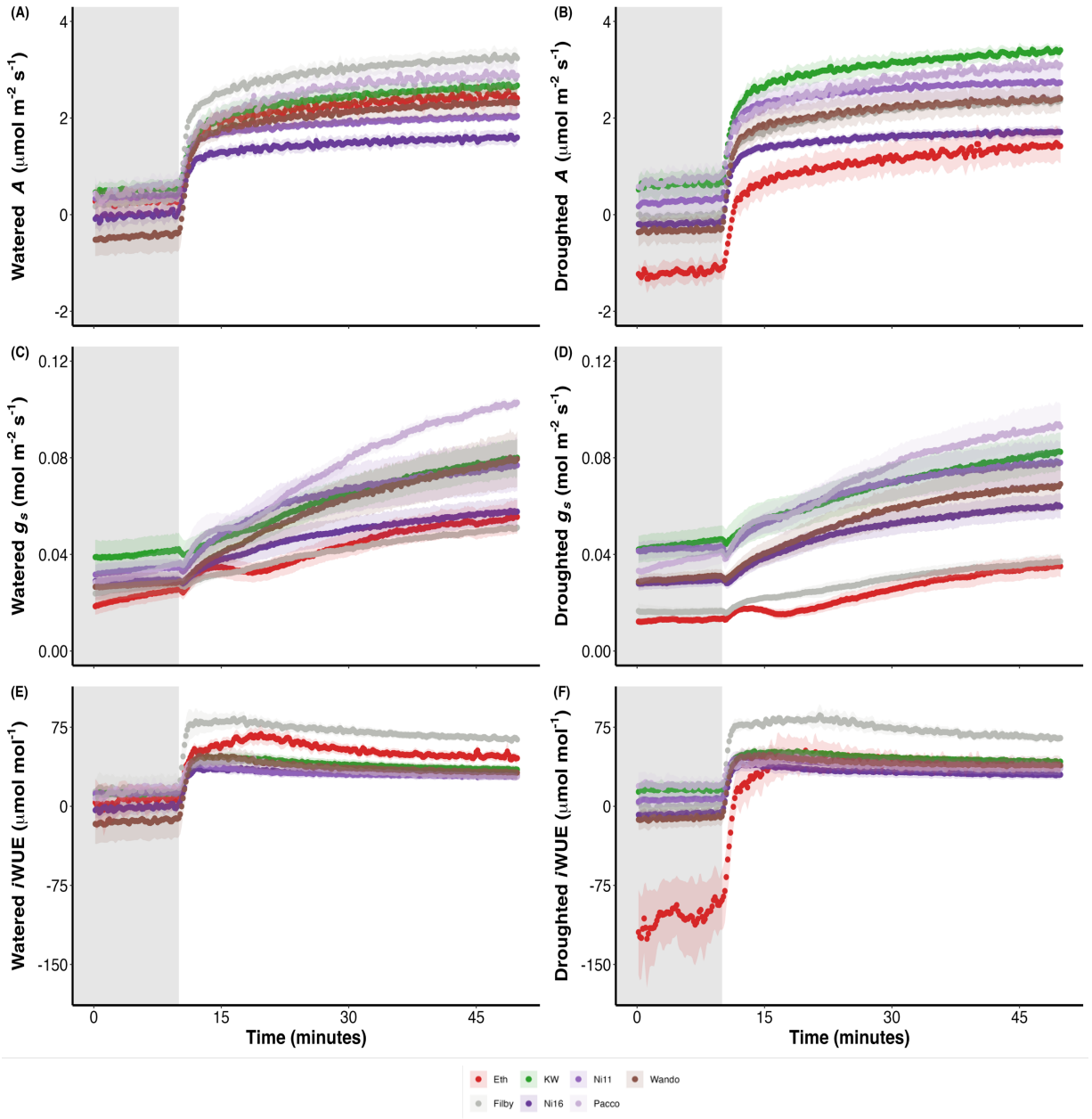

Figure 4.18. Variation in pod assimilation (A), stomatal conductance (g_s) and intrinsic water use efficiency (iWUE) in response to a step in light intensity across P. sativum accessions under watered and droughted conditions. Assimilation in **(A)** watered and **(B)** droughted pods, stomatal conductance in **(C)** watered and **(D)** droughted pods and intrinsic water use efficiency in **(E)** watered and **(F)** droughted pods were monitored in response to an increase in light intensity from 100 to 1000 μmol m^{-2} s^{-1} photosynthetic photon flux density. Measured at 400 μmol mol^{-1} [CO_2] and 23 ºC within a bespoke Lawson Lab non-foliar gas exchange chamber (n = 5). Error bars represent mean ± SE.

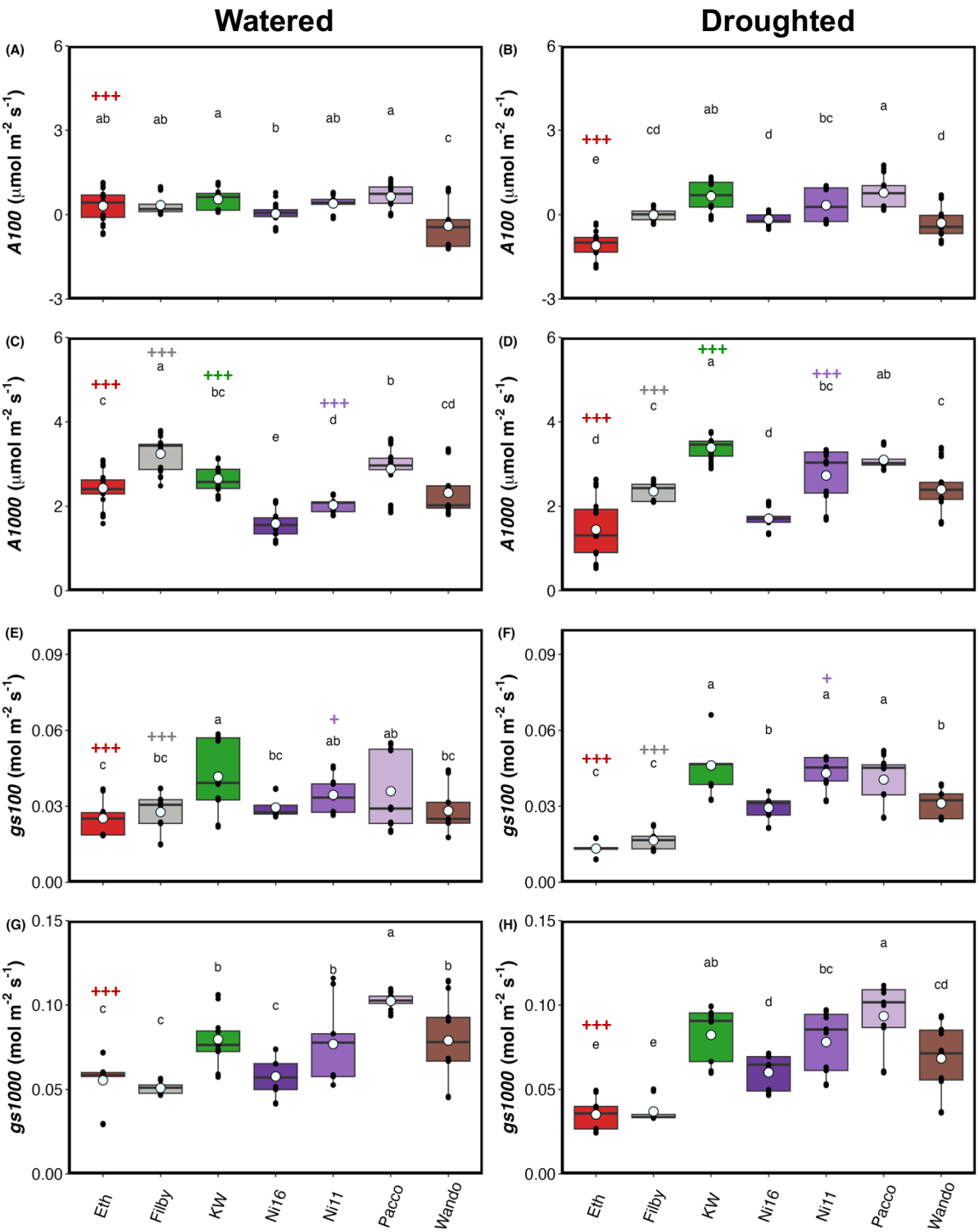

Figure 4.19. Variation in pod steady state assimilation (A) and stomatal conductance (g_s) at 100 µmol m^{-2} s^{-1} and 1000 µmol m^{-2} s^{-1} photosynthetic photon flux density (PPFD) across P. sativum accessions under watered and droughted conditions. Steady state *A* at 100 µmol m^{-2} s^{-1} PPFD (*A100*) in **(A)** watered and **(B)** droughted pods, steady state *A* at 1000 µmol m^{-2} s^{-1} PPFD (*A1000*) in **(C)** watered and **(D)** droughted pods, steady state g_s at 100 µmol m^{-2} s^{-1} PPFD (*gs100*) in **(E)** watered and **(F)** droughted pods and steady state g_s at 1000 µmol m^{-2} s^{-1} PPFD (*gs1000*) in **(G)** watered and **(H)** droughted pods, were parameterised from data collected within a step in light intensity from 100 to 1000 µmol m^{-2} s^{-1} PPFD at 400 µmol mol^{-1} [CO_2] and 23 ºC within a bespoke Lawson Lab non-foliar gas exchange chamber (n = 5). *A100* and *gs100* were calculated from the average of the last five data points before PPFD was increased to 1000 µmol m^{-2} s^{-1} PPFD. Whilst *A1000* and *gs1000* were calculated from the last five data points at 1000 µmol m^{-2} s^{-1} PPFD. White dots symbolise the mean, whilst error bars represent mean ± SE. Different letters above each error bar represent significant differences in one of the steady state parameters between the different *P. sativum* accessions ($P < 0.05$; TukeyHSD). The presence of + of the same colour indicates a significant difference within an individual accession between watered and droughted conditions in one of the steady state parameters, whereby + is $P < 0.05$, ++ is $P < 0.01$ and +++ is $P < 0.001$ (TukeyHSD).

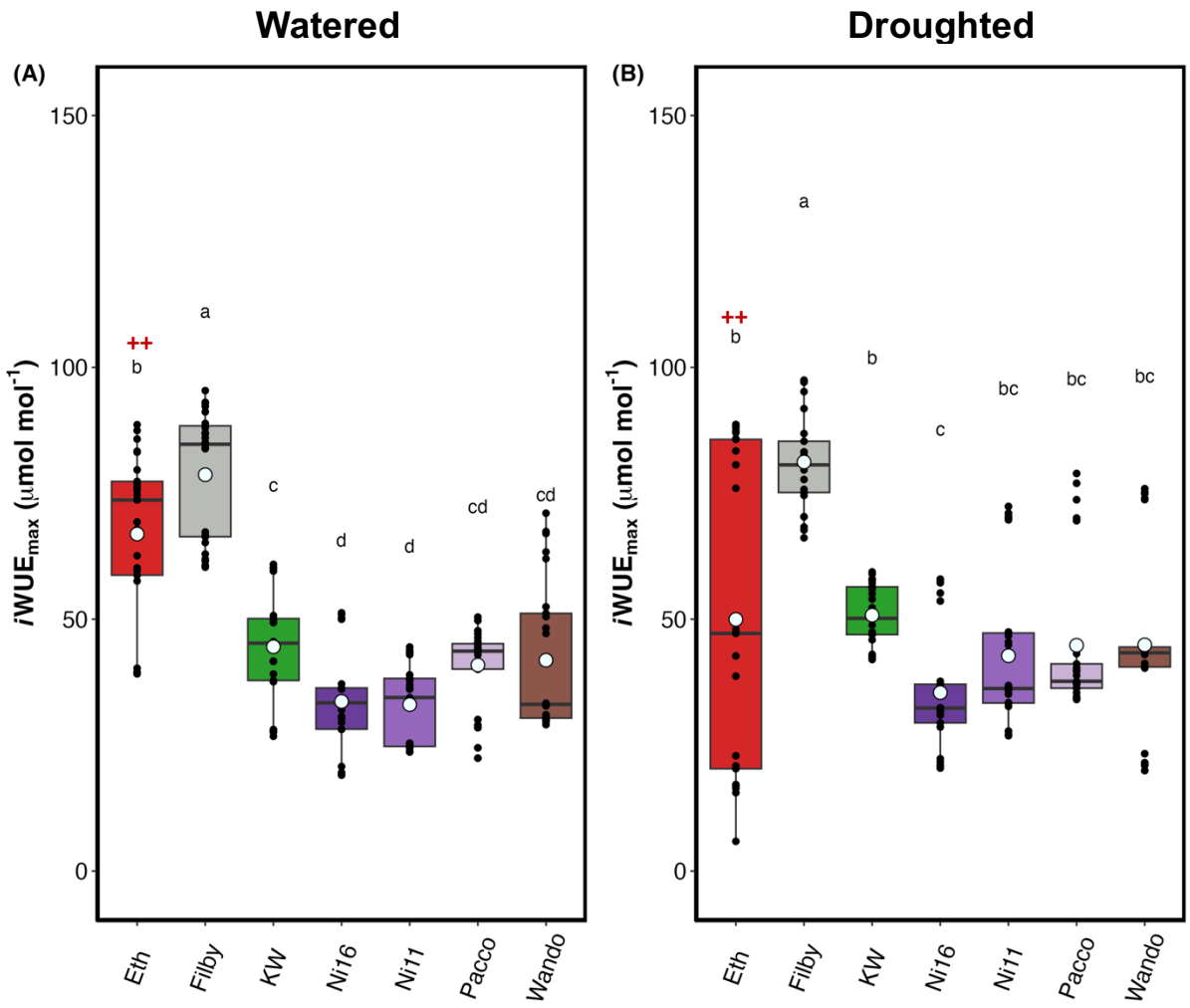

Figure 4.20. Variation in pod maximum intrinsic water use efficiency (iWUE$_{max}$) across P. sativum accessions under watered and droughted conditions. **(A)** watered and **(B)** droughted *i*WUE$_{max}$ were parameterised from data collected within a step in light intensity from 100 to 1000 µmol m^{-2} s^{-1} PPFD at 400 µmol mol^{-1} [CO_2] and 23 °C within a bespoke Lawson Lab non-foliar gas exchange chamber (n = 5). *i*WUE$_{max}$ was calculated from the average of five data points (observations 115-119) after PPFD was increased to 1000 µmol m^{-2} s^{-1} PPFD, where *i*WUE was generally at the highest and most stable rate. White dots symbolise the mean, whilst error bars represent mean ± SE. Different letters above each error bar represent significant differences in *i*WUE$_{max}$ between the different *P. sativum* accessions ($P < 0.05$; TukeyHSD). The presence of + of the same colour indicates a significant difference within an individual accession between watered and droughted conditions in *i*WUE$_{max}$, whereby + is $P < 0.05$, ++ is $P < 0.01$ and +++ is $P < 0.001$ (TukeyHSD).

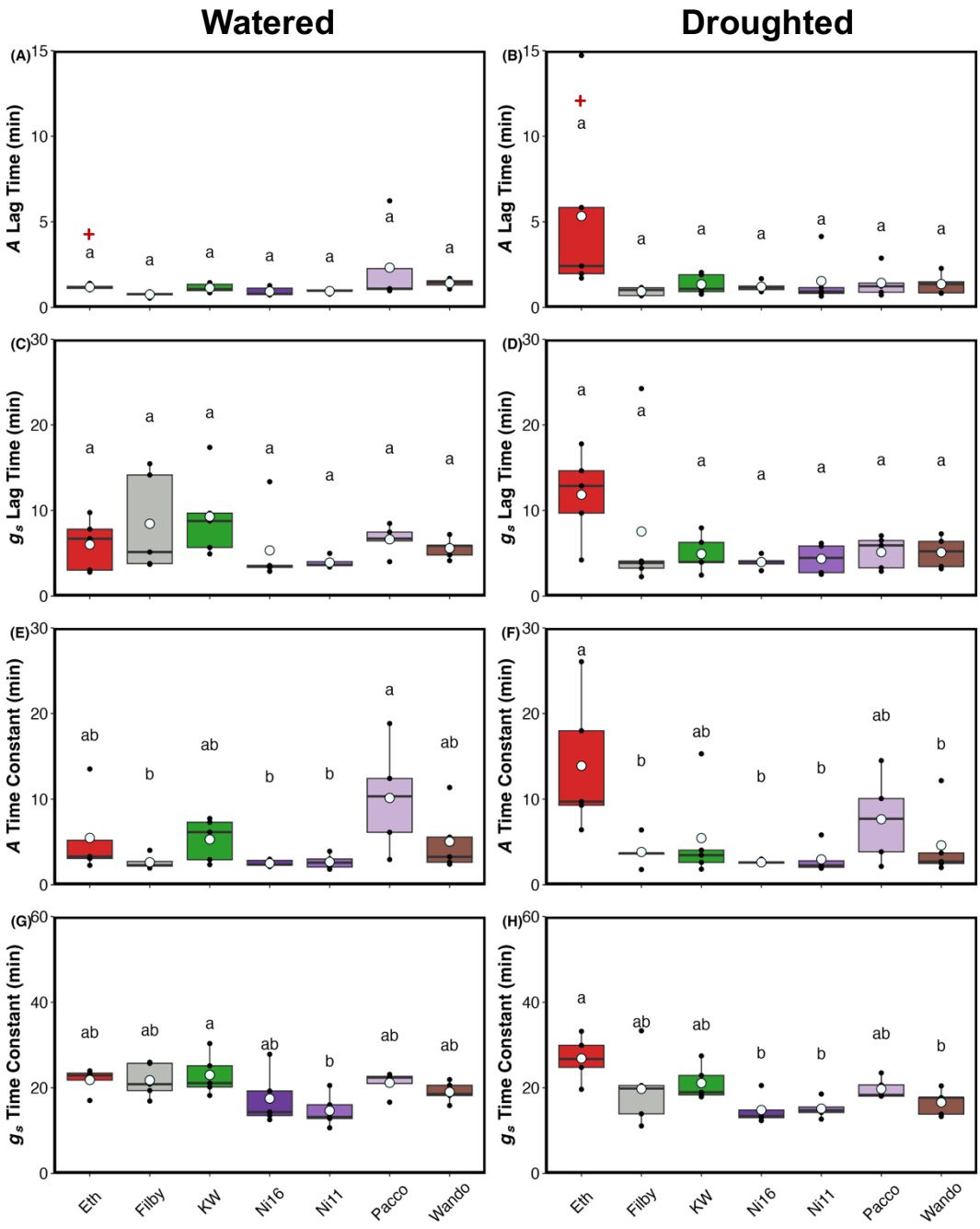

Figure 4.21. Variation in pod assimilation (A) and stomatal conductance (g_s) lag-time and time constants in response to a step in light intensity across P. sativum accessions under watered and droughted conditions. Lag-time (initial temporal delay in the response of *A* and g_s to a light intensity change) in assimilation in **(A)** watered and **(B)** droughted pods, g_s lag-time in **(C)** watered and **(D)** droughted pods, as well as time constants (time taken for *A* and g_s to reach steady state) in assimilation in **(E)** watered and **(F)** droughted pods and g_s time constants in **(G)** watered and **(H)** droughted pods were calculated via the Vialet-Chabrand et al. (2013) model. Pods were measured in response to an increase in light intensity from 100 to 1000 µmol m^{-2} s^{-1} photosynthetic photon flux density at 400 µmol mol^{-1} [CO_2] and 23 °C within a bespoke Lawson Lab non-foliar gas exchange chamber (n = 5). Error bars represent mean ± SE. Different letters above each error bar represent significant differences in either *A* or g_s lag-times or time constants between the different *P. sativum* accessions ($P < 0.05$; TukeyHSD). The presence of + of the same colour indicates a significant difference within an individual accession between watered and droughted conditions in either *A* or g_s lag-times or time constants, whereby + is $P < 0.05$, ++ is $P < 0.01$ and +++ is $P < 0.001$ (TukeyHSD).

4.3.4.6. Variation in Pod Temperature Under Watered and Droughted Conditions

Significant variation was identified in pod temperature between the different *P. sativum* accessions and experimental conditions ($F_{(6)}$ = 14.11, P < 0.001) (***Fig.4.22***). The greatest pod temperatures were observed within watered (24.75 ± 0.06 ^{o}C) and droughted (24.98 ± 0.05 ^{o}C) Ni16, with a significant difference identified to all watered accessions (excluding Ni11) in watered pod temperature (TukeyHSD; P < 0.05) and to all droughted accessions (exempting Pacco) in droughted pod temperature (TukeyHSD; P < 0.05) (***Fig.4.22***). KW exhibited the lowest droughted pod temperature (22 ± 0.09 ^{o}C) and was significantly different to Ni16, Ni11, Pacco and Wando (TukeyHSD; P < 0.05), whilst Filby had a significantly lower watered pod temperature (20.8 ± 0.04 ^{o}C) to all watered accessions (excluding Wando) (TukeyHSD; P < 0.05) (***Fig.4.22***). Interestingly, under both experimental conditions, the semi-leafless accessions (Ni11 and Pacco) exhibited significantly higher pod temperatures than the leafless accession (Filby) (TukeyHSD; P < 0.05), whilst no significant differences were observed between Ni11 and Pacco under either condition (TukeyHSD; P > 0.05) (***Fig.4.22***). Droughted pods generally had a higher temperature than watered pods, with a significant difference identified in pod temperatures between watered and droughted conditions within the individual accession of Filby (TukeyHSD; P < 0.001) and Wando (TukeyHSD; P < 0.001) (***Fig.4.22***). A negative correlation was identified between pod temperature and iWUE$_{max}$ for both watered (R = -0.55, P < 0.001) and droughted (R = -0.52, P < 0.01) conditions (***Fig.4.23***).

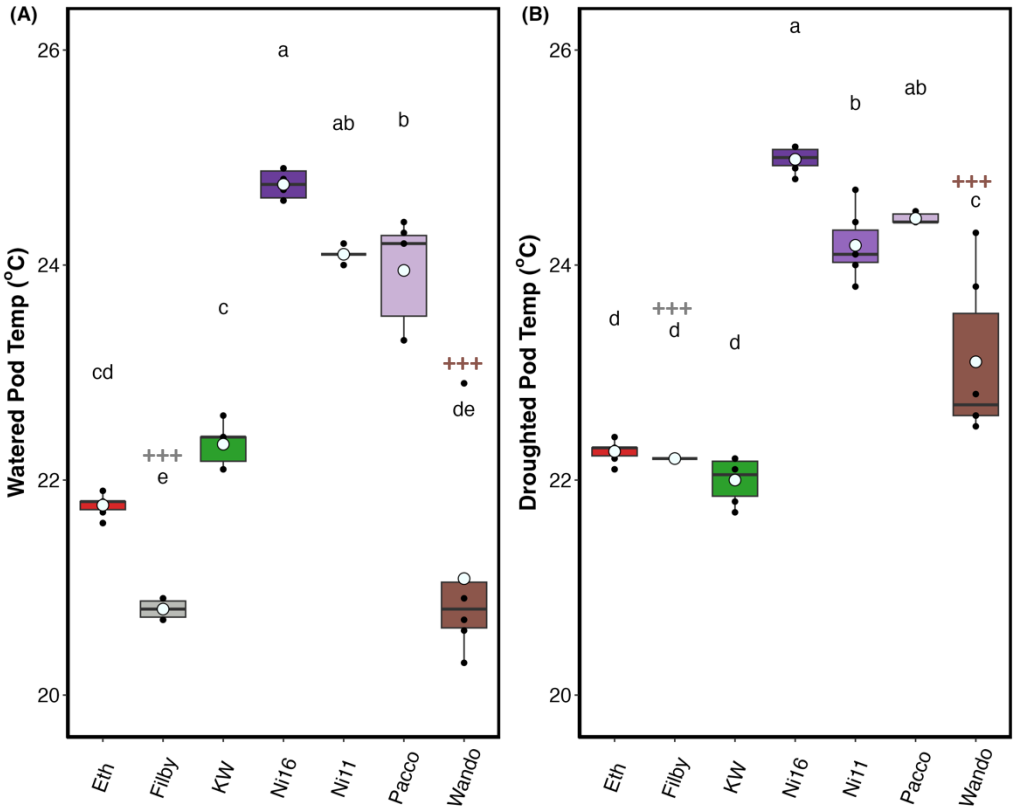

Figure 4.22. Variation in pod temperatures across P. sativum accessions under watered and droughted conditions. Temperature was observed in **(A)** watered and **(B)** droughted pods using a ^{FLIR}T500-Series thermal camera under standard growth conditions (300 µmol m^{-2} s^{-1} ± 10 µmol m^{-2} s^{-1} photosynthetic photon flux density and 23°C). White dots symbolise the mean, whilst error bars represent mean ± SE. Different letters above each error bar represent significant differences in pod temperature between the *P. sativum* accessions (P < 0.05; TukeyHSD). The presence of + of the same colour indicates a significant difference within an individual accession between watered and droughted conditions in pod temperature, whereby + is P < 0.05, ++ is P < 0.01 and +++ is P < 0.001 (TukeyHSD).

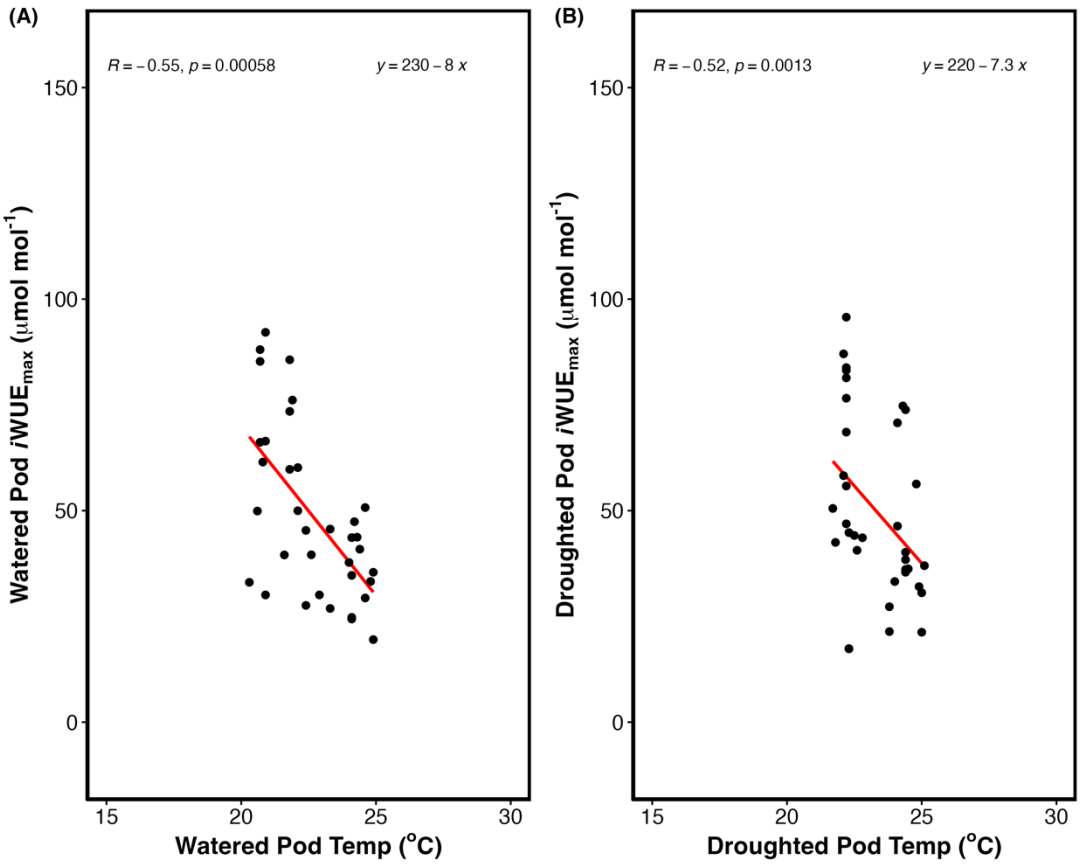

Figure 4.23. Spearmans correlation between pod iWUE$_{max}$ and temperature under watered and droughted conditions. Spearman's correlation coefficients (R) and linear regressions (represented as equations and red lines) were calculated between watered pod temperature and **(A)** watered *i*WUE$_{max}$ (maximum rate *i*WUE; A/g_s) and between droughted pod temperature and **(B)** droughted *i*WUE$_{max}$. A ^{FLIR}T500-Series thermal camera was used under standard growth conditions (300 µmol m^{-2} s^{-1} ± 10 µmol m^{-2} s^{-1} photosynthetic photon flux density (PPFD) and 23°C) to generate pod temperatures. Whilst *i*WUE$_{max}$ was calculated from the average of five data points (observations 115-119) after PPFD was increased to 1000 µmol m^{-2} s^{-1}, where *i*WUE was around the highest and most stable rate. Measured at 400 µmol mol^{-1} [CO_2] and 23 °C within a bespoke Lawson Lab non-foliar gas exchange chamber. $P < 0.05$ indicates a significant relationship (n = 5).

4.3.5. Variation in Yield Under Watered and Droughted Conditions

4.3.5.1. Grain Yield

Significant variation was identified in pod dry weight (DW) ($F_{(6)} = 5.19$, $P < 0.001$), seed DW ($F_{(6)} = 4.98$, $P < 0.001$) and number of seeds ($F_{(6)} = 3.64$, $P < 0.01$) between the different *P. sativum* accessions and experimental conditions (***Fig.4.24***). Whilst a significant difference was observed in all grain yield parameters (pod and seed DW, number of seeds and pods, pod length and total pod DW) between the different *P. sativum* accessions ($P < 0.001$) and in total pod DW ($F_{(1)} = 11.85$, $P < 0.001$) and number of pods ($F_{(1)} = 9.79$, $P < 0.01$) between the different experimental conditions (***Fig.4.24, Appendix Table.A2.1&A2.2***). For biomass yield parameter results please see ***Chapter 3 Section 3.3.5.2***.

Eth generally had the lowest grain yield for both experimental conditions, with a significantly lower watered (W) and droughted (D) pod length (W: 2.64 ± 0.07 cm, D: 2.59 ± 0.08 cm), pod DW (W: 0.20 ± 0.01 g, D: 0.17 ± 0.01 g) and seed DW (W: 0.15 ± 0.01 g, D: 0.13 ± 0.01 g) to all watered and droughted accessions respectively (TukeyHSD; $P < 0.05$) (***Fig.4.24A-D&K-L***). Eth was also significantly lower to Ni16, Ni11, Pacco and Wando in watered (1.92 ± 0.11) and droughted (1.55 ± 0.13) number of seeds (TukeyHSD; $P < 0.05$) respectively (***Fig.4.24G&H***). However Eth had the highest watered (17.67 ± 1.99) and droughted (14.83 ± 2.80) number of pods, with a significant difference in watered number of pods to all watered accessions (TukeyHSD; $P < 0.05$) and in droughted number of pods to all droughted accessions (TukeyHSD; $P < 0.05$) (***Fig.4.24E&F***). In contrast watered Wando (4.17 ± 0.17) and

droughted Ni11 (3.33 ± 0.42) had the lowest number of pods, with a significant difference to Eth and Pacco in watered number of pods (TukeyHSD; $P < 0.05$) and to Eth in droughted number of pods (TukeyHSD; $P < 0.05$) (***Fig.4.24E&F***). Filby exhibited a significantly lower watered total pod DW (2.20 ± 0.39 g) to Ni16, Ni11, Pacco and Wando (TukeyHSD; $P < 0.05$) and a significantly lower droughted total pod DW (2.08 ± 0.31 g) to Ni16 and Wando (TukeyHSD; $P < 0.05$) (***Fig.4.24I&J***).

The greatest overall watered grain yield was generally attributed with Wando, with a significantly greater watered total pod DW (5.07 ± 0.33 g) to Filby (TukeyHSD; $P < 0.05$), watered seed DW (0.88 ± 0.10 g) to all watered accessions (exempting Ni16), watered pod DW (1.21 ± 0.13 g) to all watered accessions (TukeyHSD; $P < 0.05$) and watered number of seeds (4.08 ± 0.41) to Eth, Filby and KW (TukeyHSD; $P < 0.05$) (***Fig.4.24A,C,G&I***). Whilst the greatest overall droughted grain yield was associated with Ni16, with a significantly greater droughted total pod DW (4.87 ± 0.53 g) to Eth, Filby and KW (TukeyHSD; $P < 0.05$), droughted pod length (8.03 ± 0.35 cm) to all droughted accessions (excluding Ni11) (TukeyHSD; $P < 0.05$), droughted seed DW (1.10 ± 0.12 g) to all droughted accessions (TukeyHSD; $P < 0.05$), droughted pod DW (1.39 ± 0.14 g) to all droughted accessions (exempting Wando) (TukeyHSD; $P < 0.05$) and droughted number of seeds (4.62 ± 0.43) to Eth, Filby and KW (TukeyHSD; $P < 0.05$) (***Fig.4.24B,D,H,J&L***). Whilst the greatest watered pod length was observed within Ni11 (7.5 ± 0.32 cm), which had a significant difference to all watered accessions (par Ni16) (TukeyHSD; $P < 0.05$) (***Fig.4.24K***).

Droughted pod DW was generally higher than watered conditions, with a significant difference identified between watered and droughted Ni16 (TukeyHSD; $P < 0.001$) (***Fig.4.24A&B***). Whilst droughted seed DW was also generally higher than watered conditions, with a significant difference identified between watered and droughted Ni16 (TukeyHSD; $P < 0.001$) (***Fig.4.24C&D***). Droughted Ni16 was also significantly greater in the number of seeds than watered Ni16 (TukeyHSD; $P < 0.01$) (***Fig.4.24G&H***). However no significant difference was identified in pod length, total pod DW or in the number of pods between watered and droughted conditions within each individual accession (TukeyHSD; $P > 0.05$) (***Fig.4.24E-F&I-L***).

4.3.5.2. Relationship Between Yield and Pod A_{sat400}

To examine the impact of pod assimilation on yield, biomass (from ***Chapter 3 Section 3.3.5.2***) and grain yield parameters were correlated against pod A_{sat400} for both watered and droughted conditions (***Table.4.4***). Droughted pod A_{sat400} had a significant negative correlation to the majority of droughted biomass yield parameters including: plant height (R = -0.53, $P < 0.01$), plant DW (R = -0.61, $P < 0.001$), number of leaves (R = -0.39, $P < 0.05$), number of stipules (R = -0.34, $P < 0.05$), number of stems (R = -0.64, $P < 0.001$), stipule DW (R = -0.41, $P < 0.05$) and stem DW (R = -0.60, $P < 0.001$) (***Table.4.4***). Watered A_{sat400} also exhibited significant negative correlations to watered number of leaves (R = -0.40, $P < 0.05$), watered leaf DW (R = -0.46, $P < 0.01$) and watered stem DW (R = -0.44, $P < 0.01$) (***Table.4.4***). Significant negative correlations were also identified between watered pod A_{sat400} and the majority of watered grain yield parameters including: pod DW (R = -0.49, $P < 0.01$), number of seeds (R = -0.50,

P < 0.01), seed DW (R = -0.48, P < 0.01) and pod length (R = -0.54, P < 0.001) (***Table.4.4***).

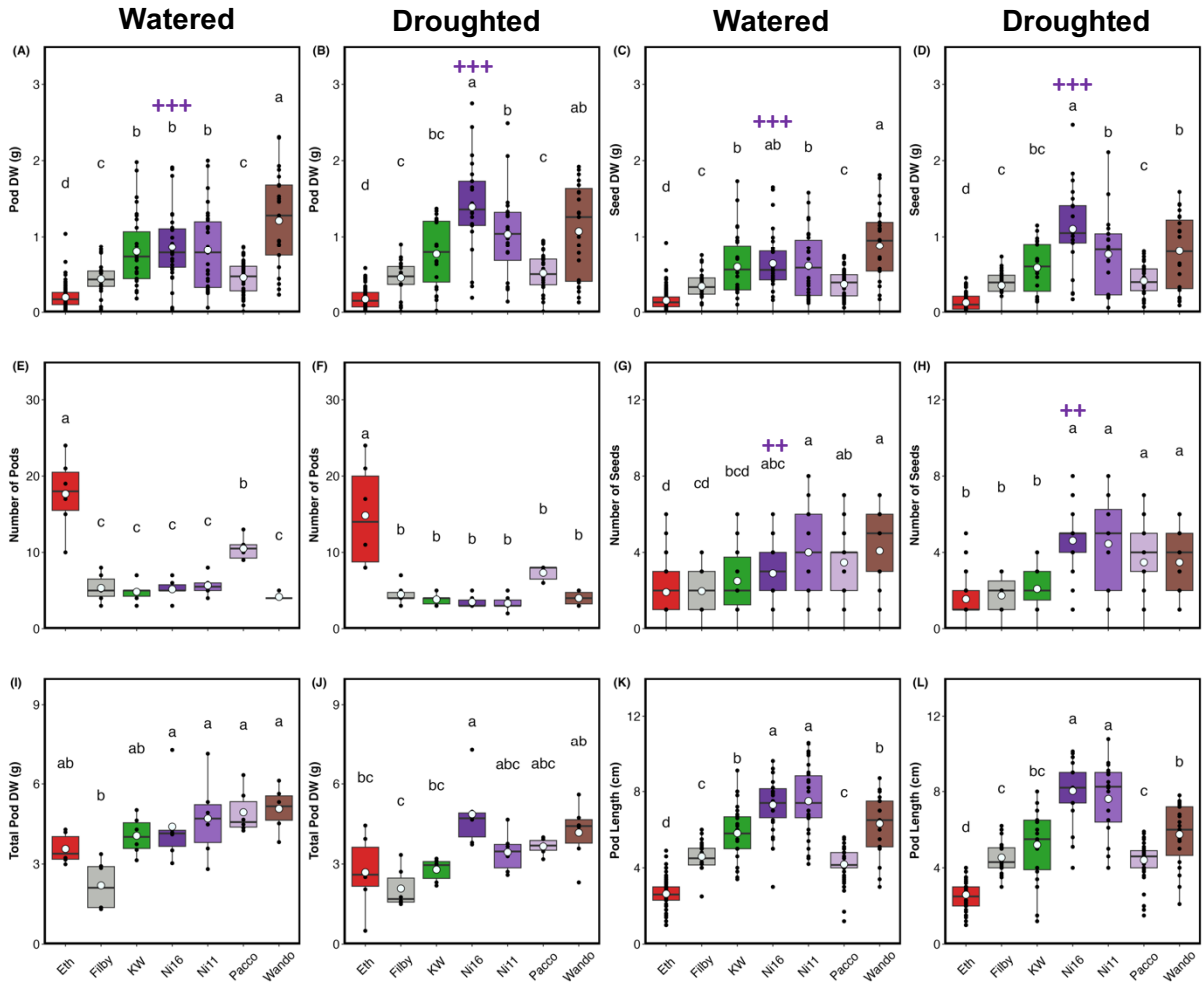

Figure 4.24. Variation in grain yield parameters across P. sativum accessions under watered and droughted conditions. Grain yield parameters are represented by watered **(A)** pod dry weight (DW), **(E)** number of pods, **(I)** total pod dry weight, **(C)** seed DW, **(G)** number of seeds and **(K)** pod length, as well as droughted **(B)** pod dry weight (DW), **(F)** number of pods, **(J)** total pod dry weight, **(D)** seed DW, **(H)** number of seeds and **(L)** pod length. Dry weights were measured after a constant weight had been reached and pod lengths were measured via ImageJ (version 1.53). White dots symbolise the mean, whilst error bars represent mean ± SE (n = 6). Different letters above each error bar represent significant differences across the different *P. sativum* accessions in one of the grain yield parameters (P < 0.05; TukeyHSD). The presence of + of the same colour indicates a significant difference within an individual accession between watered and droughted conditions in one of the grain yield parameters, whereby + is P < 0.05, ++ is P < 0.01 and +++ is P < 0.001 (TukeyHSD).

Table 4.4. Spearmans correlation coefficient table showing the relationship between grain and biomass yield components and pod A_{sat400} under watered and droughted conditions. Whereby *A* at 400 µmol mol^{-1} atmospheric CO_2; C_a (A_{sat400}) (measured in µmol m^{-2} s^{-1}) was measured within a bespoke Lawson Lab non-foliar gas exchange chamber at 23 °C and 1000 µmol m^{-2} s^{-1} photosynthetic photon flux density. Grain yield parameters are represented by the number of pods, number of seeds, pod length, pod dry weight (DW), seed DW and total pod DW, whilst biomass yield parameters are represented by plant height, plant DW, number and DW of stems, leaves and stipules and tendril DW. Pod lengths were measured (in cm) via ImageJ (version 1.53), whilst dry weights (DW) were measured (in g) after a constant weight was reached. Spearman's correlation coefficients (R) were calculated for each yield component against pod A_{sat400} measurement for both watered and droughted conditions, with the darker red boxes representing a strong negative correlation, whilst the dark green boxes represent a strong positive correlation. Statistical significance between yield parameters and pod A_{sat400} are illustrated as asterisks, whereby * is $P < 0.05$, ** is $P < 0.01$ and *** is $P < 0.001$ (n = 5).

Yield Parameter	Pod A_{sat400}	
	Watered	Droughted
Plant Height	-0.047	** -0.53
Plant DW	-0.3	*** -0.61
Number of Leaves	* -0.4	* -0.39
Number of Stipules	-0.12	* -0.34
Number of Stems	0.19	*** -0.64
Leaf DW	** -0.46	-0.3
Stipule DW	-0.17	* -0.41
Stem DW	** -0.44	*** -0.6
Tendril DW	0.26	-0.16
Number of Pods	0.12	-0.17
Pod DW	** -0.49	0.093
Number of Seeds	** -0.5	0.092
Seed DW	** -0.48	0.11
Pod Length	*** -0.54	0.073
Total Pod DW	-0.3	-0.19

4.4. Discussion

The impacts of drought on agricultural production are increasing, thus identifying lines that have high photosynthetic rates and yield potential under future climatic conditions has become an important way to increase food production to meet demands (Kim et al., 2019; Faralli and Lawson, 2020; Bagheri et al., 2023). The majority of studies that explore natural variation for future breeding programmes mainly focus on foliar tissues, however it is becoming increasingly apparent that non-foliar tissues play an important role in carbon assimilation, especially when foliar tissues are compromised (Hu et al., 2019; Simkin et al., 2020; Henry et al., 2020; Garrido et al., 2023; Lawson and Milliken, 2023; Antonietta et al., 2024; Milliken et al., 2024). Although genetic variation in non-foliar photosynthesis has previously been examined by Molero and Reynolds (2020) in wheat spikes, and natural variation in the contribution of alfalfa pod wall photosynthesis to grain filling (Wang et al., 2016) and the variation in responses of durum wheat ears to drought stress across varieties (Martínez-Peña et al., 2022) have been previously studied, to date natural variation in pea pod photosynthesis, yield and responses of stomatal anatomy/kinetics under drought stress is yet to be fully evaluated using modern techniques, despite Atkins et al. (1977) previously highlighting the potential carboxylation activities of the pod walls of peas (Lawson and Milliken, 2023). Subsequently, the present study utilised current physiological techniques, including a bespoke Lawson Lab non-foliar gas exchange chamber (***Fig.4.2***) to assess natural variation in pod photosynthesis in pea populations, whilst establishing differences in pod stomatal and photosynthetic responses to light intensity changes under watered and droughted conditions. Whereby significant variation in the

pods existed between the different *P. sativum* accessions for the majority of measured parameters under both experimental conditions (***Fig.4.3-4.24***).

4.4.1. Variation in Photosynthetic Rates and Yield Under Drought

The pods were photosynthetically active under both watered and droughted conditions for the majority of gas exchange parameters (***Fig.4.6-4.8&4.18-4.20***), with significant variation apparent in pod A_{sat400}, whereby greater photosynthetic rates were observed in the fully leafless accession (Filby) under watered conditions and elite accession (KW) under droughted conditions (***Fig.4.6&4.8***). The greater photosynthetic rates in the leafless accession may have been driven by the lack of shading from foliar tissues, which supports the findings of Bianculli et al. (2016) who suggested that soybean pod assimilation increased in defoliated lines, due to greater solar irradiance able to reach the pods (Bianculli et al., 2016; Cho et al., 2023). However, in the present study the leafless accession when subjected to drought stress, decreased in pod A_{sat400} potentially generated from a decline in gs_{400} and dark respiration rate, resulting in both restricted atmospheric and re-fixed/respiratory CO_2 sources for photosynthesis, with the former supported by the increase in pod temperature under drought, which is often indicative of stomatal closure (***Fig.4.6-4.9&4.22***) (Simkin et al., 2020; Pignon et al., 2021b; Javadian et al., 2023; Lawson and Milliken, 2023). Whilst the higher pod photosynthetic capability of the elite accession (KW) under drought conditions maybe the result of generally higher pod gs_{400}, which potentially maintained the atmospheric CO_2 supply even under drought stress and was further supported by the positive relationship identified between pod A and g_s (especially under drought) (***Fig.4.6-4.8***),

such findings emphasise the variation that exists within non-foliar photosynthesis due to potential fluctuations in CO_2 sources (Rouhi et al., 2007; Henry et al., 2020; Lawson and Milliken, 2023). It is also interesting to note that the A/C_a curves (***Fig.4.6A&B***) appeared linear, this may suggest the utilisation of a carbon capture mechanism similar to that in C_4 plants, with PEPC potentially restricting the CO_2 limitation that often surrounds Rubisco, possibly reinforcing the proposed mechanism of non-foliar carbon fixation by Blanke and Lenz (1989) (***Fig.4.1***), however further investigation into the molecular pathways of non-foliar photosynthesis are required to confirm this (Blanke and Lenz, 1989; Zhou et al., 2019; Henry et al., 2020).

Pod A_{sat400} was generally greater under droughted conditions (***Fig.4.6&4.8***), such findings agree with those of Ma et al. (2001) in chickpeas who reported that water-stressed pods had higher photosynthetic rates than well-watered varieties, reinforcing that non-foliar tissues may act as compensatory mechanisms under stress environments, possibly conferred by the drought tolerant mechanisms mentioned in ***Chapter 4 Section 4.1*** (Ma et al., 2001; Hu et al., 2019; Lawson and Milliken, 2023). The ability of the pods to act as a compensatory source of carbon assimilation was further supported by the negative relationships generally identified between biomass parameters and pod A_{sat400} under drought conditions (***Table.4.4***), suggesting that a decrease in biomass through possible leaf and stipule abscission (to reduce overall plant water-loss) drove an increase in photosynthesis in the pods to compensate for the loss of foliar tissues (Rouhi et al., 2007; Hu et al., 2014; Zhan et al., 2014; Henry et al., 2020; Antonietta et al., 2024). Unexpectedly, drought had a general positive impact on some grain yield parameters (including pod and seed DW) (***Fig.4.24***),

however no correlation was found between grain yield parameters and pod A_{sat400} under drought stress whilst a negative relationship was identified under watered conditions (***Table.4.4***). Subsequently, there may have been a disconnection between pod A_{sat400} and grain yield, possibly due to gas-exchange measurements being acquired before the pod filling stage (to avoid complexities surrounding non-foliar gas exchange as a result of 3D areas and the implications on boundary layer conductance), which may have excluded the total contribution of re-fixation from embryonic/seed respiratory CO_2 (Atkins et al., 1977; Simkin et al., 2020; Lawson and Milliken, 2023; Milliken et al., 2024; Song and Zhu, 2024). Whilst discrepancies may also be from the different contributions of foliar (with drought having limited impact upon foliar tissues in ***Chapter 3***), stem or tendril (as well as other green photosynthetic organs) photosynthesis to grain yield and therefore future studies could take into consideration the impact of embryonic respiration, as well as the amount each photosynthetically active tissue contributes to overall grain yield (Murchie et al., 2023; Milliken et al., 2024).

4.4.2. Variation in Pod Stomatal and Photosynthetic Responses to Light Intensity Changes Under Drought

Significant variation was identified in operating efficiency of PSII (F_q'/F_m') in the pods in response to changes in light intensity and a light induction, with drought/heat tolerant accession (Wando) exhibiting the greatest performance in comparison to the landrace (Eth), which may have had a subsequent impact on some grain yield parameters with decreases in F_q'/F_m' often indicative of potential photoinhibition and energy loss

(***Fig.4.3-4.5&4.24&Table.4.1-4.3***) (Zhang et al., 2016; Lawson and Vialet-Chabrand, 2024). Interestingly, drought had little to no impact on any of the chlorophyll fluorescence parameters in the pods (***Fig.4.3-4.5***), in agreement with Tambussi et al. (2005) who found no significant differences in chlorophyll fluorescence parameters between well-watered and water-stressed wheat ears and with Martinez et al. (2003) who reported that wheat ear bracts did not decrease in F_q'/F_m' under drought (Martinez et al., 2003; Tambussi et al., 2005).

Significant variation was also identified in pod *A* and g_s responses to a step increase in light intensity, with similar trends in pod *A1000* observed to those previously mentioned in pod A_{sat400} (***Fig.4.18-4.19***). Responses of *A* and g_s to a step in light intensity can often be driven by stomatal anatomy and kinetics, especially under drought (Lawson et al., 2012; Lawson and Blatt, 2014; McAusland et al., 2016; Li et al., 2017; Bertolino et al., 2019; Caine et al., 2023). However within the present study, g_s was only influenced by pore length (PL) under drought stress (***Fig.4.16&4.17***), this positive relationship could explain the physiological performance of the elite accession (KW) under drought, with a larger PL enabling higher rates of pod gs_{400} and therefore greater fixation of atmospheric CO_2, whilst also maintaining a cooler and more optimal pod temperature for carbon assimilation (***Fig.4.6,4.8,4.11&4.22***) (Fanourakis et al., 2015; Urban et al., 2017b). Although higher g_s are often associated with lower *i*WUE (due to greater water loss), within the present study cooler pod temperatures were associated with a greater $i\text{WUE}_{max}$ (***Fig.4.23***), and therefore, in the case of KW pods, the corresponding increase in *A* (driven by both cooler pod temperatures and increased CO_2 uptake through larger stomata) may have efficiently maintained

*i*WUE$_{max}$ under drought stress (***Fig.4.6,4.8,4.11,4.20&4.22***), further emphasising the functionality of pea pod stomata (Lawson and Blatt, 2014; McAusland et al., 2016; Kardiman and Ræbild, 2018; Simkin et al., 2020; Conesa et al., 2020; Lawson and Milliken, 2023).

Interestingly within the present study drought had no impact upon pod SD, SS or gs_{max} (***Fig.4.10-4.12***), which contrasts the findings of Li et al. (2017) in wheat ears, who found water stress reduced SD and stomatal width/size in several ear organs (including the awns, glumes, lemmas and paleas). Subsequently the mild drought stress utilised here may not have been enough to trigger pod stomatal anatomy changes but was possibly enough to initiate an increase in the amount of photosynthesis occurring in the pods potentially through variation in underlying signalling pathways yet to be explored (***Fig.4.6-4.19***) (Ma et al., 2001; Tokarz et al., 2021; Tian et al., 2022; Lawson and Milliken, 2023; Antonietta et al., 2024). Despite the general lack of variation in pod SD (***Fig.4.10***), under both experimental conditions increases in SD lead to greater maximum anatomical g_s (gs_{max}), whilst SS had no impact (***Fig.4.14&4.15***), such findings are in agreement with that of foliar tissues, whereby increases in gs_{max} are frequently reported to coincide with an increase in SD (although these are normally accompanied by a decrease in SS) (Franks and Casson, 2014; Bertolino et al., 2019; Caine et al., 2023). Whilst a higher gs_{max} often results in decreased *i*WUE, within the present study accessions with the highest gs_{max} did not generally have the lowest *i*WUE$_{max}$ (***Fig.4.12&4.20***) (Dow et al., 2014a; Bertolino et al., 2019). Despite the rapid g_s kinetics experienced by watered Ni11 and droughted Ni16, they also exhibited the lowest *i*WUE$_{max}$, which may be attributed to the generally

lower assimilation and respiration rates (especially in Ni16) (***Fig.4.8-4.9&4.18-4.21***), highlighting that WUE in these pod tissues was potentially restricted by CO_2 supply and emphasising the variation that exists in *i*WUE through disconnections in *A* and g_s responses (McAusland et al., 2016; Lawson and Blatt, 2014; Faralli et al., 2019; Eyland et al., 2021; Nguyen et al., 2023).

Intriguingly, the greater pod temperatures and lower $iWUE_{max}$ experienced by the semi-leafless accessions (Ni11 and Pacco) and Ni16 in comparison to the leafless accession (***Fig.4.20&4.22***), suggests that the leafless accession; although slower in kinetics, had more functional stomata, possibly through greater irradiance being able to reach the pods (Bianculli et al., 2016; Simkin et al., 2020; Cho et al., 2023; Lawson and Milliken, 2023). However, under drought stress the leafless accession could not out-perform the elite variety (KW; due to the mechanisms previously mentioned) and therefore a cross between these two accessions, as well as those that were high yielding may provide opportunities for greater pea pod stomata functionality and photosynthetic potential under future climatic conditions (Simkin et al., 2020; Garrido et al., 2023; Lawson and Milliken, 2023) (***Fig.4.6,4.8&4.18-4.20***).

4.4.3. Limitations

This study was limited by the number and variation in morphology/heritage of accessions, with only one type of semi-leafless afila, semi-leafless stipules reduced, fully leafless and landrace accession utilised, which were not fully representative of the diverse pea germplasm currently available, thus future studies could screen a

greater pea population of naturally varying accessions. Such studies could also utilise a more severe level of drought stress to fully explore the impact of future climatic conditions on pod stomata, photosynthesis and yield. Furthermore, the difference in CO_2 from atmospheric and respiratory sources were not determined, thus future studies could utilise other approaches such as membrane inlet mass spectrometry (MIMS) chambers to determine differences in ^{14}C from the two supplies. Future studies could also measure the pods after seed filling to consider the impact of embryonic respiration on assimilation rates and grain yield, whilst the use of shading experiments could be used to determine grain yield contributions from different photosynthetic tissues. Finally, comparisons to field conditions could provide a more accurate representation of pod photosynthesis under natural/agricultural settings (Simkin et al., 2020; Lawson and Milliken, 2023; Murchie et al., 2023; Milliken et al., 2024).

4.4.4. Conclusions

In summary, pea pods were shown to be photosynthetically active and have functional stomata under both watered and water restricted conditions, and natural variation was identified in the pods for the majority of physiological parameters measured. The higher pod photosynthetic activity and functionality observed in the leafless accession was potentially generated by greater light reaching the pods, due to the lack of shading normally attributed with the presence of foliar tissues. Although, under drought stress, reductions in stomatal conductance and dark respiration rates may have limited pod photosynthesis in the leafless accession in comparison to the elite variety (KW), which potentially had more functional stomata under drought stress. The increase in pod

photosynthesis alongside the reduction in biomass yield parameters under drought stress, supports the idea that non-foliar tissues act as compensatory mechanisms for carbon assimilation when foliar tissues are compromised. However drought did not impact PSII operating efficiency or stomatal anatomy, indicating that the mild drought utilised within this study was enough to trigger an increase in non-foliar photosynthesis but not enough to trigger detrimental impacts on pod anatomy or induce photoinhibition. Nonetheless, the variation in pod photosynthetic activity and functionality of stomata reinforces that greater consideration should be given to non-foliar tissues when screening varieties and highlights potentially novel traits that could be combined with current breeding programmes for enhanced pea production under future climatic conditions (Simkin et al., 2020; Lawson and Milliken, 2023; Murchie et al., 2023; Milliken et al., 2024).

4.4.5. Take Home Messages

- Pea pods naturally varied in photosynthetic activity and stomatal functionality, with increased photosynthesis observed under drought stress when biomass yield parameters declined (especially number of leaves/stipules), supporting that non-foliar tissues act as compensatory mechanisms when foliar tissues are compromised.

- The leafless accession (Filby) exhibited greater photosynthetic rates and stomatal functionality (especially under watered conditions), possibly attributed to a greater amount of light able to reach the pods, due to the absence of shading normally induced by foliar tissues.

- The elite variety (KW) had greater photosynthetic rates under drought stress, potentially due to a higher stomatal conductance driven by larger stomatal pores to facilitate increased atmospheric CO_2 fixation and evaporative cooling, whilst limited impacts from water loss were identified.

- Drought did not impact the operating efficiency of PSII, however variations in this parameter potentially drove differences in grain yield.

- The negative relationship under watered conditions between pod A_{sat400} and grain yield parameters, as well as the lack of any significant relationship under drought stress, may be due to discrepancies in grain yield contributions from

the different photosynthetically active tissues and the amount of respiration contributed from the respiring seed as the pod matures.

- Under both experimental conditions increases in gs_{max} were primarily caused by a greater density of stomata. However, drought had no impact on SD, SS or gs_{max} and therefore the mild drought utilised was enough to trigger an increase in pod photosynthesis but not enough to induce changes in stomatal anatomy within accessions.

- The present study highlights potentially novel and beneficial traits in non-foliar tissues that when combined with current breeding programmes may enhance pea production under future climatic conditions.

Chapter 5: General Discussion

5.1. Overview

When domestication of crops first began, selecting for enhanced photosynthetic and/or stomatal characteristics were not considered. Subsequently, as the impacts of climate change on agriculture (including drought) are becoming more pronounced, alternative strategies including exploration into the natural variation that exists within crop photosynthetic capacity and stomatal responses are required to increase yields under future climatic conditions to sustainably meet food demands by 2050 (Billen et al., 2024; Galanakis, 2024; Knorr and Augustin, 2024). As peas consist of an assortment of conventional leafed, semi-leafless and leafless varieties (*see* ***Table.2.1***) and contain green non-foliar structures (pods), they present an ideal model for the examination of variation in both foliar and non-foliar photosynthesis and other beneficial traits (including stomatal characteristic that relate to drought tolerance). Increased pea productivity is key to meet the increasingly popular demand for alternative sources of protein (Mikic et al., 2011; Tulbek et al., 2017; Moreau et al., 2018; Tran et al., 2022; Lawson and Milliken, 2023; Tayeh et al., 2023; Rogers et al., 2024; Milliken et al., 2024).

The aims of this study were to determine the extent of natural variation in foliar photosynthetic capacity and yield amongst different varieties of pea and establish photosynthetic and stomatal responses to changes in light intensity (*see* ***Chapter 2***). Pea varieties (after the initial screen in ***Chapter 2***), were selected based on photosynthetic capacity, stomatal and *i*WUE performances, as well as variation in leaf structures/morphologies and heritage. Selected varieties were examined for natural variation in the traits mentioned above and the impact of drought on functional traits

(*see* ***Chapter 3***). A bespoke Lawson Lab non-foliar gas exchange chamber was utilised to assess the extent of natural variation in non-foliar pea pod photosynthesis and stomatal conductance under watered and droughted environments (*see* ***Chapter 4***). The work within this study highlights the extent of variation in pea physiology in both foliar and non-foliar tissues and emphasises the potential for genetic screening programmes of pea varieties to enhance productivity under future climatic conditions.

5.2. Variation in Photosynthesis/Photosynthetic Capacity and the Impact on Yield

Although variation in photosynthetic capacity has been studied across many different species (Wright et al., 2004; Hikosaka and Shigeno, 2009; Lawson et al., 2012) and within species of barley (Stevens et al., 2021), wheat (Driever et al., 2014; Silva-Pérez et al., 2020; McAusland et al., 2020), soybean (Sakoda et al., 2016) and rice (Acevedo-Siaca et al., 2021), relatively little exploration has occurred to date into the natural variation in photosynthetic capacity of *P. sativum*, especially across the different foliar tissues, including leaves and stipules (Heath and Hebblethwaite, 1985; Nemeskéri et al., 2015). In ***Chapters 2*** and ***3*** significant variation were reported in photosynthetic capacity in both types of foliar tissues, unsurprisingly the elite variety KW exhibited higher photosynthetic capacity than landrace accessions (Elatius and Eth) (***Fig.2.8&3.8***). Such findings were expected as landraces can contain undesirable traits as explored within ***Chapters 2*** and ***3,*** whereby the excessive height demonstrated by the landrace accessions potentially drove their low photosynthetic

capacities (***Fig.2.25&3.25, Table.2.10&3.8***) (Faralli and Lawson, 2020; Schmidt et al., 2023).

Variation in foliar photosynthetic capacity can be influenced by numerous traits (as reviewed in ***Chapter 1***), including protein abundance and leaf/stipule mass per area (LMA/SMA), although protein content did not impact photosynthetic capacity in ***Chapter 2***, LMA/SMA had a positive association with photosynthetic capacity within ***Chapters 2*** and ***3*** (***Fig.2.10,2.24&3.24***) (Poorter et al., 2009; Parry et al., 2011; Ren et al., 2019). Positive relationships between LMA and photosynthetic capacity have previously been attributed with enhanced leaf thickness which enables greater exposure of chloroplasts to intercellular airspaces and CO_2 concentration surrounding the chloroplasts, which can increase photosynthetic rates, emphasising that LMA/SMA is a beneficial trait when exploring the drivers of variation in photosynthetic capacity. It would also be interesting to determine the cellular structures and organisation of the higher photosynthetic capacity and LMA/SMA accessions from ***Chapters 2*** and ***3*** to explore whether chlorophyll positioning was a key driver of greater photosynthetic rates (Poorter et al., 2009; Ren et al., 2019).

Utilisation of a bespoke Lawson Lab non-foliar gas exchange chamber also enabled variation in pea pod photosynthetic rates to be observed (***Chapter 4***). The significant variation in the CO_2-saturated rate of *A* at 400 μmol mol^{-1} atmospheric [CO_2] (A_{sat400}) observed (in ***Chapter 4***), reinforces the greater photosynthetic ability of elite accession (KW) whilst also highlighting the importance of non-foliar photosynthesis especially for the leafless accession (Filby) (further explored in ***Chapter 4***) (***Fig.4.8***) (Heath and Hebblethwaite, 1985, Heath et al., 1994; Lawson and Milliken, 2023; Milliken et al.,

2024). Intriguingly, although the mild drought inflicted within ***Chapters 3*** and ***4*** generally had limited impact upon most foliar physiological traits measured (including photosynthetic capacity) (***Fig.3.8***), within the pods, A_{sat400} was generally greater under drought (***Fig.4.8***). It has been previously reported that non-foliar materials can act as compensatory mechanisms when foliar tissues are compromised (Ma et al., 2001; Hu et al., 2019; Lawson and Milliken, 2023). Yet, despite little impact of drought on photosynthesis measured at an individual leaf/stipule level (in ***Chapter 3***), the significant negative relationship between the number of leaves/stipules and pod A_{sat400} (***Table.4.4***), highlighted that the level of drought administered could have driven foliar abscission of older leaves (not measured for photosynthesis) to prevent resource wastage, reduce overall plant water loss and in turn trigger an increase in pod photosynthesis possibly through signalling pathways yet to be fully investigated in non-foliar tissues (Ma et al., 2001; Rouhi et al., 2007; Hu et al., 2014; Zhan et al., 2014; Henry et al., 2020; Tokarz et al., 2021; Tian et al., 2022; Antonietta et al., 2024).

There is an ongoing debate as to whether photosynthetic capacity directly correlates to grain yield. In the majority of studies including that of Driever et al., (2014) and Silva-Pérez et al. (2020) in wheat, Stevens et al. (2021) in barley and Priyadarsini et al., (2022) in rice no significant relationship between capacity and yield were identified. It was therefore unsurprising that within the present study a general lack of significance was observed between foliar photosynthetic capacity and grain yields (***Chapters 2*** and ***3***) (***Table.2.10&3.8***), as photosynthetic capacity is usually measured under optimal conditions and therefore does not represent photosynthesis realised in the field, often leading to a disconnection between photosynthesis and final yield (Lawson et al., 2012; Driever et al., 2014; Acevedo-Siaca et al., 2020; Stevens et al., 2021).

These discrepancies (mentioned above) may instead explain the physiological performance of the elite drought/heat tolerant accession (Wando), which exhibited one of the highest grain yields (under watered conditions) seen in ***Chapters 2*** and ***4***, despite lower rates of foliar J_{max} (***Chapters 2*** and ***3***) (***Fig.2.8,2.25,3.8&4.24***). However, within the pods Wando displayed high levels of operating efficiency of PSII (F_q'/F_m'), which may instead explain some of the greater grain yields (***Fig.4.3-4.5&4.24***) and is consistent with findings explored in ***Chapter 3*** for the landrace accession, which displayed high F_q'/F_m' and biomass yields (***Fig.3.1-3.3&3.25***). These findings reinforce that chlorophyll fluorescence (which measures realised photosynthetic rates) may be a more accurate physiological tool when evaluating the determinants of greater yield (Murchie and Lawson, 2013; Pszczółkowski et al., 2023).

5.3. Variation in Photosynthetic and Stomatal Responses to Changes in Light Intensity

Under normal agricultural settings, crops are subjected to dynamic conditions, with even small cloud movements influencing the amount of sunlight received and in turn the responses of stomata and photosynthesis (Matthews et al., 2017; Faralli et al., 2019; Long et al., 2022). In ***Chapters 2-4*** both rates of A and g_s naturally varied between the different *P. sativum* accessions in response to light intensity changes and step increases in light intensity (which mimic the movement of a passing cloud) (***Fig.2.5-2.6,2.19-2.20,3.4-3.5,3.17-3.18,4.18-4.19***). Variation in A and g_s to light intensity changes/increases are often attributed to differences in stomatal anatomy (density and size) and kinetics, with different combinations of stomatal density (SD)

and size (SS) previously linked to changes in stomatal rapidity and both operational g_s and maximum anatomical g_s (gs_{max}) (McAusland et al., 2016; Bertolino et al., 2019; Conesa et al., 2020; Faralli and Lawson, 2020; McAusland et al., 2020; Caine et al., 2023). Intriguingly, within the present study the anatomical drivers of operational g_s varied, ranging from generally no impact of SD and SS on operational g_s (in ***Chapter 3***) to a greater abundance of smaller stomata increasing operational g_s (in ***Chapter 2***) (***Fig.2.17,2.18,3.15,3.16,4.16&4.17***). Whereas gs_{max} was primarily driven by SD for ***Chapters 2-4*** (although gs_{max} was also influenced by SS in ***Chapter 3***) (***Fig.2.15,2.16,3.13,3.14,4.14&4.15***). Such findings were expected, as gs_{max} is predominantly calculated through SD and SS, whereas operational g_s can be influenced by factors other than stomatal anatomy, including differences in guard cell biochemistry (not measured), therefore the lack of impact of SD and SS on operational g_s in ***Chapter 3*** may have been influenced more by non-stomatal anatomy factors possibly generated through the reduction in the number and variety of *P. sativum* accessions utilised between experiments (Dow et al., 2014a; Dow et al., 2014b, McElwain et al., 2016; Bertolino et al., 2019; Conesa et al., 2020; Xiong and Flexas, 2020). Nonetheless, the differences seen in the anatomical drivers of operational g_s and gs_{max} reinforces the natural variation that existed in *P. sativum* within this study (Faralli and Lawson, 2020).

Operational g_s and gs_{max} can also influence *i*WUE, with reductions in these parameters often leading to greater *i*WUE, as observed within ***Chapters 2*** and ***3***, with lower operational g_s potentially generating the high $i\text{WUE}_{max}$ seen within the semi-leafless accession (Ni11) (***Fig.2.19-2.21&3.17-3.19***) (Dow et al., 2014a; Bertolino et al., 2019). However, the influence of gs_{max} was less apparent (in ***Chapters 2-4***), with accessions

with greater *i*WUE$_{max}$ generally not exhibiting a low gs_{max} (***Fig.2.13,2.21,3.11,3.19,4.12&4.20***). Such findings could be due to operational g_s being a measured trait that responds to "real-time" changes, whilst gs_{max} is a theoretical trait that is typically not achieved under natural settings (Lawson et al., 2012; Dow et al., 2014a; Dow et al., 2014b; Bertolino et al., 2019; Conesa et al., 2020). As previously mentioned operational g_s and *i*WUE can also be impacted by stomatal kinetics, with faster stomata able to respond quicker to environmental cues, limiting the lag that exists between *A* and g_s and in turn improve photosynthetic induction and reduce water loss, with such responses being imperative under water-limiting environments (such as drought) (Lawson and Blatt, 2014; Kardiman and Ræbild, 2018; Lawson and Vialet-Chabrand, 2019; Nguyen et al., 2023). However within the present study, limited variation was observed for the majority of stomatal kinetic parameters (***Fig.2.22,3.20&4.21***) and where significant variation was observed, little to no connection could be made between high *i*WUE$_{max}$ accessions and rapid stomatal responses (*see* ***Chapters 2-4***). In these cases operational g_s (*see* ***Chapters 2*** and ***3***) or low pod *A* (*see* ***Chapter 4***) played a more pivotal role in *i*WUE$_{max}$ regulation. However, the limited impacts of stomatal kinetics on *i*WUE may also be due to the fact that only the rapidity of stomatal opening and not closure was determined and therefore stomatal closure may have a greater influence on *i*WUE$_{max}$, subsequently future studies could take this into consideration (Vialet-Chabrand et al., 2013; Lawson and Blatt, 2014; Lawson and Vialet-Chabrand, 2019).

Interestingly, the highest (and in some cases lowest) *i*WUE$_{max}$ accessions appeared to be interchangeable throughout the entire study, with the semi-leafless (Ni11 and Pacco), leafless (Filby) or near-isogenic (Ni11 and Ni16) accessions exhibiting the

highest iWUE$_{max}$ within one (or two) of the experiments (***Fig.2.21,3.19&4.20***). Although variations in iWUE$_{max}$ may have been driven by fluctuations in operational g_s or A (previously mentioned), it may also suggest that the reduction of foliar tissue and/or the genetic background of the near-isogenic lines contain potentially beneficial drought tolerant mechanisms and untapped genes yet to be fully explored for enhanced productivity under future climatic conditions (Lafond et al., 1981; Snoad et al., 1985; Baigorri et al., 1999; Nemeskéri et al., 2015; Checa et al., 2020; Szablińska-Piernik and Lahuta, 2021; Bagheri et al., 2023).

5.4. Variation between Leaves, Stipules and Pods

As peas contain more than one green tissue capable of photosynthesising and have multiple foliar tissue types (leaves and stipules) (***Fig.2.1***), this provides an extra layer of natural variation to explore, especially amongst the semi-leafless and leafless varieties (Nemeskéri et al., 2015; Simkin et al., 2020; Lawson and Milliken, 2023). Although the fully leafless accession (Filby) experienced cooler pod temperatures (under both watered and droughted conditions) when compared to the semi-leafless accessions (Ni11 and Pacco) within ***Chapter 4***, at a whole plant level (in ***Chapter 3***), the leafless accession exhibited the highest temperatures (***Fig.3.21&4.22***). These results were expected as the total loss of foliar tissue, would reduce the surface area for water loss, although such features could be beneficial under drought, optimal temperatures must be maintained for a plant to efficiently photosynthesise (Perez and Feeley, 2018; Szablińska-Piernik and Lahuta, 2021; Bagheri et al., 2023). Subsequently, as explored in ***Chapter 3***, the semi-leafless afila accessions (Pacco)

higher *i*WUE$_{max}$ under drought (mentioned previously) and greater ability to maintain cooler whole plant temperatures in comparison to the leafless and semi-leafless stipules reduced accession (Ni11), suggested that transformation of leaves into tendrils, but not a total loss of foliar tissues (due to the presence of stipules) may prevent overheating and maintain WUE for greater survival under drought stress (***Fig.3.19,3.21&4.22***) (Moreau et al., 2018; Checa et al., 2020; Tran et al., 2022). It has previously been established that stipules have a more efficient response to water deficit via a greater ability to perform osmotic adjustments of potassium, magnesium and chloride ions than other foliar structures, which may explain the performance of Pacco as well as the greater *i*WUE$_{max}$ of the stipules reported in ***Chapters 2*** and ***3*** in comparison to the leaves (Gonzalez et al., 2002). Such findings emphasise the need to consider more than just standard leaf tissues when evaluating beneficial traits (***Fig.2.21&3.19***) (Checa et al., 2020; Tran et al., 2022).

However, standard leaf tissues should not be ruled out, with stipules previously reported as being less efficient at gas exchange through high respiration rates, compact mesophyll cells and reduced source to sink exportation (Giovanardi et al., 2018), as conferred within ***Chapters 2*** and ***3***, whereby the leaves were generally higher for most gas exchange parameters than the stipules (although were not always significant) (***Fig.2.6,2.8,2.20,3.5,3.8&3.18***). It should also be noted that photosynthetic and stomatal conductance rates of the leaves and stipules were around 4-5x greater than that of the pods (when observing *A1000* in ***Chapters 3*** and ***4***) (***Fig.3.18&4.19***). Yet despite the lower rates, pods still contain many beneficial traits and have been shown within the present study to act as a compensatory mechanism for foliar tissues (even under mild drought stress), with key genetic traits yet to be fully

explored for increased photosynthesis and productivity under future climatic conditions. Consequently, breeding programmes and/or scientific studies should evaluate and incorporate multiple photosynthetic tissues to enhance the discovery of beneficial features/genes (Simkin et al., 2020; Henry et al., 2020; Tran et al., 2022; Lawson and Milliken, 2023).

5.5. Limitations and Further Research

As mentioned within ***Chapters 2-4***, this study was primarily limited by the number of accessions utilised, this restricted the amount of natural variation to be explored within the study and meant that the responses of the landrace, leafless and semi-leafless accessions were based on only one/two varieties (of each type). Furthermore, the plants (when under standard watering) were grown under optimal conditions, that were not fully representative of natural agricultural settings with the influence of nitrogen-fixing bacteria on photosynthetic capacity under field settings not taken into consideration. Unfortunately, the level of drought imposed in ***Chapters 3*** and ***4*** was not severe, thus the full impact of drought stress was not fully captured. It would therefore be interesting to determine variation in gas exchange under field conditions when utilising a greater number of varieties that are exposed to nitrogen fixation and to a more severe level of drought (Boussadia et al., 2010; Driever et al., 2014; Wang et al., 2018; Faralli and Lawson, 2020; Yang et al., 2021). Greater investigation into the calculations of non-foliar C_i and the contributions from respiratory and atmospheric CO_2 sources (through possible membrane inlet mass spectrometry measurements) are also required to fully explore the variation in photosynthetic capacity in non-foliar

tissues (Simkin et al., 2020; Lawson and Milliken, 2023; Milliken et al., 2024; Song and Zhu, 2024). Peas also contain more than just one type of green non-foliar tissue, with stems and tendrils potentially photosynthesising and contributing to yield, especially within the leafless accession, thus shading experimentation involving pods, stems, tendrils and foliar tissues could be undertaken to fully explore the contribution each region has on final yield and if there are any underlying genetic traits yet to be identified (Côté and Grodzinski, 1990; Simkin et al., 2020; Tokarz et al., 2021). Whilst a study by Price and Hedley (1980) identified differing levels of chlorophyll content and Rubisco and PEPC enzyme activity in the pod walls between green and yellow pea pod varieties, subsequently utilisation of a non-foliar gas exchange chamber on yellow podded varieties may capture the photosynthetic rates and potentially beneficial traits of yellow pods.

5.6. Conclusions

Significant variation was identified for the majority of physiological parameters measured, especially in A_{sat400}, photosynthetic capacity and photosynthetic and stomatal responses to light intensity changes/increases across the *P. sativum* accessions for both types of foliar tissues and the pods. Limited impact of foliar photosynthetic capacity was observed on grain yield, however findings suggested that chlorophyll fluorescence may be a more efficient way of analysing the drivers of yield. Despite the lower photosynthetic rates of the pods in comparison to the foliar tissues, it was apparent that even under mild drought stress the pods were likely acting as compensatory mechanisms for foliar tissues, which in conjunction with possible

drought tolerant mechanisms observed within the semi-leafless and leafless accessions, highlights the potential for considering more than just normal leaf tissues for identification of beneficial traits. The substantial screening undertaken and extensive variation observed in *P. sativum* across multiple tissue types within this study not only highlights the benefits of the technologies utilised but underscores the extent of variation that exist even amongst a small population of peas, with considerable natural variation yet to be explored in the wider pea germplasm for enhanced productivity under future climatic conditions (Nemeskéri et al., 2015; Faralli and Lawson, 2020; Simkin et al., 2020; Lawson and Milliken, 2023).

5.7. Final Take Home Messages

- Significant variation existed in the majority of physiological parameters measured (including A_{sat400}, photosynthetic capacity and stomatal and photosynthetic responses to light intensity changes) (***Chapters 2-4***).

- Elite accessions generally had a higher foliar photosynthetic capacity in comparison to landrace accessions, potentially driven through differences in LMA/SMA and biomass features (such as plant height).

- Foliar photosynthetic capacity had limited impact on grain yield, whilst chlorophyll fluorescent techniques appeared a more efficient way to determine the drivers of grain yield.

- Pods were observed as being photosynthetically active (although at lower rates than foliar tissues), with greater performances in A_{sat400} seen by elite and leafless accessions, whilst the pods may have compensated for foliar tissues even under mild drought stress.

- Accessions with high $i\text{WUE}_{max}$ appeared to be interchangeable throughout the entire study, potentially generated by fluctuations in operational g_s (or A), rather than gs_{max} or stomatal kinetics.

- Semi-leafless, near-isogenic and leafless accessions potentially contain beneficial traits for drought tolerance, with a greater capability of maintaining iWUE$_{max}$.

- The presence of stipules over leaves (and not a total loss of foliar tissues) potentially maintained cooler whole plant temperatures. However, leaves were generally greater than stipules for the majority of gas exchange parameters.

- The variation presented within this study in both foliar and non-foliar tissues highlights the potential to improve pea productivity through enhanced photosynthetic capacity, stress tolerant mechanisms and photosynthetic/stomatal responses.

Chapter 6: References

Abi-Ghanem, R., Bodah, E.T., Wood, M. and Braunwart, K., 2013. Potential breeding for high nitrogen fixation in Pisum sativum L.: germplasm phenotypic characterization and genetic investigation. *American Journal of Plant Sciences*, **4**(8), 1597–1600.

Abi-Ghanem, R., Carpenter-Boggs, L. and Smith, J.L., 2011. Cultivar effects on nitrogen fixation in peas and lentils. *Biology and Fertility of Soils*, **47**(1), 115–120.

Acevedo-Siaca, L.G., Coe, R., Quick, W.P. and Long, S.P., 2021. Variation between rice accessions in photosynthetic induction in flag leaves and underlying mechanisms. *Journal of Experimental Botany*, **72**(4), 1282–1294.

Acevedo-Siaca, L.G., Coe, R., Wang, Y., Kromdijk, J., Quick, W.P. and Long, S.P., 2020. Variation in photosynthetic induction between rice accessions and its potential for improving productivity. *New Phytologist*, **227**(4), 1097–1108.

Acosta-Rangel, A., Ávila-Lovera, E., De Guzman, M.E., Torres, L., Haro, R., Arpaia, M.L., Focht, E. and Santiago, L.S., 2018. Evaluation of leaf carbon isotopes and functional traits in avocado reveals water-use efficient cultivars. *Agriculture, Ecosystems and Environment*, **263**, 60–66.

Aggour, A. R., 1999. Inheritance of tolerance to high temperature stress in pea (Pisum sativum L.). *Annals of Agric. Sci. Moshtohor*, **37**(4), 2651–2671.

Ali, A.A., Xu, C., Rogers, A., McDowell, N.G., Medlyn, B.E., Fisher, R.A., Wullschleger, S.D., Reich, P.B., Vrugt, J.A., Bauerle, W.L., Santiago, L.S. and Wilson, C.J., 2015. Global-scale environmental control of plant photosynthetic capacity. *Ecological Applications*, **25**(8), 2349–2365.

Alonso-Blanco, C., Aarts, M.G.M., Bentsink, L., Keurentjes, J.J.B., Reymond, M., Vreugdenhil, D. and Koornneef, M., 2009. What has natural variation taught us about plant development, physiology, and adaptation? *Plant Cell*, **21**(7), 1877–1896.

Amaral, J., Lobo, A.K. and Carmo-Silva, E., 2024. Regulation of Rubisco activity in crops. *New Phytologist*, **241**(1), 35–51.

Annicchiarico, P., Nazzicari, N., Laouar, M., Thami-Alami, I., Romani, M. and Pecetti, L., 2020. Development and proof-of-concept application of genome-enabled selection for pea grain yield under severe terminal drought. *International Journal of Molecular Sciences*, **21**(7), 2414.

Antonietta, M., Martinez, D. and Guiamet, J.J., 2024. Delayed senescence and crop performance under stress: always a functional couple?. *Journal of Experimental Botany*, **75**(14), 4244–4257.

Arab, M.M., Askari, H., Aliniaeifard, S., Mokhtassi-Bidgoli, A., Estaji, A., Sadat-Hosseini, M., Sohrabi, S.S., Mesgaran, M.B., Leslie, C.A., Brown, P.J. and Vahdati, K., 2023. Natural variation in photosynthesis and water use efficiency of locally adapted Persian walnut populations under drought stress and recovery. *Plant Physiology and Biochemistry*, **201**, 107859.

Araújo, S.S., Beebe, S., Crespi, M., Delbreil, B., González, E.M., Gruber, V., Lejeune-Henaut, I., Link, W., Monteros, M.J., Prats, E. and Rao, I., 2015. Abiotic stress responses in legumes: strategies used to cope with environmental challenges. *Critical Reviews in Plant Sciences*, **34**(1-3), 237–280.

Araújo, W.L., Fernie, A.R. and Nunes-Nesi, A., 2011. Control of stomatal aperture: A renaissance of the old guard. *Plant Signaling and Behavior*, **6**(9), 1305–1311.

Araus, J.L., Sanchez-Bragado, R. and Vicente, R., 2021. Improving crop yield and resilience through optimization of photosynthesis: panacea or pipe dream? *Journal of Experimental Botany*, **72**(11), 3936–3955.

Armstrong, E.L., Pate, J.S. and Tennant, D., 1994. The field pea crop in South Western Australia–patterns of water use and root growth in genotypes of contrasting morphology and growth habit. *Functional Plant Biology*, **21**(4), 517–532.

Aschan, G. and Pfanz, H., 2003. Non-foliar photosynthesis - A strategy of additional carbon acquisition. *Flora*, **198**(2), 81–97.

Aschemann-Witzel, J., Gantriis, R.F., Fraga, P. and Perez-Cueto, F.J.A., 2020. Plant-based food and protein trend from a business perspective: markets, consumers, and the challenges and opportunities in the future. *Critical Reviews in Food Science and Nutrition*, 1–10.

Asseng, S., Guarin, J.R., Raman, M., Monje, O., Kiss, G., Despommier, D.D., Meggers, F.M. and Gauthier, P.P.G., 2020. Wheat yield potential in controlled-environment vertical farms. *Proceedings of the National Academy of Sciences of the United States of America*, **117**(32), 19131–19135.

Atkins, C.A., Kuo, J., Pate, J.S., Flinn, A.M. and Steele, T.W., 1977. Photosynthetic Pod Wall of Pea (Pisum sativum L.) Distribution of Carbon Dioxide-fixing Enzymes in Relation to Pod Structure. *Plant Physiology*, **60**(5), 779–786.

AuBuchon-Elder, T., Coneva, V., Goad, D.M., Jenkins, L.M., Yu, Y., Allen, D.K. and Kellogg, E.A., 2020. Sterile spikelets contribute to yield in sorghum and related grasses. *Plant Cell*, **32**(11), 3500–3518.

Baggett, J. R. and Kean, D., 1987. 'Oregon 523' Freezing Pea. *HortScience*, **22**(2), 330–331.

Bagheri, M., Santos, C.S., Rubiales, D. and Vasconcelos, M.W., 2023. Challenges in pea breeding for tolerance to drought: Status and prospects. *Annals of Applied Biology*, **183**(2), 108–120.

Bahar, N.H.A., Lo, M., Sanjaya, M., Van Vianen, J., Alexander, P., Ickowitz, A. and Sunderland, T., 2020. Meeting the food security challenge for nine billion people in 2050: What impact on forests? *Global Environmental Change*, **62**, e102056.

Baigorri, H., Antolín, M.C. and Sánchez-Dıaz, M., 1999. Reproductive response of two morphologically different pea cultivars to drought. *European Journal of Agronomy*, **10**(2), 119–128.

Barnes, M.L., Breshears, D.D., Law, D.J., van Leeuwen, W.J.D., Monson, R.K., Fojtik, A.C., Barron-Gafford, G.A. and Moore, D.J.P., 2017. Beyond greenness: Detecting temporal changes in photosynthetic capacity with hyperspectral reflectance data. *PLoS ONE*, **12**(12), e0189539.

Baslam, M., Mitsui, T., Hodges, M., Priesack, E., Herritt, M.T., Aranjuelo, I. and Sanz-Sáez, Á., 2020. Photosynthesis in a changing global climate: Scaling up and scaling down in crops. *Frontiers in Plant Science*, **11**, 882.

Basu, P.S., Chaturvedi, S.K., Gaur, P.M., Mondal, B., Meena, S.K., Das, K., Kumar, V., Tewari, K. and Sharma, K., 2022. Physiological mechanisms of tolerance to drought and heat in major pulses for improving yield under stress environments. *Advances in plant defense mechanisms*. IntechOpen.

Battle, M.W., Vialet-Chabrand, S., Kasznicki, P., Simkin, A.J. and Lawson, T., 2024. Fast stomatal kinetics in sorghum enables tight coordination with photosynthetic responses to dynamic light intensity and safeguards high water use efficiency. *Journal of Experimental Botany*, erae389.

Bean, R.C., Porter, G.G. and Barr, B.K., 1963. Photosynthesis & Respiration in Developing Fruits . III. Variations in Photosynthetic Capacities during Color Change in Citrus. *Plant Physiology*, **38**(3), 285–290.

Becerra-Tomás, N., Díaz-López, A., Rosique-Esteban, N., Ros, E., Buil-Cosiales, P., Corella, D., Estruch, R., Fitó, M., Serra-Majem, L., Arós, et al., 2018. Legume consumption is inversely associated with type 2 diabetes incidence in adults: A prospective assessment from the PREDIMED study. *Clinical Nutrition*, **37**(3), 906–913.

Benjamin, J.G. and Nielsen, D.C., 2006. Water deficit effects on root distribution of soybean, field pea and chickpea. *Field crops research*, **97**(2-3), 248–253.

Berners-Lee, M., Kennelly, C., Watson, R. and Hewitt, C.N., 2018. Current global food production is sufficient to meet human nutritional needs in 2050 provided there is radical societal adaptation.

Elementa, **6**(1), 52.

Bertolino, L.T., Caine, R.S. and Gray, J.E., 2019. Impact of stomatal density and morphology on water-use efficiency in a changing world. *Frontiers in Plant Science*, **10**, 225.

Bianculli, M.L., Aguirrezábal, L.A., Irujo, G.A.P. and Echarte, M.M., 2016. Contribution of incident solar radiation on leaves and pods to soybean seed weight and composition. *European Journal of Agronomy*, **77**, 1–9.

Billen, G., Aguilera, E., Einarsson, R., Garnier, J., Gingrich, S., Grizzetti, B., Lassaletta, L., Le Noë, J. and Sanz-Cobena, A., 2024. Beyond the Farm to Fork Strategy: Methodology for designing a European agro-ecological future. *Science of the Total Environment*, **908**, 168160.

Blanke, M., 2002. Photosynthesis of strawberry fruit. In: *Acta Horticulturae*. International Society for Horticultural Science, **567**, 373–376.

Blanke, M.M. and Lenz, F., 1989. Fruit photosynthesis. *Plant, Cell & Environment*, **12**(1), 31–46.

Blankenagel, S., Yang, Z., Avramova, V., Schön, C.C. and Grill, E., 2018. Generating plants with improved water use efficiency. *Agronomy*, **8**(9), 194.

Blatt, M.R., Jezek, M., Lew, V.L. and Hills, A., 2022. What can mechanistic models tell us about guard cells, photosynthesis, and water use efficiency?. *Trends in Plant Science*, **27**(2), 166–179.

Blessing, C.H., Mariette, A., Kaloki, P. and Bramley, H., 2018. Profligate and conservative: Water use strategies in grain legumes. *Journal of Experimental Botany*, **69**(3), 349–369.

Bota, J., Flexas, J. and Medrano, H., 2001. Genetic variability of photosynthesis and water use in Balearic grapevine cultivars. *Annals of Applied Biology*, **138**(3), 353–361.

Boussadia, O., Steppe, K., Zgallai, H., Ben El Hadj, S., Braham, M., Lemeur, R. and Van Labeke, M.C., 2010. Effects of nitrogen deficiency on leaf photosynthesis, carbohydrate status and biomass production in two olive cultivars 'Meski' and 'Koroneiki'. *Scientia Horticulturae*, **123**(3), 336–342.

Brownlee, C., 2018. Stomatal Physiology: Cereal Successes. *Current Biology*, **28**(9), R551–R553.

Bueckert, R.A., Wagenhoffer, S., Hnatowich, G. and Warkentin, T.D., 2015. Effect of heat and precipitation on pea yield and reproductive performance in the field. Canadian journal of plant science, **95**(4), 629–639.

Burgess, A.J., Masclaux-Daubresse, C., Strittmatter, G., Weber, A.P., Taylor, S.H., Harbinson, J., Yin, X., Long, S., Paul, M.J., Westhoff, P. and Loreto, F., 2023. Improving crop yield potential: Underlying biological processes and future prospects. *Food and Energy Security*, **12**(1), e435.

Burlacot, A., Burlacot, F., Li-Beisson, Y. and Peltier, G., 2020. Membrane Inlet Mass Spectrometry: A Powerful Tool for Algal Research. *Frontiers in Plant Science*, **11**, 1302.

Burstin, J., Salloignon, P., Chabert-Martinello, M., Magnin-Robert, J.B., Siol, M., Jacquin, F., Chauveau, A., Pont, C., Aubert, G., Delaitre, C. and Truntzer, C., 2015. Genetic diversity and trait genomic prediction in a pea diversity panel. *BMC genomics*, **16**, 1–17.

Busch, F.A., 2024. Photosynthetic Gas Exchange in Land Plants at the Leaf Level. In: *Covshoff, S. (eds) Photosynthesis: Methods and Protocols. Methods in Molecular Biology*, **2790**, 41–61. Humana, New York, NY: Springer US.

Caine, R. S., Harrison, E. L., Sloan, J., Flis, P. M., Fischer, S., Khan, M. S., Nguyen, P. T., Nguyen, L. T., Gray, J. E. and Croft, H., 2023. The influences of stomatal size and density on rice abiotic stress resilience. *New Phytologist*, **237**(6), 2180–2195.

Cano, A., Fortunati, E., Cháfer, M., Kenny, J.M., Chiralt, A. and González-Martínez, C., 2015. Properties and ageing behaviour of pea starch films as affected by blend with poly(vinyl alcohol). *Food Hydrocolloids*, **48**, 84–93.

Carlson, K.M. and Garrett, R.D., 2018. Environmental Impacts of Tropical Soybean and Palm Oil Crops. *Oxford Research Encyclopedia of Environmental Science*.

Cassia, R., Nocioni, M., Correa-Aragunde, N. and Lamattina, L., 2018. Climate change and the impact of greenhouse gasses: CO2 and NO, friends and foes of plant oxidative stress. *Frontiers in Plant Science*, **9**, 273.

Cen, Y.P. and Sage, R.F., 2005. The regulation of Rubisco activity in response to variation in temperature and atmospheric CO2 partial pressure in sweet potato. *Plant Physiology*, **139**(2), 979–990.

Chang, T.G., Song, Q.F., Zhao, H.L., Chang, S., Xin, C., Qu, M. and Zhu, X.G., 2020. An in situ approach to characterizing photosynthetic gas exchange of rice panicle. *Plant Methods*, **16**(1), 92.

Chater, C.C.C., Caine, R.S., Fleming, A.J. and Gray, J.E., 2017. Origins and evolution of stomatal development. *Plant Physiology*, **174**(2), 624–638.

Checa, O.E., Rodriguez, M., Wu, X. and Blair, M.W., 2020. Introgression of the Afila Gene into Climbing Garden Pea (Pisum sativum L.). *Agronomy*, **10**(10), 1537.

Chen, B., Shi, Y., Sun, Y., Lu, L., Wang, L., Liu, Z. and Cheng, S., 2024. Innovations in functional genomics and molecular breeding of pea: exploring advances and opportunities. *Abiotech*, **5**(1), 71–93.

Cheng, L. and Fuchigami, L.H., 2000. Rubisco activation state decreases with increasing nitrogen content in apple leaves. *Journal of Experimental Botany*, **51**(351), 1687–1694.

Cho, Y.B., Stutz, S.S., Jones, S.I., Wang, Y., Pelech, E.A. and Ort, D.R., 2023. Impact of pod and seed photosynthesis on seed filling and canopy carbon gain in soybean. *Plant physiology*, **193**(2), 966–979.

Chovancek, E., Zivcak, M., Brestic, M., Hussain, S. and Allakhverdiev, S.I., 2021. The different patterns of post-heat stress responses in wheat genotypes: the role of the transthylakoid proton gradient in efficient recovery of leaf photosynthetic capacity. *Photosynthesis Research*, **1**, 1–15.

Condon, A.G., Richards, R.A., Rebetzke, G.J. and Farquhar, G., 2002. Improving intrinsic water-use efficiency and crop yield. *Crop science*, **42**(1), 122–131.

Conesa, M.À., Muir, C.D., Molins, A. and Galmés, J., 2020. Stomatal anatomy coordinates leaf size with Rubisco kinetics in the Balearic Limonium. *AoB Plants*, **12**(1), plz050.

Conklin, P.A., Strable, J., Li, S. and Scanlon, M.J., 2019. On the mechanisms of development in monocot and eudicot leaves. *New Phytologist*, **221**(2), 706–724.

Côté, R. and Grodzinski, B., 1990. Photosynthesis, Photorespiration and Partitioning in Leaflets, Stipules and Tendrils of Pisum sativum. *Current Research in Photosynthesis*, **1**, 2873–2876.

Côté, R., Gerrath, J.M., Peterson, C.A. and Grodzinski, B., 1992. Sink to source transition in tendrils of a Semileafless mutant, Pisum sativum cv curly. *Plant physiology*, **100**(4), 1640–1648.

Couchoud, M., Salon, C., Girodet, S., Jeudy, C., Vernoud, V., and Prudent, M., 2020. Pea Efficiency of Post-drought Recovery Relies on the Strategy to Fine-Tune Nitrogen Nutrition. *Frontiers in Plant Science*, **11**, 204.

Coyne, C.J., Kumar, S., Wettberg, E.J.B., Marques, E., Berger, J.D., Redden, R.J., Ellis, T.H.N., Brus, J., Zablatzká, L. and Smýkal, P., 2020. Potential and limits of exploitation of crop wild relatives for pea, lentil, and chickpea improvement. *Legume Science*, **2**(2), e36.

Crous, K.Y., Uddling, J. and De Kauwe, M.G., 2022. Temperature responses of photosynthesis and respiration in evergreen trees from boreal to tropical latitudes. *New Phytologist*, **234**(2), 353–374.

Ćupina, B., Krstić, D., Mikić, A., Erić, P., Vučković, S. and Pejić, B., 2010. The effect of field pea (Pisum sativum L.) companion crop management on red clover (Trifolium pratense L.) establishment and productivity. *Turkish Journal of Agriculture and Forestry*, **34**(4), 275–283.

Dahl, W.J., Foster, L.M. and Tyler, R.T., 2012. Review of the health benefits of peas (Pisum sativum L.). *British Journal of Nutrition*, **108**(SUPPL. 1), S3–S10.

Daley, P.F., Raschke, K., Ball, J.T. and Berry, J.A., 1989. Topography of photosynthetic activity of leaves obtained from video images of chlorophyll fluorescence. *Plant Physiology*, **90**(4), 1233–1238.

Damour, G., Vandame, M. and Urban, L., 2008. Long-term drought modifies the fundamental relationships between light exposure, leaf nitrogen content and photosynthetic capacity in leaves of the lychee tree (Litchi chinensis). *Journal of Plant Physiology*, **165**(13), 1370–1378.

Daszkowska-Golec, A. and Szarejko, I., 2013. Open or close the gate - Stomata action under the control of phytohormones in drought stress conditions. *Frontiers in Plant Science*, **4**(MAY), 138.

de la Peña, T.C. and Pueyo, J.J., 2012. Legumes in the reclamation of marginal soils, from cultivar and inoculant selection to transgenic approaches. *Agronomy for Sustainable Development*, **32**(1), 65–91.

de la Riva, E.G., Olmo, M., Poorter, H., Ubera, J.L. and Villar, R., 2016. Leaf mass per area (LMA) and its relationship with leaf structure and anatomy in 34 Mediterranean woody species along a water availability gradient. *PloS one*, **11**(2), e0148788.

De Souza, A.P. and Long, S.P., 2018. Toward improving photosynthesis in cassava: characterizing photosynthetic limitations in four current African cultivars. *Food and energy security*, **7**(2), e00130.

De Souza, A.P., Wang, Y., Orr, D.J., Carmo-Silva, E. and Long, S.P., 2020. Photosynthesis across African cassava germplasm is limited by Rubisco and mesophyll conductance at steady state, but by stomatal conductance in fluctuating light. *New Phytologist*, **225**(6), 2498–2512.

DEFRA (2020). Department for Environment, Food & Rural Affairs Farming statistics - provisional crop areas, yields and livestock populations on 1 June 2020 – United Kingdom, GOV.UK. Accessed on 08 October 2024. https://www.gov.uk/government/statistics/farming-statistics-provisional-crop-areas-yields-and-livestock-populations-at-1-june-2020-united-kingdom.

Dhillon, L.K., Lindsay, D., Yang, T., Zakeri, H., Tar'an, B., Knight, J.D. and Warkentin, T.D., 2022. Biological nitrogen fixation potential of pea lines derived from crosses with nodulation mutants. *Field Crops Research*, **289**, 108731.

Dietz, K.J., Zörb, C. and Geilfus, C.M., 2021. Drought and crop yield. *Plant Biology*, **23**(6), 881–893.

Ding, D., Zhao, Y., Guo, H., Li, X., Schoenau, J. and Si, B., 2018. Water footprint for pulse, cereal, and oilseed crops in Saskatchewan, Canada. *Water (Switzerland)*, **10**(11), 1–24.

Dittberner, H., Korte, A., Mettler-Altmann, T., Weber, A.P.M., Monroe, G. and de Meaux, J., 2018. Natural variation in stomata size contributes to the local adaptation of water-use efficiency in Arabidopsis thaliana. *Molecular Ecology*, **27**(20), 4052–4065.

Domingues, T.F., Meir, P., Feldpausch, T.R., Saiz, G., Veenendaal, E.M., Schrodt, F., Bird, M., Djagbletey, G., Hien, F., Compaore, H., Diallo, A., Grace, J. and Lloyd, J., 2010. Co-limitation of photosynthetic capacity by nitrogen and phosphorus in West Africa woodlands. *Plant, Cell and Environment*, **33**(6), 959–980.

Dong, N., Prentice, I.C., Wright, I.J., Evans, B.J., Togashi, H.F., Caddy-Retalic, S., McInerney, F.A., Sparrow, B., Leitch, E. and Lowe, A.J., 2020. Components of leaf-trait variation along environmental

gradients. *New Phytologist*, **228**(1), 82–94.

Dow, G.J., Berry, J.A. and Bergmann, D.C., 2014a. The physiological importance of developmental mechanisms that enforce proper stomatal spacing in Arabidopsis thaliana. *The New phytologist*, **201**(4), 1205–1217.

Dow, G.J., Bergmann, D.C. and Berry, J.A., 2014b. An integrated model of stomatal development and leaf physiology. *New Phytologist*, **201**(4), 1218–1226.

Drake, P. L., Froend, R. H. and Franks, P. J., 2013. Smaller, faster stomata: scaling of stomatal size, rate of response, and stomatal conductance. *Journal of Experimental Botany*, **64**(2), 495–505.

Driesen, E., Van den Ende, W., De Proft, M. and Saeys, W., 2020. Influence of environmental factors light, CO2, temperature, and relative humidity on stomatal opening and development: A review. *Agronomy*, **10**(12), 1975.

Driever, S.M., Lawson, T., Andralojc, P.J., Raines, C.A. and Parry, M.A.J., 2014. Natural variation in photosynthetic capacity, growth, and yield in 64 field-grown wheat genotypes. *Journal of Experimental Botany*, **65**(17), 4959–4973.

Driever, S.M., Simkin, A.J., Alotaibi, S., Fisk, S.J., Madgwick, P.J., Sparks, C.A., Jones, H.D., Lawson, T., Parry, M.A.J. and Raines, C.A., 2017. Increased sbpase activity improves photosynthesis and grain yield in wheat grown in greenhouse conditions. *Philosophical Transactions of the Royal Society B: Biological Sciences*, **372**(1730), 20160384.

Driscoll, A.W., Bitter, N.Q., Sandquist, D.R. and Ehleringer, J.R., 2020. Multidecadal records of intrinsic water-use efficiency in the desert shrub Encelia farinosa reveal strong responses to climate change. *Proceedings of the National Academy of Sciences of the United States of America*, **117**(31), 18161–18168.

Du, T., Meng, P., Huang, J., Peng, S. and Xiong, D., 2020. Fast photosynthesis measurements for phenotyping photosynthetic capacity of rice. *Plant Methods*, **16**(1), 6.

Du, X., Zhang, X., Chen, X., Jin, W., Huang, Z. and Kong, L., 2024. Drought stress reduces the photosynthetic source of subtending leaves and the transit sink function of podshells, leading to reduced seed weight in soybean plants. *Frontiers in Plant Science*, **15**, 1337544.

Duursma, R.A., 2015. Plantecophys-an R package for analysing and modelling leaf gas exchange data. *PloS one*, **10**(11), e0143346.

Easlon, H.M., Nemali, K.S., Richards, J.H., Hanson, D.T., Juenger, T.E. and McKay, J.K., 2014. The physiological basis for genetic variation in water use efficiency and carbon isotope composition in Arabidopsis thaliana. *Photosynthesis Research*, **119**(1–2), 119–129.

Edwards, E.J., 2019. Evolutionary trajectories, accessibility and other metaphors: the case of C4 and CAM photosynthesis. *New Phytologist*, **223**(4), 1742–1755.

Elazab, A., Moraga, F. and del Pozo, A., 2021. Photosynthetic organs contributions to grain yield genetic gains in Chilean winter wheat. *Agronomy Journal*, **113**(6), 5006–5026.

Elliott-Kingston, C., Haworth, M., Yearsley, J. M., Batke, S. P., Lawson, T. and McElwain, J. C., 2016. Does size matter? Atmospheric CO2 may be a stronger driver of stomatal closing rate than stomatal size in taxa that diversified under low CO2. *Frontiers in Plant Science*, **7**, 197656.

Elliott, J., Deryng, D., Müller, C., Frieler, K., Konzmann, M., Gerten, D., Glotter, M., Flörke, M., Wada, Y., Best, N. et al., 2014. Constraints and potentials of future irrigation water availability on agricultural production under climate change. *Proceedings of the National Academy of Sciences of the United States of America*, **111**(9), 3239–3244.

Ellis, T.H.N., Hofer, J.M., Vikeli, E., Ambrose, M.J., Higuera-Poveda, P., Wingen, L.U. and Chayut, N.,

2021. Diversity of pod shape in Pisum. *Diversity*, **13**(5), 203.

Elsheery, N.I. and Cao, K.F., 2008. Gas exchange, chlorophyll fluorescence, and osmotic adjustment in two mango cultivars under drought stress. *Acta Physiologiae Plantarum*, **30**, 769–777.

Ennajeh, M., Vadel, A.M., Cochard, H. and Khemira, H., 2010. Comparative impacts of water stress on the leaf anatomy of a drought-resistant and a drought-sensitive olive cultivar. *The Journal of Horticultural Science and Biotechnology*, **85**(4), 289–294.

Evans, J.R., 1989. Photosynthesis and nitrogen relationships in leaves of C3 plants. *Oecologia*, **78**(1), 9–19.

Evans, J.R., 2013. Improving photosynthesis. *Plant Physiology*, **162**(4), 1780–1793.

Evans, J.R., 2020. Mesophyll conductance: walls, membranes and spatial complexity. *New Phytologist*, **229**(4), 1864–1876.

Evans, L.T. and Fischer, R.A., 1999. Yield potential: its definition, measurement, and significance. *Crop science*, **39**(6), 1544–1551.

Evans, J.R. and von Caemmerer, S., 1996. Carbon dioxide diffusion inside leaves. *Plant physiology*, **110**(2), 339.

Eyland, D., van Wesemael, J., Lawson, T. and Carpentier, S., 2021. The impact of slow stomatal kinetics on photosynthesis and water use efficiency under fluctuating light. *Plant Physiology*, **186**(2), 998–1012.

Faisal, M., Sarnaik, A.P., Kannoju, N., Hajinajaf, N., Asad, M.J., Davis, R.W. and Varman, A.M., 2024. RuBisCO activity assays: a simplified biochemical redox approach for in vitro quantification and an RNA sensor approach for in vivo monitoring. *Microbial Cell Factories*, **23**(1), 83.

Fanourakis, D., Giday, H., Milla, R., Pieruschka, R., Kjaer, K.H., Bolger, M., Vasilevski, A., Nunes-Nesi, A., Fiorani, F. and Ottosen, C.O., 2015. Pore size regulates operating stomatal conductance, while stomatal densities drive the partitioning of conductance between leaf sides. *Annals of botany*, **115**(4), 555–565.

FAOSTAT. (2024). Crops and Livestock Products: Production/Yield Quantities of Peas, dry/green for 1970-2020. Accessed on 08 October 2024. https://www.fao.org/faostat/en/#data/QCL/visualize. Licence: CC-BY-4.0.

Faralli, M. and Lawson, T., 2020. Natural genetic variation in photosynthesis: an untapped resource to increase crop yield potential? *Plant Journal*, **101**(3), 518–528.

Faralli, M., Bontempo, L., Bianchedi, P.L., Moser, C., Bertamini, M., Lawson, T., Camin, F., Stefanini, M. and Varotto, C., 2022. Natural variation in stomatal dynamics drives divergence in heat stress tolerance and contributes to seasonal intrinsic water-use efficiency in Vitis vinifera (subsp. sativa and sylvestris). *Journal of Experimental Botany*, **73**(10), 3238–3250.

Faralli, M., Matthews, J. and Lawson, T., 2019. Exploiting natural variation and genetic manipulation of stomatal conductance for crop improvement. *Current Opinion in Plant Biology*, **49**, 1–7.

Farooq, M., Ahmad, R., Shahzad, M., Sajjad, Y., Hassan, A., Shah, M.M., Naz, S. and Khan, S.A., 2021. Differential variations in total flavonoid content and antioxidant enzymes activities in pea under different salt and drought stresses. *Scientia Horticulturae*, **287**, 110258.

Farquhar, G.D., von Caemmerer, S. and Berry, J.A., 1980. A biochemical model of photosynthetic CO2 assimilation in leaves of C3 species. *Planta*, **149**(1), 78–90.

Farquhar, G.D., O'Leary, M.H. and Berry, J.A., 1982. On the relationship between carbon isotope discrimination and the intercellular carbon dioxide concentration in leaves. *Functional Plant Biology*, **9**(2), 121–137.

Ferguson, J.N., Humphry, M., Lawson, T., Brendel, O. and Bechtold, U., 2018. Natural variation of life-history traits, water use, and drought responses in Arabidopsis. *Plant Direct*, **2**(1), e00035.

Flexas, J., Galmés, J., Gallé, A., Gulías, J., Pou, A., Ribas-Carbo, M., Tomàs, M. and Medrano, H., 2010. Improving water use efficiency in grapevines: Potential physiological targets for biotechnological improvement. *Australian Journal of Grape and Wine Research*, **16**(SUPPL. 1), 106–121.

Foyer, C.H., 2018. Reactive oxygen species, oxidative signaling and the regulation of photosynthesis. *Environmental and Experimental Botany*, **154**, 134–142.

Franks, P.J. and Casson, S., 2014. Connecting stomatal development and physiology. *New Phytologist*, **201**(4), 1079–1082.

Fraser, L.H., Greenall, A., Carlyle, C., Turkington, R. and Friedman, C.R., 2009. Adaptive phenotypic plasticity of Pseudoroegneria spicata: response of stomatal density, leaf area and biomass to changes in water supply and increased temperature. *Annals of Botany*, **103**(5), 769–775.

Furbank, R.T., Sharwood, R., Estavillo, G.M., Silva-Perez, V. and Condon, A.G., 2020. Photons to food: Genetic improvement of cereal crop photosynthesis. *Journal of Experimental Botany*, **71**(7), 2226–2238.

Galanakis, C.M., 2024. The future of food. *Foods*, **13**(4), 506.

Galdon-Armero, J., Fullana-Pericas, M., Mulet, P.A., Conesa, M.A., Martin, C. and Galmes, J., 2018. The ratio of trichomes to stomata is associated with water use efficiency in Solanum lycopersicum (tomato). *Plant Journal*, **96**(3), 607–619.

Galmés, J., Ochogavía, J.M., Gago, J., Roldán, E.J., Cifre, J. and Conesa, M.À., 2013. Leaf responses to drought stress in Mediterranean accessions of Solanum lycopersicum: Anatomical adaptations in relation to gas exchange parameters. *Plant, Cell and Environment*, **36**(5), 920–935.

Garrido, A., Conde, A., Serôdio, J., De Vos, R.C. and Cunha, A., 2023. Fruit photosynthesis: more to know about where, how and why. *Plants*, **12**(13), 2393.

Geber, M.A. and Dawson, T.E., 1997. Genetic variation in stomatal and biochemical limitations to photosynthesis in the annual plant, Polygonum arenastrum. *Oecologia*, **109**, 535–546.

Gebreegziabher, B.G. and Tsegay, B.A., 2020. Proximate and mineral composition of Ethiopian pea (Pisum sativum var. abyssinicum A. Braun) landraces vary across altitudinal ecosystems. *Cogent Food & Agriculture*, **6**(1), 1789421.

Gilbert, M.E., Zwieniecki, M.A. and Holbrook, N.M., 2011. Independent variation in photosynthetic capacity and stomatal conductance leads to differences in intrinsic water use efficiency in 11 soybean genotypes before and during mild drought. *Journal of Experimental Botany*, **62**(8), 2875–2887.

Giovanardi, M., Pantaleoni, L., Ferroni, L., Pagliano, C., Albanese, P., Baldisserotto, C. and Pancaldi, S., 2018. In pea stipules a functional photosynthetic electron flow occurs despite a reduced dynamicity of LHCII association with photosystems. *Biochimica et Biophysica Acta - Bioenergetics*, **1859**(10), 1025–1038.

Giuliani, R., Koteyeva, N., Voznesenskaya, E., Evans, M.A., Cousins, A.B. and Edwards, G.E., 2013. Coordination of leaf photosynthesis, transpiration, and structural traits in rice and wild relatives (genus Oryza). *Plant physiology*, **162**(3), 1632–1651.

Golmohammadi, M., Sofalian, O., Taheri, M., Ghanbari, A. and Rasoli, V., 2020. Changes in fruit yield and photosynthesis parameters in different olive cultivars (Olea europaea L.) under contrasting water regimes. *Acta Scientiarum Polonorum Hortorum Cultus*, **19**(3), 135–147.

Gonzalez, E.M., Arrese-Igor, C., Aparicio-Tejo, P.M., Royuela, M. and Koyro, H.W., 2002. Solute heterogeneity and osmotic adjustment in different leaf structures of semi-leafless pea (Pisum sativum L.) subjected to water stress. *Plant Biology*, **4**(5), 558–566.

Gray, A., Liu, L. and Facette, M., 2020. Flanking Support: How Subsidiary Cells Contribute to Stomatal Form and Function. *Frontiers in Plant Science*, **11**, 881.

Gresset, S., Westermeier, P., Rademacher, S., Ouzunova, M., Presterl, T., Westhoff, P. and Schön, C.C., 2014. Stable carbon isotope discrimination is under genetic control in the C4 species maize with several genomic regions influencing trait expression. *Plant Physiology*, **164**(1), 131–143.

Gresshoff, P.M., Hayashi, S., Biswas, B., Mirzaei, S., Indrasumunar, A., Reid, D., Samuel, S., Tollenaere, A., van Hameren, B., Hastwell, A., Scott, P. and Ferguson, B.J., 2015. The value of biodiversity in legume symbiotic nitrogen fixation and nodulation for biofuel and food production. *Journal of Plant Physiology*, **172**, 128–136.

Gu, J., Yin, X., Stomph, T.J. and Struik, P.C., 2014. Can exploiting natural genetic variation in leaf photosynthesis contribute to increasing rice productivity? A simulation analysis. *Plant, Cell and Environment*, **37**(1), 22–34.

Guerrieri, R., Belmecheri, S., Ollinger, S. V., Asbjornsen, H., Jennings, K., Xiao, J., Stocker, B.D., Martin, M., Hollinger, D.Y., Bracho-Garrillo, R., et al., 2019. Disentangling the role of photosynthesis and stomatal conductance on rising forest water-use efficiency. *Proceedings of the National Academy of Sciences of the United States of America*, **116**(34), 16909–16914.

Hagemann, M. and Bauwe, H., 2016. Photorespiration and the potential to improve photosynthesis. *Current Opinion in Chemical Biology*, **35**, 109–116.

Haile, G. G., Tang, Q., Sun, S., Huang, Z., Zhang, X., and Liu, X., 2019. Droughts in East Africa: Causes, impacts and resilience. *Earth-Science Reviews*, **193**, 146–161.

Han, J., Lei, Z., Flexas, J., Zhang, Y., Carriquí, M., Zhang, W. and Zhang, Y., 2018. Mesophyll conductance in cotton bracts: Anatomically determined internal CO2 diffusion constraints on photosynthesis. *Journal of Experimental Botany*, **69**(22), 5433–5443.

Han, J., Lei, Z., Zhang, Y., Yi, X., Zhang, W. and Zhang, Y., 2019. Drought-introduced variability of mesophyll conductance in Gossypium and its relationship with leaf anatomy. *Physiologia Plantarum*, **166**(3), 873–887.

Hanci, F. and Cebeci, E., 2019. Relationships among cultivated peas and their wild relatives: Molecular and morphological characterization. *Bangladesh Journal of Botany*, **48**(4), 1011–1019.

Harrison, E. L., Arce Cubas, L., Gray, J. E. and Hepworth, C., 2020. The influence of stomatal morphology and distribution on photosynthetic gas exchange. *The Plant Journal*, **101**(4), 768–779.

Harrison, E.P., Olcer, H., Lloyd, J.C., Long, S.P. and Raines, C.A., 2001. Small decreases in SBPase cause a linear decline in the apparent RuBP regeneration rate, but do not affect Rubisco carboxylation capacity. *Journal of Experimental Botany*, **52**(362), 1779–1784.

Hasanuzzaman, M., Zhou, M. and Shabala, S., 2023. How does stomatal density and residual transpiration contribute to osmotic stress tolerance?. *Plants*, **12**(3), 494.

Hatfield, J.L. and Dold, C., 2019. Water-use efficiency: Advances and challenges in a changing climate. *Frontiers in Plant Science*, **10**, 103.

He, P., Wright, I.J., Zhu, S., Onoda, Y., Liu, H., Li, R., Liu, X., Hua, L., Oyanoghafo, O.O. and Ye, Q., 2019. Leaf mechanical strength and photosynthetic capacity vary independently across 57 subtropical forest species with contrasting light requirements. *New Phytologist*, **223**(2), 607–618.

Heath, M.C. and Hebblethwaite, P.D., 1985. Solar radiation interception by leafless, semi-leafless and leafed peas (Pisum sativum) under contrasting field conditions. *Annals of Applied Biology*, **107**(2), 309–318.

Heath, M.C., Pilbeam, C.J., McKenzie, B.A. and Hebblethwaite, P.D., 1994. Plant architecture, competitive ability and crop productivity in food legumes with particular emphasis on pea (*Pisum sativum* L.) and faba bean (*Vicia faba* L.). In: Muehlbauer F, Kaiser W (eds) Expanding the production and use of cool season food legumes. *Current plant science and biotechnology in agriculture*, **19**. Springer, Dordrecht, 771–790.

Hein, J.A., Sherrard, M.E., Manfredi, K.P. and Abebe, T., 2016. The fifth leaf and spike organs of barley (Hordeum vulgare L.) display different physiological and metabolic responses to drought stress. *BMC plant biology*, **16**, 1–12.

Hellwig, T., Abbo, S., Sherman, A. and Ophir, R., 2021. Prospects for the natural distribution of crop wild-relatives with limited adaptability: The case of the wild pea Pisum fulvum. *Plant Science*, **310**, 110957.

Henry, R.J., Furtado, A. and Rangan, P., 2020. Pathways of photosynthesis in non-leaf tissues. *Biology*, **9**(12), 438.

Hepworth, C., Caine, R.S., Harrison, E.L., Sloan, J. and Gray, J.E., 2018. Stomatal development: focusing on the grasses. *Current Opinion in Plant Biology*, **41**, 1–7.

Hetherington, A.M. and Woodward, F.I., 2003. The role of stomata in sensing and driving environmental change. *Nature*, **424**(6951), 901–908.

Hibberd, J.M. and Quick, W.P., 2002. Characteristics of C4 photosynthesis in stems and petioles of C3 flowering plants. *Nature*, **415**(6870), 451–454.

Hikosaka, K. and Shigeno, A., 2009. The role of Rubisco and cell walls in the interspecific variation in photosynthetic capacity. *Oecologia*, **160**(3), 443–451.

Hiratsuka, S., Suzuki, M., Nishimura, H. and Nada, K., 2015. Fruit photosynthesis in Satsuma mandarin. *Plant Science*, **241**, 65–69.

Hoekstra, A.Y., 2015. The water footprint: The relation between human consumption and water use. *The Water We Eat: Combining Virtual Water and Water Footprints*. Springer, Cham, 35–48.

Hong, T., Lin, H. and He, D., 2018. Characteristics and correlations of leaf stomata in different Aleurites Montana provenances. *PLoS ONE*, **13**(12), e0208899.

Hossain, M.A., Bhattacharjee, S., Armin, S.M., Qian, P., Xin, W., Li, H.Y., Burritt, D.J., Fujita, M. and Tran, L.S.P., 2015. Hydrogen peroxide priming modulates abiotic oxidative stress tolerance: Insights from ROS detoxification and scavenging. *Frontiers in Plant Science*, **6**(June), 420.

Hradilová, I., Duchoslav, M., Brus, J., Pechanec, V., Hýbl, M., Kopecký, P., Smržová, L., Štefelová, N., Vaclávek, T., Bariotakis, M., Machalová, J., Hron, K., Pirintsos, S. and Smýkal, P., 2019. Variation in wild pea (Pisum sativum subsp. elatius) seed dormancy and its relationship to the environment and seed coat traits. *PeerJ*, **2019**(1), e6263.

Hu, L., Zhang, Y., Xia, H., Fan, S., Song, J., Lv, X. and Kong, L., 2019. Photosynthetic characteristics of non-foliar organs in main C3 cereals. *Physiologia plantarum*, **166**(1), 226–239.

Hu, Y.Y., Zhang, Y.L., Luo, H.H., Li, W., Oguchi, R., Fan, D.Y., Chow, W.S. and Zhang, W.F., 2012. Important photosynthetic contribution from the non-foliar green organs in cotton at the late growth stage. *Planta*, **235**(2), 325–336.

Hu, Y.Y., Zhang, Y.L., Yi, X.P., Zhan, D.X., Luo, H.H., Soon, C.W. and Zhang, W.F., 2014. The relative contribution of non-foliar organs of cotton to yield and related physiological characteristics under water deficit. *Journal of Integrative Agriculture*, **13**(5), 975–989.

Huang, M., Shan, S., Zhou, X., Chen, J., Cao, F., Jiang, L. and Zou, Y., 2016. Leaf photosynthetic performance related to higher radiation use efficiency and grain yield in hybrid rice. *Field Crops Research*, **193**, 87–93.

Huang, W., Zhang, S.B. and Hu, H., 2014. Sun leaves up-regulate the photorespiratory pathway to maintain a high rate of CO2 assimilation in tobacco. *Frontiers in Plant Science*, **5**(DEC), 688.

Iñiguez, C., Aguiló-Nicolau, P. and Galmés, J., 2021. Improving photosynthesis through the enhancement of Rubisco carboxylation capacity. *Biochemical Society Transactions*, **49**(5), 2007–2019.

Ismail, I.M., Basahi, J.M. and Hassan, I.A., 2014. Gas exchange and chlorophyll fluorescence of pea (Pisum sativum L.) plants in response to ambient ozone at a rural site in Egypt. *Science of the total environment*, **497**, 585–593.

Jafarinasab, A., Azari, A., Siddique, K.H. and Madahhosseini, S., 2022. Variation of yield and physiological characteristics of Lathyrus sativus L. populations under terminal drought. *Agricultural Water Management*, **273**, 107886.

Javadian, M., Scott, R.L., Biederman, J.A., Zhang, F., Fisher, J.B., Reed, S.C., Potts, D.L., Villarreal, M.L., Feldman, A.F. and Smith, W.K., 2023. Thermography captures the differential sensitivity of dryland functional types to changes in rainfall event timing and magnitude. *New Phytologist*, **240**(1), 114–126.

Jiang, C., Ryu, Y., Wang, H. and Keenan, T.F., 2020. An optimality-based model explains seasonal variation in C3 plant photosynthetic capacity. *Global Change Biology*, **26**(11), 6493–6510.

Jiang, H., Hu, F., Fu, X., Chen, C., Wang, C., Tian, L. and Shi, Y., 2023. YOLOv8-Peas: a lightweight drought tolerance method for peas based on seed germination vigor. *Frontiers in Plant Science*, **14**, 1257947.

Jiao, Y., Niklas, K.J., Wang, L., Yu, K., Li, Y. and Shi, P., 2022. Influence of leaf age on the scaling relationships of lamina mass vs. area. *Frontiers in Plant Science*, **13**, 860206

Jing, R., Johnson, R., Seres, A., Kiss, G., Ambrose, M.J., Knox, M.R., Ellis, T.H.N. and Flavell, A.J., 2007. Gene-based sequence diversity analysis of field pea (Pisum). *Genetics*, **177**(4), 2263–2275.

Joseph, P., Searing, A., Watson, C. and McKeague, J., 2020. Alternative proteins: Market research on consumer trends and emerging landscape. *Meat and Muscle Biology*, **4**(2).

Kaiser, E., Morales, A., Harbinson, J., Kromdijk, J., Heuvelink, E. and Marcelis, L.F.M., 2015. Dynamic photosynthesis in different environmental conditions. *Journal of Experimental Botany*, **66**(9), 2415–2426.

Kantar, F., Shivakumar, B.G., Arrese-Igor, C., Hafeez, F.Y., González, E.M., Imran, A. and Larrainzar, E., 2010. Efficient biological nitrogen fixation under warming climates. *Climate Change and Management of Cool Season Grain Legume Crops*, 283–306.

Kardiman, R. and Ræbild, A., 2018. Relationship between stomatal density, size and speed of opening in Sumatran rainforest species. *Tree Physiology*, **38**(5), 696–705.

Kennedy, J.J., Killick, R.E., Dunn, R.J., McCarthy, M.P., Morice, C.P., Rayner, N.A. and Titchner, H.A., 2019. Global and regional climate in 2018. *Weather*, **74**(10), 332–340.

Khatun, M., Sarkar, S., Era, F. M., Islam, A. K. M. M., Anwar, M. P., Fahad, S., Datta, R., and Islam, A. K. M. A., 2021. Drought Stress in Grain Legumes: Effects, Tolerance Mechanisms and Management. *Agronomy,* **11**(12), 2374.

Kim, M., Hepler, P.K., Eun, S.O., Ha, K.S. and Lee, Y., 1995. Actin filaments in mature guard cells are radially distributed and involved in stomatal movement. *Plant Physiology*, **109**(3), 1077–1084.

Kim, W., Iizumi, T. and Nishimori, M., 2019. Global patterns of crop production losses associated with droughts from 1983 to 2009. *Journal of Applied Meteorology and Climatology*, **58**(6), 1233–1244.

Knorr, D. and Augustin, M.A., 2024. The future of foods. *Sustainable Food Technology*, **2**(2), 253–265.

Kosterin, O.E., 2017. On three cultivated subspecies of pea (Pisum sativum L.). *Vavilovskii Zhurnal Genetiki i Selektsii*, **21**(6), 694–700.

Kreplak, J., Madoui, M.A., Cápal, P., Novák, P., Labadie, K., Aubert, G., Bayer, P.E., Gali, K.K., Syme, R.A., Main, D., et al., 2019. A reference genome for pea provides insight into legume genome evolution. *Nature Genetics*, **51**(9), 1411–1422.

Kromdijk, J. and Long, S.P., 2016. One crop breeding cycle from starvation? How engineering crop photosynthesis for rising CO2 and temperature could be one important route to alleviation. *Proceedings of the Royal Society B: Biological Sciences*, **283**(1826), 20152578.

Kromdijk, J., Głowacka, K. and Long, S.P., 2020. Photosynthetic efficiency and mesophyll conductance are unaffected in Arabidopsis thaliana aquaporin knock-out lines. *Journal of Experimental Botany*, **71**(1), 318–329.

Kumar, V., Sharma, A., Soni, J.K. and Pawar, N., 2019. Physiological response of C3 , C4 and CAM plants in changeable climate. *The Pharma Innovation Journal*, **6**(9), 70–79.

Lafond, G. and Evans, L.E., 1981. A Comparative Study of Conventional, Leafless And Semi-Leafless Phenotypes Of Peas: Photosynthetic CO2 Fixation In Vitro. *Canadian Journal of Plant Science*, **61**(3), 665–671.

Lafond, G., Evans, L.E. and Ali-Khan, S.T., 1981. Comparison of near-isogenic leafed, leafless, semi-leafless, and reduced stipule lines of peas for yield and associated traits. Canadian Journal of plant science, **61**(2), 463–465.

Lara, S.W. and Tsiami, A., 2024. A Lexicon of Descriptive Sensory Terms for Peas (*Pisum sativum* L.): A Systematic Review. Foods, **13**(14), 2290.

Lauteri, M., Haworth, M., Serraj, R., Monteverdi, M.C. and Centritto, M., 2014. Photosynthetic diffusional constraints affect yield in drought stressed rice cultivars during flowering. *PloS one*, **9**(10), e109054.

Lawson, T. and Blatt, M.R., 2014. Stomatal Size, Speed, and Responsiveness Impact on Photosynthesis and Water Use Efficiency. *Plant Physiology*, **164**(4), 1556–1570.

Lawson, T. and Matthews, J., 2020. Guard cell metabolism and stomatal function. *Annual review of plant biology*, **71**(1), 273–302.

Lawson, T. and Milliken, A.L., 2023. Photosynthesis–beyond the leaf. *New Phytologist*, **238**(1), 55–61.

Lawson, T. and Vialet-Chabrand, S., 2019. Speedy stomata, photosynthesis and plant water use efficiency. *New Phytologist*, **221**(1), 93–98.

Lawson, T. and Vialet-Chabrand, S., 2024. Imaging Spatial and Temporal Variation in Photosynthesis Using Chlorophyll Fluorescence. In: *Covshoff, S. (eds) Photosynthesis: Methods and Protocols. Methods in Molecular Biology*, **2790**, 293–316. Humana, New York, NY: Springer US.

Lawson, T. and Weyers, J., 1999. Spatial and temporal variation in gas exchange over the lower surface of Phaseolus vulgaris L. primary leaves. *Journal of Experimental Botany*, **50**(337), 1381–1391.

Lawson, T., James, W. and Weyers, J., 1998. A surrogate measure of stomatal aperture. *Journal of Experimental Botany*, **49**(325), 1397–1403.

Lawson, T., Kramer, D.M. and Raines, C.A., 2012. Improving yield by exploiting mechanisms underlying natural variation of photosynthesis. *Current Opinion in Biotechnology*, **23**(2), 215–220.

Leakey, A.D.B., Ferguson, J.N., Pignon, C.P., Wu, A., Jin, Z., Hammer, G.L. and Lobell, D.B., 2019. Water Use Efficiency as a Constraint and Target for Improving the Resilience and Productivity of C3 and C4 Crops. *Annual Review of Plant Biology*, **70**(1), 781–808.

Lei, Z., Liu, F., Wright, I.J., Carriquí, M., Niinemets, Ü., Han, J., Jia, M., Atwell, B.J., Cai, X., Zhang, W. and Zhou, Z., 2022. Comparisons of photosynthetic and anatomical traits between wild and domesticated cotton. *Journal of Experimental Botany*, **73**(3), 873–885.

Leigh, A., Sevanto, S., Ball, M.C., Close, J.D., Ellsworth, D.S., Knight, C.A., Nicotra, A.B. and Vogel, S., 2012. Do thick leaves avoid thermal damage in critically low wind speeds?. *New Phytologist*, **194**(2), 477–487.

Leverett, A. and Kromdijk, J., 2024. The long and tortuous path towards improving photosynthesis by engineering elevated mesophyll conductance. *Plant, Cell & Environment*. **47**(9), 3411–3427.

Li, Y., Li, H., Li, Y. and Zhang, S., 2017. Improving water-use efficiency by decreasing stomatal conductance and transpiration rate to maintain higher ear photosynthetic rate in drought-resistant wheat. *Crop Journal*, **5**(3), 231–239.

Li, Y.T., Li, Y., Li, Y.N., Liang, Y., Sun, Q., Li, G., Liu, P., Zhang, Z.S. and Gao, H.Y., 2020. Dynamic light caused less photosynthetic suppression, rather than more, under nitrogen deficit conditions than under sufficient nitrogen supply conditions in soybean. *BMC Plant Biology*, **20**(1), 1–13.

Liang, G., Liu, J., Zhang, J. and Guo, J., 2020. Effects of drought stress on photosynthetic and physiological parameters of tomato. *Journal of the American Society for Horticultural Science*, **145**(1), 12–17.

Limousin, J.M., Misson, L., Lavoir, A.V., Martin, N.K. and Rambal, S., 2010. Do photosynthetic limitations of evergreen Quercus ilex leaves change with long-term increased drought severity?. *Plant, Cell & Environment*, **33**(5), 863–875.

Ljuština, M., Mikić, A., Mikić, A. and Ljuština, M., 2010. Early Distribution of Pea in Europe A Brief Review on the Early Distribution of Pea (Pisum sativum L.) in Europe. *Crop Res*, **47**, 457–460.

Lombardini, L., Restrepo-Diaz, H. and Volder, A., 2009. Photosynthetic light response and epidermal characteristics of sun and shade pecan leaves. *Journal of the American Society for Horticultural Science*, **134**(3), 372–378.

Lombardozzi, D.L., Smith, N.G., Cheng, S.J., Dukes, J.S., Sharkey, T.D., Rogers, A., Fisher, R. and Bonan, G.B., 2018. Triose phosphate limitation in photosynthesis models reduces leaf photosynthesis and global terrestrial carbon storage. *Environmental Research Letters*, **13**(7), e074025.

Long, S.P., Taylor, S.H., Burgess, S.J., Carmo-Silva, E., Lawson, T., De Souza, A.P., Leonelli, L. and Wang, Y., 2022. Into the shadows and back into sunlight: photosynthesis in fluctuating light. *Annual Review of Plant Biology*, **73**(1), 617–648.

Long, S.P., Marshall-Colon, A. and Zhu, X.G., 2015. Meeting the global food demand of the future by engineering crop photosynthesis and yield potential. *Cell*, **161**(1), 56–66.

Long, S.P., Zhu, X.G., Naidu, S.L. and Ort, D.R., 2006. Can improvement in photosynthesis increase crop yields? *Plant, Cell and Environment*, **29**(3), 315–330.

López-Calcagno, P.E., Brown, K.L., Simkin, A.J., Fisk, S.J., Vialet-Chabrand, S., Lawson, T. and Raines, C.A., 2020. Stimulating photosynthetic processes increases productivity and water-use efficiency in the field. *Nature Plants*, **6**(8), 1054–1063.

Lou, L., Li, X., Chen, J., Li, Y., Tang, Y. and Lv, J., 2018. Photosynthetic and ascorbate-glutathione metabolism in the flag leaves as compared to spikes under drought stress of winter wheat (Triticum aestivum L.). *PLoS One*, **13**(3), e0194625.

Lv, X., Li, Y., Chen, R., Rui, M. and Wang, Y., 2023. Stomatal responses of two drought-tolerant barley varieties with different ROS regulation strategies under drought conditions. *Antioxidants*, **12**(4), 790.

Ma, Q., Behboudian, M.H., Turner, N.C. and Palta, J.A., 2001. Gas exchange by pods and subtending leaves and internal recycling of CO2 by pods of chickpea (Cicer arietinum L.) subjected to water deficits. *Journal of Experimental Botany*, **52**(354), 123–131.

MACHEREY-NAGEL., 2023. User Manual for Protein Quantification Assay (online). Available from https://www.mn-net.com/media/pdf/ec/f9/48/Instruction-Protein-Quantification-Assay.pdf (last accessed 10 April 2024).

Macnicol, P.K. and Jacobsen, J.V., 1992. Endosperm acidification and related metabolic changes in the developing barley grain. *Plant Physiology*, **98**(3), 1098–1104.

MacWilliam, S., Wismer, M. and Kulshreshtha, S., 2014. Life cycle and economic assessment of Western Canadian pulse systems: the inclusion of pulses in crop rotations. *Agricultural Systems*, **123**, 43–53.

Magyar-Tábori, K., Mendler-Drienyovszki, N. and Dobránszki, J., 2011. Models and tools for studying drought stress responses in peas. *OMICS: A Journal of Integrative Biology*, **15**(12), 829–838.

Makino, A. and Osmond, B., 1991. Effects of nitrogen nutrition on nitrogen partitioning between chloroplasts and mitochondria in pea and wheat. *Plant Physiology*, **96**(2), 355–362.

Makino, A., 2003. Rubisco and nitrogen relationships in rice: Leaf photosynthesis and plant growth. *Soil Science and Plant Nutrition*, **49**(3), 319–327.

Martínez-Peña, R., Schlereth, A., Höhne, M., Encke, B., Morcuende, R., Nieto-Taladriz, M.T., Araus, J.L., Aparicio, N. and Vicente, R., 2022. Source-sink dynamics in field-grown durum wheat under contrasting nitrogen supplies: key role of non-foliar organs during grain filling. *Frontiers in Plant Science*, **13**, 869680.

Martinez, D.E., Luquez, V.M., Bartoli, C.G. and Guiamet, J.J., 2003. Persistence of photosynthetic components and photochemical efficiency in ears of water-stressed wheat (Triticum aestivum). *Physiologia Plantarum*, **119**(4), 519–525.

Mathobo, R., Marais, D. and Steyn, J.M., 2017. The effect of drought stress on yield, leaf gaseous exchange and chlorophyll fluorescence of dry beans (Phaseolus vulgaris L.). *Agricultural Water Management*, **180**, 118–125.

Matthews, J.S., Vialet-Chabrand, S.R. and Lawson, T., 2017. Diurnal variation in gas exchange: the balance between carbon fixation and water loss. *Plant Physiology*, **174**(2), 614–623.

Matthews, J.S.A., Vialet-Chabrand, S. and Lawson, T., 2020. Role of blue and red light in stomatal dynamic behaviour. *Journal of Experimental Botany*, **71**(7), 2253–2269.

Maurino, V.G., 2019. Using energy-efficient synthetic biochemical pathways to bypass photorespiration. *Biochemical Society Transactions*, **47**(6), 1805–1813.

Maydup, M.L., Antonietta, M., Graciano, C., Guiamet, J.J. and Tambussi, E.A., 2014. The contribution of the awns of bread wheat (Triticum aestivum L.) to grain filling: Responses to water deficit and the effects of awns on ear temperature and hydraulic conductance. *Field Crops Research*, **167**, 102–111.

Maydup, M.L., Antonietta, M., Guiamet, J.J., Graciano, C., López, J.R. and Tambussi, E.A., 2010. The contribution of ear photosynthesis to grain filling in bread wheat (Triticum aestivum L.). *Field Crops Research*, **119**(1), 48–58.

Mbava, N., Mutema, M., Zengeni, R., Shimelis, H. and Chaplot, V., 2020. Factors affecting crop water use efficiency: A worldwide meta-analysis. *Agricultural Water Management*, **228**, e105878.

McAusland, L. and Murchie, E.H., 2020. Start me up; harnessing natural variation in photosynthetic induction to improve crop yields. *New Phytologist*, **227**(4), 989–991.

McAusland, L., Atkinson, J.A., Lawson, T. and Murchie, E.H., 2019. High throughput procedure utilising chlorophyll fluorescence imaging to phenotype dynamic photosynthesis and photoprotection in leaves under controlled gaseous conditions. *Plant Methods*, **15**(1), 109.

McAusland, L., Davey, P.A., Kanwal, N., Baker, N.R. and Lawson, T., 2013. A novel system for spatial and temporal imaging of intrinsic plant water use efficiency. *Journal of Experimental Botany*, **64**(16), 4993–5007.

McAusland, L., Vialet-Chabrand, S., Davey, P., Baker, N.R., Brendel, O. and Lawson, T., 2016. Effects of kinetics of light-induced stomatal responses on photosynthesis and water-use efficiency. *The New phytologist*, **211**(4), 1209–1220.

McAusland, L., Vialet-Chabrand, S., Jauregui, I., Burridge, A., Hubbart-Edwards, S., Fryer, M.J., King, I.P., King, J., Pyke, K., Edwards, K.J., Carmo-Silva, E., Lawson, T. and Murchie, E.H., 2020. Variation in key leaf photosynthetic traits across wheat wild relatives is accession dependent not species dependent. *New Phytologist*, **228**(6), 1767–1780.

McClain, A.M. and Sharkey, T.D., 2020. Building a better equation for electron transport estimated from Chl fluorescence: accounting for nonphotosynthetic light absorption. *New Phytologist*, **225**(2), 604.

McClain, A.M., Cruz, J.A., Kramer, D.M. and Sharkey, T.D., 2023. The time course of acclimation to the stress of triose phosphate use limitation. *Plant, Cell & Environment*, **46**(1), 64–75.

McElwain, J.C., Yiotis, C. and Lawson, T., 2016. Using modern plant trait relationships between observed and theoretical maximum stomatal conductance and vein density to examine patterns of plant macroevolution. *New Phytologist*, **209**(1), 94–103.

McKown, K.H. and Bergmann, D.C., 2020. Stomatal development in the grasses: lessons from models and crops (and crop models). *New Phytologist*, **227**(6), 1636–1648.

Mikic, A., Mihailovic, V., Cupina, B., Kosev, V., Warkentin, T., Mcphee, K., Ambrose, M., Hofer, J. and Ellis, N., 2011. Genetic background and agronomic value of leaf types in pea (Pisum sativum). *Ratarstvo i povrtarstvo*, **48**(2), 275–284.

Milliken, A.L., Fan, M., Mathan, J., Davey, P. and Lawson, T., 2024. Measuring Nonfoliar Photosynthesis. In: *Covshoff, S. (eds) Photosynthesis: Methods and Protocols. Methods in Molecular Biology*, **2790**, 77–94. Humana, New York, NY: Springer US.

Mishra, A., Bruno, E., and Zilberman, D., 2021. Compound natural and human disasters: Managing drought and COVID-19 to sustain global agriculture and food sectors. *Science of The Total Environment*, **754**, 142210.

Moisa, C., Copolovici, D., Lupitu, A., Lazar, L. And Copolovici, L., 2019. Drought stress influence on pea plants (Pisum sativum l.). *Scientific and Technical Bulletin, Series: Chemistry, Food Science and Engineering*, **16**, 20–24.

Molero, G. and Reynolds, M.P., 2020. Spike photosynthesis measured at high throughput indicates genetic variation independent of flag leaf photosynthesis. *Field Crops Research*, **255**, 107866.

Momayyezi, M., Rippner, D.A., Duong, F.V., Raja, P.V., Brown, P.J., Kluepfel, D.A., Earles, J.M., Forrestel, E.J., Gilbert, M.E. and McElrone, A.J., 2022. Structural and functional leaf diversity lead to variability in photosynthetic capacity across a range of Juglans regia genotypes. *Plant, Cell & Environment*, **45**(8), pp.2351–2365.

Moran, J.F., Becana, M., Iturbe-Ormaetxe, I., Frechilla, S., Klucas, R.V. and Aparicio-Tejo, P., 1994. Drought induces oxidative stress in pea plants. *Planta*, **194**, 346–352.

Moreau, C., Hofer, J.M., Eléouët, M., Sinjushin, A., Ambrose, M., Skøt, K., Blackmore, T., Swain, M., Hegarty, M., Balanzà, V. and Ferrándiz, C., 2018. Identification of Stipules reduced, a leaf morphology gene in pea (Pisum sativum). *New Phytologist*, **220**(1), 288-299.

Müller, A., Schneider, J.F., Degrossoli, A., Lupilova, N., Dick, T.P. and Leichert, L.I., 2017. Systematic in vitro assessment of responses of roGFP2-based probes to physiologically relevant oxidant species. *Free Radical Biology and Medicine*, **106**, 329–338.

Münchinger, I.K., Hajek, P., Akdogan, B., Caicoya, A.T. and Kunert, N., 2023. Leaf thermal tolerance and sensitivity of temperate tree species are correlated with leaf physiological and functional drought resistance traits. *Journal of Forestry Research*, **34**(1), 63–76.

Murchie, E.H. and Lawson, T., 2013. Chlorophyll fluorescence analysis: A guide to good practice and understanding some new applications. *Journal of Experimental Botany*, **64**(13), 3983–3998.

Murchie, E.H., Reynolds, M., Slafer, G.A., Foulkes, M.J., Acevedo-Siaca, L., McAusland, L., Sharwood, R., Griffiths, S., Flavell, R.B., Gwyn, J. and Sawkins, M., 2023. A 'wiring diagram'for source strength traits impacting wheat yield potential. *Journal of Experimental Botany*, **74**(1), 72–90.

Naim-Feil, E., Toren, M., Aubert, G., Rubinstein, M., Rosen, A., Eshed, R., Sherman, A., Ophir, R., Saranga, Y. and Abbo, S., 2017. Drought response and genetic diversity in Pisum fulvum, a wild relative of domesticated pea. *Crop Science*, **57**(3), 1145–1159.

Nardini, A., 2022. Hard and tough: the coordination between leaf mechanical resistance and drought tolerance. *Flora*, **288**, 152023.

Nemeskéri, E., and Helyes, L., 2019. Physiological Responses of Selected Vegetable Crop Species to Water Stress. *Agronomy,* **9**(8), 447.

Nemeskéri, E., Molnár, K., Vígh, R., Nagy, J. and Dobos, A., 2015. Relationships between stomatal behaviour, spectral traits and water use and productivity of green peas (Pisum sativum L.) in dry seasons. *Acta physiologiae plantarum*, **37**, 1–16.

Nguyen, G.N., Norton, S.L., Rosewarne, G.M., James, L.E. and Slater, A.T., 2018. Automated phenotyping for early vigour of field pea seedlings in controlled environment by colour imaging technology. *PLoS One*, **13**(11), e0207788.

Nguyen, T.B.A., Lefoulon, C., Nguyen, T.H., Blatt, M.R. and Carroll, W., 2023. Engineering stomata for enhanced carbon capture and water-use efficiency. *Trends in Plant Science*, **28**(11), 1290–1309.

Nunes-Nesi, A., Nascimento, V.D.L., De Oliveira Silva, F.M., Zsögön, A., Araújo, W.L. and Sulpice, R., 2016. Natural genetic variation for morphological and molecular determinants of plant growth and yield. *Journal of Experimental Botany*, **67**(10), 2989–3001.

Nunes, T.D.G., Zhang, D. and Raissig, M.T., 2020. Form, development and function of grass stomata. *Plant Journal*, **101**(4), 780–799.

Olle, M., Williams, I.H., Rosa, E. and Tamm, S., 2020. Finding best field pea (Pisum sativum L.) cultivars for breeding in Northern climatic conditions. *Acta Agriculturae Scandinavica Section B: Soil and Plant Science*, **70**(1), 1–7.

Ortiz, D. and Salas-Fernandez, M.G., 2022. Dissecting the genetic control of natural variation in sorghum photosynthetic response to drought stress. *Journal of experimental botany*, **73**(10), 3251–3267.

Ortiz, D., Hu, J. and Salas Fernandez, M.G., 2017. Genetic architecture of photosynthesis in Sorghum bicolor under non-stress and cold stress conditions. *Journal of Experimental Botany*, **68**(16), 4545–4557.

Osman, H.S., 2015. Enhancing antioxidant–yield relationship of pea plant under drought at different growth stages by exogenously applied glycine betaine and proline. Annals of Agricultural Sciences, **60**(2), 389–402.

Ouyang, W., Struik, P.C., Yin, X. and Yang, J., 2017. Stomatal conductance, mesophyll conductance, and transpiration efficiency in relation to leaf anatomy in rice and wheat genotypes under drought. *Journal of Experimental Botany*, **68**(18), 5191–5205.

Oxborough, K. and Baker, N.R., 1997. Resolving chlorophyll a fluorescence images of photosynthetic efficiency into photochemical and non-photochemical components–calculation of qP and F_v'/F_m'; without measuring F_o'. *Photosynthesis research*, **54**, 135–142.

Paarlberg, R., Bhattacharya, A., Huang, J., Karembu, M., Pray, C. and Wesseler, J., 2024. The uptake of new crop science: Explaining success, and failure. *Food Policy*, **122**, 102572.

Pallas Jr, J.E. and Michel, B.E., 1971. Infrared energy as a factor in controlled environments. *Physiologia Plantarum*, **25**(2), 165–168.

Palliotti, A., Cartechini, A. and Nasini, L., 2001. Grapevine adaptation to continuous water limitation during the season. *Advances in Horticultural Science*, **15**(1–4), 39–45.

Pandey, J., Devadasu, E., Saini, D., Dhokne, K., Marriboina, S., Raghavendra, A.S. and Subramanyam, R., 2023. Reversible changes in structure and function of photosynthetic apparatus of pea (*Pisum sativum*) leaves under drought stress. *The Plant Journal*, **113**(1), 60–74.

Pantin, F. and Blatt, M.R., 2018. Stomatal response to humidity: Blurring the boundary between active and passive movement. *Plant Physiology*, **176**(1), 485–488.

Parry, M.A., Reynolds, M., Salvucci, M.E., Raines, C., Andralojc, P.J., Zhu, X.G., Price, G.D., Condon, A.G. and Furbank, R.T., 2011. Raising yield potential of wheat. II. Increasing photosynthetic capacity and efficiency. *Journal of experimental botany*, **62**(2), 453-467.

Pater, D., Mullen, J.L., McKay, J.K. and Schroeder, J.I., 2017. Screening for natural variation in water use efficiency traits in a diversity set of brassica napus L. identifies candidate variants in photosynthetic assimilation. *Plant and Cell Physiology*, **58**(10), 1700–1709.

Perez, T.M. and Feeley, K.J., 2018. Increasing humidity threatens tropical rainforests. *Frontiers in Ecology and Evolution*, **6**, 68.

Peterhansel, C., Blume, C. and Offermann, S., 2013. Photorespiratory bypasses: How can they work? *Journal of Experimental Botany*, **64**(3), 709–715.

PGRO. (2022). Processors and Growers Research Organisation - Pulse market update September 2022. Accessed on 26 May 2024. https://www.pgro.org/pulse-market-update-september-2022.

PGRO. (2024). Processors and Growers Research Organisation - Pulse market update September 2024. Accessed on 08 October 2024. https://www.pgro.org/pulse-market-update-september-2024/.

Picoli, M.C.A., Rorato, A., Leitão, P., Camara, G., Maciel, A., Hostert, P. and Sanches, I.D.A., 2020. Impacts of public and private sector policies on soybean and pasture expansion in mato Grosso-Brazil from 2001 to 2017. *Land*, **9**(1), 20.

Pignon, C.P., Leakey, A.D.B., Long, S.P. and Kromdijk, J., 2021a. Drivers of Natural Variation in Water-Use Efficiency Under Fluctuating Light Are Promising Targets for Improvement in Sorghum. *Frontiers in Plant Science*, **12**.

Pignon, C.P., Fernandes, S.B., Valluru, R., Bandillo, N., Lozano, R., Buckler, E., Gore, M.A., Long, S.P., Brown, P.J. and Leakey, A.D., 2021b. Phenotyping stomatal closure by thermal imaging for GWAS and TWAS of water use efficiency-related genes. *Plant physiology*, **187**(4), 2544–2562.

Pilorgé, E., Kezeya, B., Stauss, W., Muel, F. and Mergenthaler, M., 2021. Pea and rapeseed acreage and land use for plant-based meat alternatives in the EU. *OCL*, **28**, 54.

Pingali, P.L., 2012. Green revolution: Impacts, limits, andthe path ahead. *Proceedings of the National Academy of Sciences of the United States of America*, **109**(31), 12302–12308.

Poorter, H., Niinemets, Ü., Poorter, L., Wright, I.J. and Villar, R., 2009. Causes and consequences of variation in leaf mass per area (LMA): a meta-analysis. *New phytologist*, **182**(3), 565–588.

Price, D.N. and Hedley, C.L., 1980. Developmental and Varietal Comparisons of Pod Carboxylase Levels in Pisum sativum L. *Annals of Botany*, **45**(3), 283–294.

Priyadarsini, P., Lal, M.K., Pandey, R., Kumar, M., Malini, M.K., Das, A., Sehgal, V.K., Gopala Krishnan, S., Chinnusamy, V. and Pal, M., 2022. Variability in photosynthetic traits is associated with biomass accumulation and grain yield in basmati rice germplasm. *Plant Physiology Reports*, **27**(4), 618–624.

Pszczółkowski, P., Sawicka, B., Skiba, D., Barbaś, P. and Noaema, A.H., 2023. The Use of Chlorophyll Fluorescence as an Indicator of Predicting Potato Yield, Its Dry Matter and Starch in the Conditions of Using Microbiological Preparations. Applied Sciences, **13**(19), 10764.

Purushothaman, R., Krishnamurthy, L., Upadhyaya, H.D., Vadez, V. and Varshney, R.K., 2017. Genotypic variation in soil water use and root distribution and their implications for drought tolerance in chickpea. *Functional Plant Biology*, **44**(2), 235–252.

Puthur, J.T., Shackira, A.M., Saradhi, P.P. and Bartels, D., 2013. Chloroembryos: A unique photosynthesis system. *Journal of Plant Physiology*, **170**(13), 1131–1138.

Quebbeman, J.A. and Ramirez, J.A., 2016. Optimal allocation of leaf-level nitrogen: Implications for covariation of Vcmax and Jmax and photosynthetic downregulation. *Journal of Geophysical Research: Biogeosciences*, **121**(9), 2464–2475.

Raines, C.A., 2011. Update on Photosynthetic Carbon Assimilation Increasing Photosynthetic Carbon Assimilation in C3 Plants to Improve Crop Yield: Current and Future Strategies. *Plant physiology*, **155**(1), 36–42.

Rangan, P., Furtado, A. and Henry, R.J., 2016. New evidence for grain specific C4 photosynthesis in wheat. *Scientific reports*, **6**(1), 1–12.

Rasskazova, I. and Kirse-Ozolina, A., 2020. Field pea Pisum sativum L. as a perspective ingredient for vegan foods: a review. *Research For Rural Development*, **35**, 125–131.

Ray, D.K., Mueller, N.D., West, P.C. and Foley, J.A., 2013. Yield Trends Are Insufficient to Double Global Crop Production by 2050. *PLoS ONE*, **8**(6), e66428.

Ray, D.K., West, P.C., Clark, M., Gerber, J.S., Prishchepov, A. V and Chatterjee, S., 2019. Climate change has likely already affected global food production. *PLoS ONE*, **14**(5), e0217148.

Ren, T., Weraduwage, S.M. and Sharkey, T.D., 2019. Prospects for enhancing leaf photosynthetic capacity by manipulating mesophyll cell morphology. *Journal of Experimental Botany*, **70**(4), 1153–1165.

Ricroch, A.E., Guillaume-Hofnung, M. and Kuntz, M., 2018. The ethical concerns about transgenic crops. *Biochemical Journal*, **475**(4), 803–811.

Rispail, N., Wohor, O.Z., Osuna-Caballero, S., Barilli, E. and Rubiales, D., 2023. Genetic diversity and population structure of a wide Pisum spp. core collection. *International Journal of Molecular Sciences*, **24**(3), 2470.

Rivera-Amado, C., Molero, G., Trujillo-Negrellos, E., Reynolds, M. and Foulkes, J., 2020. Estimating organ contribution to grain filling and potential for source upregulation in wheat cultivars with a

contrasting source–sink balance. *Agronomy*, **10**(10), 1527.

Rogers, H., Dora, M., Tsolakis, N. and Kumar, M., 2024. Plant-based Food Supply Chains: Recognising Market Opportunities and Industry Challenges of Pea Protein. *Applied Food Research*, **4**(2), 100440.

Rouhi, V., Samson, R., Lemeur, R. and Van Damme, P., 2007. Photosynthetic gas exchange characteristics in three different almond species during drought stress and subsequent recovery. *Environmental and experimental botany*, **59**(2), 117–129.

Roux, B. and Leonhardt, N., 2018. The regulation of ion channels and transporters in the guard cell. In *Advances in Botanical Research*. Academic Press. **87**, 171–214.

Ruggiero, A., Punzo, P., Landi, S., Costa, A., Van Oosten, M.J. and Grillo, S., 2017. Improving plant water use efficiency through molecular genetics. *Horticulturae*, **3**(2), 1–22.

Rungruangmaitree, R. and Jiraungkoorskul, W., 2017. Pea, Pisum sativum, and its anticancer activity. *Pharmacognosy Reviews*, **11**(21), 39–42.

Sadras, V.O., Lake, L., Leonforte, A., McMurray, L.S. and Paull, J.G., 2013. Screening field pea for adaptation to water and heat stress: Associations between yield, crop growth rate and seed abortion. *Field Crops Research*, **150**, 63–73.

Sage, R.F., Way, D.A. and Kubien, D.S., 2008. Rubisco, Rubisco activase, and global climate change. *Journal of Experimental Botany*, **59**(7), 1581–1595.

Sainju, U.M., Lenssen, A.W., Allen, B.L., Jabro, J.D. and Stevens, W.B., 2019. Pea Growth, Yield, and Quality in Different Crop Rotations and Cultural Practices. *Agrosystems, Geosciences & Environment*, **2**(1), 1–9.

Sakoda, K., Tanaka, Y., Long, S.P. and Shiraiwa, T., 2016. Genetic and physiological diversity in the leaf photosynthetic capacity of soybean. *Crop Science*, **56**(5), 2731–2741.

Sakoda, K., Yamori, W., Shimada, T., Sugano, S.S., Hara-Nishimura, I. and Tanaka, Y., 2020. Higher stomatal density improves photosynthetic induction and biomass production in Arabidopsis under fluctuating light. *Frontiers in Plant Science*, **11**, 589603.

Sanchez-Bragado, R., Elazab, A., Zhou, B., Serret, M.D., Bort, J., Nieto-Taladriz, M.T. and Araus, J.L., 2014. Contribution of the ear and the flag leaf to grain filling in durum wheat inferred from the carbon isotope signature: Genotypic and growing conditions effects. *Journal of Integrative Plant Biology*, **56**(5), 444–454.

Sanchez-Bragado, R., Molero, G., Reynolds, M.P. and Araus, J.L., 2016. Photosynthetic contribution of the ear to grain filling in wheat: A comparison of different methodologies for evaluation. *Journal of Experimental Botany*, **67**(9), 2787–2798.

Santos, C.S., Carbas, B., Castanho, A., Vasconcelos, M.W., Vaz Patto, M.C., Domoney, C. and Brites, C., 2019. Variation in pea (Pisum sativum L.) seed quality traits defined by physicochemical functional properties. *Foods*, **8**(11), 570.

Schmidt, S.B., Brown, L.K., Booth, A., Wishart, J., Hedley, P.E., Martin, P., Husted, S., George, T.S. and Russell, J., 2023. Heritage genetics for adaptation to marginal soils in barley. *Trends in Plant Science*, **28**(5), 544–551.

Seibt, U., Rajabi, A., Griffiths, H. and Berry, J.A., 2008. Carbon isotopes and water use efficiency: Sense and sensitivity. *Oecologia*, **155**(3), 441–454.

Serraj, R., Krishnamurthy, L., Kashiwagi, J., Kumar, J., Chandra, S. and Crouch, J.H., 2004. Variation in root traits of chickpea (Cicer arietinum L.) grown under terminal drought. *Field Crops Research*, **88**(2–3), 115–127.

Shamim, M.J., Kaga, A., Tanaka, Y., Yamatani, H. and Shiraiwa, T., 2022. Analysis of physiological variations and genetic architecture for photosynthetic capacity of Japanese soybean germplasm. *Frontiers in Plant Science*, **13**, 910527.

Sharkey, T.D., 1985. Photosynthesis in intact leaves of C3 plants: Physics, physiology and rate limitations. *The Botanical Review*, **51**(1), 53–105.

Sharkey, T.D., 2016. What gas exchange data can tell us about photosynthesis. *Plant, Cell & Environment*, **39**(6), 1161–1163.

Sharkey, T.D., 2019. Is triose phosphate utilization important for understanding photosynthesis. *Journal of Experimental Botany*, **70**(20), 5521–5525.

Sharma, V., Sinha, A.K., Chaudhary, S., Priyadarshini, A., Tripathi, B.N. and Kumar, S., 2012. Genetic analysis of structure and function of stipules in pea Pisum sativum. *Proc. Ind. Nat. Sci. Acad*, **78**, 9–34.

Sharwood, R.E., 2017. Engineering chloroplasts to improve Rubisco catalysis: prospects for translating improvements into food and fiber crops. *New Phytologist*, **213**(2), 494–510.

Shen, Y., Johnson, E.N., Syrovy, L.D., Warkentin, T.D., Devini, D.S. and Shirtliffe, S.J., 2022. Evaluation of yield and agronomic performance of leafed and semi-leafless pea blends. *Agronomy Journal*, **114**(5), 2762–2773.

Sherrard, M.E., Maherali, H. and Latta, R.G., 2009. Water stress alters the genetic architecture of functional traits associated with drought adaptation in Avena barbata. *Evolution*, **63**(3), 702–715.

Sherstneva, O., Khlopkov, A., Gromova, E., Yudina, L., Vetrova, Y., Pecherina, A., Kuznetsova, D., Krutova, E., Sukhov, V., Vodeneev, V. and Allakhverdiev, S., 2021. Analysis of chlorophyll fluorescence parameters as predictors of biomass accumulation and tolerance to heat and drought stress of wheat (Triticum aestivum) plants. *Functional Plant Biology*, **49**(2), 155–169.

Shevela, D., Schröder, W.P. and Messinger, J., 2018. Liquid-phase measurements of photosynthetic oxygen evolution. In: *Methods in Molecular Biology*. Humana Press Inc., 197–211.

Sikder, S., Foulkes, J., West, H., De Silva, J., Gaju, O., Greenland, A. and Howell, P., 2015. Evaluation of photosynthetic potential of wheat genotypes under drought condition. *Photosynthetica*, **53**, 47–54.

Silva-Pérez, V., De Faveri, J., Molero, G., Deery, D.M., Condon, A.G., Reynolds, M.P., Evans, J.R. and Furbank, R.T., 2020. Genetic variation for photosynthetic capacity and efficiency in spring wheat. *Journal of Experimental Botany*, **71**(7), 2299–2311.

Simkin, A.J., Faralli, M., Ramamoorthy, S. and Lawson, T., 2020. Photosynthesis in non-foliar tissues: implications for yield. *Plant Journal*, **101**(4), 1001–1015.

Simkin, A.J., López-Calcagno, P.E. and Raines, C.A., 2019. Feeding the world: Improving photosynthetic efficiency for sustainable crop production. *Journal of Experimental Botany*, **70**(4), 1119–1140.

Singh, S.K. and Reddy, K.R., 2011. Regulation of photosynthesis, fluorescence, stomatal conductance and water-use efficiency of cowpea (Vigna unguiculata [L.] Walp.) under drought. *Journal of Photochemistry and Photobiology B: Biology*, **105**(1), 40–50.

Slattery, R.A. and Ort, D.R., 2015. Photosynthetic energy conversion efficiency: Setting a baseline for gauging future improvements in important food and biofuel crops. *Plant Physiology*, **168**(2), 383–392.

Smith, N.G., Keenan, T.F., Colin Prentice, I., Wang, H., Wright, I.J., Niinemets, Ü., Crous, K.Y., Domingues, T.F., Guerrieri, R., Yoko Ishida, F., et al., 2019. Global photosynthetic capacity is optimized to the environment. *Ecology Letters*, **22**(3), 506–517.

Smýkal, P., Aubert, G., Burstin, J., Coyne, C.J., Ellis, N.T.H., Flavell, A.J., Ford, R., Hýbl, M., Macas, J.,

Neumann, P., McPhee, K.E., Redden, R.J., Rubiales, D., Weller, J.L. and Warkentin, T.D., 2012. Pea (Pisum sativum L.) in the Genomic Era. *Agronomy*, **2**(2), 74–115.

Smýkal, P., Hradilová, I., Trněný, O., Brus, J., Rathore, A., Bariotakis, M., Das, R.R., Bhattacharyya, D., Richards, C., Coyne, C.J. and Pirintsos, S., 2017. Genomic diversity and macroecology of the crop wild relatives of domesticated pea. *Scientific Reports*, **7**(1), 1–12.

Smýkal, P., Kenicer, G., Flavell, A.J., Corander, J., Kosterin, O., Redden, R.J., Ford, R., Coyne, C.J., Maxted, N., Ambrose, M.J. and Ellis, N.T.H., 2011. Phylogeny, phylogeography and genetic diversity of the Pisum genus. *Plant Genetic Resources: Characterisation and Utilisation*, **9**(1), 4–18.

Snoad, B., 1981. Plant form, growth rate and relative growth rate compared in conventional, semi-leafless and leafless peas. *Scientia Horticulturae*, **14**(1), 9–18.

Snoad, B., Monti, L. M., and Frusciante, L., 1985. The effects of heterozygosity at the af, st and tl loci in peas. *Theoretical and applied genetics*, **71**(1), 39–43.

Song, G., Wang, Q. and Jin, J., 2020. Leaf photosynthetic capacity of sunlit and shaded mature leaves in a deciduous forest. *Forests*, **11**(3), 318.

Song, Q. and Zhu, X.G., 2024. Techniques for photosynthesis phenomics: gas exchange, fluorescence, and reflectance spectrums. *Crop and Environment*, **3**(3), 147–158.

Stagnari, F., Maggio, A., Galieni, A. and Pisante, M., 2017. Multiple benefits of legumes for agriculture sustainability: an overview. *Chemical and Biological Technologies in Agriculture*, **4**(1), 1–13.

Stepanova, N., Tarakhovskaya, E., Soboleva, A., Orlova, A., Basnet, A., Smolenskaya, A., Frolova, N., Bilova, T., Kamionskaya, A., Frolov, A. and Medvedev, S., 2024a. Green Light Drives Embryonic Photosynthesis and Protein Accumulation in Cotyledons of Developing Pea (Pisum sativum L.) Seeds. *Agronomy*, **14**(10), 2367.

Stepanova, N., Zhilkina, T., Kamionskaya, A. and Smolikova, G., 2024b. Non-Foliar Photosynthesis in Pea (Pisum sativum L.) Plants: Beyond the Leaves to Inside the Seeds. *Plants*, **13**(20), 2945.

Stevens, J., Jones, M.A. and Lawson, T., 2021. Diverse physiological and physical responses among wild, landrace and elite barley varieties point to novel breeding opportunities. *Agronomy*, **11**(5), 921.

Sui, X., Shan, N., Hu, L., Zhang, C., Yu, C., Ren, H., Turgeon, R. and Zhang, Z., 2017. The complex character of photosynthesis in cucumber fruit. *Journal of Experimental Botany*, **68**(7), 1625–1637.

Syrovy, L.D., Banniza, S. and Shirtliffe, S.J., 2015. Yield and agronomic advantages of pea leaf type mixtures under organic management. *Agronomy Journal*, **107**(1), 113–120.

Szablińska-Piernik, J. and Lahuta, L.B., 2021. Metabolite profiling of semi-leafless pea (Pisum sativum L.) under progressive soil drought and subsequent re-watering. *Journal of Plant Physiology*, **256**, 153314.

Tafesse, E. G., Gali, K. K., Reddy Lachagari, V. B., Bueckert, R., and Warkentin, T. D., 2021. Genome-Wide Association Mapping for Heat and Drought Adaptive Traits in Pea. *Genes,* **12**(12), 1897.

Tafesse, E.G., Warkentin, T.D., Shirtliffe, S., Noble, S. and Bueckert, R., 2022. Leaf pigments, surface wax and spectral vegetation indices for heat stress resistance in pea. *Agronomy*, **12**(3), 739.

Takahashi, S., Monda, K., Negi, J., Konishi, F., Ishikawa, S., Hashimoto-Sugimoto, M., Goto, N. and Iba, K., 2015. Natural variation in stomatal responses to environmental changes among Arabidopsis thaliana ecotypes. *PLoS ONE*, **10**(2), e0117449.

Tambussi, E.A., Bort, J., Guiamet, J.J., Nogués, S. and Araus, J.L., 2007. The photosynthetic role of ears in C3 cereals: Metabolism, water use efficiency and contribution to grain yield. *Critical Reviews in*

Plant Sciences, **26**(1), 1–16.

Tambussi, E.A., Maydup, M.L., C A, C., Guiamet, J.J. and Araus, J.L., 2021. Ear photosynthesis in C3 cereals and its contribution to grain yield: methodologies, controversies and perspectives. *Journal of Experimental Botany*, **72**(11), 3956–3970.

Tambussi, E.A., Nogués, S. and Araus, J.L., 2005. Ear of durum wheat under water stress: Water relations and photosynthetic metabolism. *Planta*, **221**(3), 446–458.

Tanaka, A., Fujita, K. and Kikuchi, K., 1974. Nutrio-physiological studies on the tomato plant: I. Outline of growth and nutrient absorption. *Soil Science and Plant Nutrition*, **20**(1), 57–68.

Tanaka, Y., Shiraiwa, T., Nakajima, A., Sato, J. and Nakazaki, T., 2008. Leaf gas exchange activity in soybean as related to leaf traits and stem growth habit. *Crop Science*, **48**(5), 1925–1932.

Tanaka, Y., Sugano, S.S., Shimada, T. and Hara-Nishimura, I., 2013. Enhancement of leaf photosynthetic capacity through increased stomatal density in Arabidopsis. *New Phytologist*, **198**(3), 757–764.

Tayeh, N., Aubert, G., Pilet-Nayel, M.L., Lejeune-Hénaut, I., Warkentin, T.D. and Burstin, J., 2015. Genomic tools in pea breeding programs: Status and perspectives. *Frontiers in Plant Science*, **6**(NOVEMBER), 1–13.

Tayeh, N., Hofer, J., Aubert, G., Jacquin, F., Turner, L., Kreplak, J., Paajanen, P., Le Signor, C., Dalmais, M., Pflieger, S. and Geffroy, V., 2023. afila, the origin and nature of a major innovation in the history of pea breeding. *bioRxiv*, 2023-07.

Tian, H., Zhou, Q., Liu, W., Zhang, J., Chen, Y., Jia, Z., Shao, Y. and Wang, H., 2022. Responses of photosynthetic characteristics of oat flag leaf and spike to drought stress. *Frontiers in Plant Science*, **13**, 917528.

Timmerman-Vaughan, G.M., Mills, A., Whitfield, C., Frew, T., Butler, R., Murray, S., Lakeman, M., McCallum, J., Russell, A. and Wilson, D., 2005. Linkage mapping of QTL for seed yield, yield components, and developmental traits in pea. *Crop Science*, **45**(4), 1336–1344.

Tinoco-Ojanguren, C. and Pearcy, R.W., 1993. Stomatal dynamics and its importance to carbon gain in two rainforest Piper species: I. VPD effects on the transient stomatal response to lightflecks. *Oecologia*, **94**, 388–394.

Tokarz, K.M., Wesołowski, W., Tokarz, B., Makowski, W., Wysocka, A., Jędrzejczyk, R.J., Chrabaszcz, K., Malek, K. and Kostecka-Gugała, A., 2021. Stem photosynthesis—A key element of grass pea (Lathyrus sativus L.) acclimatisation to salinity. *International Journal of Molecular Sciences*, **22**(2), 685.

Tomás, M., Medrano, H., Pou, A., Escalona, J.M., Martorell, S., Ribas-Carbó, M. and Flexas, J., 2012. Water-use efficiency in grapevine cultivars grown under controlled conditions: effects of water stress at the leaf and whole-plant level. *Australian Journal of Grape and Wine Research*, **18**(2), 164–172.

Tran, C.T., Becker, H.C. and Horneburg, B., 2022. Agronomic performance of normal-leafed and semi-leafless pea (Pisum sativum L.) genotypes. *Crop Science*, **62**(4), 1430–1442.

Tran, T.A., Vassileva, V., Petrov, P. and Popova, L.P., 2013. Cadmium-induced structural disturbances in Pisum sativum leaves are alleviated by nitric oxide. *Turkish Journal of Botany*, **37**(4), 698–707.

Trivedi, P., Batista, B.D., Bazany, K.E. and Singh, B.K., 2022. Plant–microbiome interactions under a changing world: responses, consequences and perspectives. *New Phytologist*, **234**(6), 1951–1959.

Trněný, O., Brus, J., Hradilová, I., Rathore, A., Das, R.R., Kopecký, P., Coyne, C.J., Reeves, P., Richards, C. and Smýkal, P., 2018. Molecular evidence for two domestication events in the pea crop. *Genes*, **9**(11), 535.

Tschiersch, H., Borisjuk, L., Rutten, T. and Rolletschek, H., 2011. Gradients of seed photosynthesis and its role for oxygen balancing. *BioSystems*, **103**(2), 302–308.

Tulbek, M.C., Lam, R.S.H., Wang, Y.C., Asavajaru, P. and Lam, A., 2017. Pea: A Sustainable Vegetable Protein Crop. In: *Sustainable Protein Sources*. Academic Press. Elsevier Inc., 145–164.

Uhlarik, A., Ćeran, M., Živanov, D., Grumeza, R., Skøt, L., Sizer-Coverdale, E. and Lloyd, D., 2022. Phenotypic and genotypic characterization and correlation analysis of pea (Pisum sativum L.) diversity panel. *Plants*, **11**(10), 1321.

Urban, L., Aarrouf, J. and Bidel, L.P., 2017a. Assessing the effects of water deficit on photosynthesis using parameters derived from measurements of leaf gas exchange and of chlorophyll a fluorescence. *Frontiers in plant science*, **8**, 304622.

Urban, J., Ingwers, M., McGuire, M.A. and Teskey, R.O., 2017b. Stomatal conductance increases with rising temperature. *Plant signaling & behavior*, **12**(8), e1356534.

van Bezouw, R.F.H.M., Keurentjes, J.J.B., Harbinson, J. and Aarts, M.G.M., 2019. Converging phenomics and genomics to study natural variation in plant photosynthetic efficiency. *Plant Journal*, **97**(1), 112–133.

Vatén, A. and Bergmann, D.C., 2012. Mechanisms of stomatal development: An evolutionary view. *EvoDevo*, **3**(1), 1–9.

Vialet-Chabrand, S., Dreyer, E. and Brendel, O., 2013. Performance of a new dynamic model for predicting diurnal time courses of stomatal conductance at the leaf level. *Plant, Cell and Environment*, **36**(8), 1529–1546.

Vialet-Chabrand, S., Matthews, J.S.A., Simkin, A.J., Raines, C.A. and Lawson, T., 2017. Importance of fluctuations in light on plant photosynthetic acclimation. *Plant Physiology*, **173**(4), 2163–2179.

Voss-Fels, K.P., Stahl, A. and Hickey, L.T., 2019. Q&A: Modern crop breeding for future food security. *BMC Biology*, **17**(1), 1–7.

Vouraki, S., Papanikolopoulou, V., Irakli, M., Parissi, Z., Abraham, E.M. and Arsenos, G., 2023. Legume Grains as an Alternative to Soybean Meal in the Diet of Intensively Reared Dairy Ewes. *Sustainability*, **15**(2), 1028.

Wall, S., Cockram, J., Vialet-Chabrand, S., Van Rie, J., Gallé, A. and Lawson, T., 2023. The impact of growth at elevated [CO2] on stomatal anatomy and behavior differs between wheat species and cultivars. *Journal of Experimental Botany*, **74**(9), 2860–2874.

Wang, H., Hou, L., Wang, M. and Mao, P., 2016. Contribution of the pod wall to seed grain filling in alfalfa. *Scientific Reports*, **6**(1), 26586.

Wang, Q., Liu, J. and Zhu, H., 2018. Genetic and molecular mechanisms underlying symbiotic specificity in legume-rhizobium interactions. *Frontiers in Plant Science*, **9**, 313.

Wang, X.Q., Sun, H., Zeng, Z.L. and Huang, W., 2023. Within-branch photosynthetic gradients are more related to the coordinated investments of nitrogen and water than leaf mass per area. *Plant Physiology and Biochemistry*, **198**, 107681.

Warkentin, T.D., Smýkal, P., Coyne, C.J., Weeden, N., Domoney, C., Bing, D.J., Leonforte, A., Xuxiao, Z., Dixit, G.P., Boros, L. and McPhee, K.E., 2015. Pea. *Grain legumes*, 37–83.

Weeden, N.F., 2018. Domestication of pea (Pisum sativum L.): The case of the Abyssinian pea. *Frontiers in Plant Science*, **9**, 515.

Weyers, J. D., and Johansen, L. G. 1985. Accurate estimation of stomatal aperture from silicone rubber

impressions. *New phytologist*, **101**(1), 109–115.

Whitney, S.M., Houtz, R.L. and Alonso, H., 2011. Update on Understanding and Manipulating Rubisco Biogenesis Advancing Our Understanding and Capacity to Engineer Nature's CO2-Sequestering Enzyme, Rubisco. *Plant Physiology*, **155**, 27–35.

Wijewardene, I., Shen, G. and Zhang, H., 2021. Enhancing crop yield by using Rubisco activase to improve photosynthesis under elevated temperatures. *Stress Biology*, **1**(1), 2.

Wilson, D.R., Hanson, R. and Jermyn, W.A., 1981. Growth and water use of conventional and semi-leafless peas. In *Proceedings of the Agronomy Society of New Zealand*, **11**, 35–39.

Windsor, N., Boatwright, L., Boyles, R., Bridges, W., Rubiales, D. and Thavarajah, D., 2024. Characterizing Dry Pea (Pisum sativum L.) for Improved Nutritional Traits and the Potential for Biofortification. *Legume Science*, **6**(3), e250.

Winther, L., Rasmussen, S.K., Poulsen, G. and Lange, C.B.A., 2023. Assessment of Genetic Diversity and Protein Content of Scandinavian Peas (Pisum sativum). *Agronomy*, **13**(9), 2307.

Wright, I.J., Reich, P.B., Westoby, M., Ackerly, D.D., Baruch, Z., Bongers, F., Cavender-Bares, J., Chapin, T., Cornelissen, J.H., Diemer, M. and Flexas, J., 2004. The worldwide leaf economics spectrum. *nature*, **428**(6985), 821–827.

Wright, I.J., Westoby, M. and Reich, P.B., 2002. Convergence towards higher leaf mass per area in dry and nutrient-poor habitats has different consequences for leaf life span. *Journal of ecology*, **90**(3), 534–543.

Wu, D.T., Li, W.X., Wan, J.J., Hu, Y.C., Gan, R.Y. and Zou, L., 2023. A comprehensive review of pea (Pisum sativum L.): chemical composition, processing, health benefits, and food applications. *Foods*, **12**(13), 2527.

Wullschleger, S.D., 1993. Biochemical limitations to carbon assimilation in C3 plants—a retrospective analysis of the A/Ci curves from 109 species. *Journal of experimental botany*, **44**(5), 907–920.

Xiong, D. and Flexas, J., 2020. From one side to two sides: the effects of stomatal distribution on photosynthesis. *New Phytologist*, **228**(6), 1754–1766.

Xiong, D., Douthe, C. and Flexas, J., 2018. Differential coordination of stomatal conductance, mesophyll conductance, and leaf hydraulic conductance in response to changing light across species. *Plant Cell and Environment*, **41**(2), 436–450.

Xu, Z. and Zhou, G., 2008. Responses of leaf stomatal density to water status and its relationship with photosynthesis in a grass. *Journal of experimental botany*, **59**(12), 3317–3325.

Yamori, W. and von Caemmerer, S., 2009. Effect of rubisco activase deficiency on the temperature response of CO2 assimilation rate and rubisco activation state: Insights from transgenic tobacco with reduced amounts of rubisco activase. *Plant Physiology*, **151**(4), 2073–2082.

Yamori, W., Hikosaka, K. and Way, D.A., 2014. Temperature response of photosynthesis in C3, C4, and CAM plants: Temperature acclimation and temperature adaptation. *Photosynthesis Research*, **119**(1–2), 101–117.

Yan, S., Weng, B., Jing, L. and Bi, W., 2023. Effects of drought stress on water content and biomass distribution in summer maize (Zea mays L.). *Frontiers in Plant Science*, **14**, 1118131.

Yan, Y., Hou, P., Duan, F., Niu, L., Dai, T., Wang, K., Zhao, M., Li, S. and Zhou, W., 2021. Improving photosynthesis to increase grain yield potential: an analysis of maize hybrids released in different years in China. *Photosynthesis Research*, **150**(1), 295–311.

Yang, X., Lu, M., Wang, Y., Wang, Y., Liu, Z. and Chen, S., 2021. Response mechanism of plants to drought stress. *Horticulturae*, **7**(3), 50.

Yarnell, S. H. 1950. The Role of the Regional Vegetable Breeding Laboratory in Breeding and Testing New Vegetable Varieties. *Proceedings of the Florida State Horticultural Society*, **63**,102–107.

Ye, Z.P., Kang, H.J., An, T., Duan, H.L., Wang, F.B., Yang, X.L. and Zhou, S.X., 2020. Modeling Light Response of Electron Transport Rate and Its Allocation for Ribulose Biphosphate Carboxylation and Oxygenation. *Frontiers in Plant Science*, **11**.

Yin, Q., Tian, T., Kou, M., Liu, P., Wang, L., Hao, Z. and Yue, M., 2020. The relationships between photosynthesis and stomatal traits on the Loess Plateau. *Global Ecology and Conservation*, **23**, e01146.

Yin, X., Gu, J., Dingkuhn, M. and Struik, P.C., 2022. A model-guided holistic review of exploiting natural variation of photosynthesis traits in crop improvement. *Journal of Experimental Botany*, **73**(10), 3173–3188.

Yin, X., Struik, P.C., Romero, P., Harbinson, J., Evers, J.B., Van Der Putten, P.E.L. and Vos, J., 2009. Using combined measurements of gas exchange and chlorophyll fluorescence to estimate parameters of a biochemical C3 photosynthesis model: A critical appraisal and a new integrated approach applied to leaves in a wheat (Triticum aestivum) canopy. *Plant, Cell and Environment*, **32**(5), 448–464.

Yoon, D.-K., Ishiyama, K., Suganami, M., Tazoe, Y., Watanabe, M., Imaruoka, S., Ogura, M., Ishida, H., Suzuki, Y., Obara, M., Mae, T. and Makino, A., 2020. Transgenic rice overproducing Rubisco exhibits increased yields with improved nitrogen-use efficiency in an experimental paddy field. *Nature Food*, **1**(2), 134–139.

Zargar, S.M., Gupta, N., Nazir, M., Mahajan, R., Malik, F.A., Sofi, N.R., Shikari, A.B. and Salgotra, R.K., 2017. Impact of drought on photosynthesis: Molecular perspective. *Plant Gene*, **11**, 154–159.

Zentner, R.P., Lafond, G.P., Derksen, D.A., Nagy, C.N., Wall, D.D. and May, W.E., 2004. Effects of tillage method and crop rotation on non-renewable energy use efficiency for a thin Black Chernozem in the Canadian Prairies. *Soil and Tillage Research*, **77**(2), 125–136.

Zhan, D., Yang, Y., Hu, Y., Zhang, Y., Luo, H. and Zhang, W., 2014. Contributions of nonleaf organs to the yield of cotton grown with different water supply. *The Scientific World Journal*, **2014**(1), 602747.

Zhang, C., Zhan, D.X., Luo, H.H., Zhang, Y.L. and Zhang, W.F., 2016. Photorespiration and photoinhibition in the bracts of cotton under water stress. *Photosynthetica*, **54**(1), 12–18.

Zhang, Q., Peng, S. and Li, Y., 2019a. Increase rate of light-induced stomatal conductance is related to stomatal size in the genus Oryza. *Journal of Experimental Botany*, **70**(19), 5259–5269.

Zhang, X., Pu, P., Tang, Y., Zhang, L. and Lv, J., 2019b. C4 photosynthetic enzymes play a key role in wheat spike bracts primary carbon metabolism response under water deficit. *Plant Physiology and Biochemistry*, **142**, 163–172.

Zhang, Y., Zhang, Y., Wang, Z. and Wang, Z., 2011. Characteristics of canopy structure and contributions of non-leaf organs to yield in winter wheat under different irrigated conditions. *Field Crops Research*, **123**(3), 187–195.

Zhao, T., and Dai, A., 2015. The Magnitude and Causes of Global Drought Changes in the Twenty-First Century under a Low-Moderate Emissions Scenario. *Journal of Climate*, **28**(11), 4490–4512.

Zhao, W., Sun, Y., Kjelgren, R. and Liu, X., 2015. Response of stomatal density and bound gas exchange in leaves of maize to soil water deficit. *Acta Physiologiae Plantarum*, **37**, 1–9.

Zhao, X., Nie, G., Yao, Y., Ji, Z., Gao, J., Wang, X. and Jiang, Y., 2020a. Natural variation and genomic prediction of growth, physiological traits, and nitrogen-use efficiency in perennial ryegrass under low-nitrogen stress. *Journal of Experimental Botany*, **71**(20), 6670–6683.

Zhao, W., Liu, L., Shen, Q., Yang, J., Han, X., Tian, F. and Wu, J., 2020b. Effects of water stress on photosynthesis, yield, and water use efficiency in winter wheat. *Water*, **12**(8), 2127.

Zhou, H., Akçay, E. and Helliker, B.R., 2019. Estimating C_4 photosynthesis parameters by fitting intensive A/C_i curves. *Photosynthesis research*, **141**, 181–194.

Zhu, X.G., Long, S.P. and Ort, D.R., 2010. Improving photosynthetic efficiency for greater yield. *Annual Review of Plant Biology*, **61**, 235–261.

Zlatev, Z. and Lidon, F.C., 2012. An overview on drought induced changes in plant growth, water relations and photosynthesis. *Emir. J. Food Agric.*, **24**(1), 57–72.

Chapter 7: Appendices

Appendix 1.

Table A1.1. One-way ANOVA table of yield parameters compared between the P. sativum accessions. Pod length was measured (in cm) via ImageJ (version 1.53), whilst dry weights (DW) were measured (in g) after a constant weight was reached. Statistical significance in yield parameters between the different *P. sativum* accessions are illustrated as asterisks, whereby * is $P < 0.05$, ** is $P < 0.01$ and *** is $P < 0.001$ (n = 3-6).

Yield Type	Parameter	DF	*F* value	*P* value	Sig
Grain	Number of Pods	13	5.45	2.09E-06	***
	Pod DW	13	26.93	<2E-16	***
	Total Pod DW	13	5.75	9.84E-07	***
	Pod Length	13	61.54	<2E-16	***
	Number of Seeds	13	23.81	<2E-16	***
	Seed DW	13	24.91	<2E-16	***
Biomass	Plant Height	13	82.12	<2E-16	***
	Plant DW	13	13.49	2.07E-13	***
	Number of Stems	13	29.06	<2E-16	***
	Stem DW	13	24.34	<2E-16	***
	Number of Leaves	13	14.62	3.65E-14	***
	Leaf DW	13	10.94	1.54E-11	***
	Number of Stipules	13	149.30	<2E-16	***
	Stipule DW	13	37.94	<2E-16	***
	Tendril DW	13	19.73	<2E-16	***

Appendix 2.

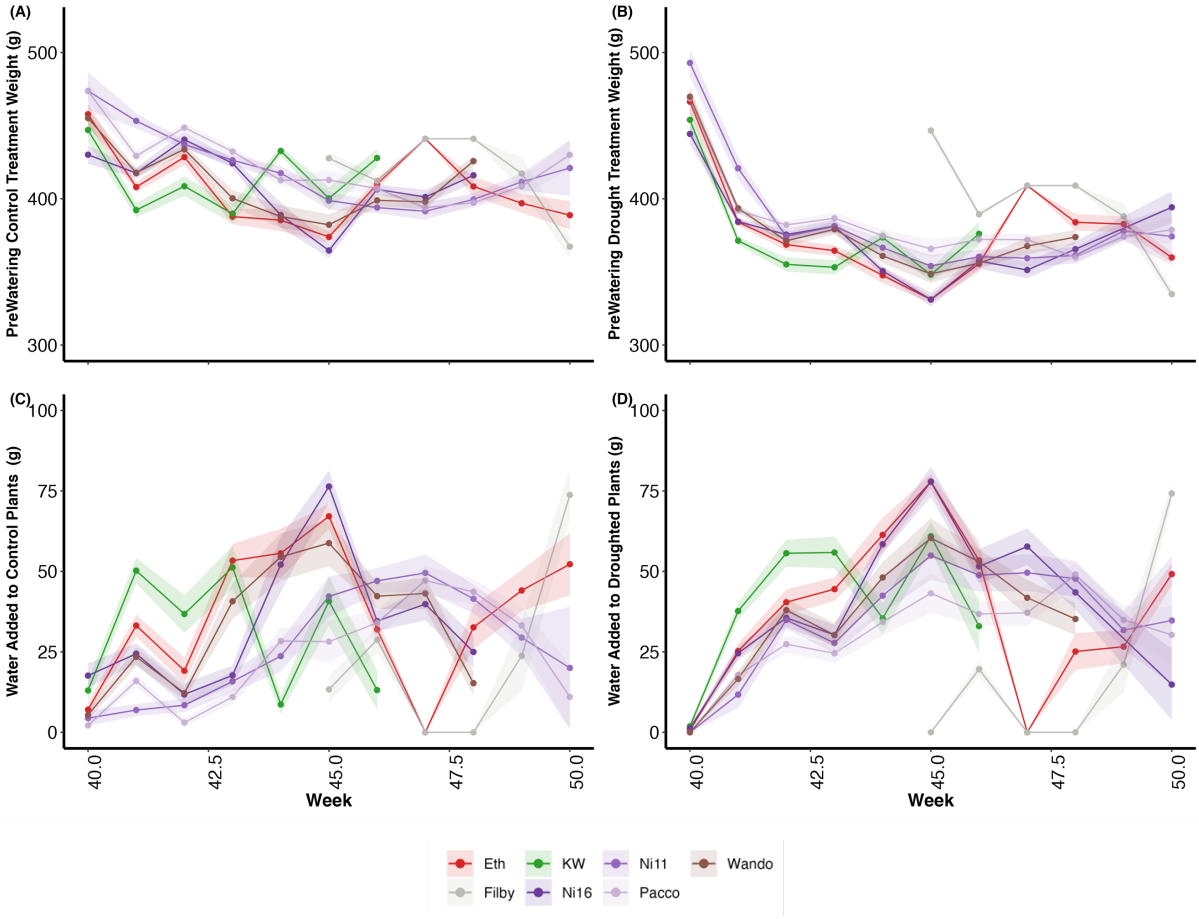

Figure A2.1. Weekly watering weights and amount of water added to watered and droughted plants. Plants were weighed daily to maintain the correct weight according to their relative soil water content (RSWC; 50 % for droughted (409 grams) and 80% for watered plants (440 grams)) calculated via the Moisa et al. (2019) RSWC method. **(A)** watered and **(B)** droughted plants were weighed before watering and the weight of water needed to reach their RSWC weight were calculated for both **(C)** watered and **(D)** droughted plants. Filby (grey) was grown later as it is a leafless accession and was utilised for pod measurements within ***Chapter 4***. Error bars represent mean ± SE (on a daily basis; n = 2-10).

Table A2.1. One-way ANOVA table of grain and biomass yield parameters compared between the P. sativum accessions. Dry weights (DW) were measured (in g) after a constant weight was reached. Statistical significance in yield parameters between the different accessions are illustrated as asterisks, whereby * is $P < 0.05$, ** is $P < 0.01$ and *** is $P < 0.001$ (n = 6).

Yield Type	Parameter	DF	*F* value	*P* value	Sig
Grain	Number of Pods	6	38.75	<2E-16	***
	Pod DW	6	87.54	<2E-16	***
	Total Pod DW	6	10.17	4.56E-08	***
	Pod Length	6	220.78	<2E-16	***
	Number of Seeds	6	34.89	<2E-16	***
	Seed DW	6	67.95	<2E-16	***
Biomass	Plant Height	6	56.97	<2E-16	***
	Plant DW	6	21.77	2.88E-14	***
	Number of Stems	6	69.19	<2E-16	***
	Stem DW	6	174.94	<2E-16	***
	Number of Leaves	6	270.12	<2E-16	***
	Leaf DW	6	120.15	<2E-16	***
	Number of Stipules	6	335.90	<2E-16	***
	Stipule DW	6	121.68	<2E-16	***
	Tendril DW	6	69.92	<2E-16	***

Table A2.2. One-way ANOVA table of grain and biomass yield parameters compared between watered and droughted experimental conditions. Dry weights (DW) were measured (in g) after a constant weight was reached. Statistical significance in yield parameters between the different accessions are illustrated as asterisks, whereby * is $P < 0.05$, ** is $P < 0.01$ and *** is $P < 0.001$ (n = 6).

Yield Type	Parameter	DF	*F* value	*P* value	Sig
Grain	Number of Pods	1	9.79	2.56E-03	**
	Pod DW	1	3.32	0.07	NSD
	Total Pod DW	1	11.85	9.78E-04	***
	Pod Length	1	0.01	0.91	NSD
	Number of Seeds	1	0.13	0.72	NSD
	Seed DW	1	3.38	0.07	NSD
Biomass	Plant Height	1	3.29	0.07	NSD
	Plant DW	1	33.71	1.72E-07	***
	Number of Stems	1	25.68	3.15E-06	***
	Stem DW	1	42.96	8.04E-09	***
	Number of Leaves	1	26.40	2.40E-06	***
	Leaf DW	1	64.11	1.78E-11	***
	Number of Stipules	1	14.73	2.69E-04	***
	Stipule DW	1	18.88	4.61E-05	***
	Tendril DW	1	11.44	1.18E-03	**